

REPORT DOCUMENTATION PAGE				<i>Form Approved</i> <i>OMB No. 0704-0188</i>	
<small>The public reporting burden for this collection of information is estimated to average 1 hour per response, including the time for reviewing instructions, searching existing data sources, gathering and maintaining the data needed, and completing and reviewing the collection of information. Send comments regarding this burden estimate or any other aspect of this collection of information, including suggestions for reducing the burden, to Department of Defense, Washington Headquarters Services, Directorate for Information Operations and Reports (0704-0188), 1215 Jefferson Davis Highway, Suite 1204, Arlington, VA 22202-4302. Respondents should be aware that notwithstanding any other provision of law, no person shall be subject to any penalty for failing to comply with a collection of information if it does not display a currently valid OMB control number.</small> PLEASE DO NOT RETURN YOUR FORM TO THE ABOVE ADDRESS.					
1. REPORT DATE (DD-MM-YYYY) 08-05-2009		2. REPORT TYPE Master's Thesis		3. DATES COVERED (From - To) DEC 2008 - MAY 2009	
4. TITLE AND SUBTITLE Surfacing Rescue Container Concept Design for Trident Submarines				5a. CONTRACT NUMBER N62271-97-G-0026	
				5b. GRANT NUMBER	
				5c. PROGRAM ELEMENT NUMBER	
6. AUTHOR(S) Joshua Jonathan LaPenna				5d. PROJECT NUMBER	
				5e. TASK NUMBER	
				5f. WORK UNIT NUMBER	
7. PERFORMING ORGANIZATION NAME(S) AND ADDRESS(ES) Massachusetts Institute of Technology				8. PERFORMING ORGANIZATION REPORT NUMBER	
9. SPONSORING/MONITORING AGENCY NAME(S) AND ADDRESS(ES) Naval Postgraduate School Monterey, CA 93943				10. SPONSOR/MONITOR'S ACRONYM(S) NPS	
				11. SPONSOR/MONITOR'S REPORT NUMBER(S)	
12. DISTRIBUTION/AVAILABILITY STATEMENT 1. DISTRIBUTION STATEMENT A. Approved for public release; distribution is unlimited.					
13. SUPPLEMENTARY NOTES					
14. ABSTRACT In the wake of the KURSK tragedy, world navies have brought their full attention to the submarine rescue problem. While many rescue systems exist, none have been able to sufficiently address the gamut of scenarios that place submariners in peril. One rescue strategy utilizes a submarine escape capsule commonly referred to as a Surfacing Rescue Container (SRC). The United States has never adopted the underlying strategy. This paper recognizes the SRC concept as the most reliable means of rescue, and proposes a modular SRC concept design (LSRC) which utilizes a modified Trident II D-5 missile tube as its host. The design is intended for use on the U.S. Navy's next generation ballistic missile submarine (SSBN) but may be back-fitted on current U.S. Navy Ohio class and U.K. Royal Navy Vanguard Class submarines with significant alteration. Technical analyses include a minimum weight design approach for internally stiffened right circular cylinders exposed to external hydrostatic pressure, an analytical and numerical structural analysis of imperfect ring stiffened cylinders, and a seakeeping analysis for cylindrical spar buoys.					
15. SUBJECT TERMS					
16. SECURITY CLASSIFICATION OF:			17. LIMITATION OF ABSTRACT UU	18. NUMBER OF PAGES 189	19a. NAME OF RESPONSIBLE PERSON Sean Tibbitts, Educational Technician
a. REPORT	b. ABSTRACT	c. THIS PAGE			19b. TELEPHONE NUMBER (Include area code) (831) 656-2319 civins@nps.edu

Surfacing Rescue Container Concept Design for Trident Submarines

By

Joshua J. LaPenna

B.S., Mechanical Engineering, University of New York at Buffalo
Master of Business Administration, University of Hawai'i at Mānoa

Submitted to the Department of Mechanical Engineering
in Partial Fulfillment of the Requirements for the Degrees of

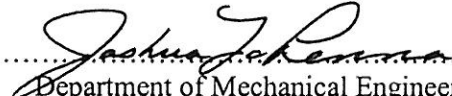
Naval Engineer
and
Master of Science in Mechanical Engineering
at the
Massachusetts Institute of Technology

June 2009


© 2009 Joshua J. LaPenna. All rights reserved

The author hereby grants MIT and the U.S. Government permission to reproduce and distribute
publicly paper and electronic copies of this thesis document.


Signature of Author.....


Department of Mechanical Engineering
May 08, 2009

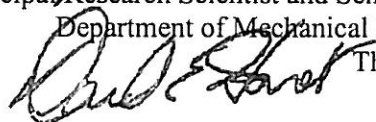
Certified by.....


Tomasz Wierzbicki, Professor of Mechanical Engineering
Department of Mechanical Engineering
Thesis Advisor

Certified by.....


Yuming Liu, Principal Research Scientist and Senior Lecturer
Department of Mechanical Engineering
Thesis Reader

Accepted by.....


David E. Hardt, Professor of Mechanical Engineering
Chairman, Department Committee of Graduate Studies
Department of Mechanical Engineering

(INTENTIONALLY LEFT BLANK)

Surfacing Rescue Container Concept Design for Trident Submarines

by

Joshua Jonathan LaPenna

Submitted to the Department of Mechanical Engineering
on May 8th, 2009 in partial fulfillment of the requirements
for the degree of Naval Engineer and
Master of Science in Mechanical Engineering

ABSTRACT

In the wake of the *KURSK* tragedy, world navies have brought their full attention to the submarine rescue problem. While many rescue systems exist, none have been able to sufficiently address the gamut of scenarios that place submariners in peril. One rescue strategy utilizes a submarine escape capsule commonly referred to as a Surfacing Rescue Container (SRC). Although SRCs have been employed in several submarine designs over the last four decades, the United States has never adopted the underlying strategy. This paper recognizes the SRC concept as the most reliable means of rescue, and proposes a modular SRC concept design (LSRC) which utilizes a modified Trident II D-5 missile tube as its host. The design is intended for use on the U.S. Navy's next generation ballistic missile submarine (SSBN) but may be back-fitted on current U.S. Navy Ohio class and U.K. Royal Navy Vanguard Class submarines with significant alteration. Technical analyses include a minimum weight design approach for internally stiffened right circular cylinders exposed to external hydrostatic pressure, an analytical and numerical structural analysis of imperfect ring stiffened cylinders, and a seakeeping analysis for cylindrical spar buoys.

Thesis Supervisor: Tomasz Wierzbicki

Title: Professor of Mechanical Engineering

(INTENTIONALLY LEFT BLANK)

EXECUTIVE SUMMARY

LCDR Joshua LaPenna, an Engineering Duty Officer enrolled in the Naval Construction and Engineering Program at the Massachusetts Institute of Technology (MIT), critiques the U.S. Navy's submarine Search and Rescue (SAR) strategy, and disputes the SRDRS's (Submarine Rescue Diving and Recompression System) role as the primary means of submarine rescue. Alternatively, a Surfacing Rescue Container (SRC) concept design is proposed with hopes of being considered onboard the next generation nuclear ballistic missile submarine (SSBN). Submarine "escape capsules", like the SRC, have been employed in several submarine designs over the last four decades; however, the United States has never adopted the underlying strategy. In the light of recent U.S. submarine collisions, this paper re-examines their use.

A comparative analysis of rescue capabilities and relevant historical data is used to make a case for rescue strategies employing SRCs as the cornerstone of submarine SAR. This analysis claims that group-assisted rescue methods, such as the SRDRS and Submarine Rescue Chamber, are too slow to be used as a primary means of rescue. By implementing SRCs onboard U.S. submarines, Time-To-First-Rescue (TTFR) can be significantly reduced (SRDRS: 36+ hours, SRC: 1+ hours). The LaPenna Surfacing Rescue Container (LSRC) concept incorporates many of the lessons learned from the ill-fated Russian submarine *KURSK*, and introduces the idea of modularity as it applies to rescue systems of this kind. The LSRC will use a modified Trident II D-5 missile tube as its host, and can be used to bring 70 survivors to the surface in the event a submarine is disabled. Once on the surface, the capsule serves as both a life raft and decompression chamber until help arrives. The LSRC shares the same dimensions as a D-5 missile, displaces 43 long-tons and has a positive submerged buoyancy of 3,516 lbm. To fully implement this concept as the U.S. Navy's primary means of rescue, 145 capsules are required to outfit a submarine fleet of 71 boats.

As part of the structural analysis, a scantling optimization routine was written to optimize the LSRC's pressure hull with respect to weight. This program was used to test millions of scantling arrangements based on classical shell failure formulations and elastic buckling equations. The optimal designs were then compared with results obtained using the UK MoD optimization algorithm (MNSTRL) and a FEA was performed. Once the structure was modeled, various imperfections were introduced to assess the structure's resistance to out-of-fairness (OOF). The results were then compared to those obtained by the Naval Sea Systems Command office of Survivability and Structural Integrity (NAVSEA 05P). The final pressure hull design has two compartments and is uniformly stiffened by small T-frames. The pressure hull is rated for operations as deep as 1,666 feet and has a collapse depth in excess of 2,500 feet. Although the pressure hull was designed to fail by axisymmetric shell yield, results suggest that the pressure hull is susceptible to multi-wave failure modes. Thus, additional analysis will be necessary should the concept be developed further. Mass distribution calculations indicate that the LSRC will exhibit poor stability characteristics due to small values of \overline{BG} (31.6 inches). Having a freeboard of only 1.8 feet, there is little room for additional ballast. For this reason, reductions in load will be necessary to improve \overline{BG} . These calculations include a weight margin of 10%, evenly applied to all weight groups.

Although a detailed cost analysis was not performed, a comparative analysis with the SRDRS program requires that each LSRC be produced at a cost no greater than \$1.2M. This figure assumes that missile tube modifications and support systems can be rolled into new ship construction costs. In conclusion, the LSRC is an example of what *could* be done to improve the U.S. Navy's submarine SAR program. Contrary to this thesis's title, the LSRC concept should not be interpreted as a niche solution, applicable only to Trident submarines. Rather, it is the concept of a modular SRC which is housed in a pressure tight chamber (i.e. tube) that can be placed anywhere on a submarine.

(INTENTIONALLY LEFT BLANK)



LaPenna Surfacing Rescue Container (LSRC)

(INTENTIONALLY LEFT BLANK)

BIOGRAPHY

LCDR LaPenna is a native of Buffalo, New York. He graduated from the University of New York at Buffalo in 1996 with a Bachelor of Science in Mechanical Engineering, focusing in mechanical systems. During the summer of 1993, he participated in an internship at NASA Langley Space Research Center; and conducted research in the Non-Destructive Testing (NDT) of riveted lap joints using thermosonic stress analysis. Two years before graduation, LCDR LaPenna joined the U.S. Navy under the Nuclear Propulsion Officer Candidate (NUPOC) program.



After graduating from Nuclear Power School in Orlando, Florida, LCDR LaPenna reported for training at the Prototype Reactor Facility in Ballston Spa, New York, where he qualified Engineering Officer of the Watch on the MARF nuclear reactor (S7G). After completing Submarine School in 1998, LCDR LaPenna reported to the nuclear ballistic missile submarine *USS WYOMING* (SSBN 742). He completed five deterrent patrols onboard the *WYOMING*, and held jobs as the Main Propulsion Assistant (MPA), Reactor Controls Officer (RCA), and the Tactical Systems Officer (TSO). It was onboard the *WYOMING* that LCDR LaPenna qualified as a Submarine Warfare Officer (Submarine Dolphins), and Nuclear Engineer (S8G).

After detaching from the *WYOMING*, LCDR LaPenna transferred to Commander Submarine Force U.S. Pacific Fleet (COMSUBPAC), Pearl Harbor, Hawaii. There he worked in the Offices of Operations (N3) and Tactical Readiness and Training (N7); he held jobs as the Command Center Watch Officer (CCWO), Mine Warfare Officer, and Support Operations Officer. In these positions, LCDR LaPenna conducted numerous submarine war game exercises, participated in live torpedo firing exercises (SINKEXs), and conducted underway operations near the North Pole (ICEXs). He also worked close with allied navies in the Pacific theater and conducted underway operations onboard JMSDF and ROK Navy diesel-electric submarines.

While serving at COMSUBPAC, LCDR LaPenna obtained a Master of Business Administration (MBA) from the University of Hawaii at Mānoa. In 2003 he accepted a lateral transfer to the Engineering Duty Officer (EDO) community, and was given orders to the Naval Diving and Salvage Training Center (NDSTC), Panama City Beach, Florida. There he obtained Basic Diving Officer (BDO) qualifications as a deep-sea diver, and qualified on the Mk-16, Mk-20, Mk-21 and SCUBA diving apparatus, graduating first in his class.

In July of 2004, he reported to Portsmouth Naval Shipyard (PNS) in Kittery, Maine. At PNS he served as the Shipyard Diving Officer and the *USS JACKSONVILLE* (SSN 699) Non-Nuclear Assistant Project Superintendent (APS(NN)), as well as the Ship Safety Officer and the Work Integration Leader (AIT Coordinator). As an APS(NN) at PNS, LCDR LaPenna managed and coordinated various aspects of repair during the *JACKSONVILLE*'s Engineering Refueling Overhaul (ERO).

After taking his degrees from MIT, LCDR LaPenna will report to the Supervisor of Salvage and Diving at the Naval Sea Systems Command (NAVSEA) in Washington, DC.

LCDR LaPenna is married to the former Jennifer L. Thomas of Binghamton, New York. He has two daughters, Madeline Linda and Ava Helen.

(INTENTIONALLY LEFT BLANK)

Dedication

James John LaPenna

Acknowledgments

Yuanli Bai
Scott Barrasso
James Benzing
David Burke
Ian Carter
Hamish Fowler
Wayne Frey
Remlee Green
Katie Harris
Yaning Li
Yuming Liu
Angie Locknar
Ralph Olesen
John Standing
Michael Triantafyllou
Mark Van Emmerik
Jonathan Whatmore
Tomasz Wierzbicki
Bill Will

Special Thanks

None of this work would have been possible without the support of my wife Jennifer. She is the great woman behind the ordinary man.

(INTENTIONALLY LEFT BLANK)

PREFACE

The concept of group escape from a distressed submarine via a capsule housed within a watertight enclosure, such as a missile tube, first came to me while serving onboard the *USS WYOMING* (SSBN 742). After researching this topic, I realized that this idea is not entirely original. However, a detailed study as it applies to the Trident II D-5 missile system has never been done. This thesis was written to more fully explore how this concept could be implemented onboard U.S. submarines.

I truly believe in this concept. The U.S. submarine force is second to none; however, her rescue strategy for distressed submarines (DISSUB) is largely incomplete and would benefit from using group rescue systems such as the surfacing rescue containers (SRC)¹ used abroad. The basis for this conclusion is discussed more fully in chapter 1. It is my opinion that the “best case” Submarine Rescue Diving and Recompression System (SRDRS) response time is unacceptable. I salute the engineers who have developed the SRDRS, and applaud them for their success in developing a system that can overcome the hurdles associated with deploying a rescue capability anywhere in the world with a time to first rescue (TTFR) of only 3+ days. Given the hurdles at hand; mainly, DISSUB notification, DISSUB localization, Submarine Rescue Vehicle (SRV) deployment, DISSUB hatch mating and crew decompression, the SRDRS performance is impressive. However, we are not victims of these hurdles. On the contrary, our submarine SAR strategy created them. These hurdles exist because of a flawed rescue strategy that places the entire burden of submarine rescue upon a single fly-away system. If the rescue strategy relied on SRCs, with the SRDRS and Submarine Escape and Immersion Equipment (SEIE) suit as backups, every hurdle listed above would no longer apply. When utilizing SRCs, TTFR is spoken on the order of hours rather than days, and crew survival becomes a tangible expectation.

It is my expectation that few people within the Naval Sea Systems Command (NAVSEA) organization will take this paper seriously. This is unfortunate. Ideas such as this will never be popular; they do not improve the submarine’s stealth or lethality, they do not fit neatly into overarching guidance such as *Seapower 21* or the new *Maritime Strategy*, and more importantly, they cost money. In addition, the SRC will add weight to an already weight limited platform and will require precious real estate. Resistance will also come as a result of the strong design paradigm that exists within U.S. submarine development organizations. Finally, the idea is different; it will force designers to rethink survivability and the way we design submarines, and may even require that we adopt practices used by our former adversaries.

It is recognized that this thesis does not meet all the requirements of a true “concept design” as is accustomed to those within NAVSEA. Academically, this work is sound. A great deal of effort was made to ensure that the results were accurate and not misleading. However, I am in no way infallible and encourage others to critique my work. In the spirit of MIT, an effort was made to explore this problem with classical, if not fundamental, equations and techniques. For example, rather than simply use published design codes for developing the LSRC pressure hull, more traditional equations were used to demonstrate a more thorough understanding of the topic. In addition, an effort was made to experiment with and utilize newly developed software.

¹ Not to be confused with Submarine Rescue Chambers such as the McCann Bell.

(INTENTIONALLY LEFT BLANK)

CONTENTS

1 Introduction.....	21
1.1 Motivation.....	21
1.2 Background.....	23
1.2.1 SRC History	23
1.2.2 Current use of SRCs.....	24
1.2.3 Design Challenges	25
1.3 A Case for SRCs	27
1.3.1 Advantages and Disadvantages.....	27
1.3.2 Response Time.....	28
1.3.3 U.S. Submarine SAR Capability Gap	32
1.3.4 Conclusion	36
2 LSRC Design and Analysis	37
2.1 Design Overview	37
2.1.1 LSRC Concept	37
2.1.2 Design Process	39
2.2 Systems and Payloads	40
2.2.1 MMT Operation and Ejection Control.....	40
2.2.2 Communications and Navigation.....	42
2.2.3 Electrical Power and Lighting.....	42
2.2.4 Decompression System	43
2.2.5 Ventilation.....	43
2.2.6 Atmosphere Monitoring and Control.....	44
2.2.7 Dewatering System	46
2.2.8 Crew Supplies	47
2.2.9 Payloads and Adjustments	48
2.3 Arrangements.....	50
2.3.1 LSRC Structure, Bulkheads and Hatches.....	50
2.3.2 Outer “Command” Chamber.....	50
2.3.3 Inner Chamber	51
2.4 Structural.....	60
2.4.1 Pressure Hull Analysis	60

2.4.2 Modes of Failure	60
2.4.3 King Frames	69
2.4.4 End Caps	72
2.4.5 LSRC Hull Design	77
2.4.6 Conclusions and Recommendations	103
2.5 Stability and Seakeeping	104
2.5.1 Weight Distribution	104
2.5.2 Static Stability	104
2.5.3 Dynamic Stability	107
2.6 Cost	131
3 Conclusions and Observations	133
4 Future Work	135
4.1 Ejection Phase and Accent Phase	135
4.2 Missile Tube Systems and Interface	136
4.3 Psychological Effects (Claustrophobia)	136
4.4 Temperature	136
Bibliography	137
Acronyms	139
Terms and Definitions (Structural Analysis)	143
Terms and Definitions (Seakeeping Analysis)	147
Appendix I. SRC Designs	151
Appendix II. Historical Submarine Escape and Rescue Data	155
Appendix III. NAVSEA HY80 Stress-Strain Curve Data	159
Appendix IV. Full Factorial Scantling Optimization Routine (FFSOR)	163
Appendix V. FFSOR Results – Design A	173
Appendix VI. FFSOR Results – Design B (Small Frame)	175
Appendix VII. FFSOR Results – Design B (King Frame)	177
Appendix VIII. Seakeeping Solver for Cylindrical Spar Buoys	179
Appendix IX. Seakeeping Results	189

LIST OF FIGURES

Figure 1. Separable Compartment (SC) concept.....	23
Figure 2. The “Gabler” rescue sphere.....	24
Figure 3. Longitudinal cross-section of <i>KURSK</i>	25
Figure 4. Blast-proof crew rescue system and emergency notification	25
Figure 5. SRC placement. Type 209/1500.....	26
Figure 6. SRDRS response timeline	29
Figure 7. SRC response timeline	30
Figure 8. Submarine escape and rescue regimes with historical data	32
Figure 9. Double functionality. Alfa class SSN SRC	37
Figure 10. SRC located at the pressure hull. Type 209/1500.....	38
Figure 11. LSRC accessibility arrangements.....	39
Figure 12. MMT remote operation and ejection system.....	41
Figure 13. COTS atmosphere monitoring equipment.....	45
Figure 14. CO ₂ removal systems.....	46
Figure 15. SRC arrangement and crew supplies	47
Figure 16. LSRC profile drawings and system arrangements.....	53
Figure 17. LSRC cross-sectional view.....	54
Figure 18. Outer “command” chamber	55
Figure 19. Submarine – LSRC access hatch	56
Figure 20. Outer chamber system arrangement	57
Figure 21. Topside arrangement	57
Figure 22. LSRC seating arrangement.....	58
Figure 23. Indian Navy Type 209/1500 rescue sphere seating arrangement	59
Figure 24. SRC seating arrangements.....	59
Figure 25. Simplified LSRC structural design.....	60
Figure 26. Modes of failure.	61
Figure 27. Ring stiffener eccentricities	68
Figure 28. King frame scantling dimensions and definitions	69
Figure 29. End-cap designs.....	72
Figure 30. Dome geometry	73
Figure 31. Elliptical dome membrane stresses.....	74
Figure 32. Torispherical dome design curves	76
Figure 33. Design A.....	77
Figure 34. Design B	77
Figure 35. Design A finite element model.....	81

Figure 36. Axisymmetric imperfection (OOF)	83
Figure 37. FFSOR solutions	84
Figure 38. Frame cross sections	85
Figure 39. Design A, Von Mises stress at 2,500 feet	86
Figure 40. *BUCKLE analysis results, Mode 1, Design A	87
Figure 41. Frame tripping analysis	88
Figure 42. OOF effects on collapse depth (Method 1, Design A)	89
Figure 43. ABAQUS TM *BUCKLE analysis results, Mode 1, Design B	90
Figure 44. OOF effects on collapse depth	91
Figure 45. Von Mises stress at collapse depth (Method 2, Design B)	92
Figure 46. Deformed geometry – Post failure (Method 2, Design B)	92
Figure 47. Deformed geometry – Post failure (Method 1, Design B)	93
Figure 48. Deformed geometry – Post failure (Method 2, Design B)	93
Figure 49. <i>Paramarine</i> TM model (Design A)	96
Figure 50. <i>Paramarine</i> TM model (Design B)	96
Figure 51. Shell failure regimes	100
Figure 52. DTMB pressure hull data comparison	101
Figure 53. U.S. submarine pressure hull comparison	101
Figure 54. Range of surfaced and submerged stability	105
Figure 55. Wave superposition, and the frequency-domain time-domain relationship	107
Figure 56. Properties of a time invariant system	108
Figure 57. Sign convention for translatory and angular displacement	109
Figure 58. Added mass of an ellipsoid of revolution	116
Figure 59. Probability density functions	123
Figure 60. Sea state 3. RAOs and sea spectrum	129
Figure 61. Sea state 4. RAOs and sea spectrum	129
Figure 62. Sea state 3. Time space simulation in pitch	130
Figure 63. Sea state 4. Time space simulation in pitch	130
Figure 64. Small frame scantling dimensions and definitions	146
Figure 65. Seakeeping analysis dimensions	149

LIST OF TABLES

Table 1. SRC and SRDRS advantages and disadvantages.....	28
Table 2. Frame stability guidelines.....	68
Table 3. Scantling design guidelines.....	80
Table 4. FFSOR optimization result	85
Table 5. Design A analysis results	86
Table 6. Design B analysis results	89
Table 7. Safety factors	94
Table 8. <i>Paramarine</i> TM (MNSTRL) optimization results for Design A.	97
Table 9. <i>Paramarine</i> TM (MNSTRL) optimization results for Design B.	98
Table 10. FFSOR-NAVSEA qualitative comparison	102
Table 11. LSRC mass distribution data	104
Table 12. Static stability characteristics.....	104
Table 13. NATO STANAG 4154 operability criteria.....	126
Table 14. Seakeeping results.....	128

(INTENTIONALLY LEFT BLANK)

1 INTRODUCTION

1.1 MOTIVATION

On August 12th, 2000 the Russian attack submarine *KURSK* (K-141) suffered a fantastic casualty that killed all but 23 of her crewmembers. When I first heard of the casualty, I remember first being amazed that an Oscar class submarine could sustain so much damage. I was worried for the sailors onboard, but was relieved when I heard that the boat had sunk in just 350 feet of water. In terms of submarine operating depths, this is very shallow. Especially considering the *KURSK* itself was more than 500 feet in length. As a submariner and deep-sea diver, I was convinced that these men could be saved. Instead, all 23 men died while waiting to be rescued.

The events leading to her demise are not nearly as important as the lessons to be learned, and there are many. It has been ascertained that a poorly maintained 65-76 torpedo exploded *inside* the pressure hull. After a much larger secondary explosion, the first four compartments of the *KURSK* were flooded. Contemplating escape or rescue, survivors occupying the four intact compartments gathered in the ninth compartment underneath the escape trunk. Russian naval pathologists believe that all 23 men died of carbon monoxide poisoning. Evidence resulting from the *KURSK*'s salvage suggests that a flash-fire occurred in the ninth compartment due to high partial pressures of oxygen and the heat generated from a seawater reaction with the superoxide chemical cartridges being used to generate oxygen. Within minutes of this fire the crew most likely died from the now toxic submarine atmosphere. Unfortunately, there is no way of knowing exactly how long the survivors lived. Notes written by the crew prove that all 23 men were alive for at least 6 hours and 17 minutes. It was also observed that no attempt was made acoustically (i.e. hull tapping) to signal the Russian SRV *PRIZ* when it attempted to mate with the aft escape trunk just 32 hours after the first explosion².

When focusing on the details of the *KURSK* tragedy it is easy to miss the big picture. The fact that these men died from a flash-fire is almost irrelevant. They could just as easily have died from hypothermia, carbon dioxide poisoning, or drowning as a result of seawater leaks. The biggest lesson from the *KURSK* tragedy is *time*. Time killed these men. Notes written by the crew suggest that all 23 men were uninjured following the second explosion. If these men were to survive at all, they needed to get off the submarine within the first few hours. Had these men attempted escape on their own using individual SEIE suits³ some may have survived; however, the submarine's depth and the risk of hypothermia most likely swayed the crew's decision to await rescue. Unfortunately, this decision cannot always be reversed. If exposed to elevated pressures (due to seawater or air leaks) equivalent to just 60 feet of seawater for more than an hour, the entire crew will no longer have the option to escape without risking decompression sickness⁴. For this reason, solely relying on a rescue strategy that forces men to await rescue is

² Widely unappreciated by western media, this response time was deemed slow and uncoordinated. Given that the published SRDRS response time is 72 hours, this sentiment is not without its own hypocrisy.

³ Known to the Russian navy as ISP-60s (*Individualnoe Sredstvo Podvodnika*)

⁴ "In the ninth compartment, there are 23 sailors. We feel bad, weakened by carbon dioxide....Pressure is increasing in the compartment. If we head for the surface we won't survive the decompression. We won't last more than a day." – Captain Lieutenant Sergei Sadilenko, *KURSK* [37].

ill-posed; It prevents men from acting quickly at intermediate depths, and after a short time, puts them in a situation where individual escape is no longer an option.

This lesson should have been learned following the tragic sinking of the Peruvian submarine *BAP PACOCHA* (SS-48) (formerly *USS ATULE*) in 1988. While transiting on the surface off the coast of Peru, the *PACOCHA* suffered a collision with a Japanese trawler. In less than five minutes the *PACOCHA* was on the bottom some 140 feet below the surface. Twenty-two men were trapped inside the submarine contemplating the same questions (i.e. escape or rescue) as those onboard the *KURSK*. Communication with rescuers above revealed that the U.S. Navy had activated its emergency McCann rescue team, and that the survivors were to remain calm and await their rescue. However, due to delays in deploying the rescue chamber, and the slowly worsening atmospheric conditions within the submarine, it was finally decided that all men should escape using Steinke hoods⁵. At 140 feet this method of escape proved successful, and all twenty-two men exited the submarine via the forward escape trunk, the last leaving some twenty-three hours after the collision. Unfortunately, many of the men had incurred decompression obligations and developed decompression sickness within minutes of reaching the surface. While transporting the men to decompression chambers, one man died and another was severely brain damaged.

All things considered, the escape was successful. However, the submariners should have performed a hooded ascent immediately after reaching the bottom (or at least after learning that rescue teams had formed on the surface). Once again, *time* killed/injured these men. These two tragedies are excellent examples of why group-assisted rescue methods, when solely relied upon, are inadequate and unconstructive. In the first few hours following the casualty these men made the decision to await rescue based on the atmospheric conditions *at that time*. Only time revealed that their lithium hydroxide canisters were inefficiently removing CO₂, that leaks in the pressure hull were causing the submarine atmosphere to become hyperbaric, and that the seawater entering the battery well was creating toxic chlorine gas.

It is the objective of this thesis to investigate the use of modular escape capsules onboard U.S. submarines. Such devices solve the “time problem” and may be used at considerable depths⁶. Historically, the “escape capsule” concept has taken many forms (e.g. SRCs, RRGs, SRGs and SCs); however, the SRC has emerged as the most promising design. Access to a well designed SRC could have saved the lives of those mentioned above. The problem associated with outfitting submarines with SRCs is not engineering in nature; rather, it is political, and will only be deemed feasible when it is made a priority. Many may argue that there just isn’t enough room onboard a submarine for such a device. Somehow however, designers found room onboard a Project 705 (NATO classification: Alfa) SSN, and a Type 209 SSK; they just made it a priority. Thus was the motivation for this thesis. If a SRC cannot be realized onboard a Trident submarine, then it will never find its way into the United States Navy.

⁵ All but three escaped using Steinke hoods. The last three survivors escaped utilizing SCUBA bottles which were placed in the escape trunk by rescue divers.

⁶ See Appendix II. *KOMSOMOLETS* (K-278)

1.2 BACKGROUND

1.2.1 SRC HISTORY

It is uncertain when the SRC concept was first conceived; however, its allure is probably as old as the submarine itself. At the end of the 1930s the Italian and Spanish navies adopted one and two-man multipurpose surfacing containers based on Geralami's patent. These containers were designed to carry submarine survivors to the surface, and then by means of a winch, be returned to a special housing in the submarine's pressure hull for subsequent use. The Malakhit [Malachite] Design Bureau, Russia's renowned underwater shipbuilding firm, further experimented with this concept in the early 1960s. These devices became known as Reusable Rescue Gear (RRG). However, long cycle times and complications during the container's retraction prevented the RRG from ever being developed past the experimental design stage.

About the same time, the Malachite Design Bureau, the Rubin Central Marine Engineering Design Bureau and the Lazurite Central Design Bureau began to develop reusable Surfacing Rescue Gear (SRG). These devices were similar to the RRGs but were designed to rescue up to 20 people at once. The SRG was housed in a specially designed chamber that was accessible to the crew from inside the submarine. Once manned, the chamber door was opened and the RRG was released. After the crew reached the surface, they would exit the container and the RRG was retrieved. When the container was fully retracted, the chamber door was closed, and the chamber interior was drained allowing the next group of survivors to enter. This process was repeated until the entire crew evacuated the disabled submarine. After completing successful tests on a Project 613A diesel submarine in 1961, the Lazurite SRG design was installed on Project 662, 670, 690, 1840 and 667A submarines [1].

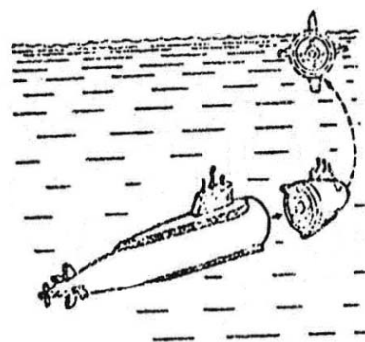


Figure 1. Separable Compartment (SC) concept

During the preliminary study of the Project 705 (NATO classification Alfa) fast attack SSN, the Malachite Design Bureau proposed that the SRG be made large enough to accommodate the entire crew. This modification would make retrieval unnecessary, and the entire crew could remain inside the container upon reaching the surface; hence, the SRC was born. Despite its large size, the SRC was married beautifully to the submarine's advanced sail design and was even integrated with the submarine's bridge. The transition from the SRG to the SRC was made possible largely due to the Alfa's small complement. Implementing this concept onboard larger submarines proved to be more difficult. This problem led to some of the most innovative group-independent escape systems yet conceived; namely, the separable compartment (SC). This concept makes no distinction between the submarine and the SRC; rather, an entire compartment is designed to separate from the submarine in the event of a casualty, leaving behind the deranged portion of the submarine. A handful of countries, including the United States, funded research to develop this concept. However, due to its scale and the overall impact on submarine design the concept was abandoned. An illustration of the SC concept can be seen in Figure 1.

1.2.2 CURRENT USE OF SRCS

The SRC was first tested with men onboard from a special test platform in the gulf of Finland in 1965, and later put to service onboard the K-64 (Project 705) in 1969. The K-64 was accepted by the Soviet Navy in December 1971 making it the first operational submarine with an SRC installed [2]. Other SRC designs can be found on most third-generation Soviet/Russian submarines; specifically, NATO classification Alfa, Mike, Sierra, Oscar, Typhoon, and Akula and possibly the Severodvinsk and Borei class. Numerous pictures of Russian SRCs can be found in Appendix I.

The only other country currently operating submarines with SRCs is India. In the early 1980s Indian admirals asked the designers at the German Ingenieur-kontor Lübeck (IKL) Design Bureau to make SRCs an integral part of the four submarines that were being purchased from the Howaldtswerke-Deutsche Werft AG (HDW) shipyard in Germany. At that time, India did not have any submarine rescue facilities of their own, and were interested in developing a rescue strategy that was reliable and inexpensive to maintain (3). Working closely with Professor Ulrich Gabler, one of the world's most renowned submarine designers, a 40 man “rescue sphere” was incorporated into the Type 209 submarine design. This project resulted in four submarines of the Shishumar class, each having a single SRC just forward of the sail (See Figure 2(a)).

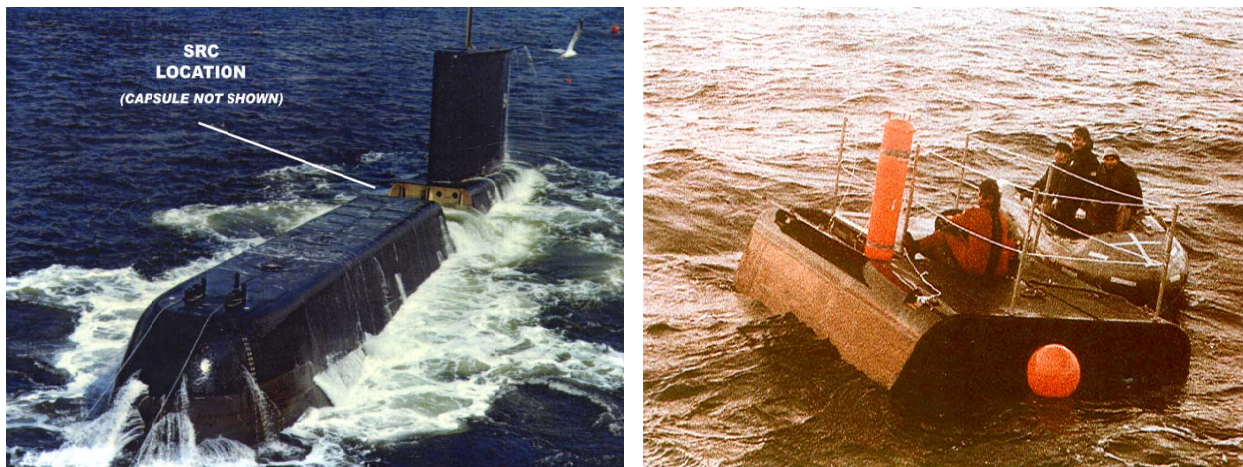


Figure 2. (a) Type 209/1500 submarine, (b) The “Gabler” or “Kockums” rescue sphere (SRC) on the surface [4]

On only one occasion was a SRC used to save men onboard a distressed submarine. On April 7, 1989, a fire broke out aboard the Soviet submarine *KOMSOMOLETS*, and despite the crew's efforts, the fire burned out of control. The submarine sank to a depth of 5,500 feet, 125 miles off the northern coast of Norway. While descending in the water column, five men entered the SRC and activated the ejection mechanism. At first, the SRC failed to release. Some seconds later the submarine was rocked by a secondary explosion (or by hitting the bottom) and the capsule rose to the surface. Due to toxic smoke and failure to equalize pressure across the upper hatch, only one man survived the escape.

1.2.3 DESIGN CHALLENGES

Implementing SRCs onboard U.S. submarines will be challenging. Russian experience has shown that the most problematic features of SRCs are the ejection/locking mechanism and the capsule's dynamic stability during ascent. To overcome these obstacles, the SRC must be designed with simplicity and robustness. Another challenge, while not entirely engineering in nature, is SRC placement. Because accessibility must be assured, this decision cannot be made without also considering the submarine's bulkhead arrangement. Ironically, submarine arrangements that maximize crew survivability impede SRC implementation. This paradox is exemplified by the Oscar class SSN. As is evident from Figure 3, only survivors in the second compartment are assured access to the SRC located in the sail. This arrangement proved fatal to the survivors onboard the *KURSK*, as the first four compartments had been flooded. The *KURSK* accident also highlighted one of the SRCs biggest disadvantages. Because the torpedoes detonated so close to the sail, the SRC was damaged and the capsule flooded. In an effort to improve SRC survivability and accessibility, system modifications were presented at the International Shipbuilding Conference in 2002. Russian speakers proposed that the submarine be divided into two rescue zones, each having a dedicated SRC protected by a blast-proof pressurized "shaft" or chamber (See Figure 4). While this modification is aimed at improving SRC survivability, it also improves crew accessibility. Unfortunately, even the modified arrangement does not assure accessibility for all crewmembers. For this reason, submarines designed with more than three manned compartments should instead employ shock-hardened access tunnels in conjunction with one or two strategically placed SRCs (See section 2.1.1).

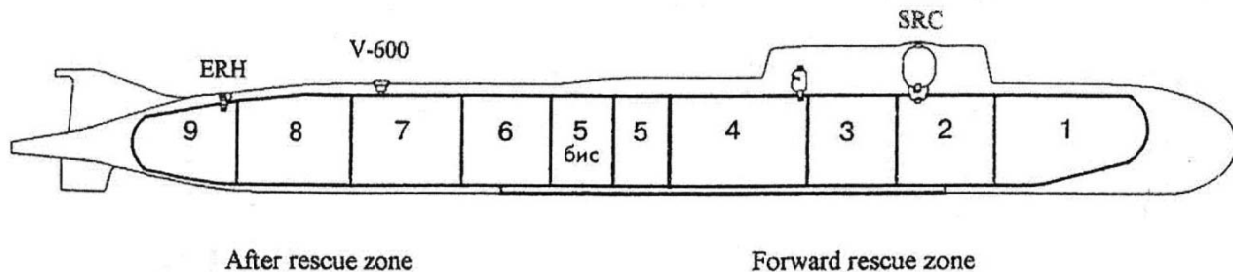


Figure 3. Longitudinal cross-section of *KURSK* [5]

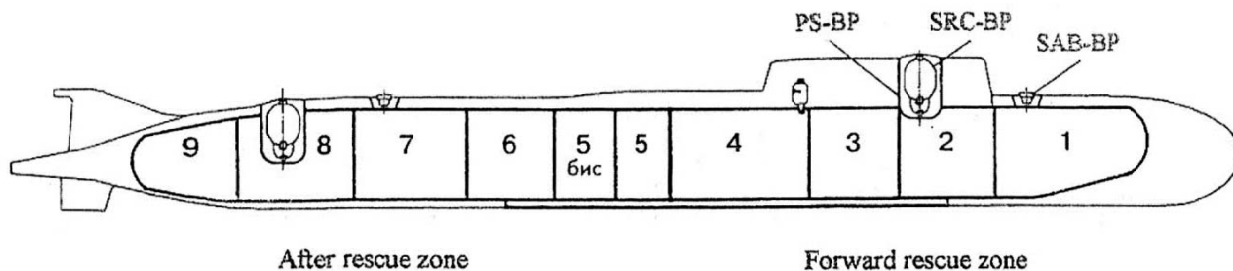


Figure 4. Blast-proof crew rescue system and emergency notification [5]

The problem of SRC placement is considerably easier for submarines with only two or three compartments. To ensure accessibility onboard the Indian Type 209/1500 submarines, designers placed the SRC directly over the forward bulkhead (See Figure 5). In this way, the capsule can be accessed from either compartment or both simultaneously. Such a design may be feasible onboard U.S. submarines. However, the large manning onboard U.S. submarines may require that wasp-waist pressure hull designs be used in conjunction with the SRC(s). For submarines designed with twin-hulls, a single SRC may be placed along the centerline of the ship, or like the Russian Project 941 (NATO classification: Typhoon), SRCs are placed above each hull for survivability and redundancy (See picture in Appendix I).

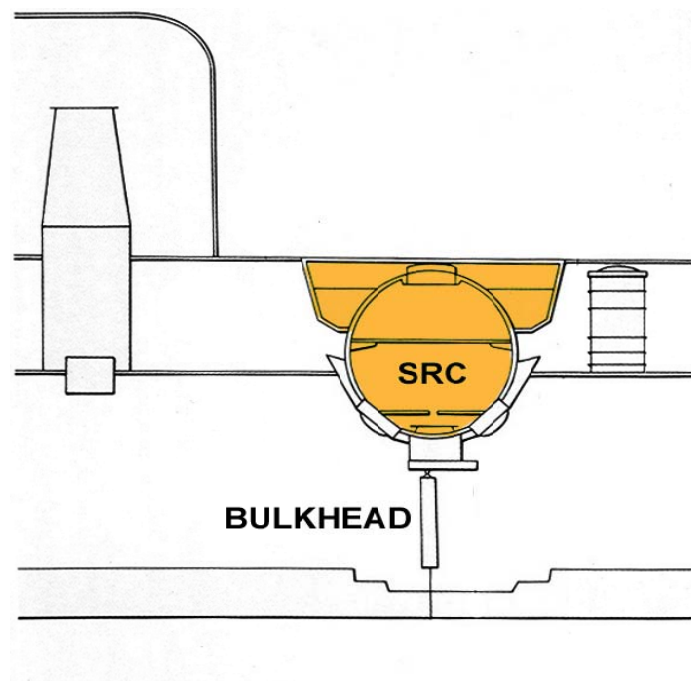


Figure 5. SRC placement. Type 209/1500 [4]

1.3 A CASE FOR SRCs

The decision to develop SRCs should not be based ROW examples alone. Thus, this section will examine the U.S. Navy's submarine escape doctrine, and will build a case for SRCs based on fundamental search and rescue (SAR) objectives and historical data. COMNAVSUBFOR OPLAN 2137 [6], published by the commander of submarine forces, defines the submarine SAR mission as follows:

“The specific mission of submarine search and rescue in the U.S. Navy is to deliver survivors from a bottomed, disabled submarine to the surface in a medically viable condition, anywhere in the world.”

This mission is currently fulfilled by three rescue systems, (1) the Mk 10 SEIE suit, (2) the submarine rescue chamber, and (3) the SRDRS, the latter two of which may be characterized as a group-assisted rescue capability. The Submarine Rescue Chamber is rated to 850 feet and can rescue up to six survivors every 1-3 hours. Like the SRDRS however, the Submarine Rescue Chamber's initial response time will vary with SUBMISS declaration and DISSUB location. The SEIE suit is immediately available to the crew for escape and may be used at any depth less than 600 feet. Proficient use of the escape trunks should allow for eight individual escapes per hour. The SRDRS is rated at 2,000 feet and can rescue 16 survivors per sortie. Each sortie has a nominal cycle time of about five hours. The initial response time (objective) for the SRDRS is 72 hours after SUBMISS has been declared. Within the U.S. Navy, the SRDRS is considered to be the primary means of submarine rescue, and the Submarine Rescue Chamber and SEIE suit are maintained as reliable back-ups. These three systems span two of the three rescue methods (i.e. individual-escape and group-assisted rescue). The third (i.e. group-independent escape), is not a part of the U.S. Navy's submarine SAR strategy. If SRCs were to be used, they would become the primary means of rescue and the SRDRS would only be relied upon as a contingency.

1.3.1 ADVANTAGES AND DISADVANTAGES

As previously discussed, the SRDRS is not in competition with the SRC concept. Rather, both systems, as well as individual escape techniques, should be used in a single strategy, each complementing the other. However, because the group-assisted rescue strategy has become the dominant rationale within the U.S. Navy, the SRDRS program will be used for purposes of comparison. Because both systems were developed to address the same problem, it is worthwhile to compare their overall effectiveness in relation to each other. To begin, a *comparative* list of advantages and disadvantages for each are listed in Table 1.

SRC ADVANTAGES

- SUBSUNK notification not necessary
- DISSUB localization does not apply
- SRV deployment does not apply
- AUWS not required
- Hatch mating not required
- SRC acts as a dry lifeboat on surface
- Reduced chance of decompression obligation
- TUP not required (decompress inside SRC)
- Improved TTFR
- Requires 1 person to deploy
- Simplicity of concept
(low probability of delay or failure)
- Cost ?

SRC DISADVANTAGES

- SRC is subject to damage
(i.e. same as submarine)
- One or more is required on *each* submarine
- Weight and space burden
- Increased ship cost (SCN)
- Cannot be used to assist foreign governments

SRDRS ADVANTAGES

- Rescue systems are maintained off submarine
- Can be used to assist foreign governments
- SDS provides more room for treatment of survivors

SRDRS DISADVANTAGES

- Requires SUBSUNK notification*
- Requires DISSUB localization*
- Requires deployment to DISSUB*
- Requires multiple rescue sorties*
- Requires TUP for decompression*
- Requires hundreds of people to deploy*
- Response subject to VOO and aircraft transport availability*
- Requires hatch mating
- TTFR > 3 days
- Complexity of concept
(high probability of delay or failure)
- Inoperable in high sea states
- Cost?

Table 1. SRC and SRDRS advantages and disadvantages

Perhaps more important than identifying the pros and cons of each system, the table above highlights just how different these two systems are. The two greatest advantages that the SRC has over the SRDRS are simplicity and TTFR. However, TTFR by itself is sufficient to warrant serious consideration. TTFR is widely recognized as the most significant factor in increasing the probability of crew survival. OPLAN 2137 fully embraces this fact and has made it part of the U.S. Navy's submarine SAR mission statement:

*“Survivability on a disabled submarine is limited based on CO₂ production and removal, cold, oxygen consumption, and the possibility of a pressurized environment or toxic gases. As a consequence, **submarine rescue is a race against time.**”*

However, the rescue systems being funded within the U.S. Navy do not fully support this sentiment. The SRDRS's slow TTFR is a direct result of the disadvantages asterisked above. Again, these disadvantages are unavoidable consequences of the group-assisted strategy.

1.3.2 RESPONSE TIME

A “best case” timeline for SRDRS deployment is depicted in Figure 6. This timeline represents the U.S. Navy's response, per plan, in the event that a U.S. attack submarine fails to transmit a check report when operating on a 24 hour communications schedule.

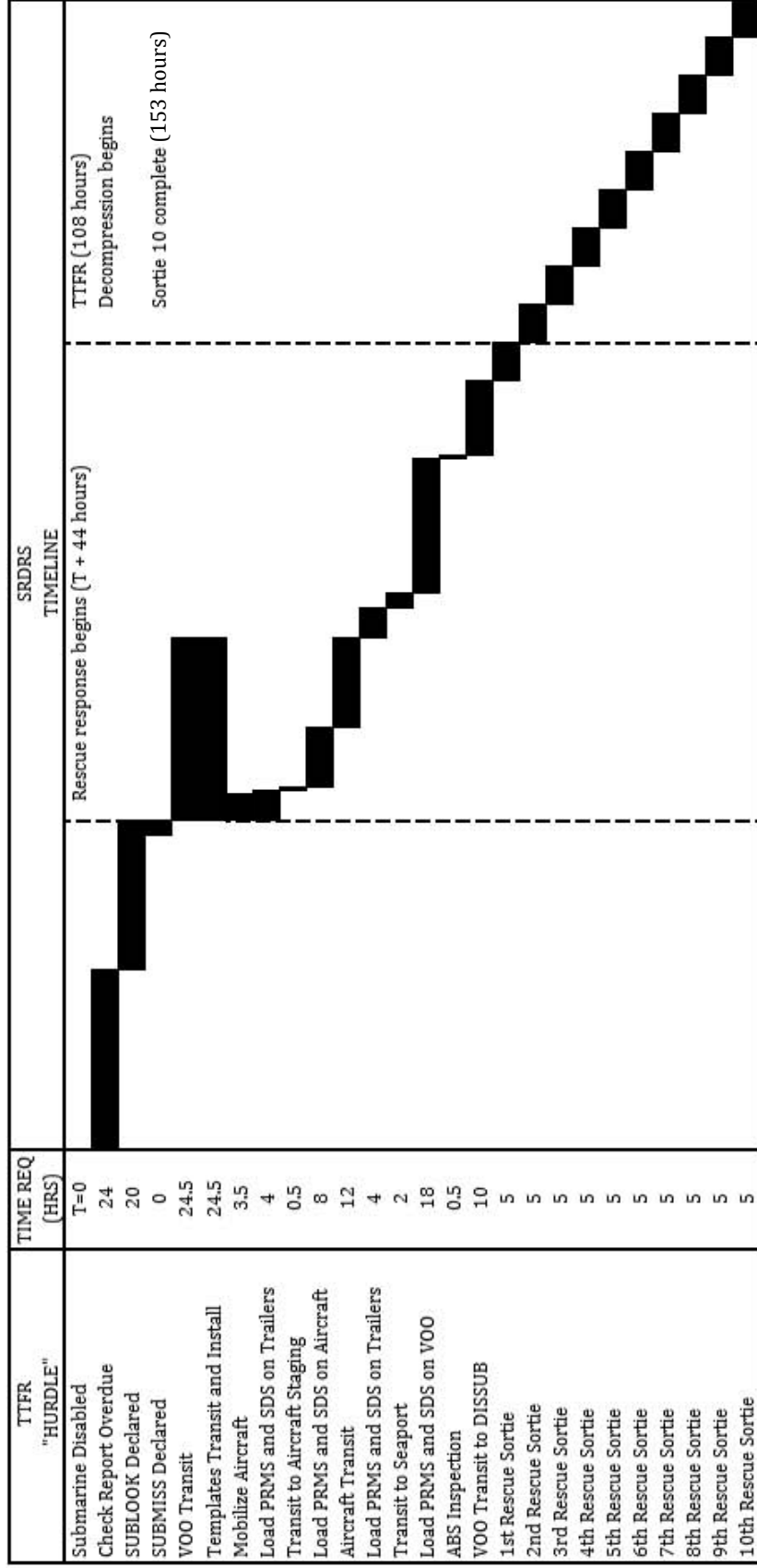


Figure 6. SRDRS response timeline

- * Assumes aircraft and VOO are immediately available
- * Assumes AUWS does not delay rescue operations
- * Assumes the treatment table of the first sortie is complete prior to sortie five
- * Assumes VOO transit and template transit/install on VOO can be done in parallel, and are complete prior PRMS/SDS arrival at seaport
- * DISSUB is 100NM from nearest seaport and VOO transits at 10kts
- * Assumes 155 men are onboard the DISSUB

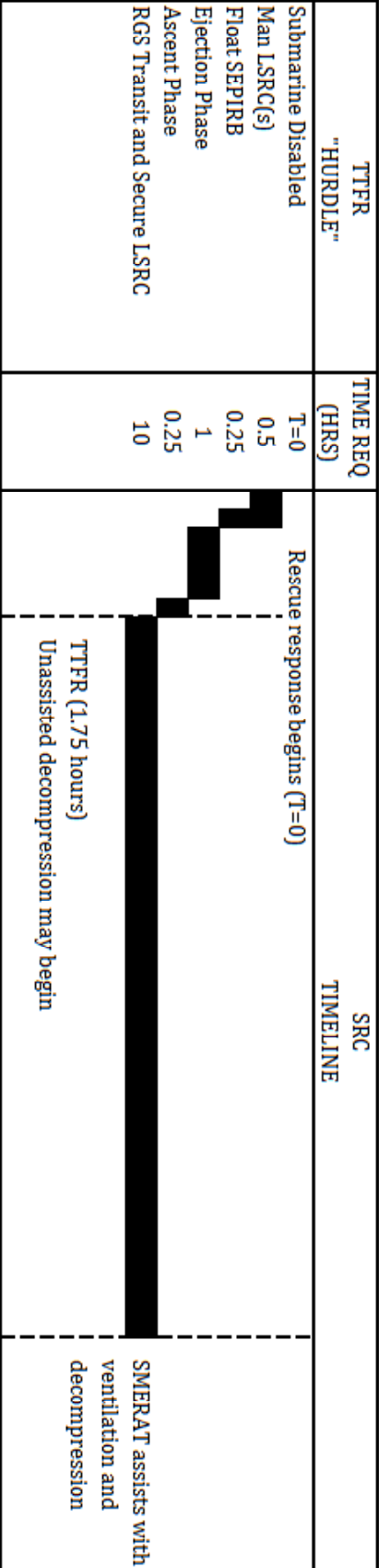


Figure 7. SRC response timeline

* Assumes RGS is immediately available
 * RGS is 100NM from LSRC and transits at 10kts
 * Assumes 140 men are onboard the DISSUB. Although LSRC manning is limited to 70 persons, larger SRCs may be designed to accommodate a crew of 155.
 * Assumes DISSUB is outfitted with two LSRCS

The first and greatest hurdle to overcome is DISSUB notification and localization. Per OPLAN 2137, a submarine's failure to transmit an accountability report will result in the declaration of SUBLOOK. Event SUBLOOK is a check on possible communication failure and is initiated by the Submarine Operational Authority (SUBOPAUTH); no rescue action is taken. By instruction, anywhere between 1 and 72 hours may elapse before SUBLOOK is initiated due to overdue accountability reports. Once declared, attempts will be made to contact the submarine. When deemed appropriate by the SUBOPAUTH, but no later than 20 hours after declaring SUBLOOK, event SUBMISS is declared. Event SUBMISS acknowledges that the submarine is overdue and submarine SAR efforts may begin. Finally, event SUBSUNK is declared when the submarine is known or presumed to be disabled and unable to surface. Due to the group-assisted rescue strategy, rescue efforts are delayed until the submarine is declared overdue. Using this strategy, it is possible that the entire crew will perish before SUBMISS is declared. The best case scenario for DISSUB alert will come from a distressed Ohio class SSBN. Because these submarines are equipped with the AN/BST-1 Submarine Emergency Communications Transmitter (SECT) Buoy, shore based facilities will learn of her sinking within minutes of reaching the bottom. Unfortunately, this automated system does not exist onboard U.S. attack submarines⁷.

Specifics of the SRDRS response immediately following event SUBMISS are listed in Figure 6. The times required to complete each task were taken directly from OPLAN 2137 and the SRDRS Concept of Operations, Revision 6. This "best case" scenario results in a TTFR of 108 hours (4.5 days), with the last survivor beginning decompression at T=153 hours (~6.4 days). Quite generously, this scenario assumes that the SRDRS response time is only 64 hours. Had the "worst case" scenario been considered, SUBMISS would not have been declared until T=92 hours (IAW OPLAN 2137). In addition, SRDRS speakers at the American Society of Naval Engineers (ASNE) Tug & Salvage Technology Symposium in 2009 admitted that meeting the 72 hour response objective has been difficult, and more realistic timelines place the SRDRS response at 96 hours. Using these numbers, the "worst case" SRDRS TTFR is 188 hours (~7.8 days) with the last man *beginning* decompression at 233 hours (~9.7 days).

A similar timeline for a typical SRC escape can be seen in Figure 7. Again, conservative values were used for each task. This timeline places TTFR at 1.75 hours. The incredible gains that can be realized using SRCs results from the group-independent escape strategy. This strategy removes the "hurdles" confronted by group-assisted rescue methods, thereby simplifying the escape and reducing TTFR.

⁷ It is unfortunate that a similar system has not yet been designed for attack submarines. SRDRS engineers and program managers have made great efforts to reduce TTFR; in many cases trimming only minutes or hours off the response time. Had SECT buoys been installed onboard SSNs the SRDRS's TTFR would have been improved by hours or even days. Having just designed the Virginia class SSN, this was a wasted opportunity that could have greatly improved submarine SAR.

1.3.3 U.S. SUBMARINE SAR CAPABILITY GAP

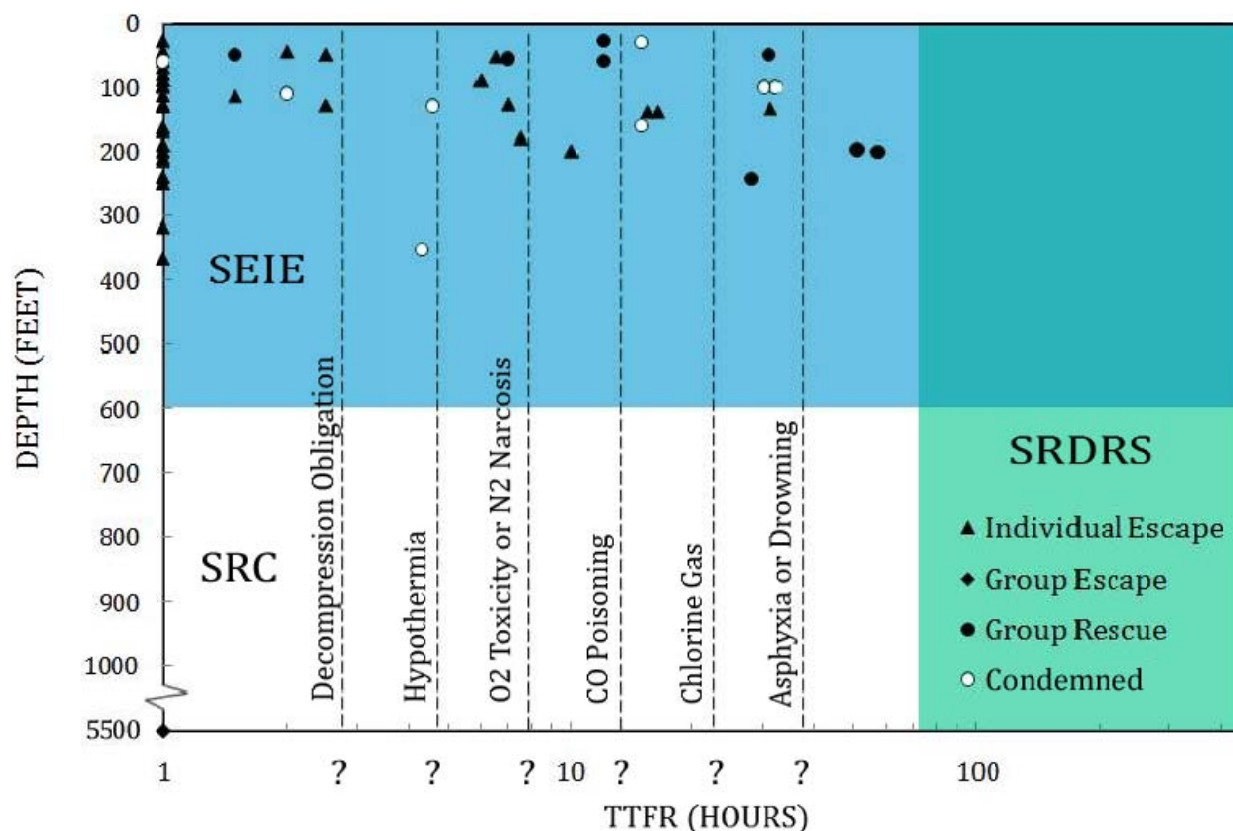


Figure 8. Submarine escape and rescue regimes with historical data⁸

The case for SCRs is further strengthened by examining rescue system capabilities in light of historical data. Figure 8 highlights the weaknesses of the U.S. Navy submarine SAR strategy. This figure was constructed entirely from historical data [7] [8] and references [6] and [9], and is not subjective. Figure 8 exploits the observation that submarine escape/rescue is primarily a function of just two variables; DISSUB depth and TTFR (or Time-to-First-Escape). Depth is plotted along the y – axis, and TTFR is plotted on log₁₀ scale along the x – axis. Every known instance of successful submarine escapes/rescues is plotted with black (filled) markers, while crews left to perish as a result of inadequate response are plotted with white (empty) markers. Colored regions of the figure indicate the Depth/TTFR coverage that is possible with current

⁸ Figure 8 makes the following assumptions: (1) Prompt escapes occurred within one hour of sinking. In most cases this is conservative. Escapes listed as “prompt” in Appendix II describe situations in which the crew attempted escape immediately following the accident. Many of these escapes occurred just minutes after flooding without individual escape gear. (2) Same day rescues occurred within 12 hours of notification. (3) Because the three escapees of U-550 were found dead on the surface, their escape time (TTFR) is not known and is assumed to have occurred within one hour. (4) The crew of *HMS Untamed* and U-526 survived for 15 hours (probably much less). (5) The SRDRS response assumes immediate notification of the submarine accident and location, and a 72 hour deployment time (i.e. “best case scenario”).

U.S. Navy systems; blue for SEIE and green for SRDRS. Because the SRDRS possesses similar capabilities as the Submarine Rescue Chamber, and to prevent the figure from appearing too cluttered, the Submarine Rescue Chamber's capability coverage is not shown. From Figure 8 the following observations are made:

- (1) A capability gap exists for scenarios at depths deeper than 600 feet and with submarine environments that become deadly within three days of the casualty (i.e. white area). This capability gap could be filled by SRCs.
- (2) All individual escapes occurred within 13 hours of the casualty, with more than half occurring within the first hour.
- (3) No submarine atmospheres have been able to sustain life for longer than 57 hours.
- (4) Only on two occasions were free/buoyant ascents deeper than 300 feet successful.

More detailed information for each of the data points is given in Appendix II. Unfortunately, many of the distressed submarines plotted in Figure 8 are not representative of "modern" designs. All but four data points used in this analysis pertain to submarines designed prior to 1950⁹. However, it is all the data that is available, and arguably, the only data that is relevant. Once again, the *KURSK*, being a modern third-generation SSN, is an important data point. No other country in the world designs submarines more survivable than Russia. While it is hard to imagine a wartime scenario more devastating than that suffered by the *KURSK*, this modern submarine could not keep her crew alive long enough to support rescue. Comparing U.S. submarine designs with that of the *KURSK*, having nine watertight compartments and a double pressure hull with 5 feet separation; the outer hull being made of three and a quarter inch thick elastic high-nickel steel and the inner pressure hull being covered with eight inches of rubber, it is difficult to believe that a submarine with a single pressure hull and only two compartments (i.e. Los Angeles class SSN) would fare any better when confronted with the kinds of casualties that put a boat on the bottom.

Additional submarine escape/rescue data is available from the British Admiralty Submarine Escape Committee (BASEC). This committee has compiled information and statistics on every known instance of past submarine escapes/rescues. This research was subsequently published in the Submarine War Damage Report No. 58 by the U.S. Hydrographic Office in 1949. Although the BASEC results are somewhat outdated, they still account for over 90% of all present day submarine escape/rescue scenarios (as of 2009). For convenience, the BASEC results as presented in reference [10] are summarized below:

⁹ Rumors exist of two separate submarine escapes (free/buoyant ascents through the torpedo tubes) occurring onboard Chinese submarines; one in 1959 (hull number 418) and another in 1987. If the rumors are true the total number of submarine escape/rescue scenarios after 1950 is seven.

Section 22-5

The escape problem on submarines can be considered in three phases as follows:

Phase 1: Survival within the submarine after damage up to the time personnel actually exist from the hull

Phase 2: Survival during the ascent to the surface

Phase 3: Survival after reaching the surface until rescued.

Section 22-6

According to British records, of all the personnel who have been carried to the bottom in known cases of sunken submarines, a total of about 500 men are believed to have survived both the initial accident or damage causing the sinking and the subsequent primary flooding. Of these 500 men, a total of 32 were rescued from three submarines of such small size that the boats were lifted bodily by cranes; 33 were saved by rescue chamber; and 46 were taken off a submarine sunk in shallow landlocked waters where raising the bow of the ship was comparatively simple and expeditious. Of the remaining 390 men who survived the initial accident, approximately 250 or 60% perished inside their respective submarines. It is probable that the principal cause of the majority of these deaths was CO₂ poisoning, in some cases due to delaying the escape attempt too long, and in others to the accelerated poisoning effect of CO₂ when present in atmosphere under high pressure. This latter condition occurs when flooding a compartment to equalize internal pressure with sea pressure to permit a skirted-trunk escape. Other known causes were drowning due to further uncontrollable or inadvertent flooding, drowning as a result of deliberately flooding a compartment to equalize internal pressure with sea pressure to permit skirted-trunk escapes with an air-lock type escape trunk. Of the 142 men who are known to have left their submarines on attempted individual escapes, 106 men or 75% reached the surface alive and survived until rescued. This represents only 27% survivors of the possible original 390. Of the 36 who left their ships on attempted escapes but did not survive, some are known to have reached the surface alive but subsequently died by drowning, exhaustion, or by prolonged immersion in cold water. The others died from various causes, among them being air embolism, asphyxiation, ruptured lung tissue due to failure to exhale during ascent, and drowning due to inhalation of water during ascent.

Section 22-7

The statistics for these escapes, although not based on enough instances to be conclusive indicate the following interesting and pertinent points:

- (a) It appears that with present equipment and techniques the chance of survival by using the individual escape method decreases about 10% for every 30-foot increase in depth, until a 250 feet and beyond, the chance of survival is very small.*

- (b) *The phase between the initial accident and the actual escape attempts is by far the most critical. Eighty-eight per cent of all subsequent deaths among personnel who survived the initial accident occurred during this period.*
- (c) *The advantage of rapid flooding over slow flooding when sea water must be admitted to a compartment to equalize internal air pressure with external sea pressure to permit escape through a skirted-trunk, is demonstrated by the fact that there were only 21% survivors after slow flooding whereas 66% survived when flooding was rapid. As would be expected, the figures also show that as the depth increases, a higher percentage of survivors results when the escape compartments are flooded rapidly rather than slowly. This is particularly marked at depths greater than 100 feet.*
- (d) *The hazard of the ascent itself, particularly when made by well trained personnel, is relatively minor for depths up to about 200 feet. Of all the men who left their submarines on individual escape attempts, either with or without an apparatus, probably less than 10% perished during the actual ascent.*
- (e) *Well over half of the survivors made "free" ascents, either entirely without breathing apparatus or with such apparatus but using it as a buoyancy bag only due to mal-operation or defective parts.*

Perhaps the most important take-away from Figure 8 is an understanding of the predicament that confronts submariners immediately after the casualty. The senior survivor must make the decision of whether or not the crew should escape by their own means or by awaiting rescue. However, in most cases an informed decision is not possible in the first few hours following the casualty. To make this decision properly, the senior survivor must understand what the submarine environment (i.e. temperature, atmosphere, etc.) will look like two or three days into the future. That is, he must know the locations of the vertical dotted lines in Figure 8. Each of these lines represents a point of no turning back or death. As was the case of the *PACOCHA*, the senior survivor believed that the crew could hold out for 48 hours; however, he was proven wrong as more information became available. Senior survivors are likely to prolong this decision in hope of more information. It is also human nature to defer decisions so long as the present condition is comfortable. In a good scenario, this may very well be the case as the submarine will still be relatively warm and the air will be of the finest quality in the first hour. Moreover, knowing that the SRDRS system exists, and that it is the most favorable option, will further delay critical reasoning. If the decision to escape via individual means is deferred too long, the crew may incur decompression obligations, thereby *removing* individual escape as an option.

To aid in this decision the Naval Submarine Medical Research Laboratory (NSMRL) has developed a decision making tool commonly referred to as the Senior Survivor Guidance

“Guardbook”¹⁰. This book contains step by step procedures which are aimed at estimating the locations of the dotted lines in Figure 8.

However, due to the dynamic environment of a distressed submarine, atmospheric estimates made within the first few hours may be misleading. At this stage of survival (i.e. Phase 1), ill-informed decisions will have dire consequences (e.g. 100% of the crew dies¹¹ awaiting more information (or rescue) vice 30% dying while attempting escape). Therefore, it is logical to pursue escape immediately following the casualty. Both historical data (above) and experimental results obtained by NSMRL support this rationale. Two experiments simulating “best case” DISSUB scenarios were conducted in 2003 and 2004 on Los Angeles class SSNs. These exercises, known as SURVIVEX 2003 and SURVIVEX 2004, were designed to measure the atmospheric degradation in the forward compartment over a seven day period while some 90+ crewmembers practiced survival techniques. Even in these controlled experiments, where the submarine’s status was known, scientists observed atmospheric conditions that, at the time, were not fully understood. In fact, temperature and humidity within the forward compartment rose so high during SURVIVEX 2004 that the exercise was terminated early; these results were not predicted. The senior survivor’s ability to predict the atmosphere of a deranged submarine two days into the future will be no better. Based on this reasoning, world navies should develop submarine SAR strategies that are centered on individual or group-independent escape methods. Presently, the SEIE suit is the only capability (within the U.S. Navy) that can support a “prompt” escape. Unfortunately, ascents using the SEIE suit are very dangerous in nature, and require a great deal of situational awareness and proficiency. Because this method of escape also requires open-ocean survival (i.e. Phase 3), it should not be relied upon as the submariners’ primary means of escape/rescue¹²

1.3.4 CONCLUSION

In conclusion, the highest percentage of crew survival will occur when the submariners escape “promptly” using dry group-independent escape methods such as the SRC. Group-assisted rescue methods such as the SRDRS are too slow to be used as a primary means of rescue, and should be maintained only for the purpose of contingency.

¹⁰ Currently, the Los Angeles class SSN Guardbook is complete, but the Ohio class SSBN, Seawolf class SSN, and Virginia class SSN Guardbooks are still in development. In addition to the senior survivor guidance Guardbook, chapter 13 of the atmosphere control manual may be used. Because the survivors’ reasoning may be impaired, NSMRL is developing an automated version of the Guardbook called SEAREX which may be loaded onto a PDA.

¹¹ See Appendix II, *HMS Untamed* (P-58), 1943.

¹² See Appendix II, *HMS Truculent* (P-315), 1950.

2 LSRC DESIGN AND ANALYSIS

2.1 DESIGN OVERVIEW

2.1.1 LSRC CONCEPT

A good SRC design will have minimal impact on the ship's war fighting capability, require few auxiliary systems, and be placed in a location that does not disrupt routine operations. The most efficient designs will have multiple functions, allowing the space occupied by the SRC to have alternate uses. Double functionality can be found on most Russian and older Soviet submarine designs where the SRC "doubles" as a submarine access trunk (See Figure 9). Therefore, an optimal design will not result unless the SRC is considered at the earliest stages of submarine design. Ultimately, the size, shape and placement of the SRC must minimize its likelihood of being damaged during a casualty, maximize crew accessibility, and support reliable and robust performance characteristics during the ejection and accent phase.

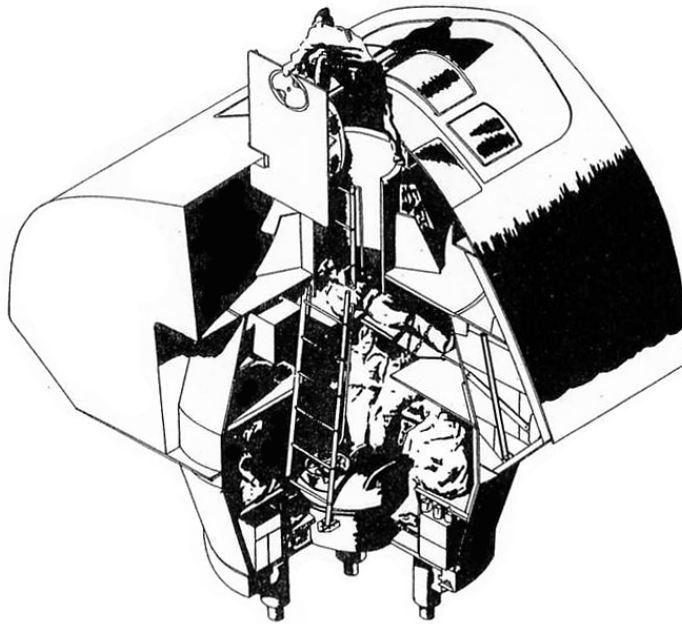


Figure 9. Double functionality. Alfa class SSN SRC [1]

The logical solution to implementing a SRC capability onboard a U.S. submarine is to imitate the design of SRCs currently in service. However, SRCs are almost entirely unique to the Russian Navy, and their designs are difficult to replicate onboard a U.S. submarine. With the exception of the Typhoon class SSBNs, Russian designs place a single SRC¹³ in the submarine's sail. Locating a SRC in the sail of a submarine precludes interference with arrangements inside the pressure hull and minimizes the likelihood of SRC fouling near the ocean floor. Unfortunately, due to fundamental design differences placing a SRC in the sail is not a feasible

¹³ Known to Russian submariners as the VSK (*Vsplyvaushchaya Spasatel'naya Kapsula*)

option for U.S. submarines¹⁴. However, positioning the SRC along the parallel mid-body, similar to those designs employed on the Russian Typhoon class and Indian Type 209/1500 submarines, may be possible (See Figure 10 and Appendix I). Placing a capsule in this location would allow the SRC to double as a Logistics Escape Trunk (LET).

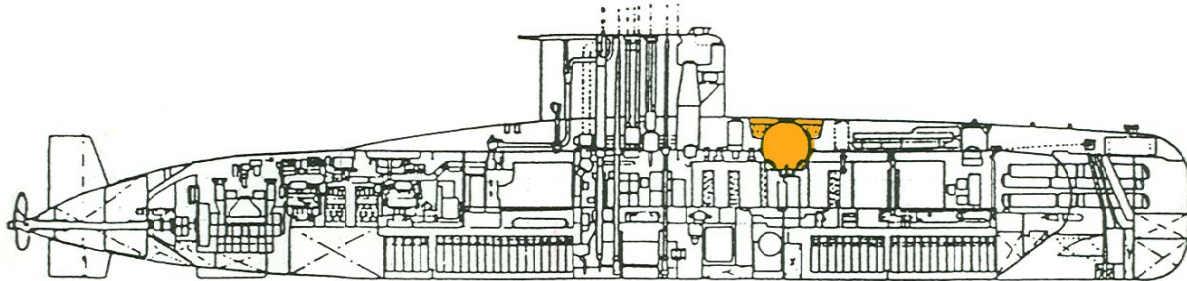


Figure 10. SRC located at the pressure hull. Type 209/1500 (IKL)

A third option is to house the SRC in a multi-mission tube (MMT) similar to the multiple all-up-round canister (MAC) tubes which are currently used onboard the U.S. Ohio Class Guided Missile Submarines (SSGN) but having greater capability. This concept, hereafter referred to as the LSRC¹⁵ concept, is well suited for the single pressure hull designs employed by the U.S. Navy, as the LSRC's center of gravity will fall below the submarine's center of buoyancy. In an attempt to marry the LSRC system to those systems currently used onboard U.S. submarines, it is proposed that the LSRC concept be first implemented onboard Trident submarines¹⁶. Because Trident submarines are already equipped with a missile compensation system (i.e. variable ballast) the additional weight imposed by the LSRC can be easily accommodated. In addition, many of the systems necessary to fully operate the MMT during the LSRC's ejection phase are already present. Hence, the focus of this paper will be to design a SRC within the confines of a Trident II D-5 missile tube. Because the Trident missile system is expected to remain in service until the middle part of the 21st century, the LSRC concept will be applicable to future submarine designs.

Unlike the missile tubes currently in use, the MMT must be designed to withstand pressures in excess of the submarine's collapse depth, and be equipped with watertight hatches affording submariners access to the LSRC. For reasons discussed in chapter 1, it is recommended that the MMT(s) be located between compartments at the bulkhead(s). This arrangement will ensure that the LSRC(s) is accessible in any casualty scenario. A second option, although less efficient, is to

¹⁴ In order to place a structure as large as a SRC in the submarine's sail, significant ballast must be placed at the keel. These weight additions are sufferable only if the submarine has enough reserve buoyancy to compensate for the additional weight. Because Russian submarines are designed with double pressure hulls, they typically possess sufficient reserve buoyancy to accommodate heavier payloads.

¹⁵ LaPenna Surfacing Rescue Container (LSRC). SRCs designed for SLBM tubes or tubes of similar size.

¹⁶ In 2002, the United States Navy announced plans to extend the life of Trident II (D-5) missiles to the year 2040 (commonly referred to as the D-5 Life Extension (D5LE) Program). Similarly, on December 4, 2006, the British Prime Minister (Tony Blair) outlined plans in Parliament to build a new generation of submarines which would carry existing Trident missiles; the last of which would leave service around 2050 [43] [44].

place one or more MMTs in a central compartment with an access tunnel connecting each compartment. This narrow crawl space would remain closed during normal operations, and would be accessed only in the case of emergency. Again, the tunnel and MMTs are placed on the centerline of the ship to enhance survivability. A schematic of each arrangement can be seen in Figure 11 below where the MMTs and LSRC access tunnel are highlighted in orange.

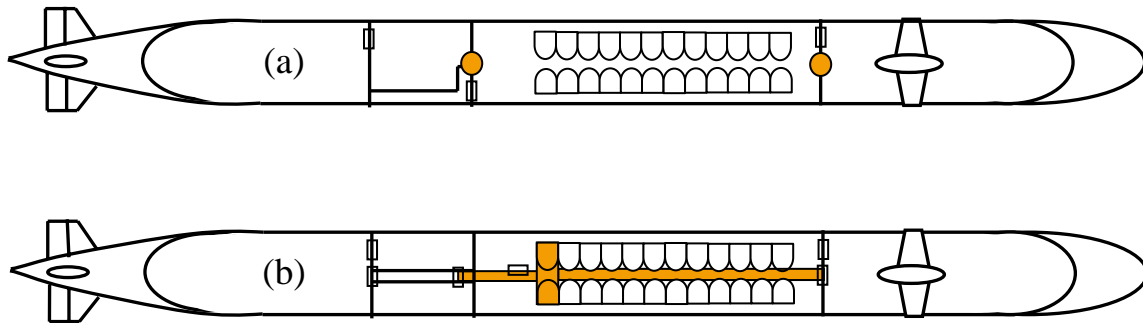


Figure 11. LSRC accessibility arrangements. (a) MMTs at bulkheads, (b) MMTs with access tunnel

If this concept is to be fully exploited, the MMT should also be designed to accommodate a wide range of other payloads, including D-5 nuclear ballistic missiles (if desired). This versatility offers the added benefit of *modularity* to the LSRC concept; a characteristic unique among SRCs. While the LSRC is expected to be a permanent payload, modularity will give authorities the option to remove the LSRC should the operational environment change or if special missions take precedence. Although specifically designed to accommodate the LSRC, it is envisioned that the MMT could also be used to deploy unmanned underwater vehicles (UUV), unmanned aerial vehicles (UAV), special operations forces (SOF) equipment or future weapon systems.

The general characteristics of the LSRC will be similar to that of the Trident II D-5 missile, having a length of 44 feet (13.41 meters) and a diameter of 83 inches (2.11 meters). Because the LSRC must be positively buoyant when manned, its weight in the full load condition will be lighter than a submarine launched ballistic missile (SLBM) (Trident II D-5: 130,000 lbm (58,500 kg)). For this reason, should the MMT be designed to accommodate a SLBM, the LSRC is ensured to be within the missile compensation system limits.

2.1.2 DESIGN PROCESS

Due to the geometry of the LSRC, it is expected that the capsule will be \overline{KG} limited. To ensure that the LSRC remains vertical during the accent phase (and is stable upon reaching the surface), it is desirable to design the capsule with a relatively large \overline{BG} . This will provide inherent stability while the capsule is submerged and will produce sufficient righting moments at the surface. Therefore, it will be important to keep the capsule as light as possible such that sufficient fixed ballast may be placed at the keel, thereby increasing \overline{BG} . Because the LSRC's structure is expected to contribute the largest percentage of weight to the full load condition, the

design process will begin with optimizing the LSRC's pressure hull based on weight (i.e. as opposed to cost). The non-dominated solutions resulting from this analysis will then serve as a starting point for the rest of the design. Because the number of sailors onboard the LSRC at the time of use unknown, a good understanding of the weight distribution will be critical to developing a safe and robust design. For this reason, computer aided design tools should be utilized to accurately calculate the weights of each component and their centers of gravity. The software used in this analysis is SolidWorks¹⁷. After the systems, payloads and furnishings are accurately modeled in the computer, fixed ballast can be added and the structure's overall mass properties can be determined. The results obtained from SolidWorks can then be used in the intact stability and seakeeping analysis to determine the LSRC's performance in a regular seaway at various sea states. At this point, the fixed ballast can be adjusted and changes can be made to the overall design to improve stability characteristics.

The technical analyses covered in this paper focus on the LSRC's structural integrity and surface stability. No consideration was given to the capsule's ejection and ascent phase, and thus remains an open area for future research. Only one pass in the design spiral was made.

2.2 SYSTEMS AND PAYLOADS

2.2.1 MMT operation and ejection control

Above all, a SRC must be reliable. For this reason the systems designed to operate the MMT muzzle door and jettison the capsule should rely upon the most basic scientific principles and physical laws. To ensure proper operation in the most degraded conditions, many systems onboard submarines already employ this design strategy (e.g. emergency main ballast tank blow system, emergency flood control system, and numerous reactor control systems). It is envisioned that the systems used to flood the MMT, rotate the locking ring and open the muzzle door be identical to those already in place for the missile tubes. These systems would need to be modified so that control valves could be operated remotely from within the LSRC, and should be certified as shock grade A items. In addition, dedicated air and hydraulic accumulators should be used to ensure MMT operation when all other ship systems are down, and remotely operated solenoid valves should be powered from the LSRC battery. Remote operation of these systems from within the escape capsule will require a break-away connection between the LSRC and the MMT¹⁸.

The ejection system would provide two functions. First, it must hold the LSRC in place while the MMT muzzle door is being operated, and secondly, it must be able to eject the capsule from the tube over a large range of angles (i.e. heel and trim) and adverse bottom currents. It is recommended that the LSRC ejection system utilize an inflatable boot or bag that would extend the length of the MMT. This method would eject the capsule based on the principle of positive displacement (i.e. vice positive pressure - such as that produced by a gas generator) and contains

¹⁷ SolidWorks Education Edition, Version 2006 SP4.1

¹⁸ By design and procedure, the crew should have the ability to float a Submarine Emergency Position Indicating Radio Beacon (SEPIRB) prior to flooding the MMT. In the event that the ejection is unsuccessful, the crew will be trapped inside the LSRC until help arrives.

no moving parts. The bag could be inflated by compressed air or be filled with seawater supplied by an air powered pump. A schematic of the ejection system can be seen in Figure 12.

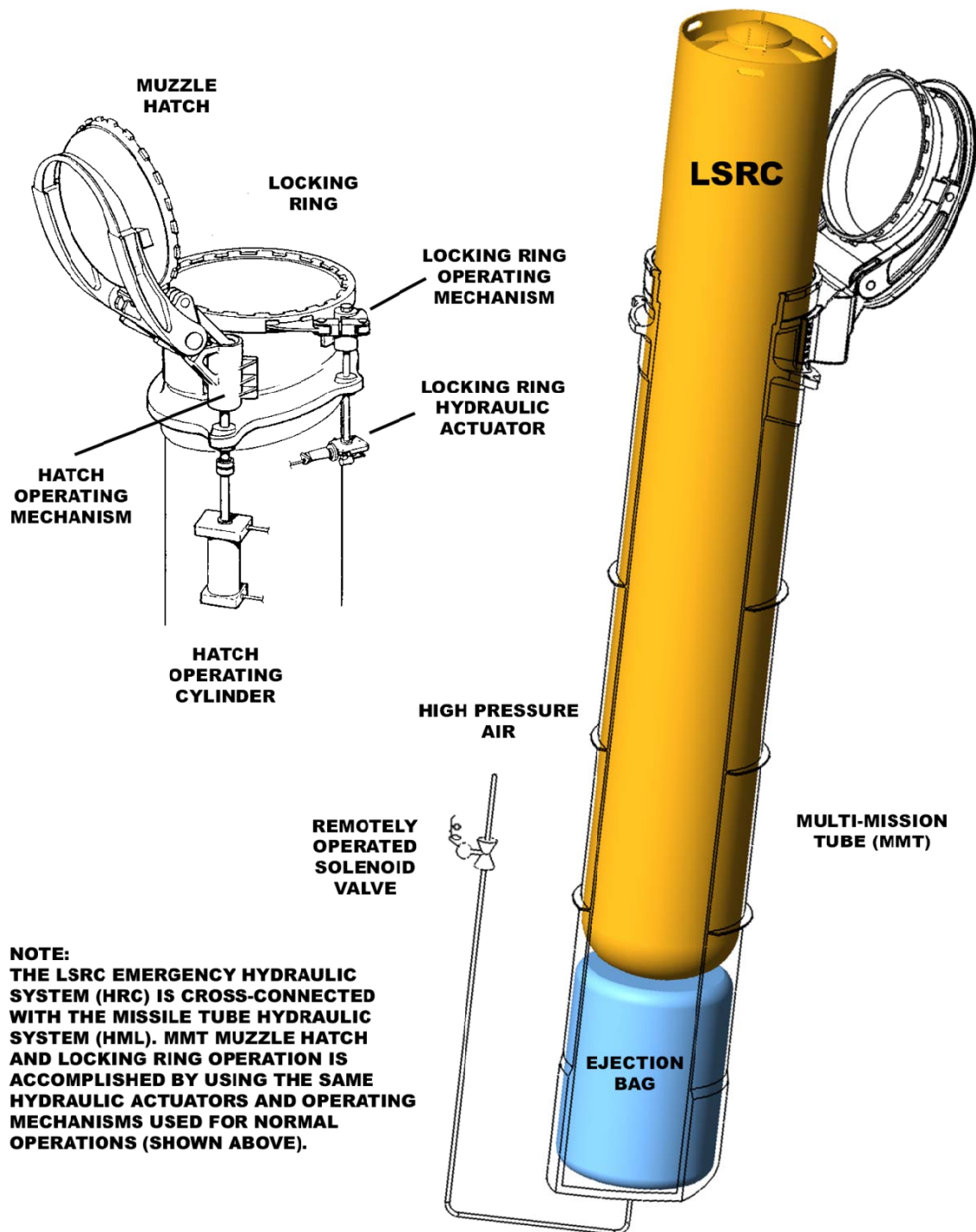


Figure 12. MMT remote operation and ejection system (concept)

2.2.2 Communications and Navigation

Upon reaching the surface, the crew will need to contact the appropriate Submarine Operational Authority (SUBOPAETH) as soon as possible. While any communications suite could be placed onboard the LSRC, it is recommended that commercial-off-the-shelf (COTS) equipment be used. Recent growth in the maritime industry has created a large need for reliable offshore communications. As a result, a wide variety of inexpensive satellite communication (SATCOM) options are commercially available. An Iridium system, for example, could be directly installed onboard the LSRC with little to no modification. Iridium SATCOM systems can be configured for secure voice communications, and can even be programmed to transmit GPS data at regular intervals. These systems are light weight, and have very low power and space requirements. Companies like Inmarsat have also been developing broadband services¹⁹ that allow users to make and receive voice calls and send and receive text and other data. It is envisioned that such systems could be coupled with onboard monitoring systems that, in addition to the relaying capsule's GPS location, could transmit a standard report containing important information such as the atmospheric conditions (air quality and temperature) within the LSRC, and a "dive profile" tabulating the duration of time that the crew has been exposed to elevated pressures both inside the stricken submarine and within the LSRC. This type of information can be used to inform the crew of their decompression obligation and will give undersea medical officers (UMO) on land the information they need to treat the crew upon arrival.

Because the LSRC is not under power, onboard navigation will be limited to reporting its location to various shore stations and displaying some form of navigation aid to prevent collision at sea. Again, commercial standards and COTS equipment should be exploited. A recent amendment to the International Convention for the Safety of Life at Sea 1974 (SOLAS) requires that all mobile offshore drilling units, cargo ships over 300 gross tons and passenger ships carrying more than 12 passengers be LRIT (Long Range Identification and Tracking) compliant. Although the LSRC will not be classified as a SOLAS ship, it can take advantage of the tracking systems being developed to meet this requirement. Inmarsat C, for example, complies with the Global Maritime Distress and Safety System (GMDSS) mandated by the SOLAS treaty, and has been chosen as the main onboard LRIT data provider by the International Maritime Organization (IMO). Such a system could be used for reliable data messaging, and will most likely be supported well into the future. The LSRC design presented in this paper is equipped with an IC system allowing for communications between the inner and outer chambers, an external phone connection for direct topside communications once the capsule has been located, UHF SATCOM, VHF (DSC) radio, and GPS systems. Navigation aids include a single submarine ID beacon or strobe, water dyes and signal flares.

2.2.3 Electrical Power and Lighting

For simplicity, a single battery may be used to supply electrical power, and all loads should be designed/chosen to accept direct current. The battery will be expected to supply sufficient power for internal lighting, the submarine ID beacon, communication and navigation, the ventilation fan, the dewatering pump, atmosphere monitoring equipment, and remotely operated

¹⁹ Inmarsat Fleet Broadband

valves within the submarine for MMT operation and ejection control. Should the crew find the need to initiate decompression on their own, the battery should have sufficient longevity to sustain independent operations for the worst case (i.e. longest) treatment table. As an added measure, the LSRC could be equipped with external connections to receive power from the aiding vessel. By design, the LSRC is a hyperbaric system suitable for manned decompression. Thus, all internal components, including the battery, must satisfy the U.S. Navy Diving and Manned Hyperbaric Systems Safety Certification Manual (SS521-AA-MAN-010).

2.2.4 Decompression System

If the atmosphere within submarine is hyperbaric at the time crew shuts the Submarine-LSRC access hatch, decompression will be necessary. The preferred means of decompression will be by assisted means. Thus, the LSRC should be designed to receive and exhaust air supplied from dive systems onboard the Rescue Gear Ship (RGS). This feature will allow qualified members of the Submarine Escape and Rescue Assistance Team (SMERAT) to have full control of the decompression evolution. These connections, in conjunction with an ungagged pressure relief valve, can also be used in a ventilation procedure²⁰ to remove carbon dioxide from the LSRC. In the event that the crew must initiate decompression on their own, valves within the capsule can be operated to equalize pressure with the outside atmosphere. To ensure that this evolution is conducted safely, procedure/warning plates can be installed above each valve and decompression tables/manuals should be onboard. Although not necessary, the LSRC should have both an inner and outer chamber (to be discussed later).

2.2.5 Ventilation

In the perfect scenario the crew will escape without any decompression obligation. Upon reaching the surface, the upper access hatch can be opened and the crew can enjoy fresh air until help arrives. However, adverse weather conditions (or less than expected freeboard²¹) may make it unsafe to ventilate in this fashion. Ventilation can then be accomplished by opening isolation valves on two vent pipes²². Both the suction and exhaust lines should drain into a seawater sump in the event that waves submerge the ventilation intake/exhaust openings. A ventilation fan can then take a suction on the sump (intake) and force fresh air to the occupants at the bottom of the capsule. Exhausted air can then exit the capsule via a similar vent line located in the upper chamber. If the crew knows that the RGS is delayed or if the battery runs low on power, the ventilation fan can be operated by a manual hand-crank on the fan casing. Although not shown in the present design, a simple snorkel device having a check valve may be used to minimize the intake of seawater.

²⁰ U.S. Navy Diving Manual (SS521-AG-PRO-010) chapter 22-5

²¹ This condition may occur if the LSRC is overmanned.

²² Although the design presented in this paper depicts two ventilation lines, this system could be incorporated into a single hull penetration.

2.2.6 Atmosphere Monitoring and Control

When the LSRC is fully manned, more than half the crew may be onboard. Given the size of the LSRC, the survivors will place a significant load on the available oxygen and produce significant levels of carbon dioxide. In addition, any contaminants produced onboard the submarine during the casualty will most likely accompany the men. To ensure that the crew is fully aware of their situation, and to adequately treat them upon reaching the surface, accurate measurements of the LSRC atmosphere should be made. Like the communication and GPS systems, atmospheric monitoring is an excellent candidate for COTS equipment²³. Due to recent activity in the offshore oil industry, saturation diving and other manned hyperbaric systems have created the need for confined space atmosphere monitoring and control. Many such systems are commercially available and should be investigated for placement onboard the LSRC.

To monitor the atmosphere within the LSRC, simple Dräger kits may be used at very little cost. Dräger offers both electronic hand-held monitoring systems as well as small portable kits containing Dräger tubes. Dräger offers over 200 tubes for accurately measuring over 500 different gases. If the atmospheric constituent data is to be sent to shore stations via the communication system, a battery powered digital system should be used as well. Analox Sensor Technology, for example, sells portable gas analyzers that are specifically designed for use onboard saturation diving systems. This company has been in the business of designing gas analyzers for DISSUB applications for years, and their equipment is currently onboard many U.S. and British submarines, as well as the SRDRS, and previously, the Deep Submergence Rescue Vehicle (DSRV). Either a fixed system such as the Analox Sub MKIIF or a portable unit such as the Analox Sub MKIIP and Analox Sub MKIIP-S²⁴ could be used with little to no modification. Geotech, for example, offers a fully compensated (pressure) portable oxygen (O₂) and carbon dioxide (CO₂) gas analyzer that is already approved by the U.S. Navy for submarines and decompression chambers. Additional features of the Geotech analyzer include ambient pressure measurement and automatic data acquisition capability. While these products are not necessarily recommended for use onboard the LSRC, it does exemplify the feasibility of such commercial products. Pictures of Dräger tubes and both the portable and fixed gas analyzer just discussed can be seen in Figure 13.

In addition to atmospheric monitoring equipment, the LSRC should be equipped with atmosphere control systems. Due to restrictions on space and power, and the short durations in which the crew is expected to occupy the capsule, the regenerative systems employed onboard nuclear submarines are not practical. Instead, non-regenerative passive (or low power) devices should be used. Further, the scope of contaminants typically removed from submarine atmospheres need not be duplicated onboard the LSRC. Because contaminants such as hydrogen, carbon monoxide, FREON, AEROSOL and Volatile Organic Compounds (VOCs) will most

²³ Although COTS equipment should be used as much as possible, experience from the ASDS program showed that many of the materials used in COTS components was often difficult to justify in accordance with the U.S. Navy Diving and Manned Hyperbaric Systems Safety Certification Manual. These lessons should be carefully examined and used as a guide in selecting COTS solutions. Other onboard items that may be designated as “toxic and flammable materials” include: signal flares, hull insulation, synthetic seat cushions, electrical components and wiring, and the lubricants used in the ventilation and dewatering equipment.

²⁴ Pending approval from the Naval Experimental Diving Unit (NEDU).

likely be present in small quantities, providing the means for removal of CO₂ alone may be sufficient.



Figure 13. COTS atmosphere monitoring equipment. (a) Dräger tubes, (b) Geotech HB1.2 (c) Analox Sub MkIIF

The removal of CO₂ from submarine atmospheres has largely been dominated by systems utilizing soda lime and lithium hydroxide absorbents. These compounds continue to be the most reliable means of CO₂ removal; although, recent innovations have made them more effective. The simplest method of removing CO₂ from the LSRC is to use the lithium hydroxide curtains currently employed onboard the U.S. submarine fleet. The curtains, manufactured by Battelle, are made from a polypropylene material that freely passes air and prevents the lithium hydroxide crystals from becoming airborne. They are inexpensive, lightweight, and small enough to be suspended between the LSRC pressure hull frames. An innovative variation of this product, manufactured by Micropore, encapsulates lithium hydroxide in a flexible polymer matrix which may be placed inside a lithium hydroxide “hopper”, or hung like a curtain. The Micropore curtain, known as ExtendAir™, comes in canisters approximately 7.5 inches tall with a diameter of 4.25 inches, each weighing about ten pounds. Roughly 25 cans per day would be needed to support a crew of 70. Yet another CO₂ removal system which could be used onboard the LSRC is the Carbon Dioxide Self-Powered Absorber (CASPA) developed by Molecular Products Ltd. The CASPA is a self-contained battery powered Soda Lime Carbon Dioxide Absorption Unit (SLCDAU). A variation of this product, also developed by Molecular Products Ltd., is the Portable Atmosphere Control Unit (PACU). This system couples the CASPA with a Self Contained Oxygen Generator (SCOG) providing a safe breathable atmosphere for up to 24 hours (for four people). Although the PACU is equipped with an emergency battery, it is designed to receive external power and could be wired to the LSRC battery. The systems described above can be seen in Figure 14.



Figure 14. CO₂ removal systems. (a) Battelle curtain, (b) Micropore curtain, (c) CASPA

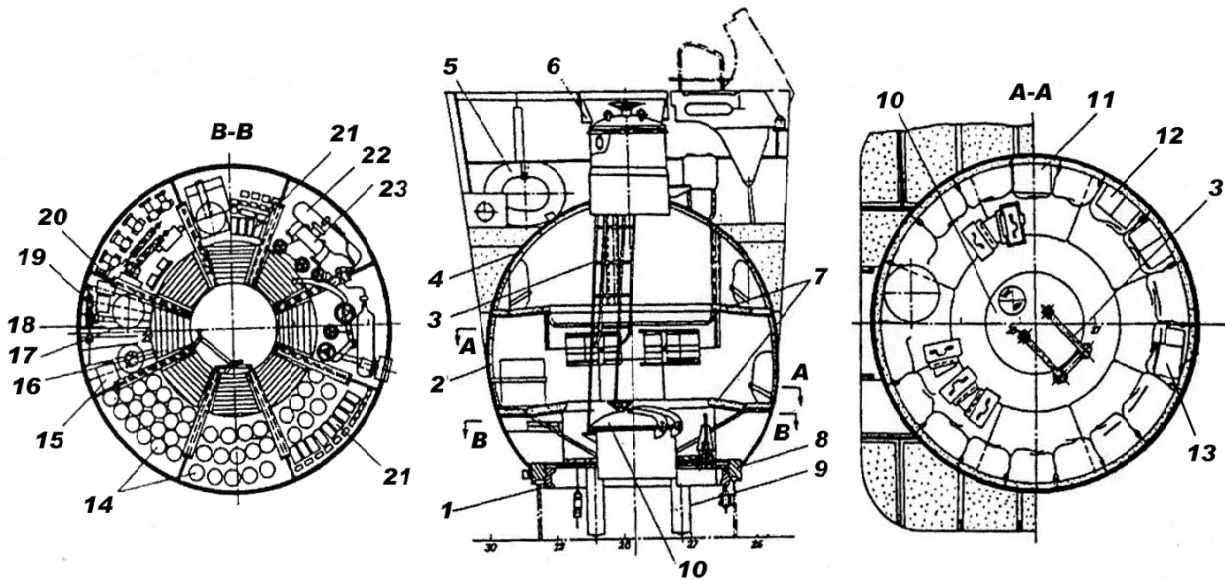
Due to human respiration, oxygen within the LSRC will be depleted over time. While waiting for the RGS it may be necessary to add oxygen to the breathable atmosphere. Oxygen generation in submarines is predominantly accomplished via the following three methods: electrolysis of water, combustion of chlorate oxygen candles, and the vaporization of liquid oxygen (LOX). For reasons of power and safety, the latter two methods should be considered for use onboard the LSRC. Because the oxygen density of LOX is similar to that of chlorate oxygen candles, neither has an advantage in terms of stowage [11]; however, a case could be made for LOX given its simplicity. Because oxygen is toxic to humans at high partial pressures, it must be added to the atmosphere in a controlled manner and monitored continuously. Light-weight Tygon[®] tubing could be affixed to the LOX tanks to ensure that oxygen is distributed evenly throughout the capsule.

2.2.7 Dewatering System

If operated properly, the LSRC should provide a warm and dry environment for the crew. However, it is expected that some seawater will enter the capsule when the ventilation system is being operated, and when the upper access hatch is open. For this reason the crew must have the ability to dewater the capsule. If the capsule were to take on water without a dewatering system, it is possible that the entire crew could be lost. This is particularly true for designs like the LSRC where the Tons Per inch Immersion (TPI) is relatively small. This system would be comprised of a single drain line receiving water from the ventilation sumps and the outer chamber's deck, and draining to a covered bilge at the bottom of the capsule. An electrically driven pump can then be used to discharge the seawater overboard. Like the ventilation fan, the dewatering pump should also be designed for manual operation. Because dewatering will only be necessary when at the surface, a low-power, low-discharge head pump may be used. Such pumps are widely available in the commercial (and recreational) boating industry, and may be suitable options for COTS procurement.

2.2.8 Crew Supplies

Although the crew will only spend a few days in the LSRC (worst case scenario), basic needs should be met. Crew supplies should include, at a minimum, sufficient drinking water to sustain the crew for the duration of the recovery (including decompression), wool blankets, first aid kits, and simple food rations such as chocolate bars and MREs. Other supplies traditionally put onboard SRCs include life rafts and fishing gear²⁵. For purposes of comparison, the cross-section of an Alfa class SSN SRC can be seen in Figure 15. This simple arrangement diagram highlights many of the crew supplies typically stocked onboard Russian SRCs.



1 – Rotating Ring; 2 – Thermal Insulation; 3 – Ladder; 4 – Pressure Hull; 5 – Life Buoy; 6 – Top Cover; 7 – Seats; 8 – Bearing Ring; 9 – Hydraulic Pusher; 10 – Bottom Cover; 11 – Radio; 12 – Warm Clothing; 13 – Gas Analyzer; 14 – Water Containers; 15 – Fishing Gear Box; 19 – Signal Cartridges; 20 – Signal Lamp; 21 – Emergency Food Supply; 22 – High Pressure Air Tank; 23 – Hand Pump.

Figure 15. Alfa class SRC arrangement and crew supplies [1]

²⁵ Given the rapid response of modern navies and the fact that the LSRC itself will serve as a lifeboat while on the surface these supplies need not be included.

2.2.9 Payloads and Adjustments

The LSRC is designed to support a crew of 70 men for three days; however, modifications to the manning and payloads could be made to extend the duration. In this analysis, each man was assumed to weigh 185 pounds with a torso no longer than 42 inches. To sustain the crew for three days, calculations were made to ensure the LSRC contained sufficient CO₂ absorbents, oxygen, drinking water and food. The following assumptions were made:

- (1) Each man will drink 85 ounces (2.5 liters) of water per day. Thus, 139 gallons (525 liters) is required to sustain the crew. In this analysis, 210 canteens were distributed evenly throughout the capsule; one canteen per man for each of the three days.
- (2) Each man will consume approximately 30 ounces (0.84 kilograms) of O₂ per day. This consumption rate assumes that the crew is at rest and breathing normally. Thus, 389 pounds (176 kilograms) of LOX is required.
- (3) The required weight for CO₂ removal was calculated based on data provided from Micropore Inc. when using ExtendAir CO₂ absorbents. A total of 74 canisters of Micropore curtains weighing 10.2 pounds (4.6 kilograms) per can are necessary to sustain the crew for three days. Thus, 750 (340.2 kilograms) pounds of CO₂ absorbents are required.
- (4) Prepackaged “group” meals similar to the U.S. Army’s MREs were estimated at 40 pounds (18.1 kilograms) per day. Thus, a total of 120 pounds (54.4 kilograms) is required to sustain the crew for the LSRC’s duration.

Finally, 300 pounds (136 kilograms) was allotted for ten wool blankets and six first aid kits. Structural and individual system weights were based on commercial products and actual component weight as calculated by computer aided design tools. At the concept design stage, a weight margin of 10% is considered reasonable and was used in this analysis. With the exception of ballast and manning, this margin was applied to all systems and payloads. A detailed summary of all weights can be found on the following page.

<u>SWBS</u>	<u>Component</u>	<u>Weight (lbm)</u>
<u>Hull Structure</u>		<u>66,293</u>
100	Fixed Ballast**	18,388
110	Plating and Stiffeners	43,459
120	Bulkheads and Hatches	4,446
<u>Electric Plant</u>		<u>904</u>
310	Battery**	800
320	Power Cables and Panels	40
330	Lighting Distribution and Fixtures	64
<u>Command and Surveillance</u>		<u>237</u>
410	Satellite Communications	56
420	GPS and Navigation lights	68
430	Internal Communications	50
440	Radio System	63
<u>Auxiliary Systems</u>		<u>2,301</u>
510	Ventilation System	470
	Atmosphere Monitoring	51
	CO ₂ Scrubbers	750
	Oxygen Supply (LOX)**	450
520	Drainage and Dewatering System	505
590	Decompression System	75
<u>Outfit and Furnishings</u>		<u>2,588</u>
630	Hull Insulation**	1,216
640	Seat Structure and Ladder	1,172
	Wool Blankets	200
<u>Armament</u>		<u>66</u>
720	MMT and Ejection System Control	36
760	Signal Flares	30
Light Ship (100-700)		72,389
M00	Margins (10%)*	5,538
Light Ship with Margins		77,927
F00	Full Loads	<u>14,329</u>
F10	Crew (70 persons)	12,950
F30	Medical Kits and MREs	220
F50	Potable water	1,159
Full Load Condition		92,256

* M00 includes a 10% margin applied to F30 and F50 to account for mounting fixtures
(Note: margin not applied to fixed ballast)

** Location and/or weight was modified to improve BG (See section 2.4)

2.3 ARRANGEMENTS

2.3.1 LSRC Structure, Bulkheads and Hatches

In an effort to maximize internal volume, the cylindrical section of LSRC was made as long as possible, and the pressure hull was designed with internal stiffeners and torispherical end-caps. While the LSRC could be designed for stability in the horizontal direction, it was assumed that the dynamic stability in the vertical position would be the most favorable during the ascent phase and while floating at the surface. For this reason, the LSRC was arranged vertically with fixed ballast at the bottom and an exit hatch at the upper end-cap (See Figures 16 and 17).

Although the capsule could be arranged with a single compartment, it was decided to add a watertight bulkhead at the upper end of the LSRC. This bulkhead serves three functions; First and most importantly, the bulkhead provides a watertight barrier between the ocean and the crew seating (i.e. the largest compartment). As previously discussed, seawater must not be allowed to enter the capsule in large quantities unchecked. By procedure, the inner chamber hatch can be closed whenever the upper access hatch is open, thereby reducing the risk of taking on water. Secondly, if the bulkhead is made strong enough to withstand high differential pressures, the LSRC may be used as a double-lock decompression chamber. This arrangement allows for multiple decompression scenarios. Depending on the treatment table, the entire crew could be decompressed all at once within the LSRC; or, the most severely injured crewmen could be moved to the outer chamber and be extracted for subsequent surface decompression. This feature would also allow UMOs to enter the capsule to treat crewmembers experiencing abnormal symptoms. Finally, the presence of a bulkhead reduces the effective length of the pressure hull allowing for smaller scantlings within the inner chamber.

To ensure access in the event that the intact compartment is partially flooded, the submarine access hatch was placed as high as possible along the side of the escape capsule (See Figure 18). In a similar fashion, all MMT cross-connects and control valves should be located high in the submarine. This arrangement will allow survivors to enter and operate the LSRC even though the MMT is partially submerged in water²⁶.

2.3.2 OUTER “COMMAND” CHAMBER

The LSRC design places nearly all control functions in the outer chamber. This arrangement will give the senior survivor complete control of the capsule from a single location (See Figure 19). Although the “command chamber” has only one row of seating, it may accommodate up to seven men. Located beneath the seats are signal flares (water dyes, smoke grenades etc.), first aid kits, water, food rations, ventilation sumps and blankets. Located in the outboards between stiffeners are the liquid oxygen tanks, atmosphere monitoring equipment, communications handsets (i.e. IC, SATCOM and radio), the MMT and ejection control panel, the dewatering, ventilation and lighting control panel, ventilation and decompression control valves, depth and pressure gauges, and system operating manuals and/or plates. The only control valves not

²⁶ If the access tunnel arrangement in Figure 11 is used, the submarine access hatch may be located anywhere.

accessible to crewmembers in the command chamber are the drain and dewatering system isolation valves which are located in the inner chamber just below the bulkhead and in the LSRC bilge. For this reason a direct communication line (e.g. sound powered phone) exists between the command chamber and the last row of seating. The inner hatch is equipped with a small window to allow for visual communication between compartments, and both hatches are within reach of the senior survivor. Unlike most decompression chambers, the LSRC inner hatch is outward opening. While this arrangement is not ideal for lock-in/lock-out operations it is preferred in the flooding scenario. Seawater entering the outer chamber through the upper hatch is directed to the bilge via a drain located at the deck.

2.3.3 Inner Chamber

Inside the inner chamber are the crew seating, submarine access hatch, battery, ventilation fan, dewatering pump, and all electronic equipment for communications and navigation. As previously discussed, the submarine access hatch was placed high in the capsule for reasons of accessibility. This arrangement also places the hatch close to the command chamber and in view of the senior survivor. It is expected that the submarine access hatch will be one of the most challenging components of the LSRC design. While an outward opening hatch is desired, MMT configuration may require that the hatch be opened inward. For this reason the LSRC design provides additional space in the second row of seating²⁷ (See Figure 18). In addition, the area just below the bulkhead houses all the electrical equipment (i.e. communications and navigation gear, the battery and ventilation fan). This “Dry Zone” (See Figure 20) is sheltered from water by the bulkhead above and will ensure that the most vital equipment remains dry even if large quantities of water enter the capsule. As an added measure, water splashing from the side can be deflected by a simple shroud extending downward from the inner hatch perimeter.

Crew seating is comprised of ten circular benches located approximately three feet apart, vertically (See Figure 22). Including the command chamber, this arrangement provides seating for 70 men. A single ladder provides access to each level, and railings extending from the overhead are provided for safety. The seating will not be comfortable, and may require that many sailors lean forward in the “fetal” position placing their feet on either side of the crewmember seated below. The author recognizes that this seating arrangement is quite aggressive and may limit the crew’s ability to carry out simple tasks. However, in the event of an actual disaster, operational requirements (i.e. manning restrictions) may be overlooked or deliberately exceeded. For this reason, the maximum manning scenario should serve as the basis for the design (to be discussed more later). Seating in this fashion is actually on par with that of other SRC designs. Figure 23 shows an overhead picture that was taken inside an Indian Navy Type 209/1500 rescue sphere (SRC). This seating arrangement, as well as that of a Russian SRC (Project 949, NATO classification: Oscar) can be seen in Figure 24. When designing the LSRC, an all-standing arrangement was also considered. However, the risks of injury during the ascent phase and surface breaking, as well as delays that may occur during the crew’s treatment and recovery, discouraged this concept.

²⁷ LSRC seating is numbered 1-10, top to bottom.

Like the command chamber, inner chamber payloads are located in the outboards. These items include, atmosphere monitoring equipment, drinking water, MREs, first aid kits, blankets, and CO₂ curtains. In addition to the systems located in the dry zone, the inner chamber also contains a single IC handset and the dewatering pump. With the exception of those crewmembers in the last row of seating, inner chamber occupants will play no role in the LSRC's operation. Detailed schematics of the LSRC including all support systems can be seen in Figure 16.

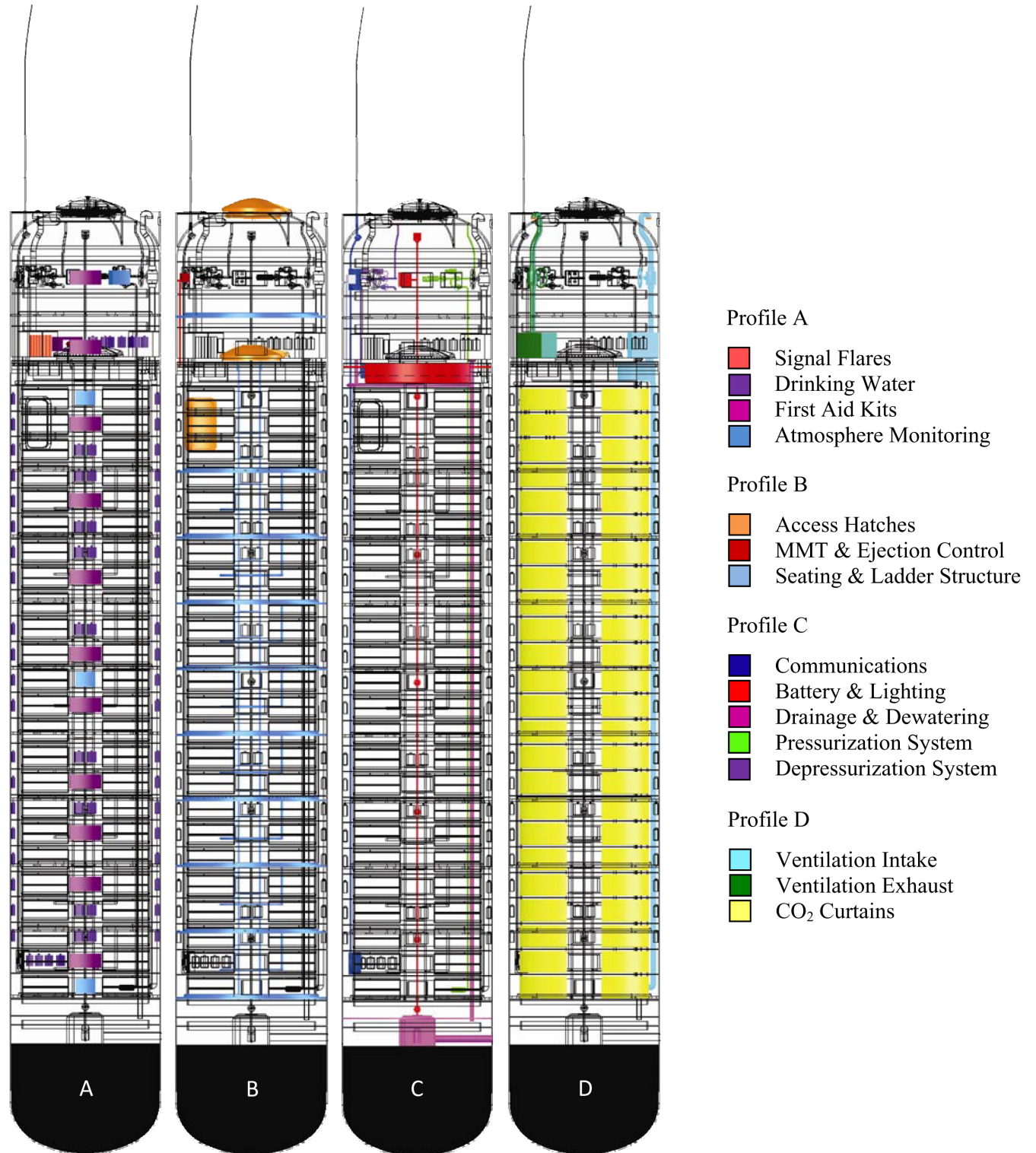


Figure 16. LSRC profile drawings and system arrangements

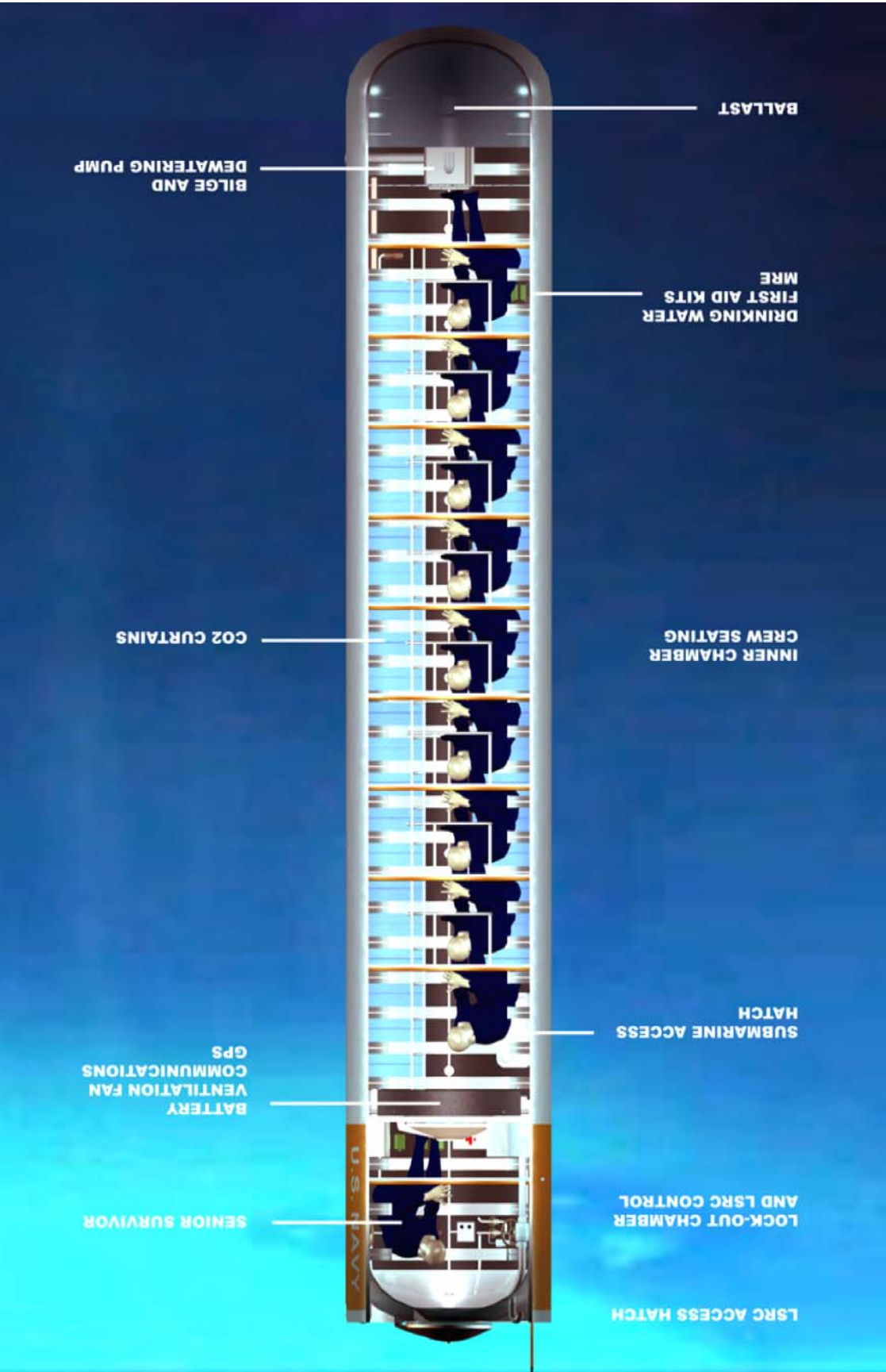


Figure 17. LSRC cross-sectional view



Figure 18. Submarine – LSRC access hatch

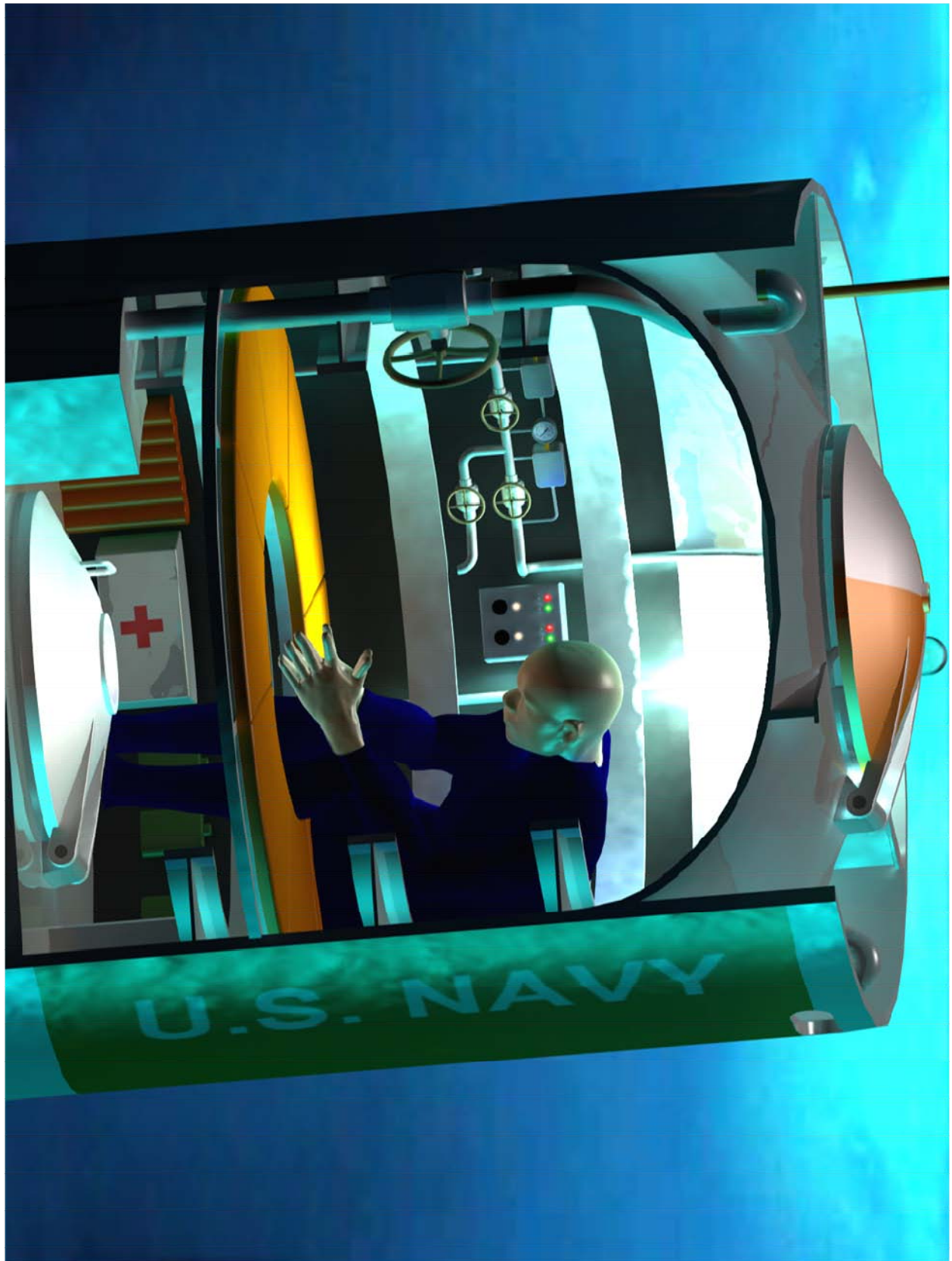


Figure 19. Outer “command” chamber

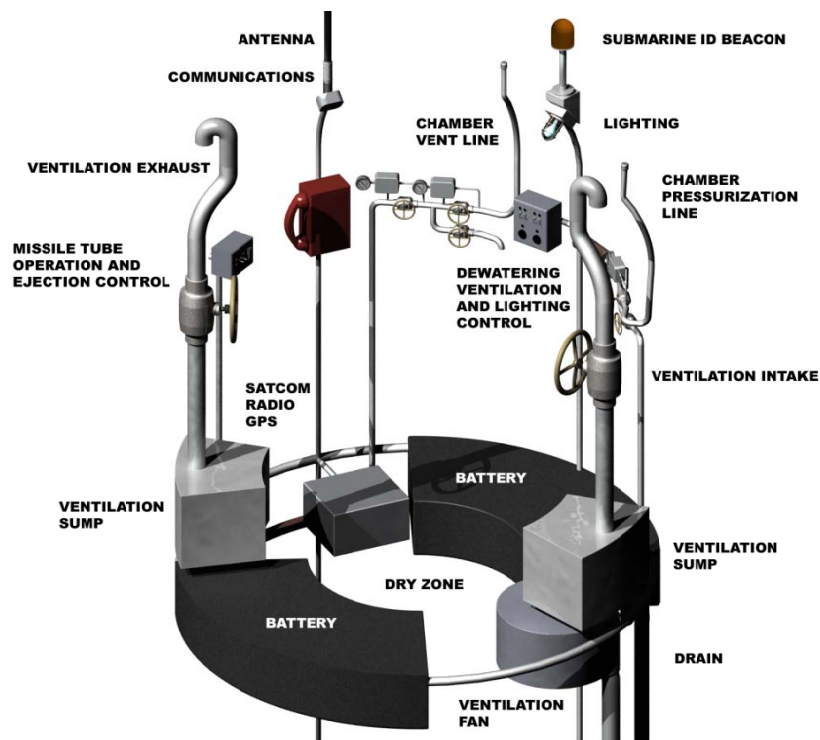


Figure 20. Outer chamber system arrangement (concept only)

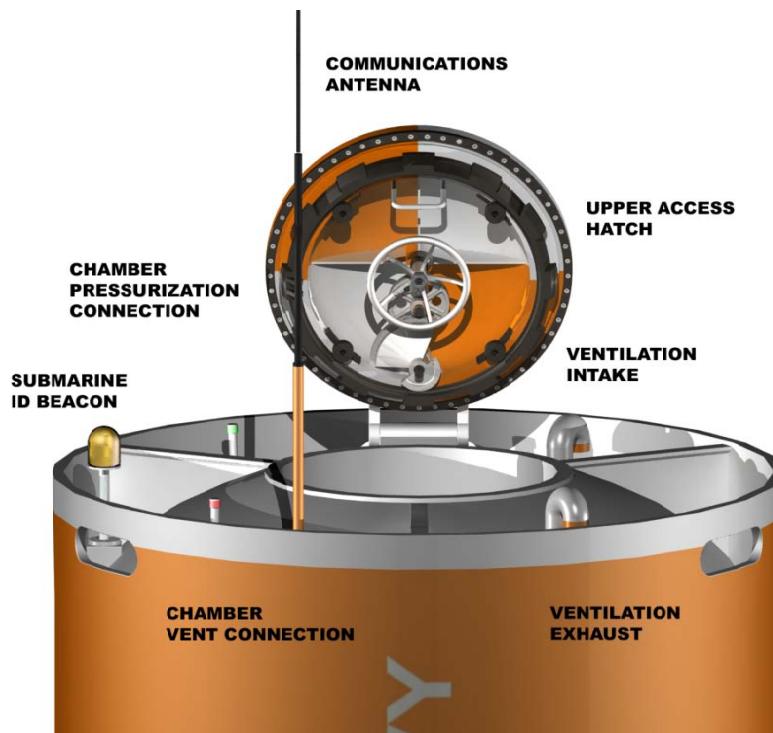


Figure 21. Topside arrangement

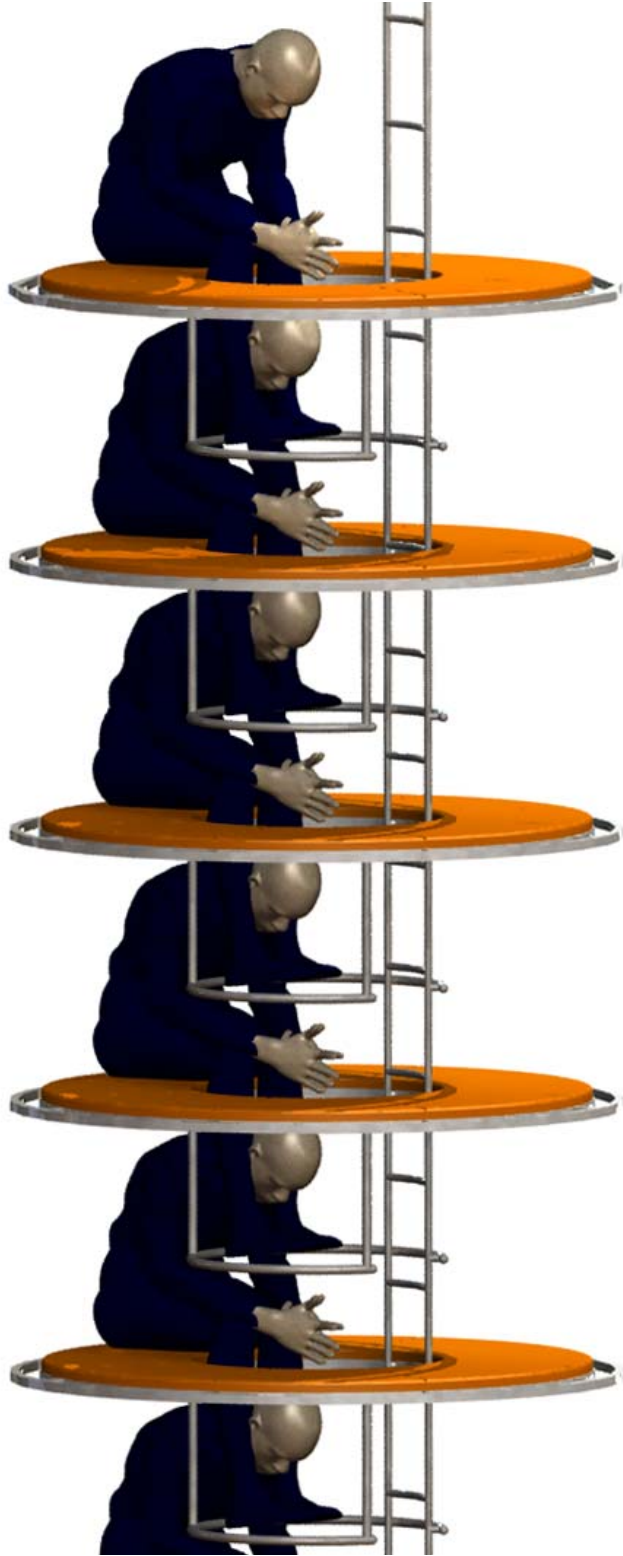


Figure 22. LSRC seating arrangement

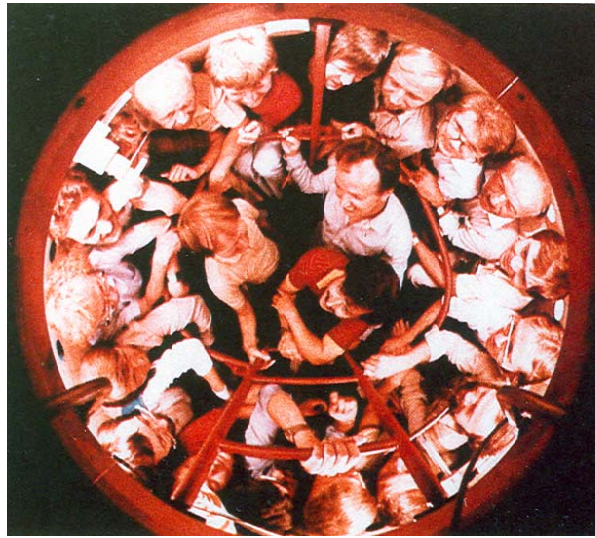


Figure 23. Indian Navy Type 209/1500 rescue sphere (SRC) seating arrangement [4]

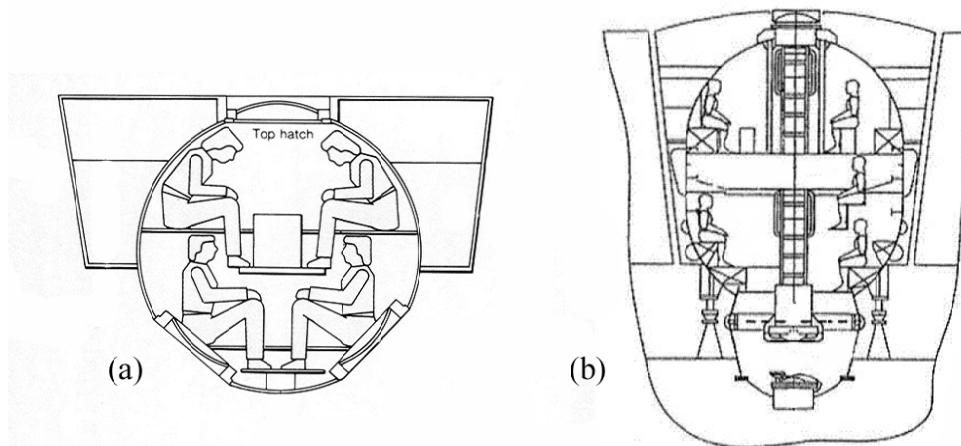


Figure 24. Seating arrangements. (a) Type 209/1500 SRC [4], (b) Project 949 SRC [5]

2.4 STRUCTURAL

2.4.1 PRESSURE HULL ANALYSIS

Before the LSRC interior could be configured, it was necessary to develop an efficient structural design for the pressure hull. The dimensions of the Trident II D-5 missile tube dictate that the LSRC should take the shape of a cylinder, thus maximizing the escape volume. The structural analysis of this shape then becomes the classical analysis of a ring stiffened closed-end cylinder exposed to external hydrostatic pressure. The analysis presented in this paper will examine this problem both numerically and analytically. It will be assumed that the pressure hull has near perfect geometry with no penetrations, and that the external pressure is uniform. A simplified drawing of the pressure hull (without bulkheads) can be seen in Figure 25.

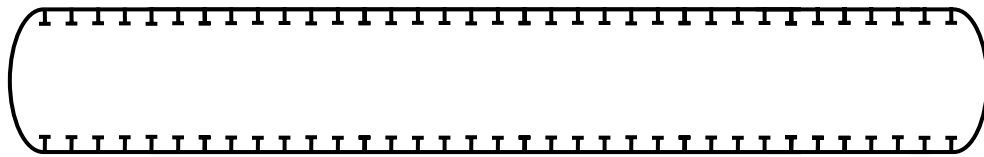


Figure 25. Simplified LSRC structural design

The integrity of the pressure vessel will be assessed based on its resistance to the following failure modes:

- Shell Yield (Axisymmetric Yield between adjacent ring stiffeners)
- Shell Lobar Buckling (Asymmetric Buckling between adjacent ring stiffeners)
- Elastic General Instability
- Frame Yielding
- Frame Instability

After the analytical solutions are presented, a parametric analysis will be done on the pressure hull to determine the most efficient scantlings and arrangement. This analysis will attempt to minimize the weight to buoyancy ratio, while meeting the necessary strength requirements for a given operating depth. Once these scantlings have been determined, a finite element analysis will be done and the final pressure vessel design will be presented.

2.4.2 MODES OF FAILURE

When the distance between bulkheads is about one or two diameters in length, thin walled cylindrical shells without stiffeners have been observed to buckle under hydrostatic pressure. This overall body collapse is commonly referred to as failure by general-instability and is sometimes called “global buckling”. General instability can be prevented by placing ringed stiffeners or “frames” along the length of the cylinder. If the frames are made strong enough to prevent failure by general instability, the unsupported length of shell between the frames now

becomes susceptible to local buckling. This mechanism of failure is commonly referred to as lobar or “asymmetric” buckling. If the cylinder is further strengthened by increasing shell plate thickness, lobar buckling will not occur, and the cylinder will remain intact until compressive hoop stresses within the plating cause the shell to fail by yield. Ideally, a submarine pressure hull would be designed to fail by all three mechanisms simultaneously. However, material and geometry imperfections make it difficult to predict buckling pressures accurately. For this reason, many submarine pressure hulls are designed to fail by yield, and frame scantlings are chosen to prevent premature failure by buckling. Examples of each failure mode can be seen in Figure 26.

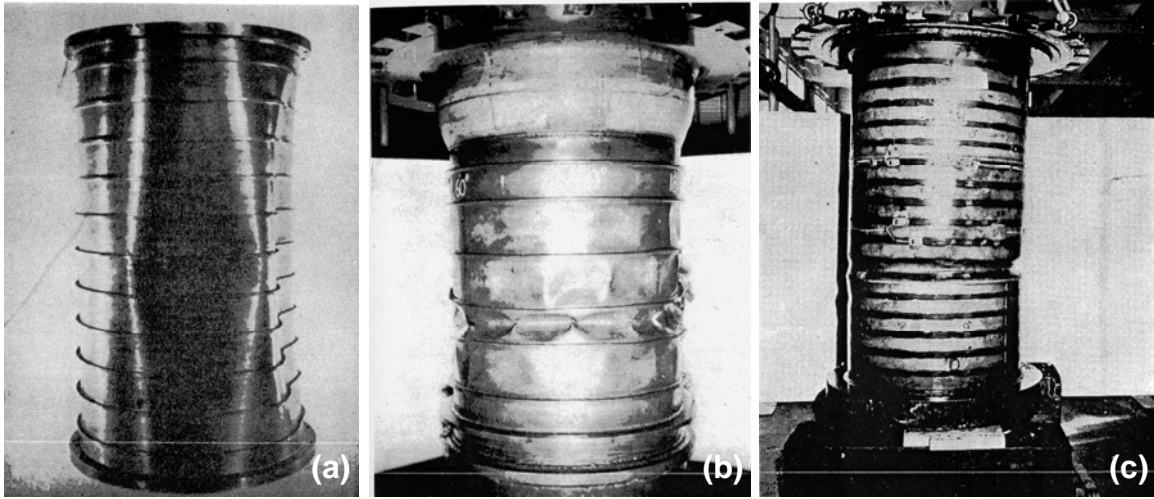


Figure 26. Modes of failure. (a) General instability, (b) Lobar buckling, (c) Shell yield. (PNA, 1967)

2.4.2.1 SHELL YIELD

When the frames are sufficiently close, preventing the premature buckling of the unsupported plate, the plate will fail by yield. This type of failure usually occurs as an “accordion pleat” (See Figure 26c) [12]. The pressure at which shell yielding occurs depends only on the yield strength of the material and the thickness to diameter ratio (t/D_o). Von Sanden and Günther [13] proposed that this yielding condition would develop first on the inside of the shell closest to the frame, and on the outside of the shell at mid-bay. Pulos and Salerno [14] expanded on this concept, and provided the following analytical solution reformulated by Jackson. The circumferential hoop stress ($\sigma_{\theta\theta}$) and the longitudinal (axial) stress (σ_{xx}) at the outer shell mid-bay (MB) region are given by:

$$\sigma_{\theta\theta MB} = \frac{pR_s}{t_s} [1 - a(F_2 + \nu F_4)] \quad (1)$$

and,

$$\sigma_{xx MB} = \frac{pR_s}{t_s} [0.5 + a(F_4)] \quad (2)$$

Where ν is Poisson's Ratio ($\nu = 0.3$ for steel), p is the external pressure given by $p = \rho g D_w S F_{SY}$, ρ is the density of salt water, g is gravity, D_w is the design collapse depth, and $S F_{SY}$ is an applied safety factor to ensure protection against shell yield in the presence of calculation and fabrication error. Accepting the recommendation by Jackson [15], a safety factor of 1.5 is applied to shell yield calculations. The circumferential hoop stress ($\sigma_{\theta\theta}$) and the longitudinal (axial) stress (σ_{xx}) at the inner shell near frame (NF) regions are given by:

$$\sigma_{\theta\theta NF} = \frac{p R_s}{t_s} [1 - a(1 - \nu F_3)] \quad (3)$$

and,

$$\sigma_{xx NF} = \frac{p R_s}{t_s} [0.5 - a(F_3)] \quad (4)$$

where a is the frame deflection parameter,

$$a = \frac{\left(1 - \frac{\nu}{2}\right)}{1 + \left(\frac{t_w t_s}{A_{eff}}\right) + \left(\frac{L_f t_s F_1}{A_{eff}}\right)} \quad (5)$$

A_{eff} is the effective frame area,

$$A_{eff} = \left(\frac{R}{R_f}\right) A_f \quad (6)$$

and F_1 , F_2 , F_3 & F_4 are the transcendental functions that define bending effects on the shell due to local framing,

$$F_1 = \frac{4}{\theta} \left| \frac{\cosh^2(\eta_1 \theta) - \cos^2(\eta_2 \theta)}{\frac{\cosh(\eta_1 \theta) \sinh(\eta_1 \theta)}{\eta_1} + \frac{\cos(\eta_2 \theta) \sin(\eta_2 \theta)}{\eta_2}} \right| \quad (7)$$

$$F_2 = \left| \frac{\frac{\cosh(\eta_1 \theta) \sin(\eta_2 \theta)}{\eta_2} + \frac{\sinh(\eta_1 \theta) \cos(\eta_2 \theta)}{\eta_1}}{\frac{\cosh(\eta_1 \theta) \sinh(\eta_1 \theta)}{\eta_1} + \frac{\cos(\eta_2 \theta) \sin(\eta_2 \theta)}{\eta_2}} \right| \quad (8)$$

$$F_3 = \sqrt{\frac{3}{1 - \nu^2}} \left| \frac{\frac{\cos(\eta_2 \theta) \sin(\eta_2 \theta)}{\eta_2} - \frac{\cosh(\eta_1 \theta) \sinh(\eta_1 \theta)}{\eta_1}}{\frac{\cosh(\eta_1 \theta) \sinh(\eta_1 \theta)}{\eta_1} + \frac{\cos(\eta_2 \theta) \sin(\eta_2 \theta)}{\eta_2}} \right| \quad (9)$$

$$F_4 = \sqrt{\frac{3}{1-\nu^2}} \left| \frac{\cosh(\eta_1\theta) \sin(\eta_2\theta)}{\eta_2} - \frac{\sinh(\eta_1\theta) \cos(\eta_2\theta)}{\eta_1} \right| \left| \frac{\cosh(\eta_1\theta) \sinh(\eta_1\theta)}{\eta_1} + \frac{\cos(\eta_2\theta) \sin(\eta_2\theta)}{\eta_2} \right| \quad (10)$$

θ is the slenderness parameter,

$$\theta = L_f \left[\frac{3(1-\nu^2)}{(R_s t_s)^2} \right]^{1/4} \quad (11)$$

η_1 and η_2 are the non-dimensional parameters,

$$\eta_1 = \frac{1}{2} \sqrt{1-\gamma} \quad \text{and} \quad \eta_2 = \frac{1}{2} \sqrt{1+\gamma} \quad (12)$$

and γ is a measure of the beam-column effect ($\gamma = 0$ implies no such effect),

$$\gamma = \frac{p_c^Y}{2E} \left(\frac{R_s}{t_s} \right)^2 \sqrt{3(1-\nu^2)} \quad (13)$$

Having solved for the circumferential and longitudinal stresses at the locations of interest (i.e. near-frame & mid-bay), an effective stress at each location can be resolved with the following equations:

$$\bar{\sigma}_{shell MB} = (\sigma_{\theta\theta MB}^2 - \sigma_{\theta\theta MB} \sigma_{xx MB} + \sigma_{xx MB}^2)^{1/2} \quad (14)$$

and,

$$\bar{\sigma}_{shell NF} = (\sigma_{\theta\theta NF}^2 - \sigma_{\theta\theta NF} \sigma_{xx NF} + \sigma_{xx NF}^2)^{1/2} \quad (15)$$

The larger of these two stresses can then be compared to the material's yield strength to assess the structure's susceptibility to shell yielding. This is known as the Hencky-Huber-Von Mises yield criterion. Although theory indicates that yielding of the shell at the frame might develop first, experiments show that this is not as critical as yielding of the shell at mid-bay [12]. Alternatively, the critical pressure for yielding (p_c^Y) can then be calculated from the following equation, where σ_Y is the yield strength of the material [14]:

$$p_c^Y = \frac{\sigma_Y \left(\frac{t_s}{R_s} \right)}{\sqrt{\frac{3}{4} + A^2 B - A G}} \quad (16)$$

where,

$$A \equiv \frac{\alpha \left(\frac{1-\nu}{2} \right)}{\alpha + \beta + (1-\beta)F_1} \quad (17)$$

$$B \equiv (F_2)^2 + F_2 F_4 (1 - 2\nu) \sqrt{\frac{0.91}{1 - \nu^2}} + (F_4)^2 (1 - \nu + \nu^2) \left(\frac{0.91}{1 - \nu^2} \right) \quad (18)$$

$$G \equiv \frac{3}{2} \left(F_2 - \nu F_4 \sqrt{\frac{0.91}{1 - \nu^2}} \right) \quad (19)$$

and α and β are the ratio of effective frame area to shell area, and the ratio of faying width to frame spacing, respectively.

$$\alpha = \frac{A_{eff}}{L_f t_s} \quad (20)$$

$$\beta = \frac{t_w}{L_f} \quad (21)$$

A solution to equation (16) can now be found through an iterative method, in which a value for γ is initially assumed (typically zero) and the critical pressure for yielding is calculated²⁸. The resulting pressure is then substituted into equation (13), and p_c^Y is recalculated. Experience shows that convergence is achieved in just a few iterations.

2.4.2.2 SHELL LOBAR BUCKLING

Asymmetric buckling (lobar buckling) can occur when the shell is relatively thin, and the frames are widely spaced. This mode of buckling is easily identifiable due to the periodic waves or “lobes” that are formed circumferentially between frames. By assuming sinusoidal displacements in the axial and circumferential directions, it can be shown that the following equation gives the critical pressure for lobar buckling of non-reinforced cylinders under hydrostatic pressure [16]:

$$p_c^{LB} = \frac{(\bar{m}^2 + n^2)^4 \left(\frac{D}{R^2} \right) + \bar{m}^4 (1 - \nu^2) C}{R (\bar{m}^2 + n^2)^2 \left(n^2 + \frac{\bar{m}^2}{2} \right)} \quad (22)$$

²⁸ These equations differ from those of Sanden and Günther in that they take into account the “beam-column” effect created by end-cap loading (i.e. $\gamma \neq 0$). However, it should be mentioned that the equations by Sanden and Günther could have been used for the LSRC design. Assuming $\gamma = 0$ is considered valid for most submarine structural configurations where the shell plating is designed to yield first and not to buckle [12].

where C and D are the axial (extensional) and bending stiffness parameters, respectively,

$$C \equiv \frac{Et_s}{1 - \nu^2} \quad \text{and} \quad D \equiv \frac{Et_s^3}{12(1 - \nu^2)} \quad (23)$$

E is Young's Modulus, m is the number of half sine waves in the axial direction, n is the number of complete sine waves in the circumferential direction, and \bar{m} is the dimensionless wave number along the axis of the cylinder. Equation (22) is solved for all positive integers of n (e.g. typically $n = 1 \dots 5$). The value of n at which the buckling pressure is lowest will be the mode of failure at which buckling occurs. For cylindrical shells without bias, it has been shown that $m = 1$. \bar{m} is defined as:

$$\bar{m} \equiv \frac{m\pi R}{L} \quad (24)$$

where $L = L_f - t_w$ (clear length enclosed by stiffeners). As it applies to this problem, the inter-frame segments of a ring stiffened cylinder can be modeled as a cylindrical shell. Although equation (22) was derived for a cylindrical shell with simply supported ends (i.e. not clamped), experiments show that it can be used to approximate the critical pressure for lobar buckling of ring stiffened cylinders with reasonable accuracy²⁹. A safety factor of 2.25 is applied to failure by lobar buckling.

2.4.2.3 ELASTIC GENERAL INSTABILITY

General instability is characterized by large “dished-in” defections along the length of the cylinder, wherein both the frame and shell deform together. This mode of failure can occur in either the elastic or inelastic stress regions, and is often the most difficult to predict. Compared to other failure modes, general instability is the most susceptible to initial deformation and defects. Available literature suggests that designing pressure vessels protected against *elastic* general instability is often sufficient (i.e. safe), so long as an appropriate safety factor is used to account for uncertainties in fabrication. Again, accepting the recommendation by Jackson [15], a safety factor of 3.75 is used for general instability calculations. In this report, the solution offered by Bryant in 1954 [12] is used to calculate the critical pressure for elastic general instability. His equation can be found below:

²⁹ For the purposes of design, the simply supported assumption errs on the side of conservatism. Coincidentally, this assumption gives more accurate results in the presence of fabrication imperfections.

$$p_c^{GI} = \frac{Et_s}{R_s} \left[\frac{\bar{m}^4}{\left(n^2 - 1 + \frac{\bar{m}^2}{2}\right)(n^2 + \bar{m}^2)^2} \right] + \frac{EI_{eff}(n^2 - 1)}{L_f R_s^3} \quad (25)$$

where \bar{m} is equation (24) with $L = L_b$ (length between bulkheads), and $R = R_s$. I_{eff} is the moment of inertia of a single frame including an “effective” length (L_{eff}) of shell plating about the neutral axis. Although L_f was originally suggested as the appropriate length for calculating the moment of inertia, many people have suggested more accurate formulations. This report will use that given by Pulos and Salerno [14] which is shown below:

$$L_{eff} = \frac{2\sqrt{R_s t_s}}{\sqrt[4]{3(1 - \nu^2)}} \left(\frac{\cosh(\theta) - \cos(\theta)}{\sinh(\theta) + \sin(\theta)} \right) \quad (26)$$

where, θ is defined by equation (11). Like the solution to equation (22), equation (25) is solved by setting $m = 1$, and calculating the critical pressure over a range of n . The value of n at which the buckling pressure is lowest will be the mode of failure at which buckling occurs.

2.4.2.4 FRAME YIELDING

Like the shell plating, the frames must also be checked for their susceptibility to failure, both by yielding and instability. If a frame should fail by either of these two methods, shell circularity will be compromised and the pressure vessel will most likely fail by general instability. The yielding condition is checked by comparing the total stress (σ_T) on the frame to the materials yield strength, where,

$$\sigma_T^{frame} = \sigma_{hoop}^{frame} + \sigma_{bending}^{frame} \leq \sigma_Y \quad (27)$$

The direct hoop stress experienced by a frame can be found from the expression below, which is derived by applying Newton’s second law to a single ring stiffener.

$$\sigma_{hoop}^{frame} = \frac{qR_f}{(A_f + t_w t_s)} \quad (28)$$

where q is the total radial load acting on a ring frame per inch of circumference. Pulos and Salerno [14] solved for this load (q) which is shown below:

$$q = pt_w \left(1 - \frac{\nu}{2}\right) \left[1 + \left(\frac{\frac{\alpha}{\beta}(1 - \beta)F_1}{\alpha + \beta + (1 - \beta)F_1}\right)\right] \quad (29)$$

where all variables are as previously defined. The direct hoop stress carried by a single frame then becomes,

$$\sigma_{hoop}^{frame} = \frac{pR_f t_w \left(1 - \frac{\nu}{2}\right)}{(A_f + t_w t_s)} \left[1 + \left(\frac{\frac{\alpha}{\beta}(1 - \beta)F_1}{\alpha + \beta + (1 - \beta)F_1}\right)\right] \quad (30)$$

The bending stress was developed by Kendrick in 1953 [17] and is shown below:

$$\sigma_{bending}^{frame} = \left(\frac{p}{p_c^{GI} - p}\right) \left[\frac{Ee \left(n_c^{GI^2} - 1\right) \left(\frac{t_s}{2} + h_w + t_{fl}\right)}{R_s^2}\right] \quad (31)$$

where e is the eccentricity from a true circle, and p_c^{GI} & n_c^{GI} are the critical values for general instability. Historically, out of roundness (e) for submarine hulls has been limited to one-half shell thickness (e.g. typically ½ inch). As the shell diameter decreases, or shell thickness increases, this limit becomes easier to obtain in manufacturing, and e may be reduced.

2.4.2.5 FRAME INSTABILITY

Frame instability under a radial load is analogous to a column under axial compression. When the slenderness ratio is large, the column is more likely to fail by buckling (i.e. instability) vice yield. Likewise, the circular frame will collapse in a two-lobe manner when the cylinder's slenderness ratio is large and it is incapable of maintaining circularity. This instability results from local buckling of either the flange or web. In practice however, it is the web that is most susceptible. In addition, local buckling of the web is greatly exacerbated when eccentricities exist in the frame's circularity (See Figure 27(a)). Buckling of the flange can often be prevented by adhering to simple scantling guidelines such as $F2$ in Table 2. For this analysis, the classical solution offered by Tokugawa [12] will be used to calculate the critical pressure for frame instability:

$$p_c^{FI} = \frac{25EI}{(2R_{NA})^3 L_f} \quad (32)$$

where, I is the moment of inertia of a single frame including a length (L_f) of shell plating, equal to the frame spacing, about the neutral axis. R_{NA} is the radius to the neutral axis of the shell-frame composite.

Another form of frame instability that should be addressed is torsional buckling. This mode of buckling is often referred to as “frame tripping” and can occur without the loss of circularity. Frames become susceptible to this type of failure when shell bending stresses create displacements and rotations about the web’s toe, or when the web buckles in radial compression. Again, the instability is exacerbated in the presence of web eccentricities (e_w) and any initial “tilt” during fabrication (See Figure 27(b)). For interior stiffeners, tests show that an initial tilt of only three degrees can be detrimental [18]. It is fortunate, however, that the frame’s resistance to premature tripping failure can be greatly improved by simply increasing the web thickness or flange breadth (IAW Table 2). This can often be done without accepting large penalties in weight or space.

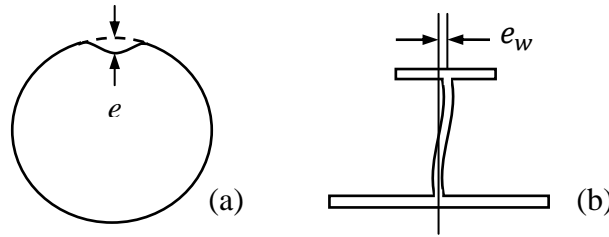


Figure 27. Ring stiffener eccentricities. (a) Out-of-Roundness (OOR), (b) Web eccentricity

The strain energy method has been found to provide an acceptable solution to the frame tripping problem. This method equates the total energy available due to external pressure to the energy required to displace the structure. The total potential energy of the buckled stiffener is then a non-linear function of the total displacements and their derivatives. For this analysis, the strain energy procedure used by SSP74 will be used³⁰.

ECCS [19]	SSP74 [20]
$E1 = \frac{h_w}{t_w} \leq 1.1 \sqrt{E/\sigma_Y}$	$F1 = \frac{h_w}{t_w} \sqrt{\sigma_Y/E} < 1.1$
$E2 = \frac{h_{fl}}{t_{fl}} \leq \sqrt{E/\sigma_Y}$	$F2 = \frac{h_{fl}}{2t_{fl}} \sqrt{\sigma_Y/E} < 0.52$
$E3 = \frac{h_w t_w^3 + t_{fl} h_{fl}^3}{6R_1 [h_w^2 t_w + t_{fl} h_{fl} (2h_w + t_{fl})]} \geq \frac{\sigma_Y}{E}$	$F3 = \frac{A^* (R_1 - R_f) R_1}{I_z} \left(\frac{\sigma_Y}{E} \right) < 2.0$
Where $I_z = h_w t_w^3 + h_{fl}^3 t_w / 12$ and A^* is a moment correction factor (not defined in this paper).	

Table 2. Frame stability guidelines

³⁰ Frame tripping analyses were performed in *Paramarine*TM software (i.e. not FFSOR).

2.4.3 KING FRAMES

For very long pressure hulls (i.e. large L_b), failure by general instability is of greater concern. For this reason, among others, internal bulkheads are often used in submarine design. The use of internal bulkheads effectively reduces L_b , and the scantlings of inter-bulkhead stiffeners can thereby be reduced. Where internal bulkheads are not necessary, or undesired, it is common practice to use king frames (also known as deep-frames) in their place. King frames are thus sized to provide the strength and rigidity of a bulkhead at a much lower weight. In U.S. submarine design, bulkheads were traditionally spaced at intervals of about 1.5 the hull diameter. This spacing was chosen such that the ballast tanks could provide sufficient buoyancy in the event that an entire compartment was flooded. Although positioning the bulkheads in this manner was largely based on survivability rather than structural optimization, it was also in agreement with the expected mode of failure in general instability (i.e. setting $L = 1.5 D_o$ in equation (24) gives $\bar{m} \approx m = 1$). As a result, pressure hull segments longer than about 1.5 the hull diameter are considered “long”, and the use of king frames is generally recommended. In designing the LSRC, the use of king frames was given particular attention. Calculations using the methods described above showed that the LSRC could be safely designed without the use of king frames ($L/D_o \approx 6$). Although outside of traditional guidance, such designs are often favored for submarines with small diameters.

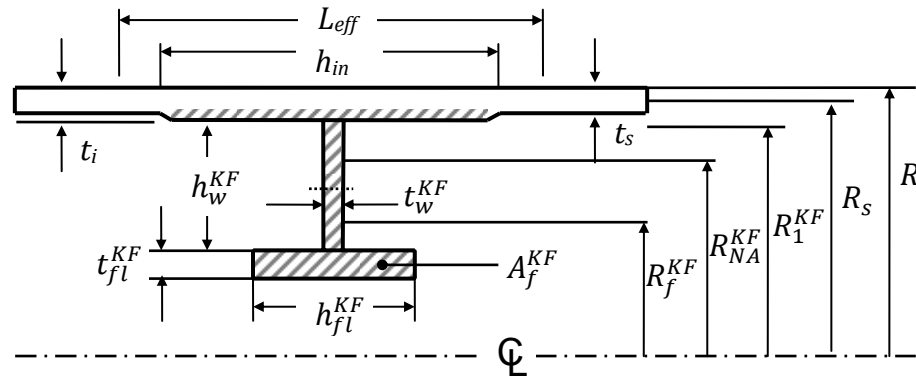


Figure 28. King frame scantling dimensions and definitions

As a first approximation, the area of the king frame should be about three times the area of a small frame. Likewise, the frame’s moment of inertia about its neutral axis should be about ten times that of a small frame. Alternatively, equation (33) offers a more formal method of sizing king frames by approximating the required moment of inertia (I_{req}^{KF}). To use this equation, the critical elastic buckling pressures for general instability must first be calculated for two separate designs. The first, P_c^{GI*} , is calculated using equation (25) with $L = L_{beff}$ (i.e. assumes king frames are present) in equation (24). For $n_c^{GI} \leq 3$, this effective length (L_{beff}) should be between $1.05L_D$ and $1.10L_D$, where L_D is the largest spacing between an adjacent bulkhead and a deep frame or between adjacent deep frames [20]. The second, P_c^{GI} , is calculated using equation (25)

with $L = L_b$ (i.e. assumes no king frames) in equation (24). The calculation of P_c^{GI} is done using the same small frames sized for $L = L_{beff}$.³¹

$$I_{req}^{KF} = I_{eff} + \frac{R_s R_{NA}^2 L_D}{E (n_c^{GI^2} - 1)} (P_c^{GI*} - P_c^{GI}) \quad (33)$$

The strength of the king frames can be found in the same manner as for the normal frames. However, open literature on king frame design often uses frame yield equations slightly different from those previously presented. The method presented below, suggested by Jackson [15], is based on the earlier work of von Sander and Günther. Similar to the small frames, the total stress in the king frame is checked against the yield strength of the frame material (See equation (27)). The direct (hoop) and bending stresses are redefined as follows:

$$\sigma_{hoop}^{KF} = \frac{F p R_f^{KF}}{A_f^{KF} + (t_w^{KF} t_s)} \quad (34)$$

$$\sigma_{bending}^{KF} = \left(\frac{p}{p_{c_{KF}}^{GI} - p} \right) \left[\frac{E e (n_{c_{KF}}^{GI^2} - 1) \left(\frac{t_s}{2} + h_w^{KF} + t_{fl}^{KF} + t_{in} \right)}{(R_{NA}^{KF})^2} \right] \quad (35)$$

$$F = t_w^{KF} \left[\frac{1 + [1 - (\nu/2)] \left(\frac{U}{V} \right)}{1 + U} \right] \quad (36)$$

$$U = \frac{2\sqrt{R t_s^3}}{A_f^{KF} + (t_w^{KF} t_s)} \left[\frac{1}{3(1 - \nu^2)} \right]^{1/4} \quad (37)$$

$$V = \frac{t_i t_w^{KF}}{A_f^{KF} + (t_i t_w^{KF})} \quad (38)$$

³¹ For example: The LSRC main compartment is 36 feet in length. Two king frames evenly spaced 12 feet apart are being considered. Thus, $L_B = 36$ & $L_D = 12$. Using $L_{beff} = 1.075 L_D$, $L_{beff} = 12.9$. The small frames are then sized for a bulkhead spacing of 12.9 feet. P_c^{GI*} is then calculated using the small frame scantlings and $L = 12.9$ in equation (24). P_c^{GI} is calculated using the same scantlings with $L = 36$. The king frame scantlings are then chosen using the results from Equation (33) and the guidelines listed in Table 2.

where $t_i = t_s + t_{in}$, and all other variables are as previously defined with the superscript “KF” denoting king frame parameters. t_{in} is defined as the thickness of the king frame insert³² (See Figure 28).

When king frames are used in a design, it is also necessary to re-evaluate the failure by elastic general instability. The three-term Bryant equation [20], equation (39), must now be used in place of equation (25). The first term of this equation addresses shell failure, while the second and third terms address the failure of the small frames and king frames, respectively. In this equation, I_{eff}^{KF} and I_{eff} are calculated using the same “effective” length of shell plating³³.

$$p_{cKF}^{GI} = \frac{Et_s}{R_s} \left[\frac{\bar{m}^4}{\left(n^2 - 1 + \frac{\bar{m}^2}{2}\right)(n^2 + \bar{m}^2)^2} \right] + \frac{EI_{eff}(n^2 - 1)}{L_f R_s R_{NA}^2} + \frac{EI_{eff}^{KF}(n^2 - 1)}{L_D R_s (R_{NA}^{KF})^2} \quad (39)$$

³² Due to the rigidity of the king frames, it is common practice to place a shaped insert at the base of the web to mitigate additional bending stresses and reduce the deflection at either side.

³³ The effective length of shell plating calculated using equation (26) for the small frame analysis was used to calculate both I_{eff}^{KF} and I_{eff} . Intuitively, one might think that the effective length applied to a king frame should differ significantly from that of the small frames. However, calculating the effective lengths for each using BS5500 and ECCS methods show that these values differ only slightly (e.g. Design B: small frame: 9.3 inches, king frame: 8.7 inches).

2.4.4 END CAPS

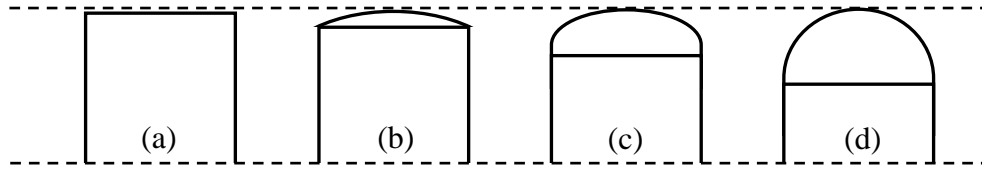


Figure 29. End-cap designs. (a) Disk, (b) Dish, (c) Elliptical, (d) Hemispherical

Before designing the pressure vessel shell, an appropriate end-cap design must be chosen. Since the Trident II D-5 missile tube was designed to accommodate an object 44 feet in length, the dimensions of the end-cap will then dictate the length over which the cylindrical shell must span. Figure 29 depicts some common options used for pressure vessel designs. While the disk and dish designs allow for greater enclosed volumes, the elliptical and hemispherical designs can be used at much greater pressures. In submarine design, the disk and dish designs are seldom used. The sharp edges where the shell meets the end-cap are difficult to model, and are typically the location of highest stress. Since the elliptical end-cap exhibits good characteristics for both volume and strength, it is the most attractive design for the LSRC and will thus be used.

In solid mechanics, end-caps such as the elliptical dome are often classified as shells in the form of surfaces of revolution. The analytical solution of such shapes can be very complicated, particularly near the cylinder-dome boundary. However, if the conditions of the shell are such that the effects of bending stress can be neglected, the problem of stress analysis can be greatly simplified [21]. For the case of the elliptical dome, it can be assumed that the bending effect due to the built-in edges are of a local character, and that the middle surface of the shell plate at some distance away from the edge undergoes uniform strain without bending. For plate thicknesses that are small relative to the dome diameter, the compressive stresses are said to be uniformly distributed across the shell thickness. Neglecting the effects of bending stresses in this manner is called membrane theory³⁴. The membrane forces N_θ (circumferential force) and N_ϕ (meridional force) can be found from applying Newton's second law to a finite area of the revolved surface in directions both tangential and normal to the surface. The equations of equilibrium in these two directions can be expressed as equations (40) and (41), respectfully [21].

$$2\pi r_0 N_\phi \sin(\phi) = -\pi p r_0^2 \quad (40)$$

$$N_\phi r_0 + N_\theta r_1 \sin(\phi) = p r_1 r_0 \quad (41)$$

where r_0 is the radius from the axis of revolution to the parallel circle, and r_1 & r_2 are the principle radii of curvature at a point on the dome surface (See Figure 30). From geometry, these radii can be written as equations (42) for the case of an ellipse.

³⁴ Although not previously discussed, membrane theory was also used to derive many of the equations for cylindrical shells. While membrane theory is sufficient for the initial selection of geometries and thicknesses, design techniques using shell theory must be used to develop the final design for submersible construction.

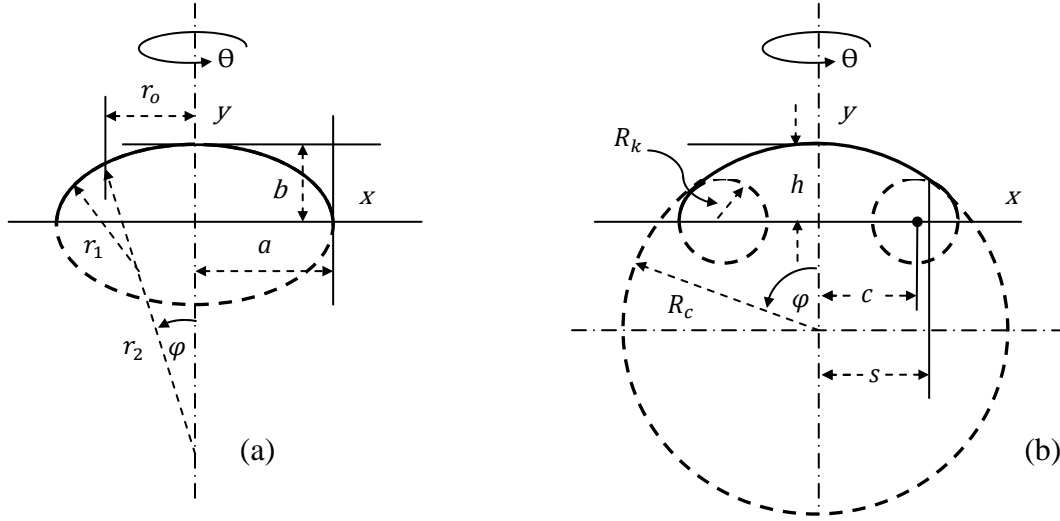


Figure 30. Dome geometry. (a) Elliptical Dome, (b) Torispherical Dome

$$r_0 = r_2 \sin(\varphi) \quad (42a)$$

$$r_1 = \frac{a^2 b^2}{(a^2 \sin^2(\varphi) + b^2 \cos^2(\varphi))^{3/2}} \quad (42b)$$

$$r_2 = \frac{a^2}{(a^2 \sin^2(\varphi) + b^2 \cos^2(\varphi))^{1/2}} \quad (42c)$$

Combining equation (40) through (42), the membrane stresses within an elliptical dome subject to external pressure (p) can be rewritten [22]:

$$\sigma_\theta = \frac{pa^2}{2t_s^e b^2} \left(\frac{b^2 - (a^2 - b^2)\sin^2(\varphi)}{\sqrt{a^2 \sin^2(\varphi) + b^2 \cos^2(\varphi)}} \right) \quad (43)$$

$$\sigma_\varphi = \frac{pa^2}{2t_s^e} \left(\frac{1}{\sqrt{a^2 \sin^2(\varphi) + b^2 \cos^2(\varphi)}} \right) \quad (44)$$

where t_s^e is the end-cap shell thickness and positive values of σ indicate tension. A plot of membrane stresses as a function of the meridional angle (φ) can be seen in Figure 31. Two conclusions can be made from this plot. (1) The maximum normal stresses occur at the dome's pole ($\varphi = 0^\circ$) and equator ($\varphi = 90^\circ$), and (2) the meridional stress is always in compression, whereas the circumferential stresses become tensile at the equator when $a^2 > 2b^2$ [21].

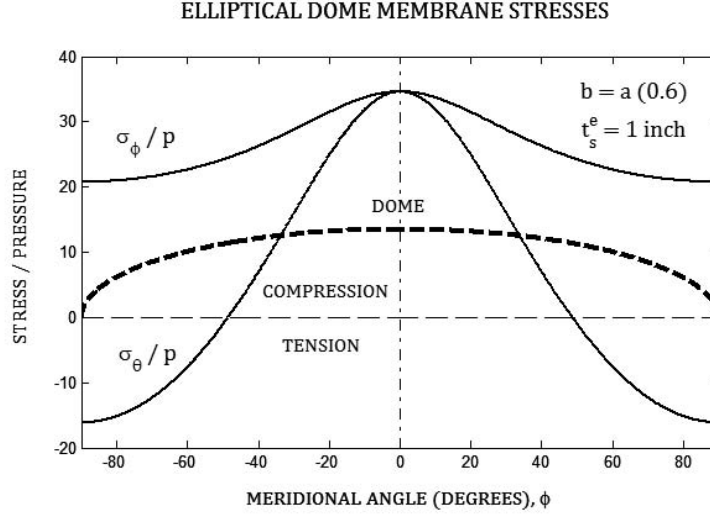


Figure 31. Elliptical dome membrane stresses

When designing for failure by yield, we can then focus our analysis on the critical regions alone. At the pole, $r_1 = r_2 = a^2/b$; hence

$$\sigma_\phi = \sigma_\theta = \frac{pa^2}{2bt_s^e} \quad (45)$$

At the equator, $r_1 = b^2/a$ and $r_2 = a$; hence

$$\sigma_\phi = \frac{pa}{2t_s^e} \quad (46a)$$

$$\sigma_\theta = \frac{pa}{t_s^e} \left(1 - \frac{a^2}{2b^2} \right) \quad (46b)$$

Due to various reasons, including ease of fabrication, the elliptical end-cap is often replaced by the torispherical dome. The torispherical dome is the surface obtained from the intersection of a spherical cap with a tangent torus. This shape very closely follows the contour of the elliptical dome, but can be defined using only two radii of curvature. The radius forming the spherical cap is often referred to as the crown radius (R_c), and that at the equator is called the knuckle radius (R_k). Using this shape, the critical yield and buckling pressures for a torispherical end-cap can be approximated using the solution obtained for a perfect sphere with similar radii of curvature. For a sphere, $r_1 = r_2 = a = b = R_o$ (outer radius). Equations (45) and (46) then become,

$$\sigma_\phi = \sigma_\theta = \frac{pR_o}{2t_s^e} \quad (47)$$

The critical pressure causing yield in the end-cap shell then becomes,

$$p_c^{Ye} = \frac{2t_s^e \sigma_Y}{R_c} \quad (48)$$

Like the cylindrical shell, the torispherical end-cap must also be checked for instability. Again, the critical buckling pressure for the torispherical end-cap is approximated using the solution for a perfect sphere under uniform external pressure. This pressure can be calculated using the solution below [16].

$$p_c^{Be} = \frac{2E}{[3(1 - \nu^2)]^{1/2}} \left(\frac{t_s^e}{R_c} \right)^2 \quad (49)$$

For engineering purposes, this solution by itself is *never* used to predict the critical buckling pressure of a submersible. Like equation (48), this equation was developed using membrane theory and nonlinearities in the pre-buckling analysis were neglected. In addition, it does not satisfy the boundary conditions at the edge of the spherical cap (clamped) and is thus limited to buckle-pattern wavelengths that are small compared to R_c . For these reasons, equation (49) can only be used to approximate the critical pressure for a torispherical end-cap if the solution is corrected by experimental data. Such correction factors are offered by many engineering societies, and take into account the many assumptions made during the equation's derivation. In addition, spherical caps are notorious for being susceptible to initial imperfections. Research has shown that there exists forms of equilibrium slightly deviated from the spherical shape [21]. These equilibrium conditions require pressures much smaller than those calculated using equation (49). As a result, the spherical dome deforms slightly and the collapse of the buckled shell occurs suddenly. It is for this reason that the circularity of the end-caps, as well as the cylindrical shell, are of such great importance in submarine construction. For practical applications, Timoshenko [23] suggests using the empirical formula below³⁵ (equation 50) for spheres when $400 \leq R_c/t_s^e \leq 2,000$ and $20^\circ \leq \varphi \leq 60^\circ$.

$$\tilde{p}_c^{Be} = \left[1 - 0.175 \left(\frac{\varphi^\circ - 20^\circ}{20^\circ} \right) \right] \left[1 - \left(\frac{0.07R_c}{400t_s^e} \right) \right] (0.3E) \left(\frac{t_s^e}{R_c} \right)^2 \quad (50)$$

Four of the most commonly used design curves³⁶, along with the equations presented above, can be seen in Figure 32. For domes with perfect geometry (and $t_s^e = 1.0$ inch), shell yield is

³⁵ See *Der Stahlbau*. Klöppel, K and Jungbluth, O. 1953, Vol. 22, pp. 121.

³⁶ (1) Britannic Majesty's Government, Sea Systems Publication No. 74 (SSP74). (2) European Recommendations for Steel Construction (ECCS). (3) British Standards Institution, Pressure Vessel Code (BS5500). (4) American Society of Mechanical Engineers, Pressure Vessel Code (ASME). Although not considered in this paper, there are many shipbuilding certification societies that maintain reliable pressure hull design codes. The American Bureau of Shipbuilding (ABS) and Germanischer Lloyd, for example, offer guidelines that are revised regularly, and are continuously validated by in-service designs.

expected to occur before buckling when $b \geq a \cdot (\sim 0.19)$. However, imperfections due to fabrication make buckling the dominant mode of failure. In general, the critical buckling pressure decreases as the radii of curvature increases. For this reason, the crown radius is used (i.e. instead of the knuckle radius) to calculate the collapse pressure of the dome. In Figure 32, the critical buckling pressure for each design code is depicted as a line. Geometry and pressure combinations falling above these lines are expected to fail. When designing the LSRC it was decided that the dome thickness should be close to, but not less than, that of the cylindrical shell, and be within the limitations of modern fabrication techniques. An upper limit of one inch was chosen, and the various design codes were used to find a suitable shape. Due to geometry requirements imposed by the design codes, only portions of each line in Figure 32(a) can be used. For example, SSP74 requires that $0.7 > R_k/R_c > 0.4$. Given the outer diameter of the LSRC (83 inches), SSP74 guidelines can only be used for domes geometries with $b \geq a \cdot (\sim 0.7)$. Using the SSP74 guidelines, Figure 32(b) shows that $t_s^e \gtrsim 0.7$ are all suitable shell thicknesses for $b/a = 0.7$, and $D_w = 2500$ feet.

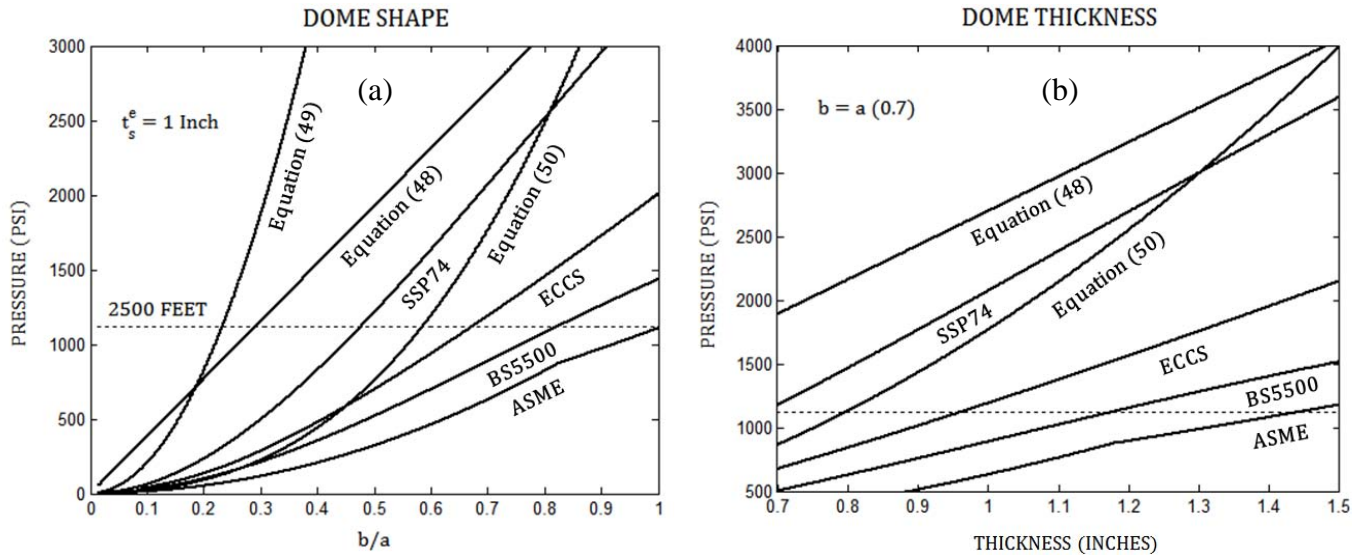


Figure 32. Torispherical dome design curves. (a) Dome Shape, (b) Dome Thickness

It was decided that SSP74 guidance would be used to design the LSRC end-caps. This decision was based on three major factors: (1) SSP74 guidance was developed specifically for submarine design, (2) The BS5500 and ASME design codes were developed primarily for industrial use, and are comparatively over-conservative, and (3) Curves developed by the ECCS and Timoshenko are based on older data which has not been revised in recent decades. The final dimensions chosen for the LSRC upper and lower end-caps were $t_s^e = 0.75$ inches and $b/a = 0.7$.

2.4.5 LSRC HULL DESIGN

This paper will attempt to optimize two basic pressure hull designs. The first design (Design A) will be stiffened by internal frames of uniform scantlings, where as the second design (Design B) will utilize two king frames in an effort to reduce the number of typical (small) frames. Both designs subdivide the pressure hull into two compartments. Diagrams of each design can be seen below in Figures 33 and 34 (All dimensions are approximate).

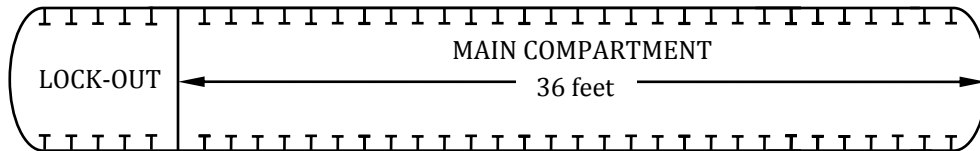


Figure 33. Design A

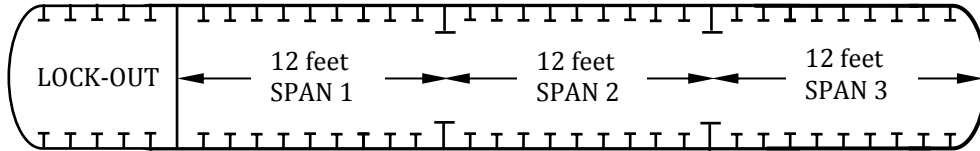


Figure 34. Design B

Clearly, the design space is not limited to the above two arrangements, and therefore, this paper does not claim to have produced the lightest design possible. Rather, it demonstrates the most direct approach to minimize the weight of a ring stiffened cylinder. To arrive at the lightest structure, it would be necessary to consider a variety of king frame arrangements and various combinations of small frames with non-uniform scantlings.

The bulkhead was placed at the upper end of the capsule to ensure that sea water does not enter the main compartment while personnel exit. The absence of such a partition could condemn the crew should excessive water enter the capsule unchecked. In addition, this arrangement provides for a space that could be used as a lock-out chamber for subsequent surface decompression. Internal vice external frames were chosen in order to maximize the internal volume, and to provide a smooth outer surface for the ejection phase and ascent. The spacing of king frames in Design B was set at 12 feet to meet the minimum bulkhead spacing requirement recommended by Jackson [15] (i.e. $L_b = [1.5 \sim 2.0] D_o$).

As mentioned earlier, shell plating in the vicinity of the bulkhead, king frames, and end-caps will be subject to additional bending stresses. To help mitigate the effects of such discontinuities, the following guidelines were used:

- Shaped inserts will be used at the base of each king frame such that $t_i = (1.3)t_s$ and $h_{in} = (L_1 + L_2)/8$, where L_1 and L_2 are the distances between the king frame and the adjacent small frames.
- At each side of the bulkhead, and extending no less than a 25% into the adjacent frame bays, the shell thickness will be increased by a factor of 1.3.
- The frame spacing for the first frame bay at either side of the discontinuity (i.e. king frame or bulkhead) will be reduced to about 80% of the value required remote from the discontinuity.
- The distance between the dome-cylinder junction and the first frame on the cylinder will not exceed half the frame spacing along the cylinder.
- The cylinder length (L_b) will be taken to extend into the end-cap (dome) by 100% of the dome's depth (b). Note: *Paramarine*TM uses 40% of the dome's depth.

The design collapse depth chosen for the LSRC is 2,500 feet (seawater). Pressure hull integrity to this depth is expected to exceed the most optimistic estimates of a Trident submarine's survivability, and will provide an additional margin to failure should the LSRC be damaged during loading and off-loading. NAVSEA document SS800-AG-MAN-010/P-9290³⁷ requires that a safety factor of 1.5 be applied for operations. Thus, a pressure hull designed for a collapse depth of 2,500 feet will be suitable for operations as deep as 1,666 feet. For the purposes of this analysis, it will be assumed that all structural components are fabricated out of HY-80 high strength steel (See Appendix III). No allowance is made for shell corrosion.

³⁷ System Certification Procedures and Criteria Manual for Deep Submergence Systems

2.4.5.1 ANALYTICAL ANALYSIS

To arrive at the lightest structure, a parametric analysis was performed on the structural dimensions that most directly impact the pressure hull's integrity. These dimensions include, shell thickness, frame spacing, web height, web thickness, flange breadth and flange thickness. By varying each of these parameters, the fundamental failure modes can be manipulated and the most efficient structures can be resolved.

Optimization of the ring-stiffened right-circular cylinder is a topic that has been well studied. Over the years, many computer aided methods have been developed to assist with pressure hull design. Although somewhat outdated, some of the more well known optimization programs include, ARE Program SD009A³⁸ and EXPRESS³⁹. More recently, programs like MNSTR (UK MoD Minimum Structural Weight), POWERPAC (NAVSEA 05), and DASH (Electric Boat) have been used for submarine design within the United States and the United Kingdom.

The parametric analysis used in this report is a straight forward application of the analytical solution outlined in sections 2.4.1 through 2.4.4. While the calculations are rather long and tedious, computers can be used to automate the process. The computer program used in this analysis, FFSOR (Full Factorial Scantling Optimization Routine)⁴⁰, calculates the critical pressures for each of the failure modes over a range of scantling parameters input by the user. The program then retains the best solutions (i.e. lowest structural weight), and plots them on an optimization graph for comparison (See Figure 37). The optimal design will be that which gives the highest margin to yield, at the lowest weight. This solution can be easily identified on the optimization graph as the point lying closest to the origin (i.e. lower left hand corner). However, since all the solutions retained in this analysis will not fail prematurely, preference will be given to the design with the lowest weight.

In an effort to limit the solution space to those designs that are best suited for submarine applications, the FFSOR was programmed to apply various design guidelines. The most fundamental of these filters is the mode of failure. During WWII, many pressure hulls were designed to fail first by lobar buckling. It was reasoned that early signs of hull deformation (or the sound of hull "popping") between the frames would alert the crew in the event of exceeding normal operating depths. As pressure hulls were designed more efficiently, it was decided that shell yield should be the preferred mode of first failure. This decision was based on the accuracy in which shell yield could be predicted, and the fact that the buckling modes were far more susceptible to imperfections. It has only been recently that submarine designers are again accepting buckling modes as the first mode of failure. This change in philosophy is a direct result of the computer aided tools that have become available to designers, in addition to the tighter tolerances that can be held during fabrication. Because of confidentiality, the equations and test data used by the U.S. Navy to accurately predict buckling modes could not be utilized in this

³⁸ **Admiralty Research Establishment.** Program SD009A: *Design of Externally Pressurized Stiffened Cylinders and Cones.*

³⁹ **British Standards Institution.** EXPRESS: *A computer Aid to the Design of Externally Pressurized Stiffened Cylinders (PD 6486)*, London, 1978

⁴⁰ See Appendix IV. The FFSOR was developed for the purposes of this paper (academics), and should not be relied upon for actual pressure hull design.

analysis. For this reason, the FFSOR was programmed to only accept solutions in which shell yield is the first mode of failure.

In addition, applicable guidelines have been programmed into the FFSOR for frame design. While not completely justified by theory, these guidelines have been shown to be reasonably valid in practice. Table 3 lists some of the additional guidelines considered in this analysis.

JACKSON [15]		McGRATTAN & PETEROS [22]	
t_s	$\cong pR/\sigma_y$	t_s	$\cong \beta_1 pR/\sigma_y \text{ (} 0.7 \leq \beta_1 \leq 0.9 \text{)}$
h_w/t_w	< 18	h_w/t_w	15 - 20
$A_f/L_f t_s$	$\cong 0.3$	$A_f/L_f t_s$	$\beta_2 \text{ (} 0.3 \leq \beta_2 \leq 0.6 \text{)}$
$L_f/2R$	0.07 - 0.10	$L_f/2R$	$\cong 0.083$
t_{fl}/t_s	0.75 - 1.0	t_{fl}/t_s	$\cong 1$
h_{fl}/h_w	0.7 - 0.8	h_{fl}	$\cong 0.75(h_w - t_{fl})$
A_f/I_f^*	$\cong E/\sigma_y R_f^2$	$h_w + t_{fl}$	5% - 10% of R
$L_b/2R$	1.5 - 2.0	* I_f = moment of inertia of frame area about frame NA	

Table 3. Scantling design guidelines

Because equation (22) requires multiple calculations (i.e. over a range of n) for a single set of pressure hull dimensions, it does not lend itself well to programming. Therefore, the Windenburg approximation will be used in place of equation (22). This approximation uses an expression that is independent of n ⁴¹, and produces results that differ from equation (22) by no more than 4%. Once an efficient design is determined, equation (22) can be used to verify the results. The Windenburg approximation (shown below) is widely accepted, and will thus be used in the parametric analysis.

$$\tilde{p}_c^{LB} = \frac{(2.42)E \left(\frac{t_s}{2R_s} \right)^{5/2}}{(1 - \nu^2)^{3/4} \left[\left(\frac{L_f - t_w}{2R_s} \right) - 0.45 \left(\frac{t_s}{2R_s} \right)^{1/2} \right]} \quad (51)$$

In summary, the analytical analysis presented in this paper (i.e. FFSOR) strives to produce the optimum pressure hull design (i.e. minimum weight) that will cause the shell to fail first by yielding, and size the frames such that premature failure by general instability will not occur.

⁴¹ Windenburg assumes $n = 2\pi R_s/(L_f - t_w)$.

2.4.5.2 NUMERICAL ANALYSIS

For the purpose of comparison, a numerical analysis was performed on each of the designs produced by the FFSOR. Designs A and B were modeled as shell elements in HyperMesh⁴² software, and were later imported into ABAQUSTM Standard⁴³ for analysis. The designs were externally loaded with uniform pressure at various depths, and critical elements were tracked for stresses, strains and displacements. A sectional view of the finite element model created for Design A can be seen in Figure 35 below.

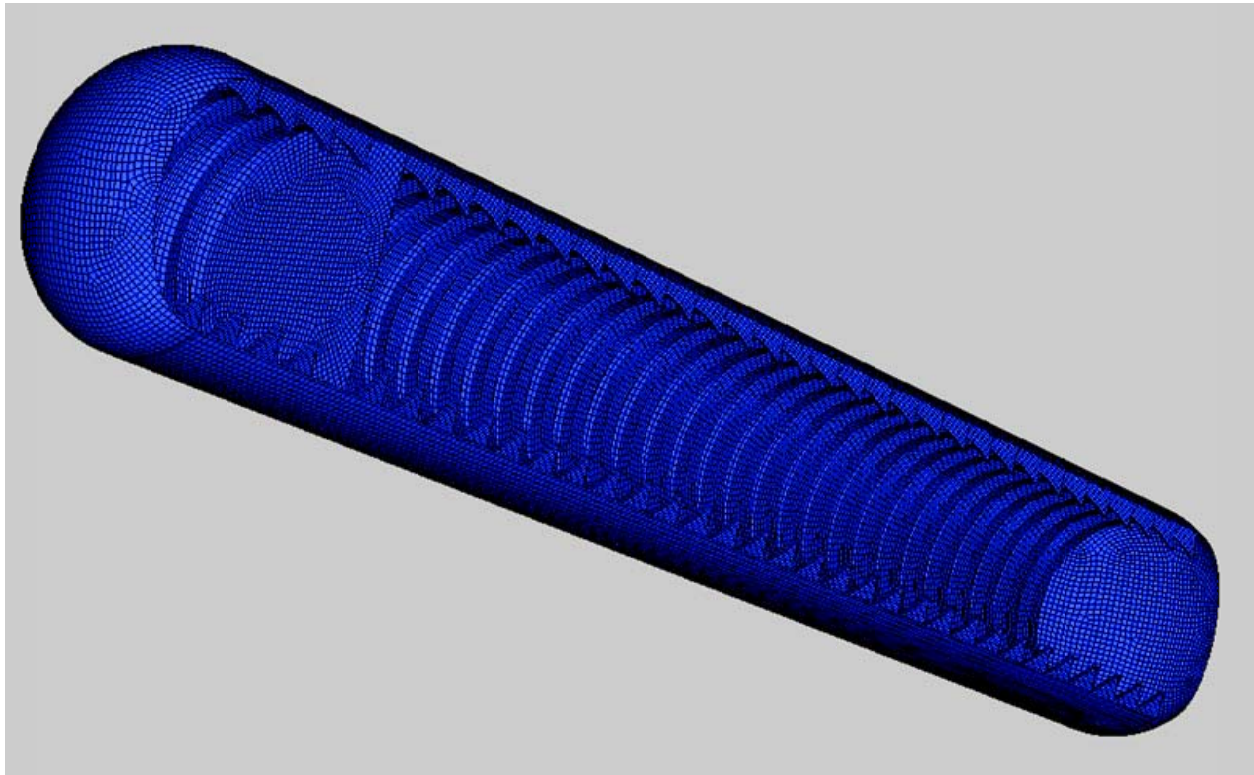


Figure 35. Design A finite element model

To assess the pressure hull's performance at 2,500 feet, a *STATIC, GENERAL analysis was performed at the appropriate load, and the Von Mises Stress was tracked for all elements. In this way, the critical elements and the largest stresses could be determined at test depth. This procedure was then repeated for depths deeper than 2,500 feet to identify the location and depth at which first yield occurred. A *BUCKLE (Linear Perturbation) analysis was then performed on the perfect geometry to identify the critical modes of elastic buckling. These results were compared to those predicted by the FFSOR, and were retained for seeding geometry imperfections (to be discussed later). Finally, a *STATIC, RIKS analysis was performed to determine the collapse depth of the structure and to visually observe the mode of failure in the presence of imperfections. The *STATIC, RIKS method is well suited for this analysis. Because

⁴² HyperWorks® Version 8.0, Altair Engineering Inc. 1995-2006

⁴³ ABAQUS/CAE Version 6.5-1, ABAQUS Inc. 2004

the RIKS method uses the load magnitude as an additional unknown; it solves simultaneously for loads and displacements. This approach provides solutions regardless of whether the response is stable or unstable [24]. In this way, the maximum load that a structure can endure can be determined by monitoring the displacements of critical members. The RIKS method also allows the user to introduce initial imperfections into the perfect geometry. In this analysis, the *IMPERFECTION feature of the RIKS method will be used to introduce out-of-fairness (OOF) eccentricities into the model.

A mesh density sensitivity analysis was not performed. The number of elements chosen for each design was sufficient enough to meet selective SSP74 guidelines, but low enough to be compiled on a PC within a reasonable amount of time. The material properties were modeled with NAVSEA HY-80 material test data (See Appendix III). While this data is expected to contain some residual stresses from fabrication, material discontinuities due to welding were not considered. The level of detail in the model is moderate, but is consistent with that used in the FFSOR. Although hatches and piping penetrations were not included in the model, the bulkhead thickness was sized at two inches to simulate the stiffness that would result from local reinforcement of the penetrations. Principle and secondary fabrication tolerances as well as internal and external secondary structure were not included.

2.4.5.3 MODELING IMPERFECTIONS

A thorough analysis of all credible imperfections must be performed to ensure that the pressure hull design will not fail prematurely. In U.S. submarine design, a very formal method is used to assess the pressure hull's strength in the presence of OOR and OOF eccentricities. In general, an OOR condition is placed at various locations about the frames' circumference and the peak stresses are calculated. This analysis, along with others including OOF conditions, are used to determine the margins of safety for each of the failure modes. Because the details of this method are classified, a comprehensive imperfection analysis was not done. At the concept design phase, forgoing this analysis is not considered unreasonable. However, because the *STATIC, RIKS method requires that imperfections be introduced into the perfect geometry, a minor effort was made at evaluating the effects of OOF.⁴⁴

The two factors that most significantly alter the buckling behavior of a structure are the imperfection size, and the imperfection shape. In the case of submarine construction where fabrication tolerances are defined by the technical authority, only the allowable magnitude of an imperfection may be known at the time of the initial design. In such cases, assuming that the imperfections are linear combinations of the eigenvectors of the linear buckling problem is a reasonable way to estimate the imperfect geometry. In this way, the buckling load's sensitivity to imperfections can be assessed. It is also reasonable to introduce initial imperfections in the shape of the static response to submerged pressure. In this analysis, OOF eccentricities were introduced

⁴⁴ Although OOR effects were not modeled in the numerical analysis, the effects of frame eccentricities were considered when designing the pressure hull (Recall that an OOR of $e = 0.5$ inches was used in the FFSOR (and *Paramarine*TM) when developing Designs A & B). For this reason, the critical loads for both frame yield and frame buckling (and consequently, general instability) are expected to be larger in the numerical analysis.

in two ways. (1) Since the pressure hull was designed to fail first by yield, an axisymmetric imperfection in the shape of the shell yield mode of failure (See Figure 26(c)) was introduced at a single frame bay far from the effects of the bulkheads and king frames (Figure 36). The maximum magnitude of this imperfection was then varied from 0.5 inches to the smallest value in which the *STATIC, RIKS method could achieve convergence. This type of analysis gives both an accurate value for the structure's collapse pressure, and the amount of OOF that can be tolerated before the operating depth is compromised. (2) The second method applies the same logic to the structure's most probable mode of buckling. For each design, a *BUCKLE analysis was performed to identify the mode of buckling with the smallest margin to failure. An imperfection was then introduced in the same manner as before in the shape of the primary buckling mode.⁴⁵ The collapse pressure resulting from this analysis was then compared to that of the first method, and the most conservative value was taken as the structure's collapse depth.

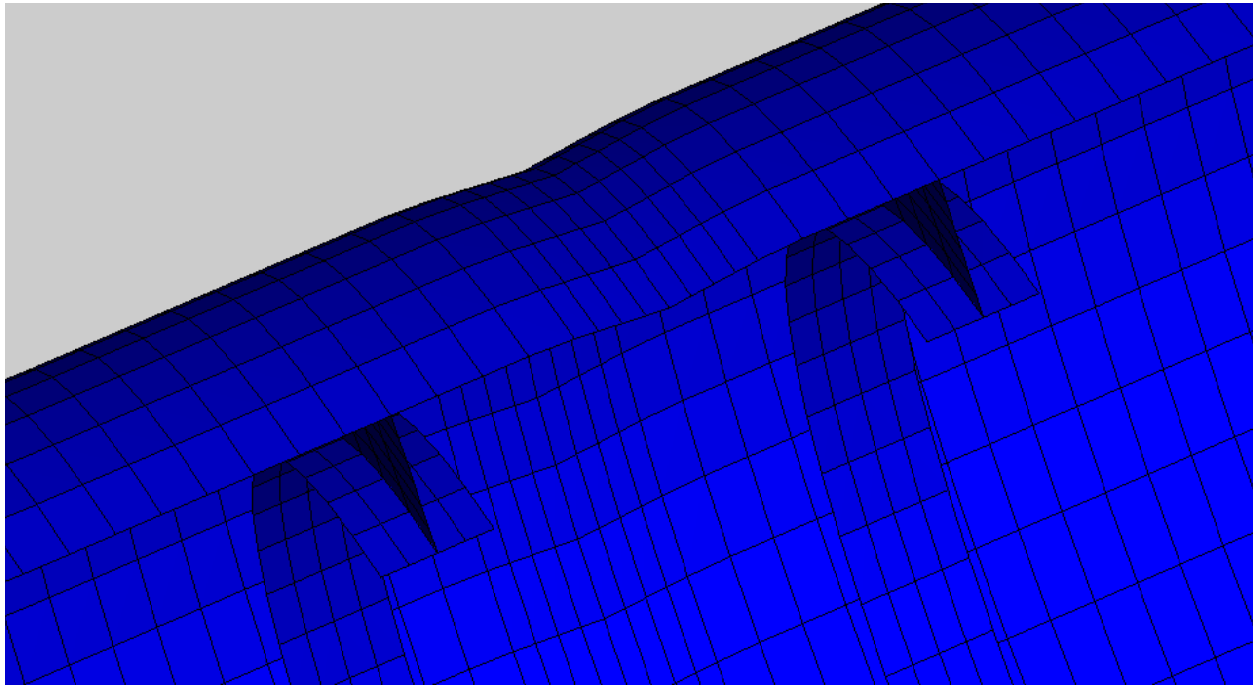


Figure 36. Axisymmetric imperfection (OOF)

⁴⁵ This paper considers the lowest buckling mode only. Similar studies have shown that the superposition of two or more modes can often result in critical failure loads smaller than that of the primary mode. For this reason, additional analysis should be performed using several mode combinations.

2.4.5.4 RESULTS

2.4.5.4.1 ANALYTICAL RESULTS (FFSOR)

The FFSOR was successfully run on both Design A & B (See results in Appendices V, VI and VII). The optimization graphs for each design can be seen below (Figure 37)⁴⁶, where P is the external pressure at 2,500 feet X 1.5 (i.e. safety factor for shell yield) and P_c is the critical pressure for failure. Since the only solutions retained in this analysis are those that fail first by shell yield, $P_c = P_c^Y$. Although the most desirable designs are those closest to the origin, it is not surprising to find that the lightest structures have the smallest margin to failure (i.e. upper left hand corner).

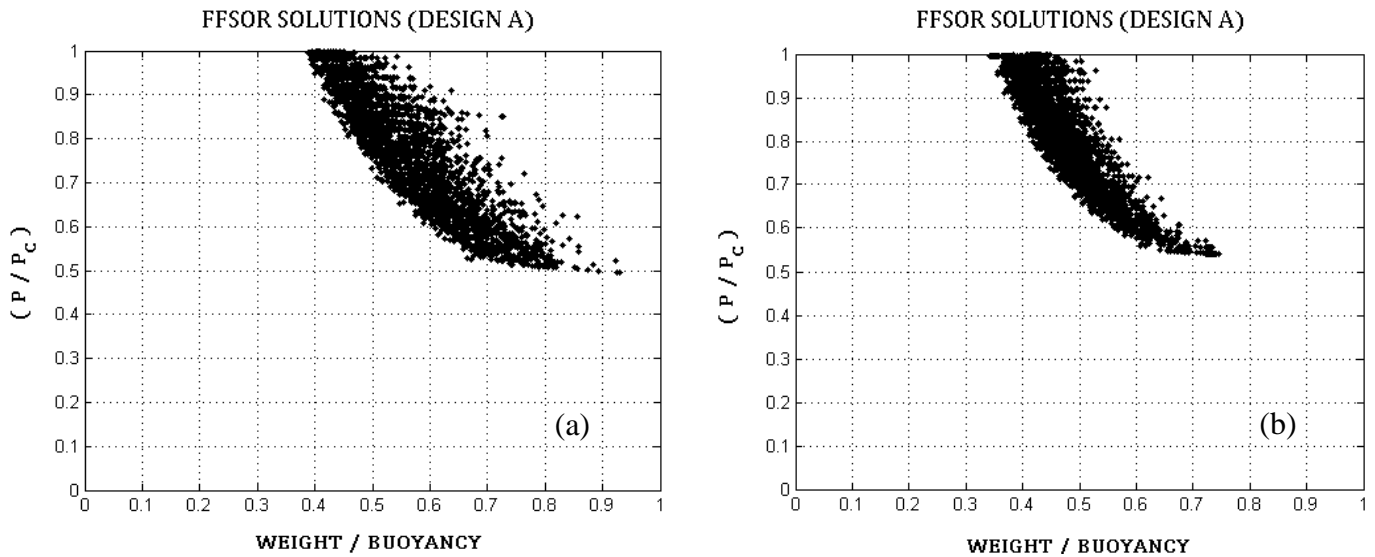


Figure 37. FFSOR solutions. (a) Design A, (b) Design B

The optimum scantlings and failure modes for each design are summarized in Table 4. Cross sections of the final frame designs can be seen in Figure 38. As expected, the safety factors for shell yield are just above the desired value. This indicates that the pressure hulls will fail first by shell yield at a depth slightly greater than 2,500 feet. Using the optimum scantlings, the results also show that both designs are almost equally likely to fail by frame yield. However, the two designs differ significantly in their ability to resist failure by lobar buckling, general instability and frame instability. The lobar buckling safety factor for Design B is only slightly larger than that required, indicating yet another possible mode of failure. On the contrary, the smaller frame spacing in Design A precludes lobar buckling from being a primary mode of failure. General instability and frame instability were not found to be critical modes of failure for either design.

A very similar analysis was performed to size the king frames used in Design B. For this analysis, the FFSOR was modified with equations (33) through (39), and takes into account the additional cross-sectional area provided by the king frame inserts. The results from this analysis

⁴⁶ Figure 37 is not a plot of all solutions. The points in each graph were selected at random to give a representative view of the design space. Number of designs analyzed: Design A: 57,200,325. Design B: 30,332,862.

show that the king frames will fail by frame yield at a depth slightly deeper than the 3,750 feet (i.e. design collapse depth X 1.5). The results of the king frame analysis can be found in Appendix VII and are summarized in Table 4 below.

Scantlings (inches)	Design A Small Frames	Design B Small Frames ⁴⁷	Design B King Frames
Shell Thickness (t_s)	0.75	0.75	N/A
Frame Spacing (L_f)	14	23	N/A
Web Height (h_w)	6	6	10
Web Thickness (t_w)	0.34375 (11/32)	0.34375 (11/32)	0.59375 (19/32)
Flange Breadth (h_{fl})	4.75	4.25	8
Flange Thickness (t_{fl})	0.65625 (21/32)	0.75	0.96875 (31/32)
Insert Breadth (h_{in})	N/A	N/A	9.2
Insert Thickness (t_{in})	N/A	N/A	0.225
Buoyancy Ratio (Buoyancy/Weight)	2.58	2.92	N/A
Slenderness Ratio (λ)	0.73	0.93	N/A
Shell Yield Safety Factor (Desired: 1.5)	1.51	1.51	N/A
Lobar Buckling Safety Factor (Desired: 2.25)	4.33	2.32	N/A
General Instability Safety Factor (Desired: 3.75)	8.79	8.44	11.74
Frame Yield Safety Factor (Desired: 1.5)	1.51	1.51	1.50
Frame Instability Safety Factor (Desired: 1.8/2.25)	11.70	7.93	6.80
Frame Tripping Safety Factor ⁴⁸	5.37	5.34	N/A

Table 4. FFSOR optimization result

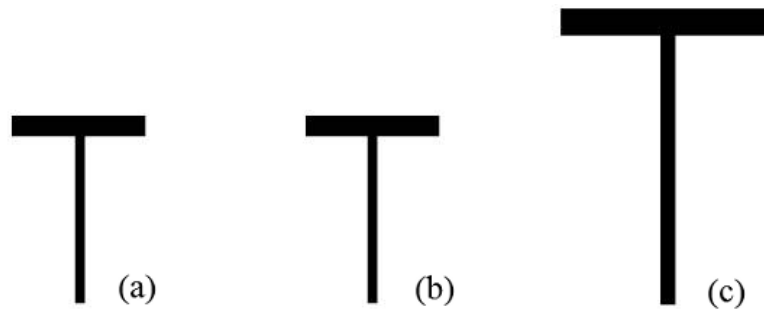


Figure 38. Frame cross-sections (drawn to scale), (a) Design A, (b) Design B small frame, (c) Design B king frame

⁴⁷ In general, the flange thickness should be slightly smaller than that of the shell. Because the FFSOR selected these parameters with equal values (i.e. $t_s = t_{fl}$), the scantlings used in the numerical analysis of Design B were modified as follows: $h_{fl} = 4.75$, $t_{fl} = 0.6875$. This change makes the scantlings for each design nearly identical, making L_f and L_b the primary differentiators.

⁴⁸ *Paramarine*TM results (Based on AMTE programs N9C & N9E). Note: Because the shell elements used in the finite element model do not have thickness, the numerical model was built using centerline dimensions. For most analyses this approximation is of no consequence. However, the frame tripping results in the numerical analyses are significantly affected due to over-sizing the web height (e.g. Design A: $h_w = 6.70$ vice 6.00 inches). For purposes of comparison, the web height used in the analytical analysis (frame tripping only) for Designs A & B were changed to 6.70 & 6.72 inches, respectively. Had the scantlings in Table 4 been used, the analytical solution for frame tripping would have resulted in a safety factor of ~ 6.65 for both Designs A & B.

2.4.5.4.2 NUMERICAL RESULTS (ABAQUS™)

DESIGN A

Analysis	Structure Weight (lbm)	P_c^Y / P_d	P_c^{FT} / P_d	Depth of First Yield (feet) ⁴⁹	Collapse Depth (feet)	Mode of Failure
Analytical	43,985	1.32	5.37	3,292	Not Calculated	Shell Yield
Numerical		1.27	5.28	3,197	4,059	Shell Yield

Table 5. Design A analysis results

The numerical results are summarized in Table 5. The *STATIC, GENERAL analysis performed at 2,500 feet showed that the maximum stress occurred on a pressure hull shell element adjacent to the shell insert near the lower end-cap. The Von Mises stress for this element is 58,517 psi. The stress concentration at this location is most likely due to the sharp variation in shell thickness inherent to the finite element model. In reality, the shell inserts would be faired to the hull, thereby minimizing the effects of such discontinuities. In general, stress contours of the pressure hull at 2,500 feet show that the highest stresses occur circumferentially at the base of each frame and at shell elements adjacent to the bulkhead. These regions can be seen in Figure 39 as red bands, circumferentially.

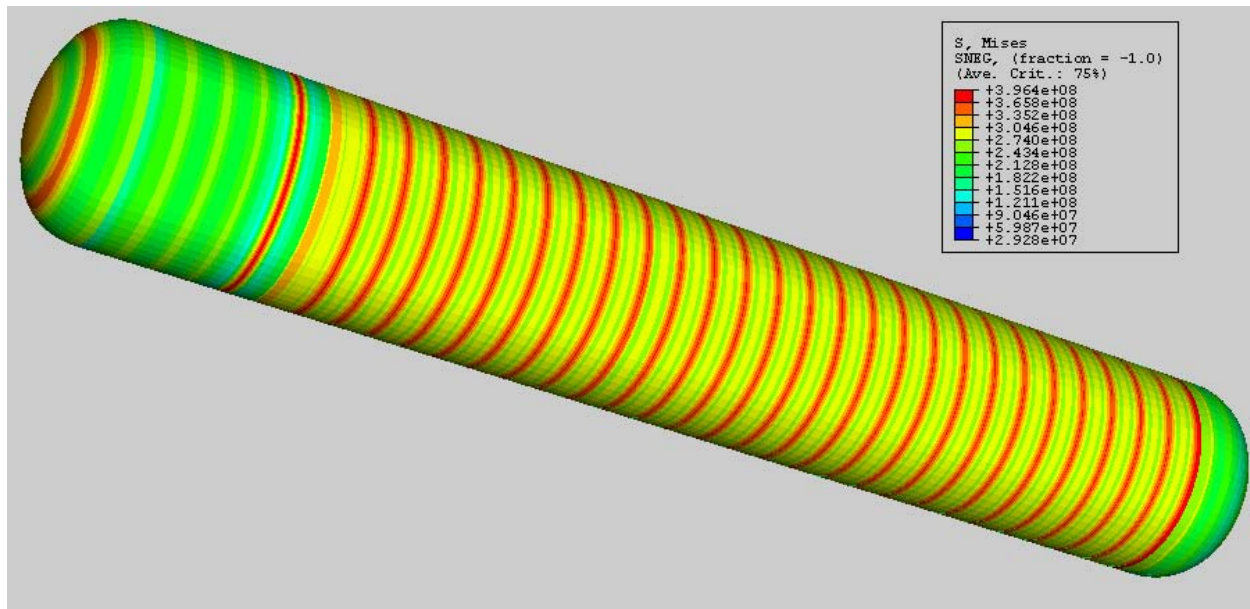


Figure 39. Design A, Von Mises stress at 2,500 feet (Note: legend in Pascals)

⁴⁹ Von Mises stress = σ_Y . Because the location of first yield differed in each of the analyses (i.e. analytical and numerical), the depths in this column should not be compared directly. The numerical result is located on a shell insert (i.e. $t_s \neq 0.75$ inches), whereas the analytical solution is the “near-frame” result (equation 15) using the scantlings in Table 4 (i.e. $t_s = 0.75$).

Analyses at depths deeper than 2,500 feet showed that first yield will occur at a shell element inside the main compartment, adjacent to the bulkhead. The depth at which this element begins to yield is 3,197 feet, corresponding to a safety factor of 1.27. This result suggests that the design guidelines of section 2.4.5.1 do not adequately suppress local bending stresses when using a design safety factor of 1.5 for shell yielding. Although the pressure hull was designed to fail by shell yield, first yield was not expected to occur at a shell insert. The analytical analysis assumes that the design guidelines of section 2.4.5.1 will preclude failure at the inserts, and that shell yielding will occur at a frame bay far from the bulkhead where $t_s = 0.75$ inches. Overlooking this result, subsequent analyses show that shell elements at the “near-frame” location (i.e. red bands in Figure 39) begin to yield at approximately 3,500 feet.

A sectional view of the field output obtained from the *BUCKLE analysis can be seen in Figure 40. The results indicate that the primary buckling mode for Design A, with perfect geometry, is frame tripping. This result does not agree with that of the FFSOR. Analytical results show that the primary mode of buckling, for Design A, is lobar buckling. However, both analyses show that the critical depth for each of these buckling modes is *relatively* close. The critical depths for frame tripping and lobar buckling, for Design A, can be seen graphically (symbol: ■) in Figure 41. The depth at which frame tripping occurs is 13,200 feet, slightly shallower than that predicted analytically (13,426 feet). Considering the depths at which the LSRC will operate, frame tripping is not likely.

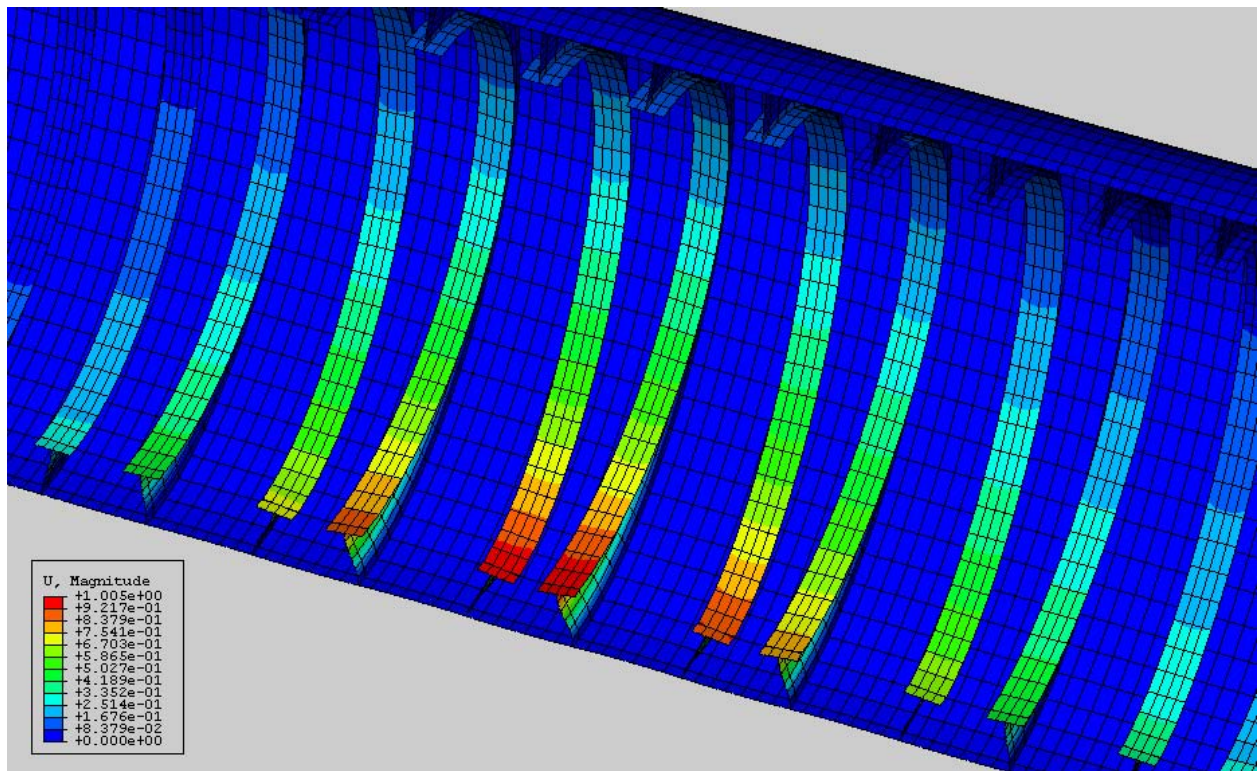


Figure 40. *BUCKLE analysis results (Displacement, U), Mode 1, Design A

Figure 40 lends itself to some interesting discussion. As stated earlier, the loss in circularity due to frame failure will cause the pressure hull to fail by general instability. The displacement

contour in Figure 40 illustrates this well. The general shape of the overall collapse can be seen as the color contour varies over thirteen consecutive frame bays. Another important observation is the mode at which frame tripping occurs. Close examination of Figure 40 suggests that frame tripping will occur at small mode numbers⁵⁰. This conclusion is based on the degree of curvature present in the frames' web. The analytical solution shows that mode $n = 0$ corresponds to the lowest buckling pressure for pure tripping. The analytical results for frame tripping can be seen in Figure 41. Figure 41(a) shows the critical buckling loads for both frame tripping and lobar buckling. It is apparent from this plot that several eigenvalues resulting from the frame tripping analysis coincide with those of lobar buckling (i.e. eigenvalue 1: $n < 4$, and eigenvalue 2: $n > 3$). At these loads, interaction exists between the two modes of buckling, and frame tripping occurs in conjunction with lobar buckling. Eigenvalues not corresponding to modes of lobar buckling indicate depths at which "pure" frame tripping occurs. Figure 41(b) displays the web shapes for the frame tripping modes $n = 0, 2, 4, 6, 8$ and 10 . In agreement with the numerical results, the web shape corresponding to mode zero is found to resemble the webs depicted in Figure 40.

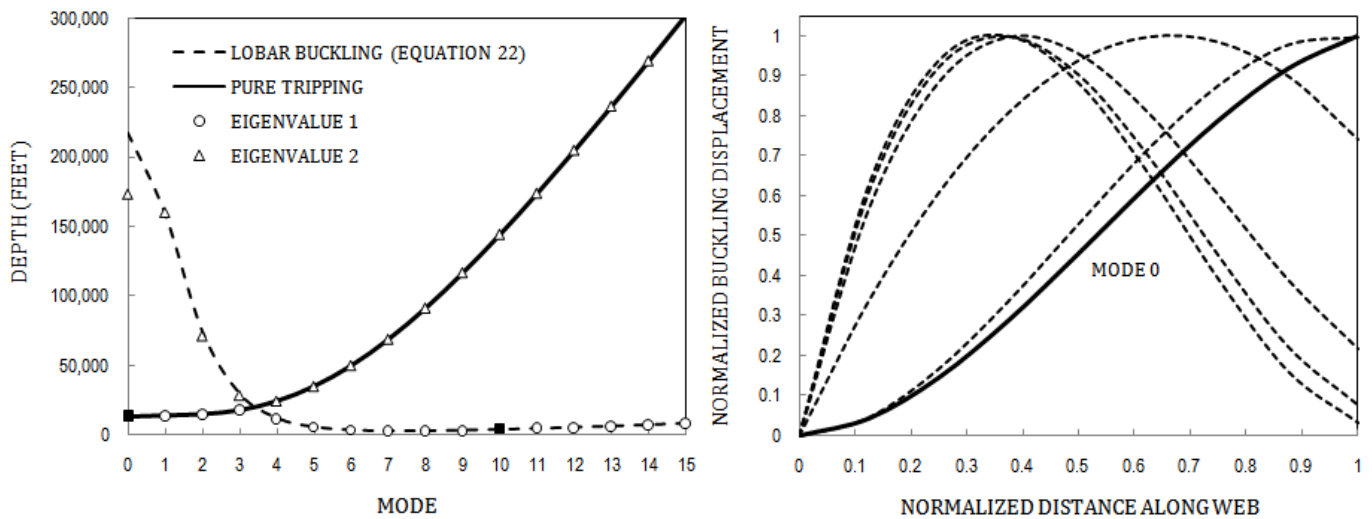


Figure 41. Frame tripping analysis. (a) Critical tripping load, (b) Tripping modes (i.e. web shape)

Results from the *STATIC, RIKS analysis show that Design A will collapse at a depth just greater than 4,059 feet. Interestingly, both Method 1 and Method 2 produced the same critical collapse depth. However, a complete analysis could only be obtained using Method 1. As mentioned earlier, frame tripping is expected to produce unstable post-buckling behavior (i.e. general instability). Due to the discontinuous response (bifurcation) at the point of buckling, the post buckling response using Method 2 could not be obtained using the ABAQUS/StandardTM RIKS method⁵¹. Fortunately, the ABAQUSTM results file (*.ODB) retains the incremental equilibrium solutions prior to collapse, and a close approximation of the critical load could be obtained. Figure 42 graphically displays the results. For each perturbation method, the

⁵⁰ Mode $n = 0$ is axisymmetric rotation of the stiffener about its toe.

⁵¹ Several *STATIC, RIKS analyses were attempted using Method 2. In each case, the response curve appeared to be retracing the original loading path once a limit was reached. The following modifications were made without success: (1) The force residual convergence criteria was tightened. (2) A limit was placed on the maximum incremental arc length. (3) Larger imperfections were built into the geometry.

displacement of a single node (in the region of interest) was tracked as the depth was increased. In Figure 42, the collapse depth can be seen as the critical values on each curve (i.e. point of inflection). Beyond this point, rapid deformation occurs at a much reduced load. As expected, the critical collapse depth increases as the perturbation magnitude is reduced. Like the Method 2 analyses, post-collapse results for Method 1 models seeded with imperfections smaller than 1/8 inches could not be obtained. For this reason, the “near perfect” curve in Figure 42 terminates in the vicinity of the collapse depth.

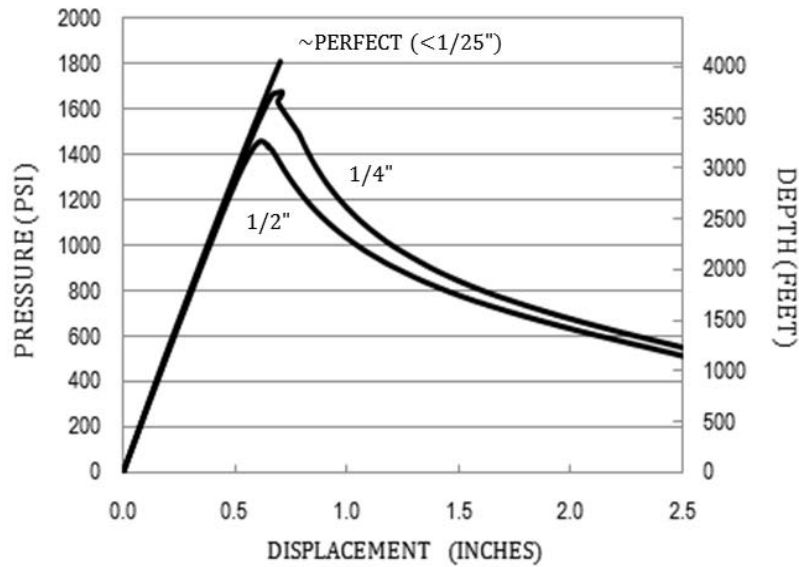


Figure 42. OOF effects on collapse depth (Method 1, Design A)

DESIGN B

Analysis	Structure Weight (lbm)	P_c^Y / P_d	P_c^{LB} / P_d	Depth of First Yield (feet) ⁵²	Collapse Depth (feet)	Mode of Failure
Analytical	42,401	1.32	2.69	3,300	Not Calculated	Shell Yield
Numerical		1.24	2.71	3,099	3,523	Shell Yield

Table 6. Design B analysis results

The numerical results are summarized in Table 6. The *STATIC, GENERAL analysis performed at 2,500 feet showed that the maximum stress occurred on a pressure hull shell element, adjacent to the fourth frame in span three. The Von Mises stress for this element is 64,332 psi, slightly larger than the “near-frame” stress of 60,603 psi calculated by equation (15) in the FFSOR. Subsequent analysis at depths deeper than 2,500 feet showed that first yield would occur at a shell element adjacent to the same frame. The depth at which this element begins to yield is 3,099 feet, approximately 200 feet shallower than that predicted by the FFSOR.

⁵² Von Mises stress, “near-frame” results (equation 15). It should be mentioned that the FFSOR assumes the shell plating will yield at mid-bay, and uses equation (16) to optimize scantlings.

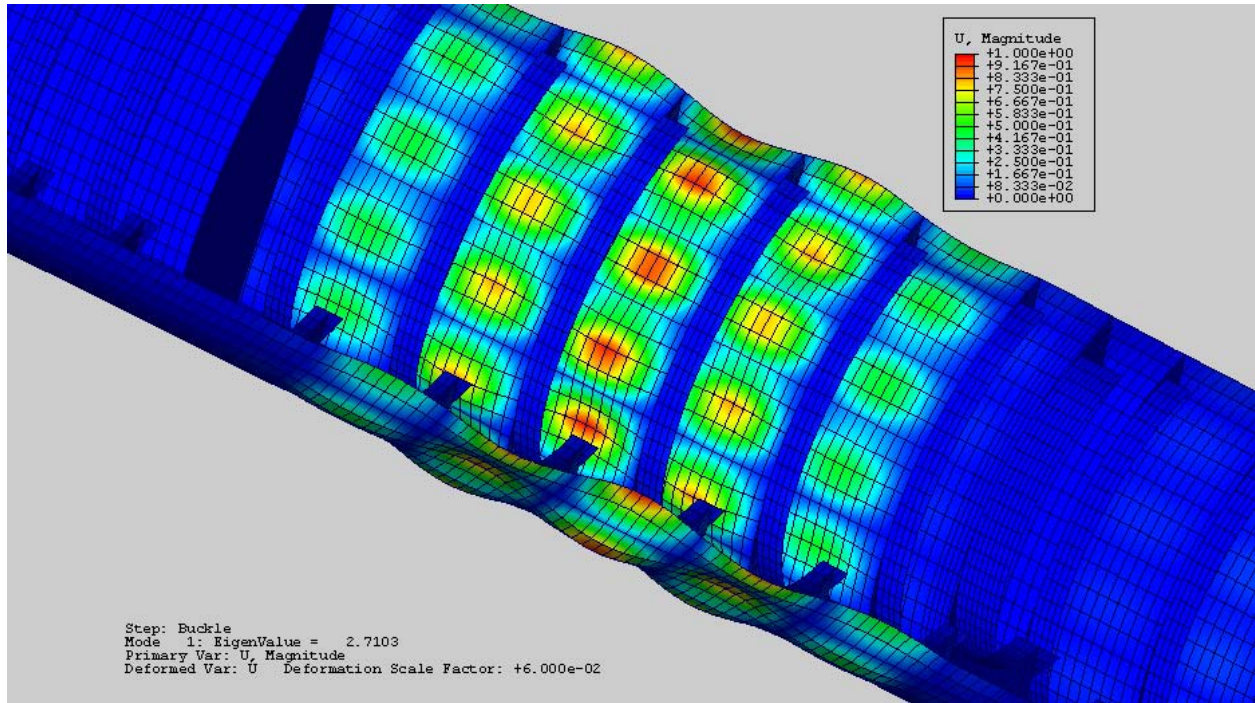


Figure 43. ABAQUS™ *BUCKLE analysis results (Displacement, U), Mode 1, Design B (Note: legend in Pascals)

A sectional view of the field output obtained from the *BUCKLE analysis can be seen in Figure 43. The results depict a classic example of lobar buckling (mode: $m = 1, n = 9$). It can be seen from the figure that the shell buckling is greatest in the compartment's middlemost bay, and diminishes at bays closer to the king frame and bulkhead. The depth at which this mode of buckling occurs is 6,775 feet, and is larger than the depth predicted by the FFSOR (5,800 feet). This discrepancy is most likely due to the different boundary conditions used by each analysis. As mentioned earlier, equation (22) was derived assuming the cylindrical shell was simply supported at each end (SS-SS). This assumption was necessary to obtain a solution based on the Donnell stability equations in the uncoupled form. The ABAQUS™ solution however, is based on shell elements that are joined at the frame web. This boundary condition is best characterized as clamped-clamped (C-C). For a general investigation of cylinder end conditions, including C-C, the *coupled* form of the Donnell stability equations must be used. Such an analysis has been outlined by Brush [16], where the critical buckling pressures for a cylinder subject to eight sets of boundary conditions have been tabulated. Extrapolating these results shows that a cylinder with dimensions similar to that of the frame bays in Design B will have a critical buckling load 2.69 times greater than the applied external hydrostatic pressure⁵³. Like the numerical analysis,

⁵³ The results of reference [41] were extrapolated as follows: The cylinder examined in reference [41] has the following dimensions: radius = a , thickness = h and length = L , where $a/h = 100$ and $L/a = 1$. The frame bays in Design B have dimensions: $a/h \approx 50$. For a given value of h , reducing a by one-half doubles the ratio of L/a . Thus, to correct the table for $a/h = 50$, one must enter the table with L/a values twice that of the actual design. Equation (22) assumes $w = w_{,xx} = u = N_{x\theta} = 0$, whereas the C-C boundary condition assumes $w = w_{,xx} = u = v = 0$. The critical pressures for each of these boundary conditions differ by a factor of 1.16. Thus, the analytical solution for lobar buckling in a single frame bay, for Design B, is equal to 1.16 times the SS-SS solution ($2.32 \times 1.16 = 2.69$).

the analytical solution for the C-C boundary conditions gives nine circumferential waves (i.e. $n = 9$). Thus, the numerical and analytical results for lobar buckling are in agreement for the case of perfect geometry.

Results from the *STATIC, RIKS analysis show that Design B will collapse at a depth just greater than 3,523 feet. Of the two imperfection shapes considered, the primary buckling mode shape (i.e. Method 2) proved to be the most limiting for this design. Figure 44 graphically displays the results. Again, the pressure hull's collapse depth is taken as the deepest depth at which an equilibrium solution could be obtained. This value appears as the highest load on each of the displacement curves. Introducing the imperfection as an axisymmetric perturbation in the shell (i.e. Method 1) resulted in a collapse depth of 3,764 feet, slightly larger than the depth of first yield (mid-bay, equation (16)) predicted by the FFSOR ($2,500 \times 1.5 = 3,750$). Figure 44 also highlights the significance of the imperfection shape. Close examination of each graph shows that the pressure hull can tolerate an axisymmetric imperfection of 1/2 inch (at 2500 feet), whereas an imperfection (OOF) of only 1/8 inch can be tolerated in the primary buckling mode shape.

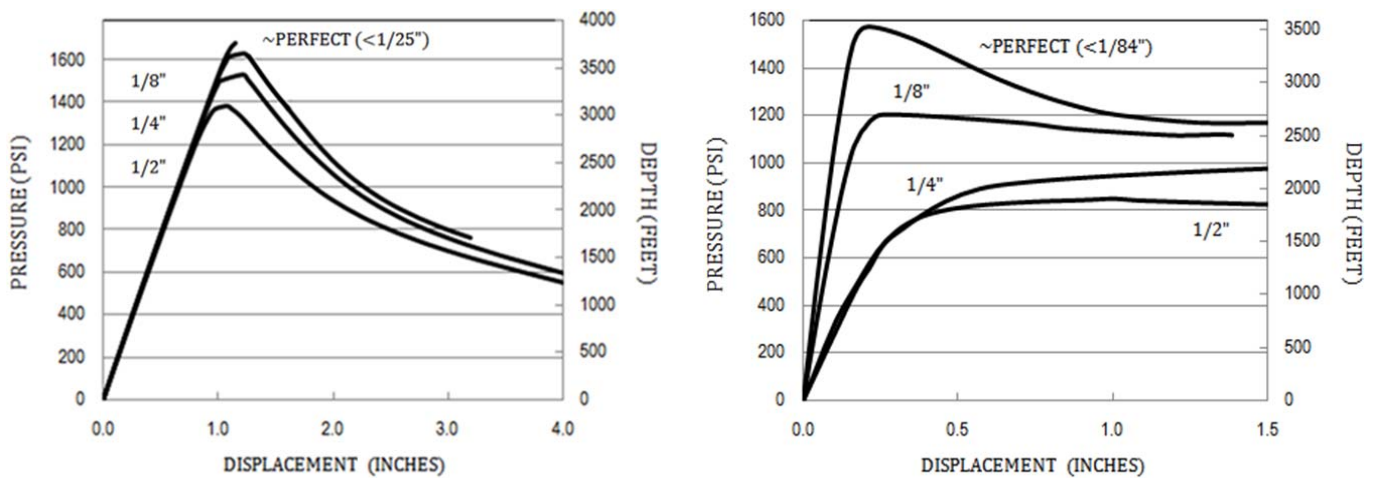


Figure 44. OOF effects on collapse depth. (a) Method 1, Design B, (b) Method 2, Design B

A visual representation of the Von Mises stress at the collapse depth for Method 2 can be seen in Figure 45, where warm colors indicate the regions of higher stress and purple elements are actively yielding. As expected, the most highly stressed areas are at mid-bay between each frame, and just below the end-cap crowns. Clearly, the influence of the perturbation shape can be seen despite the small magnitude used (i.e. Method 2: 1/84 inches). For this reason, perturbations of this shape will most likely result in elastic-plastic buckling (Figure 46). However, frame bays far from the perturbation exhibit axisymmetric yielding at the shell, mid-bay (See the lower portion of Figure 45). In the absence of any imperfections, the pressure hull in these regions will likely fail in the classical manner for shell yield. Seeding the imperfection axisymmetrically (i.e. Method 1) gave numerical results congruent with this reasoning. A visual representation of the failed pressure hull using Method 1 can be seen in Figures 47 and 48.

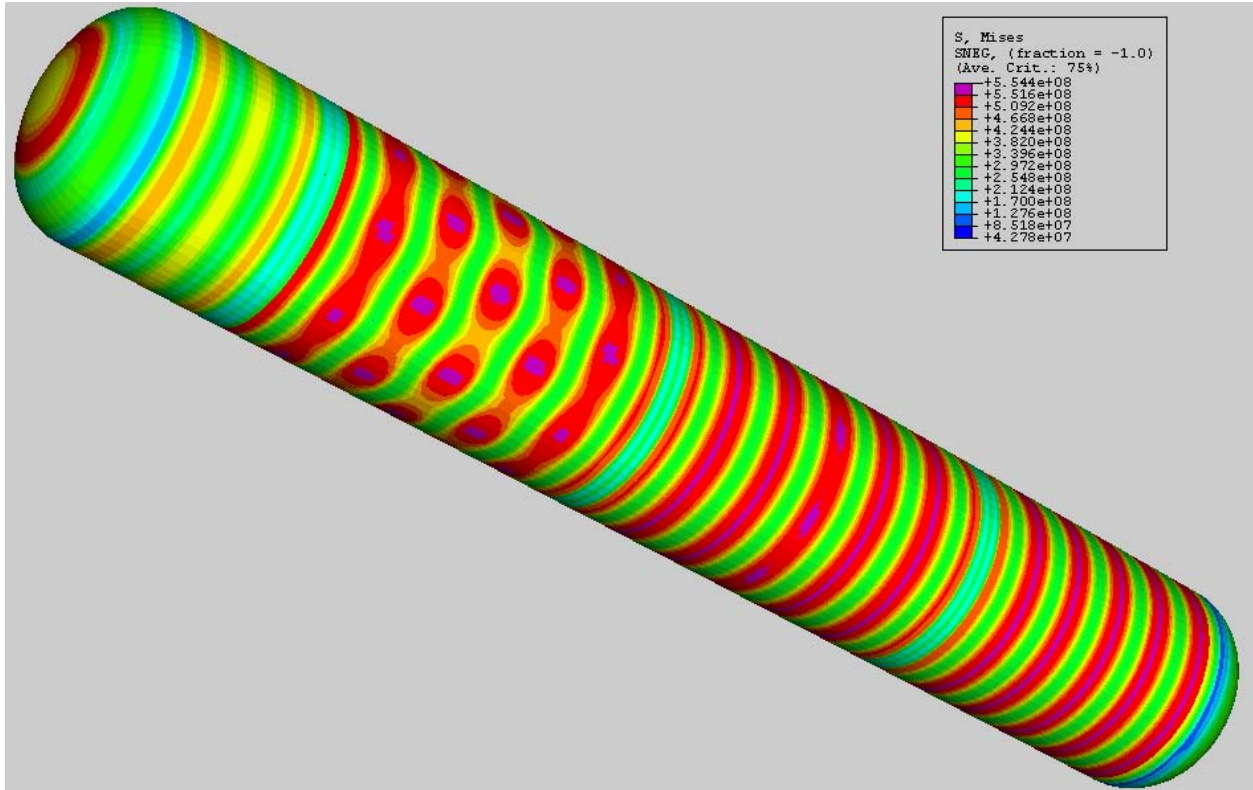


Figure 45. Von Mises stress at collapse depth (Method 2, Design B, Note: legend in Pascals)

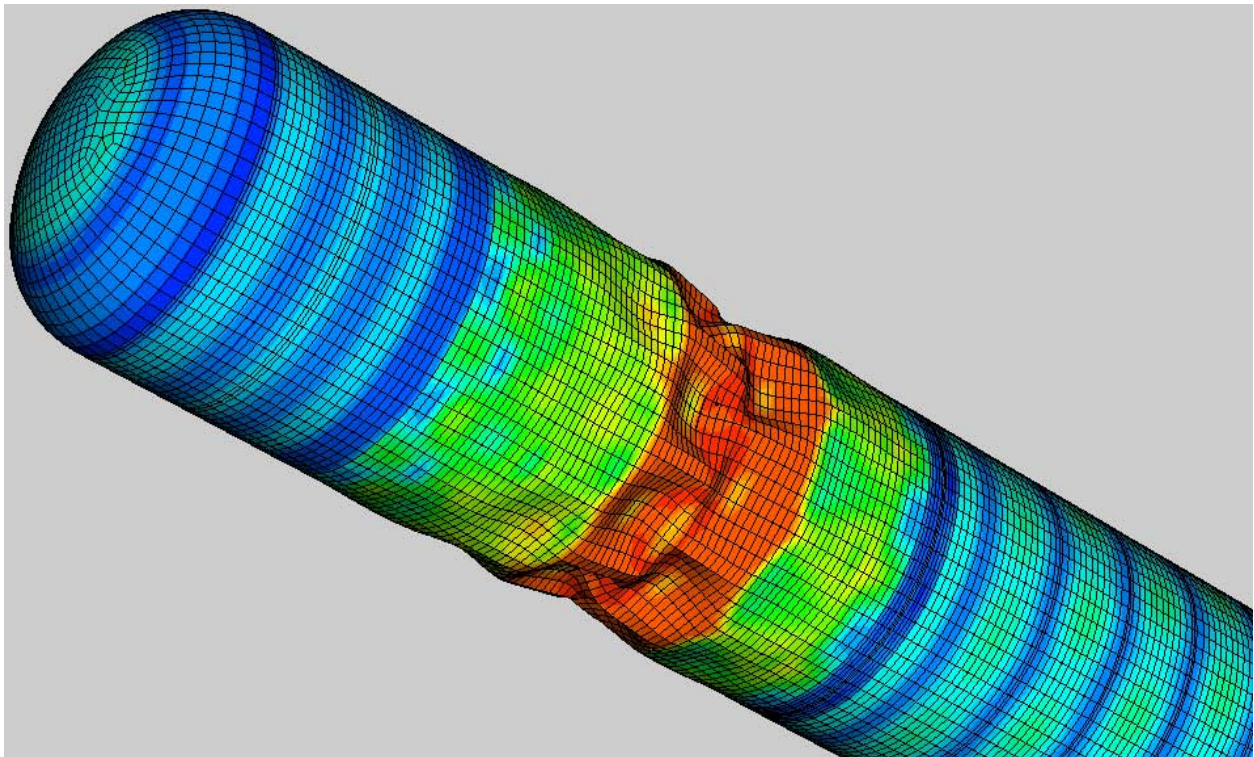


Figure 46. Deformed geometry – Post failure (Method 2, Design B)

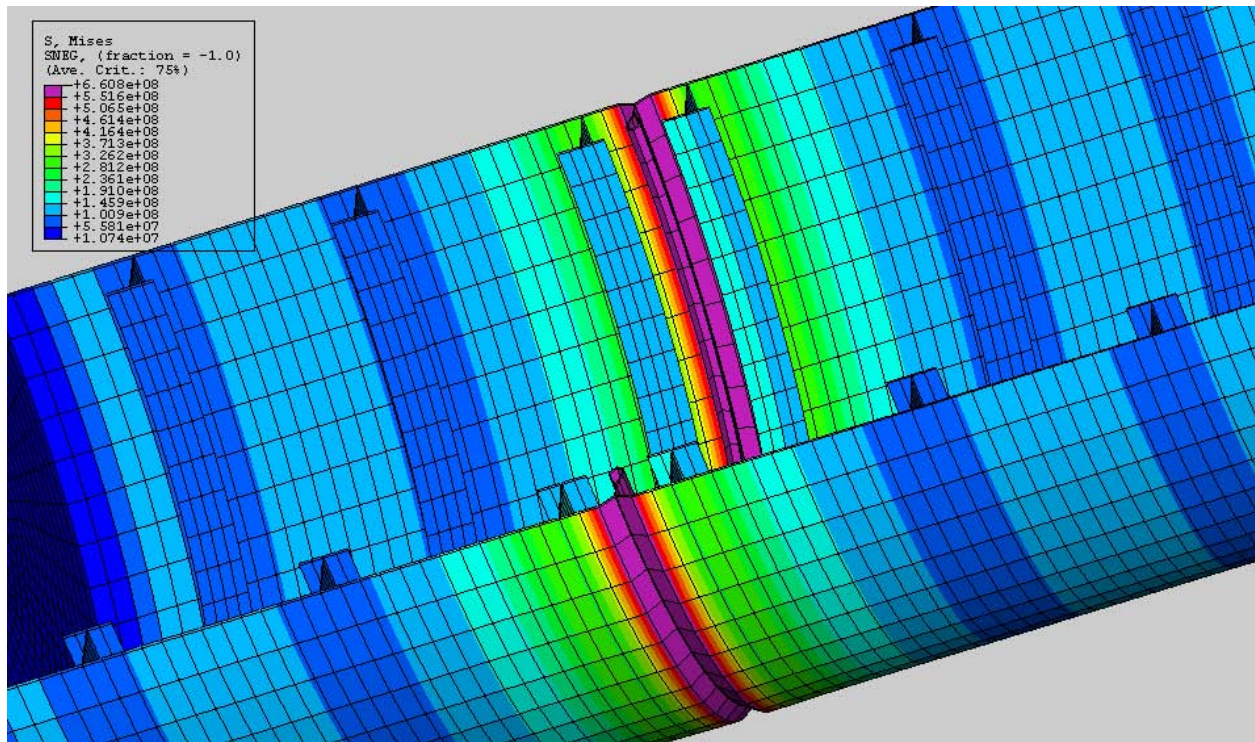


Figure 47. Deformed geometry – Post failure (Method 1, Design B, Note: legend in Pascals)

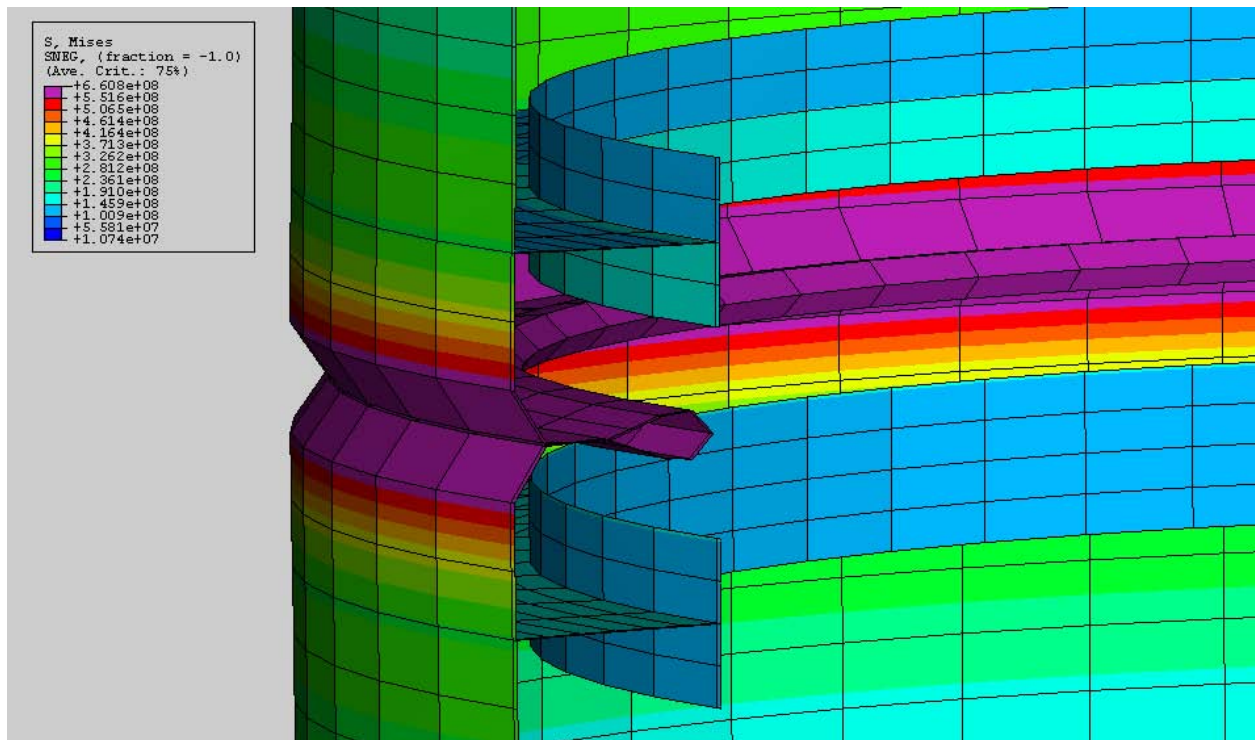


Figure 48. Deformed geometry – Post failure (Method 2, Design B, Note: legend in Pascals)

2.4.5.4.3 PRESSURE HULL DESIGN EVALUATION AND COMPARISON

It is behooving to compare the design results produced by the FFSOR with that of other optimization programs. A new program being developed by GRC Ltd., *Paramarine*^{TM54}, is well suited for such a comparison. *Paramarine*TM was initially developed in accordance with UK MoD standards, and contains a scantling optimization tool that runs the MNSTR script. However, it should be mentioned that the results of the FFSOR and *Paramarine*TM should not be compared directly⁵⁵. This is because the safety factors recommended by each are unique to the equations in which they use (See Table 7). In addition, the two programs optimize based on different criteria. While both optimization routines attempt to produce the lowest weight design that will satisfy all safety factors, *Paramarine*TM does so independently of failure mode, whereas the FFSOR considers only those designs that will fail first by shell yield.

Failure Mode	FFSOR (JACKSON [15])	<i>Paramarine</i> TM (UK MoD UNCLASS [20])
Shell Yield	1.50	1.6
Lobar Buckling	2.25	1.5
General Instability	3.75	1.8
Frame Yield	1.50	1.6
Frame Instability	1.80	2.0
King Frame Yield	1.50	1.6
King Frame Instability	2.25	2.0

Table 7. Safety factors

The *Paramarine*TM models for both Design A and Design B can be seen in Figures 49 and 50, respectively. In each of the two graphics the yellow frames indicate the pressure hull span that was optimized, and the green planes highlight the locations in which a bulkhead or king frame was placed. The results are tabulated in Tables 8 and 9. The results for both designs show that the lightest scantlings are those with the smallest frame spacing (i.e. 12 inches). In general, the opposite is true, and weight will increase as the number of frames increases. In this case, the dominant parameter is shell thickness. While the shell thickness is reasonably sized for designs with small frame spacing, *Paramarine*TM gives undesirable results when the frame spacing is large (i.e. $t_s \approx 2 - 3$ inches). Without closely examining the optimization programming that *Paramarine*TM uses, it is difficult to determine the factors that are producing these results. However, it is reasoned that the large shell thicknesses associated with large frame spacing are tied to the calculations for general instability. This conclusion is drawn from the observation that, in every case, *Paramarine*TM has produced an optimal solution that makes general instability the

⁵⁴ Graphics Research Corporation Ltd., *Paramarine*TM Version 5.0.1.

⁵⁵ One method of capturing the true difference between their results is to remove the problem's dependency on safety factors and consider a pressure vessel with perfect geometry. This can be done by using the FFSOR and *Paramarine*TM to analyze a predefined design, while matching the safety factors (e.g. $1 = SF_1 = SF_2 = SF_n$) and setting the eccentricities equal to zero. The two results should then correspond to a single design failing in the same mode, where the only difference is the depth at which failure occurs.

primary mode of failure⁵⁶. Although *this* result is not fully understood, the dependency of general instability on shell thickness is congruent with GRC documentation. *Paramarine*TM defines general instability as the lesser of two critical pressures; (1) the pressure to cause the onset of yielding in the frame flange, and (2) the pressure to cause the onset of yielding in the shell plating in way of the frame. For each set of design parameters, the optimal scantlings produced by *Paramarine*TM are limited by the first of these two pressures. According to the GRC PRSHUL/MNSTR L Systems Specification Document, the MNSTR L program precludes premature failure due to yielding at the frame flange (i.e. general instability) by increasing the shell thickness⁵⁷.

Other contributing factors that may be driving the larger shell thicknesses include: (1) excessive eccentricity, and (2) over conservative safety factors. Because the bending stresses used to calculate the aforementioned pressures are strong functions of the eccentricity, care needs to be taken when choosing a representative OOR. Within MoD standards, the OOR is typically set at 0.5% of the radius for pressure hulls with diameters between 23 and 40 feet, and approximately 1% for smaller diameter hulls. For the pressure hull in consideration (i.e. Designs A & B; Diameter = 83 inches), setting the OOR = 0.5 inches may be too conservative. In addition, the *Paramarine*TM default safety factor for lobar buckling (1.5) appears to be over conservative. Unlike the calculations for general instability, *Paramarine*TM uses an empirical design curve to calculate the critical pressure for lobar buckling. This curve assumes eccentricities $\leq 0.5\%$ are already present, and is automatically corrected for cases when eccentricity exceeds 0.5%. For this reason, applying an additional safety factor of 1.5 may be unnecessary given the simplicity of this design (i.e. Design A & B). Reducing the *Paramarine*TM inputs for both eccentricity and the lobar buckling safety factor produced results which were in closer agreement with the FFSOR.

⁵⁶ Because general instability is highly susceptible to geometry imperfections, optimizing a design to this mode of failure is normally not done.

⁵⁷ In general, modifications to shell thickness are less intrusive than modifications to the frame dimensions. This is because the frame scantlings, including flange thickness, are constrained by both the frame stability parameters ($F1$, $F2$ & $F3$) and the Faulkner optimization algorithm (used by MNSTR L).

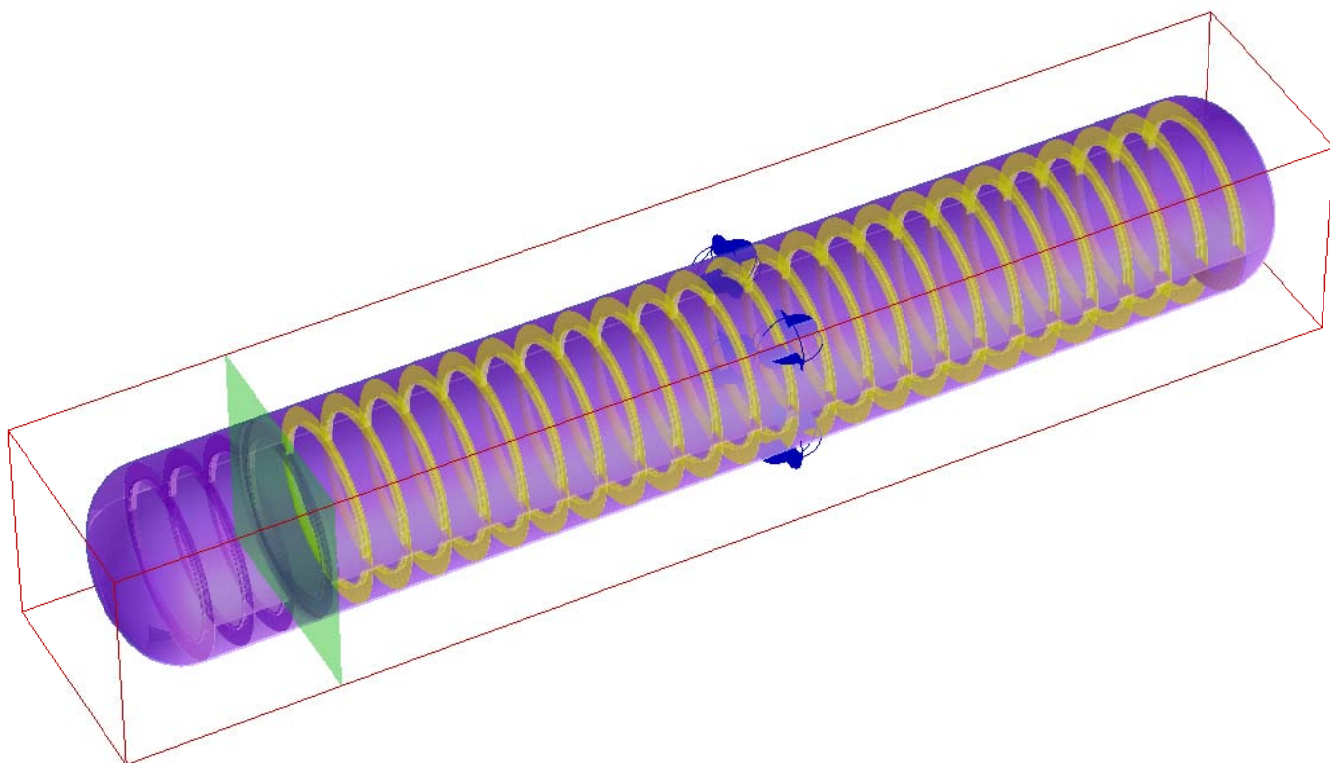


Figure 49. *Paramarine*TM model (Design A)

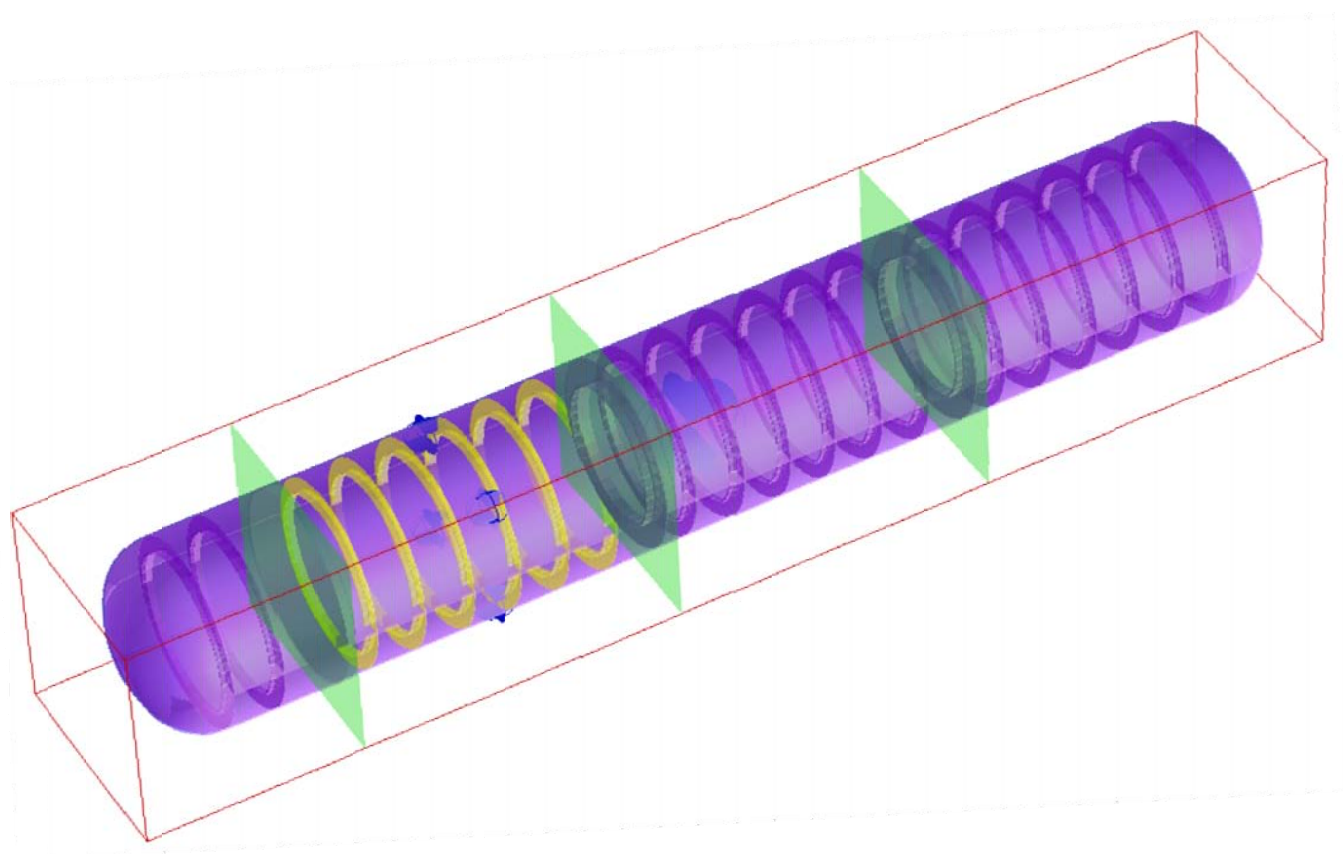


Figure 50. *Paramarine*TM model (Design B)

L_f (inches)	t_s (inches)	h_w (inches)	t_w (inches)	h_{rl} (inches)	t_{rl} (inches)	No of Frames	Compartment Weight (lbm)	Interframe Collapse (P_c/P_d)	Longitudinal (Shell) Yield (P_{ct}/P_d)	Overall Collapse (P_f/P_d)	Frame Tripping (P_{st}/P_d)
12	0.9251	6.4659	0.3195	3.6893	0.6977	33	37,721	2.24	1.62	1.80	5.05
13	0.9770	6.5966	0.3259	3.2569	0.7963	31	38,861	2.29	1.69	1.80	4.85
14	1.0214	6.0524	0.2866	4.0668	0.7588	29	39,759	2.31	1.75	1.81	4.56
15	1.0406	6.6660	0.3166	3.6654	0.7739	27	39,882	2.29	1.74	1.81	4.72
16	1.0718	6.6007	0.3218	3.7250	0.7865	25	40,367	2.29	1.77	1.81	5.04
17	1.0425	6.8778	0.3267	3.7819	0.7985	23	39,128	2.14	1.64	1.81	4.73
18	1.1310	7.1557	0.3536	3.5329	0.7721	22	41,427	2.31	1.85	1.80	5.40
19	2.0005	5.0899	0.2573	3.8738	0.7076	21	65,317	4.33	5.00	1.81	8.13
20	1.1324	6.9794	0.3402	3.4132	0.9192	20	41,113	2.19	1.78	1.81	4.97
21	2.6121	4.8340	0.2443	3.5746	0.6606	19	81,943	5.53	7.42	1.80	10.49
22	2.2700	5.2799	0.2669	4.0184	0.6697	18	72,437	4.81	5.82	1.80	9.21
23	2.3604	5.3389	0.2699	3.6735	0.7422	17	74,862	4.98	6.08	1.82	9.17
24	2.5586	5.3926	0.2728	3.7212	0.6852	16	80,180	5.37	6.84	1.81	10.20
25	2.3653	5.0493	0.2756	4.1447	0.7578	16	75,121	4.95	5.90	1.80	10.45
26	2.6163	5.2298	0.2783	3.7879	0.7653	15	81,898	5.46	6.85	1.83	10.90
27	2.8079	5.0154	0.2631	3.9633	0.7235	15	87,247	5.84	7.62	1.80	11.31
28	3.0067	5.1944	0.2655	3.9995	0.6666	14	92,534	6.24	8.40	1.81	11.85
29	2.7493	5.3781	0.2652	4.3013	0.7169	14	85,559	5.68	7.18	1.83	9.57
30	3.0268	5.4203	0.2671	3.9080	0.7223	13	93,018	6.25	8.30	1.82	10.60
31	2.7893	5.4685	0.2696	4.3736	0.7289	13	86,544	5.73	7.22	1.81	9.58
32	2.7268	5.6462	0.2931	3.9987	0.8061	12	84,622	5.58	6.89	1.80	10.41
33	2.8835	5.5510	0.2735	4.4380	0.7397	12	89,045	5.90	7.47	1.81	9.73
34	2.6530	5.5963	0.2976	4.4758	0.8184	11	82,505	5.38	6.45	1.82	10.38
35	2.5165	5.9298	0.2998	4.5130	0.8243	11	78,666	5.07	5.90	1.82	8.92
36	2.6448	5.8224	0.3019	4.5402	0.8302	11	82,380	5.33	6.33	1.83	9.74

Table 8. *Paramarine*TM (MNSTR) optimization results for $L_b = 34.89$ feet (i.e. Design A).⁵⁸

⁵⁸ *Paramarine* input parameters: Eccentricity (e) = 0.5 inches. Maximum mode number (n) = 5. Safety Factors: *Paramarine*TM defaults (UK MoD UNCLASS). $R = 41.5$ inches. (Note: P_c , P_{ct} , P_f and P_{st} are critical failure pressures used by *Paramarine*TM, and P_d is the pressure at design collapse depth (2,500 feet). Tabulated values for compartment weight and number of frames were calculated outside of *Paramarine*TM. Compartment weight does not include bulkhead weight.)

L_f (inches)	t_s (inches)	h_w (inches)	t_w (inches)	h_{rl} (inches)	t_{rl} (inches)	No of Frames	Compartment Weight (lbm)	Interframe Collapse (P_c/P_d)	Longitudinal (Shell) Yield (P_{ct}/P_d)	Overall Collapse (P_f/P_d)	Frame Tripping (P_{st}/P_d)
12	0.9251	6.3043	0.2995	3.4665	0.7319	11	12,730	2.22	1.64	1.81	4.51
13	0.9770	6.2277	0.3018	3.2840	0.7981	11	13,315	2.27	1.72	1.80	4.63
14	0.9946	6.5520	0.3112	3.1220	0.8408	10	13,299	2.23	1.69	1.81	4.38
15	1.0406	6.4950	0.3166	3.1764	0.8554	9	13,543	2.28	1.76	1.82	4.71
16	1.0718	6.2396	0.2998	3.9285	0.7324	8	13,560	2.28	1.82	1.80	4.94
17	1.0425	6.7015	0.3267	3.2773	0.8826	8	13,407	2.13	1.66	1.82	4.73
18	1.7087	4.8960	0.2538	3.8218	0.6981	7	19,424	3.72	4.03	1.80	7.66
19	1.7217	5.0899	0.2573	3.8738	0.7076	7	19,609	3.72	3.97	1.82	7.26
20	2.2119	4.7754	0.2413	3.5313	0.6526	7	24,282	4.70	5.96	1.80	9.21
21	1.9893	5.0884	0.2450	3.9719	0.6620	6	21,985	4.22	4.90	1.82	7.42
22	2.0217	5.0159	0.2669	4.0102	0.6684	6	22,366	4.26	4.94	1.80	9.40
23	2.0850	5.0720	0.2499	4.0550	0.6758	6	22,992	4.37	5.12	1.81	7.98
24	2.0118	5.3960	0.2728	4.1068	0.6845	5	22,089	4.19	4.72	1.82	8.31
25	1.7654	5.5877	0.2756	4.1532	0.7578	5	19,726	3.56	3.73	1.80	6.82
26	2.2523	5.5051	0.2783	3.7879	0.6983	5	24,460	4.66	5.56	1.81	9.13
27	2.0160	5.1405	0.2809	4.2295	0.7725	5	22,266	4.13	4.55	1.80	9.23
28	2.5776	5.0612	0.2625	3.8412	0.7099	5	27,662	5.31	6.77	1.80	10.50
29	2.2859	5.3746	0.2656	4.3057	0.7176	4	24,621	4.67	5.50	1.82	8.35
30	2.5278	5.4203	0.2671	3.9080	0.7223	4	26,966	5.17	6.44	1.80	9.19
31	2.4679	5.6087	0.2908	3.9581	0.7297	4	26,429	5.03	6.12	1.81	10.14
32	2.1532	5.3708	0.2931	4.4040	0.8061	4	23,443	4.28	4.84	1.81	9.50
33	2.2707	5.6971	0.2743	4.4471	0.7412	4	24,544	4.54	5.29	1.80	7.73
34	1.9999	5.8869	0.2976	4.4804	0.8184	4	21,965	3.82	4.24	1.82	7.63
35	2.0996	5.7815	0.2998	4.5084	0.8243	4	22,975	4.03	4.56	1.82	8.30
36	1.9073	5.6731	0.3019	4.9809	0.8302	3	20,786	3.54	3.88	1.81	7.97

Table 9. *Paramarine*TM (MNSTR) optimization results for $L_b = 12$ feet (i.e. Design B).⁵⁹

⁵⁹ Paramarine input parameters: Eccentricity (e) = 0.5 inches. Maximum mode number (n) = 5. Safety Factors: *Paramarine*TM defaults (UK MoD UNCLASS). $R = 41.5$ inches. (Note: P_c , P_{ct} , P_f and P_{st} are critical failure pressures used by *Paramarine*TM, and P_d is the pressure at design collapse depth (2,500 feet). Tabulated values for compartment weight and number of frames were calculated outside of *Paramarine*TM. Compartment weight does not include bulkhead weight.)

2.4.5.5 LSRC PRESSURE HULL SELECTION

The results of this analysis suggest that Design B (i.e. designs utilizing king frames) will be the most efficient pressure hull design for the LSRC. The performance of both designs is displayed graphically in Figures 51 through 53⁶⁰. Figure 51 is frequently used to illustrate the regimes in which a pressure hull's shell will fail. The graph is composed of three separate curves. When combined, Figure 51 may be used to estimate the critical pressure, and mode of shell failure, as a function of the unsupported length between frames. This graph assumes that the hull diameter and shell thickness remain constant, and that the frames at either end of the frame bay take no real load as the frame spacing becomes small (i.e. it is assumed that the frames merely maintain hull circularity). When the frame spacing is close, the shell is expected to fail by axisymmetric yielding. The load at which this mode of failure occurs can be estimated by the simple hoop stress formula. When the frame spacing is far, the collapse pressure can be estimated by Euler's formula for long thin tubes (i.e. two-lobe manner). Between these two extremes, there is a region in which the ratios of $t_s/2R_s$ and $L_f/2R_s$ are significant, and the values of each will govern the failure by lobar buckling. It is apparent from this graph that the lightest structures will fail at the bend where the hoop stress prediction intersects that of the Windenburg approximation. At this point the shell is the most fully loaded and the frame spacing is greatest. In practice, the precise intersection of these two curves is not known. It is for this reason that a safety factor is applied to the shell yield calculations (i.e. FFSOR: $SF_{SY} = 1.5$). While Design A has a collapse depth slightly deeper than Design B, Design B more fully utilizes the strength of the shell material. This difference resulted in a weight savings of approximately 1,584 lbs. While relatively small in comparison (~4%), this difference will allow for more flexibility when ballasting the LSRC for seakeeping characteristics.

A similar graph can be seen in Figure 52, where again, the leftmost curve represents failure by shell yield and the curve on the right corresponds to the upper limit for lobar buckling. Here, the pressure factor (Ψ) was plotted against the slenderness ratio (λ) for many of the models tested at the David Taylor Model Basin (DTMB), as well as most U.S. submarines built from 1940-1960. This graph is analogous to that of a simply supported beam under axial load, where the pressure factor is defined as the ratio of collapse pressure to the shell yield pressure given by the simple hoop stress formula ($\Psi = P_c/(t_s\sigma_Y/R_s)$), and the slenderness ratio for cylinders is defined as the following non-dimensional parameter:

$$\lambda = \left[\frac{(L_f - t_w)/2R_s}{(t_s/2R_s)^{3/2}} \left(\frac{\sigma_Y}{E} \right) \right]^{1/2} \quad (52)$$

Again, Design A stands out as the stronger pressure hull while Design B appears to be slightly more efficient. As expected, both designs fall within the shell yield regime. Because the frames actually carry a portion of the load, it is possible for the shell to achieve values of $\Psi > 1$ (i.e. Design A & B). This phenomenon illustrates the gains that can be made by exploiting low values of λ . This figure also shows that both Design A and Design B exhibit performance characteristics on par with other pressure hulls designed using similar methods.

⁶⁰ Figures 51 through 53 inclusive were developed from data of reference [40].

Figure 53 compares Design A and Design B to virtually all U.S. submarine types constructed prior to 1960. This plot is similar to Figure 52, but uses a modified pressure factor ϕ in place of Ψ . This parameter was first suggested by Wenk as a means of capturing the contribution made by the frames in supporting the shell. ϕ is defined as follows:

$$\phi = \frac{P_c}{\left(\frac{t_s^*}{R_s}\right) \sigma_Y} \quad (53a)$$

where,

$$t_s^* = \frac{t_s(L_f - t_w) + A_f}{(L_f - t_w)} \quad (53b)$$

Figure 53 illustrates the increasing trend in pressure hull efficiency for low values of λ . Both Design A and Design B fall at the higher end of this trend with good agreement.

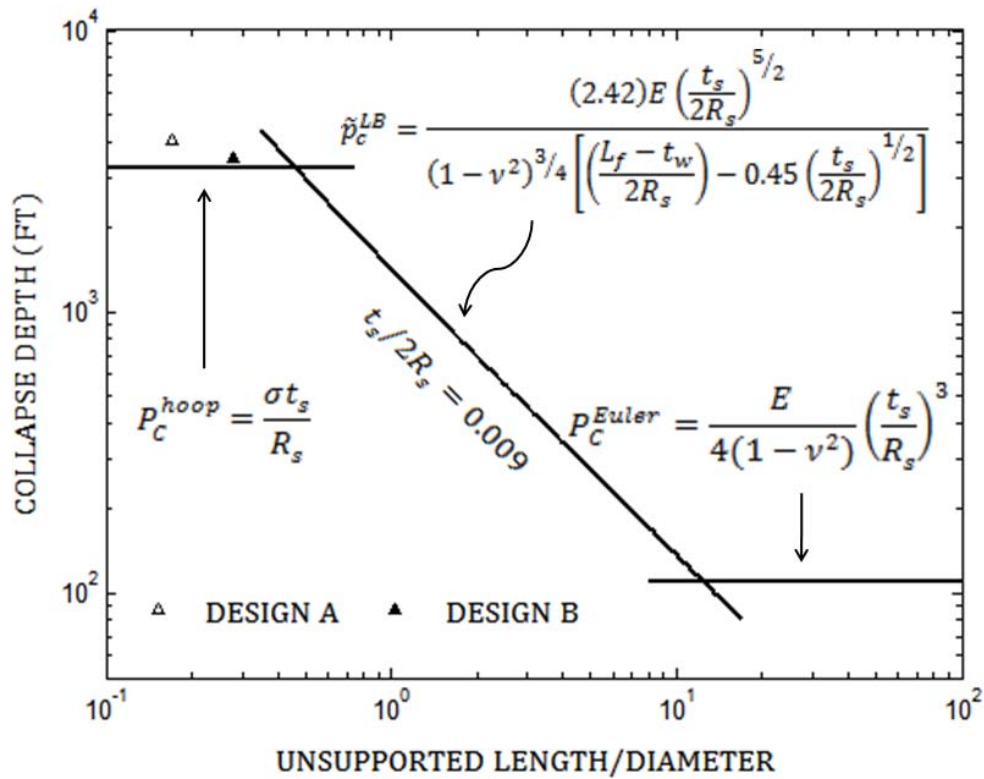


Figure 51. Shell failure regimes

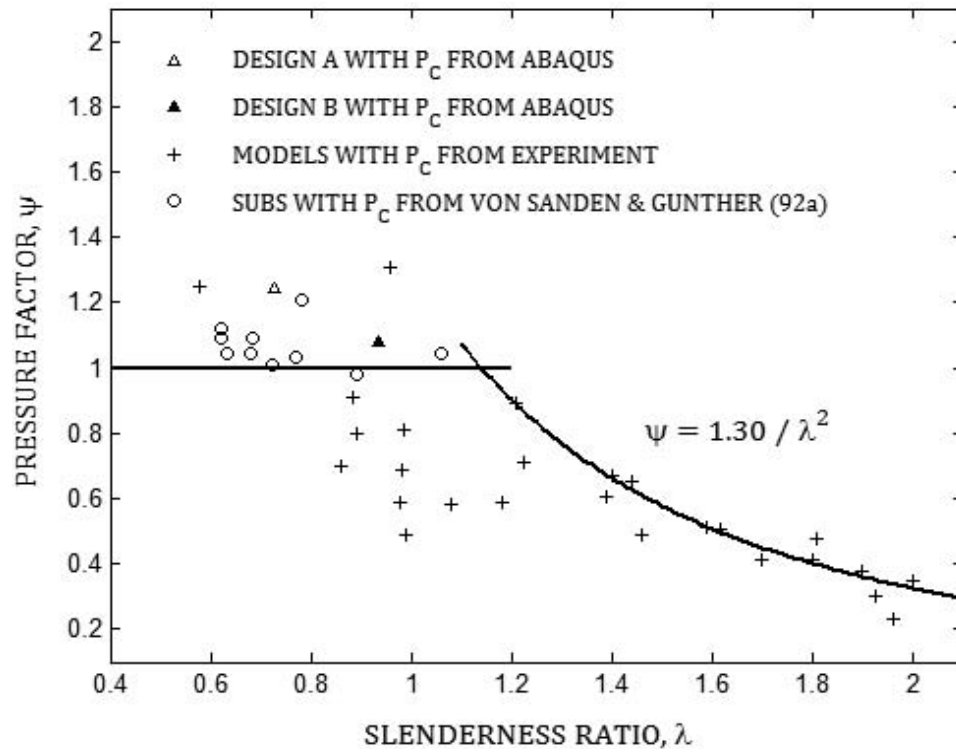


Figure 52. DTMB pressure hull data comparison

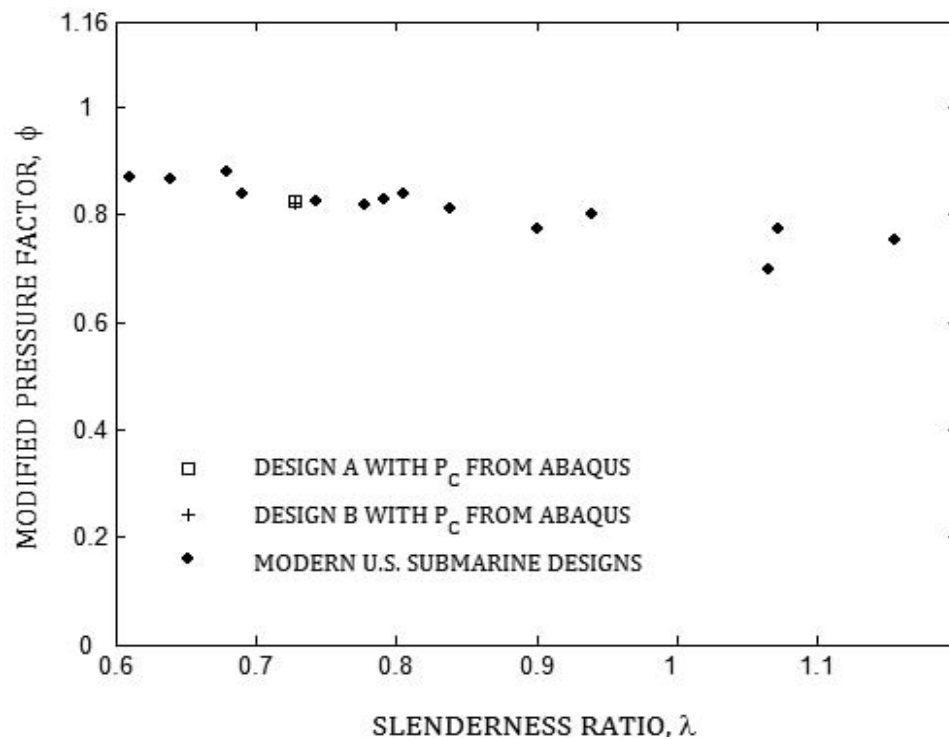


Figure 53. U.S. submarine pressure hull comparison (Prior to 1960)

In addition to comparing the LSRC designs with historical data, an effort was made to validate the designs with current NAVSEA design procedures. The results of this analysis were sent to NAVSEA 05P22 (Survivability and Structural Integrity), and were compared to those obtained using NAVSEA GAP (General Analysis Procedures) algorithms⁶¹.

While the results of the NAVSEA analysis must remain classified, some general statements can be published. Although Design B was selected as the more efficient design, its larger frame spacing makes it susceptible to multi-wave failure modes (i.e. failure modes associated with multiple modes of instability). Despite the large safety factors used, the NAVSEA analysis showed that Design B would fail prematurely at a depth shallower than 2,500 feet by multi-wave failure. Multi-wave failure modes were not considered in this paper, and the FFSOR was not designed to bar its occurrence. In addition, the NAVSEA analysis assumed an OOR of 1/2 inch and an OOF of 1/8 inches. Because neither the FFSOR nor ABAQUSTM model fully captures the combined effects of these two imperfections, similar results could not be obtained. Had a more detailed model of imperfections been used in the numerical analysis, the onset of multi-wave failure may have been observed. Like Design B, the NAVSEA analysis showed that the primary mode of failure for Design A was multi-wave failure. However, the collapse of Design A due to this mode of failure occurred at a depth slightly deeper than 2,500 feet.

Elastic analyses performed by NAVSEA were in close agreement with those obtained by the FFSOR. Again, due to the classification of the NAVSEA results the actual numbers cannot be disclosed. However, a qualitative comparison between the FFSOR results and those obtained by NAVSEA can be seen in Table 10.

Analysis	Design A (P_c/P_d)		Design B (P_c/P_d)	
	FFSOR	NAVSEA	FFSOR	NAVSEA
Shell Yield	1.506	↓	1.506	↓
Lobar Buckling	4.330	↑	2.318	↑
General Instability	8.786	↑	8.439	↑
Frame Yield	1.506	↑	1.507	↓

Table 10. FFSOR-NAVSEA qualitative comparison

Inelastic analyses performed by NAVSEA placed Design A and Design B in category one (CAT I)⁶² for general instability. Both designs were found to have critical pressures for Inelastic General Instability (IGI) at depths deeper than 2,500 feet. One area of disagreement between NAVSEA and the present analysis is the effects of OOF on collapse pressure. NAVSEA results showed that the maximum allowable OOF for Design A and Design B is ~1/7 inches and ~1/16 inches, respectively. This result suggests that the imperfection shape chosen in the ABAQUSTM analysis is not representative of the worst case shape used by NAVSEA. One final observation worth mentioning pertains to frame stresses. For both Design A and Design B, the frame stresses

⁶¹ Source Code (U.S. Navy DDS-110-2 Design Data Sheet)

⁶² Inelastic General Instability (Bond method) categories:

CAT I: Collapse between king frames

CAT II: Overall compartment collapse, including king frames

CAT III: Collapse between king frames, but influenced by non-linear behavior of the king frames

obtained using ABAQUSTM are significantly lower than those obtained using analytical procedures. Discussions with NAVSEA show similar findings. This discrepancy is common among most pressure hull analyses where frame eccentricities are not fully captured in the finite element model.

Based on weight, the results in this paper favor Design B as a valid pressure hull for the LSRC. However, in light of the results obtained by NAVSEA Design A was chosen for subsequent modeling of the concept design.

2.4.6 CONCLUSION AND RECOMMENDATIONS

In conclusion, both Designs A and B should be improved upon if they are to be considered for use in the LSRC. The results obtained by NAVSEA regarding imperfection sensitivity, multi-wave failure, and shell yield failure suggest that the actual collapse depth of the LSRC may be shallower than 2,500 feet when using the scantlings listed in Table 4. Clearly, the design procedure used in this analysis has limitations. Although the safety factors used were deemed conservative, inelastic behavior in the presence of imperfections confirms the need for a more thorough analysis. The results listed in Table 5 and 6 highlight two important outcomes of the optimization procedure outlined in this paper. First, the reader will notice that both the analytical and numerical results produce shell yield safety factors less than 1.5. Recall that the FFSOR was specifically designed to identify pressure hull designs that would *not* fail shallower than 3,750 feet (2,500 X 1.5). This outcome is a consequence of using equation (16) to determine the shell yield critical pressure. Both the analytical and numerical analyses showed that shell yield would first occur at the “near-frame” location (i.e. not at mid-bay). Because equation (16) gives close results to that of equation (14), the more limiting condition (i.e. near-frame) was overlooked. For those interested in using the procedure outlined in this paper it is suggested that equations (14) and (15) be used in place of equation (16). Second, the numerical results for Design A show that the actual collapse depth is greater than 3,750 feet (4,059 feet). This result simply implies that the pressure hull will retain some structural integrity after first yield.

Should the LSRC concept be investigated further, the structural analysis should include loads other than hydrostatic. Unlike most submersibles, the thin hull of the LSRC will be subject to significant loads when it is out of the water, both at rest while standing vertically in the missile tube, and during crane operations while being suspended with lead ballast onboard. For this reason, it may be necessary to use vertical stringers to alleviate shell loading.

Finally, a few words on *Paramarine*TM. It is not without regret that *Paramarine*TM was not used more extensively to analyze the LSRC concept. Although the MNSTR results proved undesirable for the LSRC, the structural analysis suite is perfectly suited for pressure hull design at the concept level. The pressure hull geometry is easily defined, and complex arrangements of bulkheads and stiffeners can be quickly added. *Paramarine*TM can be used to perform both elastic and inelastic analysis of the pressure hull compartments and end-caps. In addition, *Paramarine*TM version 6.0 (not yet released) is expected to be compatible with ABAQUSTM software. While this software is still under development, it is a powerful tool for anyone interested in pressure hull design.

2.5 STABILITY AND SEAKEEPING

2.5.1 WEIGHT DISTRIBUTION

A great deal of attention was given to accurately calculating the mass distribution of the LSRC. To accomplish this, the entire design was modeled in SolidWorks. As each component was created, careful attention was given to assigning the correct material type and dimension. Components too complicated to model at this stage of design, or equipment planned for COTS procurement, were modeled with the appropriate dimensions and given a density that would yield a predetermined weight. For example, the exact design of the submarine-LSRC access hatch is not known. Therefore, a model of the hatch was created with enough detail to convey the concept and was assigned a density that would allocate 800 pounds for the actual design. Upon completing the model, all mass properties, including moments of inertia, were obtained for subsequent stability analysis. The results are tabulated below (See Table 11).

Ship Characteristic	Initial Design	Modified Design
LOA (feet)	43.3	43.3
Weight (lbm)	92,256	96,595
Fixed Ballast (lbm)	18,388	23,899
\overline{KG} (feet)	19.6	18
\overline{BG} (inches)	2.6	31.6
Freeboard to upper hatch (feet)	3.6	1.8
Draft (feet)	39.2	41.0
Submerged Buoyancy (lbm)	7,855	3,516

Table 11. LSRC mass distribution data

2.5.2 STATIC STABILITY

Ship Characteristic	Modified Design
Displacement (Δ) (long-ton)	43.1
Displacement (∇) (feet ³)	1,534
Immersion (lbm/inch)	197
KM (feet)	21
KB (feet)	20.9
GM (inches)	35

Table 12. Static stability characteristics

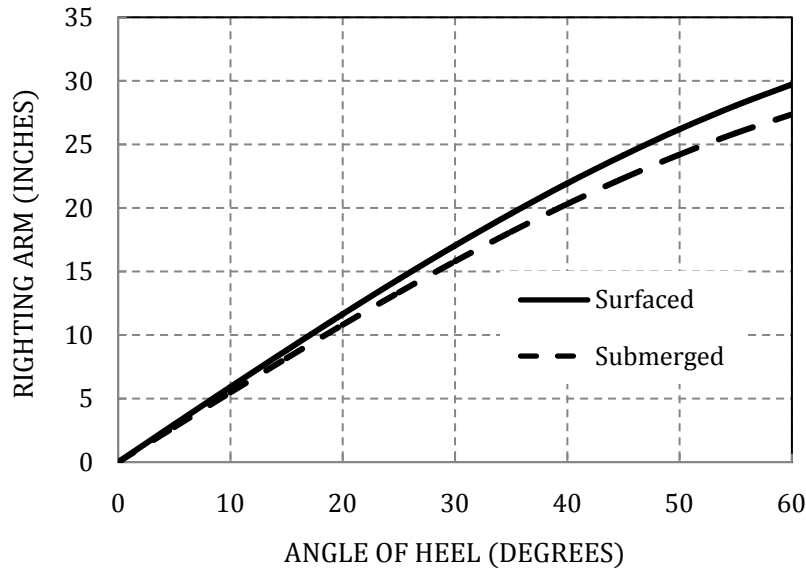


Figure 54. Range of surfaced and submerged stability (LSRC modified design)

As expected, the LSRC's mass distribution results in poor inherent stability. This is evident from the low values of \overline{BG} , \overline{GM} and \overline{GZ} shown in Tables 11 and 12, and Figure 54. In general, cylindrical spar buoys should have \overline{KG} values that are approximately 25% of the draft. Static stability can be improved by increasing \overline{BG} . As \overline{BG} increases, so will the righting moment in pitch and roll⁶³. The righting moment can be determined by simply multiplying the righting arm (\overline{GZ}) by the buoyant force (F_B) (Surfaced: $F_B = \Delta$, Submerged: $F_B = \nabla\rho$). In an effort to improve the capsule's stability the following modifications were made to the original LSRC design:

- (1) Hull insulation was removed. Hull insulation accounts for 1,216 pounds, most of which is located above the center of buoyancy. To increase \overline{BG} this weight was reallocated to fixed ballast⁶⁴.
- (2) Batteries were relocated to the bottom of the capsule, just above the dewatering system sump (bilge). Batteries account for 800 pounds of the LSRC's total weight. In an effort to shield the batteries from seawater, this weight was placed at the uppermost end of the inner compartment (i.e. dry zone); this weight falls above the center of buoyancy. Additional measures should be made to ensure the battery remains dry if it is placed at the lower end of the capsule.

⁶³ Note: A large value of \overline{BG} does not ensure dynamic stability. It can be shown that the pitch and roll motions of a slender spar buoy are resonant unless the centers of gravity and buoyancy coincide [25].

⁶⁴ This decision should be revisited. When the 33 survivors of the *USS SQUALUS* were interviewed following their rescue, cold air temperature was identified as one of their greatest hardships. This contrasts with the results obtained onboard the *USS DALLAS* during SURVIVEX 2003 where air temperatures rose nearly 10° F over three days [34]. This discrepancy may be due to the special hull treatment (SHT) used onboard the modern submarines.

- (3) LOX tanks were relocated to outboard location near the tenth row of seating. These tanks were originally placed in the command chamber so that oxygen bleeds could be controlled directly by the senior survivor. However, relocating this weight (450 pounds) to the opposite end of the capsule will improve \overline{BG} .
- (4) The freeboard to upper hatch was reduced by 50%. This modification allowed for an additional 5,511 pounds of fixed ballast. The freeboard reduction will have its greatest impact on the LSRC's ventilation system. Such a low freeboard will preclude the crew's ability to ventilate by opening the upper hatch, and may require that an extendable snorkel device be used.

The above modifications improved \overline{BG} by 29 inches. This resulted in a final \overline{BG} of just under three feet. However, this value is still too small to be relied upon for stability. Additional improvements could be made by relocating potable water and CO₂ absorbents until needed, or by reducing crew seating in rows 1-5. Other options include:

- (1) Affixing appendages to the outer hull that will improve stability during the accent phase and while at the surface.
- (2) Install inflatable bags at the upper end of the capsule. This will increase the water plane area and would allow for additional weight to be added at the keel.
- (3) Design an extension mechanism at the keel that would lock the fixed ballast in a lower position upon ejection from the MMT.

In conclusion, the surfaced and submerged static stability characteristics must be improved. It will be shown in the next section that such improvements will also result in better seakeeping characteristics. At present, these results represent the most significant technical obstacle to implementing the LSRC concept.

2.5.3 DYNAMIC STABILITY

Upon reaching the surface, the LSRC will be subject to the relentless motions of the sea. Like all sea-faring vessels, the dynamic stability of the LSRC should be understood. This is especially true for floating structures that are not under power. Good “seakeeping” characteristics are necessary to ensure that the vessel will operate as intended, and that the crew will perform as expected without injury. The geometry of the LSRC is typically referred to as a “vertical spar buoy”. Axisymmetric bodies such as the spar buoy will exhibit a resonance response that is inversely proportional to the exciting force. For this reason, spar buoys will experience large resonant responses, in a highly-tuned manner [25]. The seakeeping analysis presented in this paper is aimed at assessing the LSRC’s free response to sea states three and four. No appendages will be added to mitigate undesirable responses, and any such modifications are left for follow-on designs.

The first step in understanding how a vessel will respond in the open ocean is to characterize the environment. Because the ocean’s surface is irregular, and apparently completely random in nature, the forces imposed on the LSRC can never be fully predicted. However, the ocean’s surface does not behave without its own natural limits. For this reason, oceanographers have found that wave statistics are suitable for predicting the environment in which a vessel will operate. In addition, it has been observed that the linear superposition of regular waves having different lengths, directions and amplitudes can be used to model the ocean’s irregular surface with reasonable accuracy. This concept is illustrated in Figure 55. Although these two statements greatly over-simplify the assumptions made in linear wave theory, they form the foundation upon which all seakeeping analyses are performed.

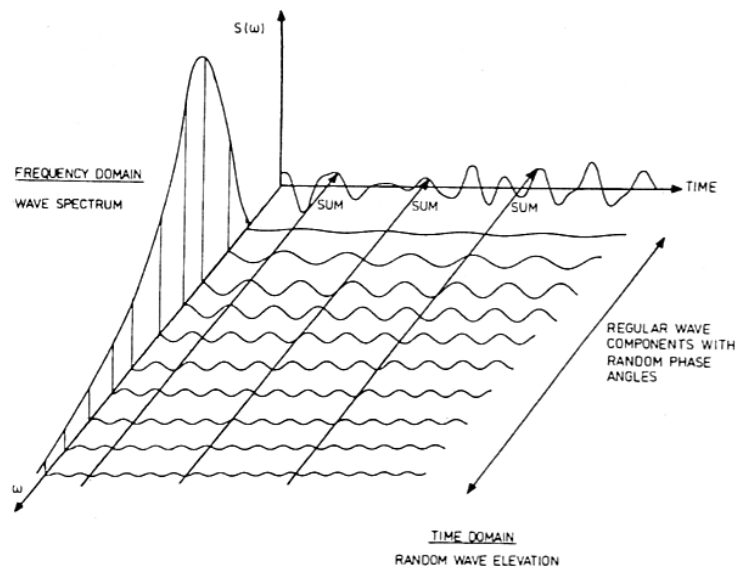


Figure 55. Wave superposition, and the frequency-domain time-domain relationship
(Courtesy of O.M. Faltinsen, Cambridge University Press [26])

Before the power of statistical mathematics can be employed, the LSRC's response to a single waveform must be understood. Assuming that the waveform is sinusoidal in nature, the wave elevation (η) (i.e. distance along the z – coordinate. See Figure 65) at any point along the x – axis is given by:

$$\eta(x, t) = a \sin(\omega t - kx) \quad (54)$$

where a is the wave amplitude, ω is the angular frequency, t is time and k is the wave number ($k = 2\pi/\lambda$). Equation (54) defines a simple harmonic progressive wave moving in the positive x – direction, where the wave elevation η is constant in y . Assuming that the water has zero viscosity and is incompressible, the idealized ocean environment can be more fully defined by a quantity known as the *velocity potential* (Φ_I)⁶⁵. In addition to defining the wave profile, the velocity potential can be used to calculate the pressure, velocity and acceleration of water particles at any point below the free surface. The velocity potential function for the aforementioned waveform, in deep water, is given by:

$$\Phi_I(x, z, t) = \frac{a\omega}{k} e^{kz} \cos(\omega t - kx) \quad (55)$$

It then follows that,

$$\frac{\partial \Phi_I}{\partial t} = -\frac{a\omega^2}{k} e^{kz} \sin(\omega t - kx) \quad (56)$$

In the next section, equations (55) and (56) will be used to define the excitation forces (i.e. forcing functions) that the LSRC would experience in a regular seaway. These forces, along with the equations of motion, will be used to solve for the system's *transfer functions*⁶⁶. Because the system under consideration is linear and time invariant, the transfer functions (H) can be used to calculate the system's response (X) to a given input (η). This relationship is described pictorially in Figure 56 below.

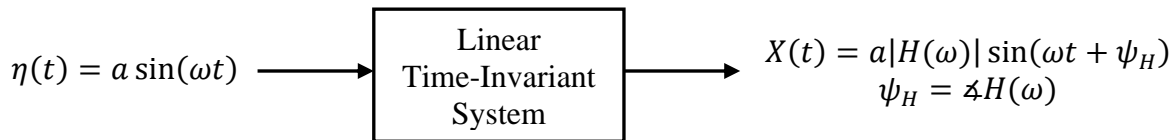


Figure 56. Properties of a time invariant system

⁶⁵ The velocity potential is defined as a function whose negative derivative in any direction yields the velocity component of the fluid in the same direction [29].

⁶⁶ The *transfer function* $H(\omega)$ is the Fourier transform of the system's impulse response ($h(t)$). The *impulse response* is simply the response of the system to a unit impulse input. The transfer function is synonymous to the Response Amplitude Operator (RAO).

2.5.3.1 EQUATIONS OF MOTION

In general, a ship floating in a train of regular waves will move in six degrees of freedom. These motions are composed of three translational components (surge, sway and heave), and three rotational components (roll, pitch and yaw) (See Figure 57). Consequently, the equations of motion will consist of six *nonlinear* equations having six unknowns. Applying linear theory to the ship's motions, these equations can be decoupled into two sets of three *linear* equations. The first set involving surge, heave and pitch, and the second; sway, roll and yaw. In the case of the LSRC, the motions of pitch and roll are equivalent, as are surge and sway. In addition, symmetry suggests that motions in heave will be decoupled from surge and pitch, and yaw can be neglected. In conclusion, the response characteristics of the LSRC can be evaluated based on evaluating three equations of motion: heave (uncoupled), and surge and pitch (coupled). The derivation of these equations can be found in the following two sections.

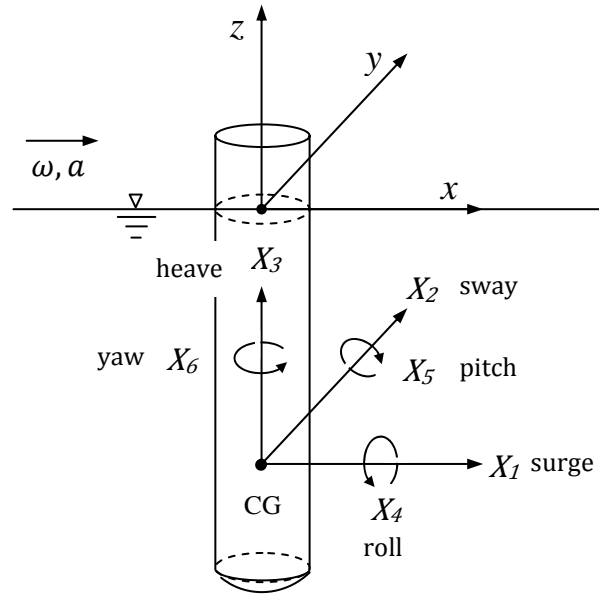


Figure 57. Sign convention for translatory and angular displacement

2.5.3.1.1 HEAVE

The LSRC can be modeled as a mass subject to an inertia force, a damping force, and a hydrostatic restoring force. Applying Newton's law in the z - direction gives:

$$(M_{33} + A_{33}) \frac{d^2 z(t)}{dt^2} + B_{33} \frac{dz(t)}{dt} + C_{33} z(t) = f_z(t) \quad (57)$$

where, M_{33} = LSRC mass, A_{33} = LSRC's added mass in heave, B_{33} = heave damping coefficient, and C_{33} = hydrostatic restoring coefficient in heave. For the velocity field defined above (equation (55)) the excitation force becomes;

$$f_z(t) \equiv F_3(t) = |F_3| \sin(\omega t + \psi_{F3}) = \text{Re}\{-|F_3|ie^{i(\omega t + \psi_{F3})}\} \quad (58)$$

where $|F_3|$ is the force magnitude, ψ_{F3} is phase shift between the incident waves and the excitation force, and i is the imaginary number $\sqrt{-1}$. Since the system is linear and time invariant, the resulting displacement will be of the form;

$$z(t) \equiv X_3(t) = |X_3| \sin(\omega t + \psi_{H3}) = \text{Re}\{-|X_3|ie^{i(\omega t + \psi_{H3})}\} \quad (59)$$

where $|X_3|$ is the heave displacement magnitude, and ψ_{H3} is the phase shift between the incident waves and the heave motion (i.e. the transfer function (H_3) phase angle). Substituting equations (58) and (59) into equation (57) and defining $\hat{F}_3 \equiv |F_3|e^{i(\psi_{F3})}$, and $\hat{X}_3 \equiv |X_3|e^{i(\psi_{H3})}$ gives:

$$\text{Re}\{-[-\omega^2(M_{33} + A_{33})\hat{X}_3 + i\omega B_{33}\hat{X}_3 + C_{33}\hat{X}_3]ie^{i\omega t}\} = \text{Re}\{-\hat{F}_3ie^{i\omega t}\} \quad (60)$$

Combining like terms gives:

$$\text{Re}\{-[-\omega^2(M_{33} + A_{33})\hat{X}_3 + i\omega B_{33}\hat{X}_3 + C_{33}\hat{X}_3 - \hat{F}_3]ie^{i\omega t}\} = 0 \quad (61)$$

Equation (61) is always true if:

$$[-\omega^2(M_{33} + A_{33}) + i\omega B_{33} + C_{33}]\hat{X}_3 = \hat{F}_3 \quad (62)$$

Rewriting the above equation in the form below gives the familiar non-dimensionalized transfer function (H_3) for the system response in heave:

$$H_3(\omega) = \frac{\hat{X}_3}{\hat{F}_3/a} = \frac{\hat{F}_3/a}{-\omega^2(M_{33} + A_{33}) + i\omega B_{33} + C_{33}} \quad (63)$$

In order to solve for the heave response complex amplitude \hat{X}_3 , the excitation force and motion coefficients must first be determined. For the problem at hand, it is valid to assume that the cylinder diameter (D_o) is sufficiently small compared to the wavelength (λ) of the incident waves. It is further assumed that the geometry of the cylinder will not produce waves of any significance in the heave motion. Therefore, the effects of diffraction and radiation can be ignored. Under these circumstances, the excitation force in the heave direction can then be approximated by the Froude-Krylov Force. This force can be calculated using the relationship below:

$$F_I^{FK} = -\rho \iint_S \left(\frac{\partial \Phi_I}{\partial t} \right) \hat{\mathbf{k}} \cdot \hat{\mathbf{n}}_s \, ds \quad (64)$$

where ρ is the density of saltwater, S is the surface upon which the forces are acting, $\hat{\mathbf{k}}$ is the unit vector in the z – direction and $\hat{\mathbf{n}}_s$ is a unit vector normal to surface S . In essence, equation (64) integrates the pressure effects due to the incident wave system over the surface of interest. When applied to the LSRC's lower end-cap, the excitation force in the z - direction (F_3) can be obtained. Due to the small variation in pressure between the dome's pole and equator, it may be assumed that the LSRC's lower end-cap is a disk (i.e. Figure (29a)). Thus, the pressure does not change along the y – axis, and the product $\hat{\mathbf{k}} \cdot \hat{\mathbf{n}}_s = 1$. For $\lambda \gg D_o$, it may also be assumed that the pressure is constant along the x – axis near $x = 0$. Under the aforementioned assumptions equation (64) reduces to:

$$F_3^{disk}(t) = -(\rho\pi R^2) \frac{\partial \Phi_I}{\partial t} \Big|_{z=-L, x=0} \quad (65)$$

Substituting equation (56) into equation (65) gives:

$$F_3^{disk}(t) = a\rho g\pi R^2 e^{-kL} \sin(\omega t) = \text{Re}\{(a\rho g\pi R^2 e^{-kL})(-ie^{i\omega t})\} \quad (66)$$

where the deep water relation $\omega^2/k = g$ was used⁶⁷. Notice that in the equation above, $\hat{F}_3^{disk} = |F_3^{disk}| = (a\rho g\pi R^2 e^{-kL})$. A slightly more accurate solution may be obtained by assuming the LSRC's lower end-cap is a dish with a depth equal to that of the ellipsoid's semiminor axis (e.g. for $b/a = 0.7 \rightarrow R_o \approx 3.7$ feet). Using spherical coordinates and relocating the origin a distance (d) below the surface (See Figure 65), equation (64) becomes:

⁶⁷ The deep water assumption is considered valid when the ratio of water depth to wave length is greater than 0.5.

$$F_3^{dish}(t) = a\rho g \int_{\pi-\beta}^{\pi} \int_0^{2\pi} e^{k(R_o \cos \phi - d)} \sin(\omega t - k(R_o \sin \phi \cos \theta)) \cos \phi R_o^2 \sin \phi d\theta d\phi \quad (67)$$

where,

$$z = R_o \cos \phi - d, \quad x = R_o \sin \phi \cos \theta, \quad \hat{\mathbf{k}} \cdot \hat{\mathbf{n}}_s = \cos \phi, \quad ds = R_o^2 \sin \phi d\theta d\phi$$

Using the trigonometric identity $\sin(a - b) = \sin(a) \cos(b) - \cos(a) \sin(b)$, we can rewrite the above equation as:

$$F_3^{dish}(t) = R_o^2 a\rho g [A \sin(\omega t) - B \cos(\omega t)] \quad (68)$$

where,

$$A \equiv \int_{\pi-\beta}^{\pi} \int_0^{2\pi} e^{k(R_o \cos \phi - d)} \cos(k R_o \sin \phi \cos \theta) \cos \phi \sin \phi d\theta d\phi \quad (69)$$

and

$$B \equiv \int_{\pi-\beta}^{\pi} \int_0^{2\pi} e^{k(R_o \cos \phi - d)} \sin(k R_o \sin \phi \cos \theta) \cos \phi \sin \phi d\theta d\phi \quad (70)$$

Because the constants A and B are known quantities, equation (68) can be rewritten as:

$$\begin{aligned} F_3^{dish}(t) &= R_o^2 a\rho g (A^2 + B^2)^{1/2} \sin(\omega t - \psi_d) \\ &= \text{Re}\{(R_o^2 a\rho g (A^2 + B^2)^{1/2} e^{i(-\psi_d)}) (-ie^{i\omega t})\} \end{aligned} \quad (71)$$

where,

$$\psi_d = \text{Arctan}(B/A) \quad (72)$$

and

$$\hat{F}_3^{dish} = |F_3^{dish}| e^{i(-\psi_d)} = (R_o^2 a\rho g (A^2 + B^2)^{1/2}) e^{i(-\psi_d)} \quad (73)$$

2.5.3.1.2 SURGE AND PITCH

Like the motion of the LSRC in the z – direction, the surge (x – direction) and pitch (rotation about the y – axis), can be derived from Newton’s Law. However, these motions are coupled and the equations of motion will need to be solved simultaneously. The equations of motion are:

$$(M_{11} + A_{11}) \frac{d^2 x}{dt^2} + (M_{15} + A_{15}) \frac{d^2 \phi}{dt^2} + B_{11} \frac{dx}{dt} + B_{15} \frac{d\phi}{dt} + C_{11}x + C_{15}\phi = f_x(t) \quad (74)$$

$$(I_{55} + A_{55}) \frac{d^2 \phi}{dt^2} + (M_{51} + A_{51}) \frac{d^2 x}{dt^2} + B_{55} \frac{d\phi}{dt} + B_{51} \frac{dx}{dt} + C_{55}\phi + C_{51}x = f_\phi(t) \quad (75)$$

Assuming rotation occurs about the cylinder’s center of gravity, and referencing all moments accordingly, $M_{15} = M_{51} = 0$ and I_{55} is the mass moment of inertia in pitch about the LSRC’s center of gravity. Due to the LSRC’s geometry it can also be shown that $C_{11} = C_{15} = C_{51} = 0$. For a vertical cylinder floating in deep water the surge and pitch excitations are given by equations (76) and (77) [26]. The wavelength is assumed to be larger than five times the diameter so that the buoy does not generate any waves of significance.

$$f_x(t) = F_1(t) = 2\rho g a A_{WP} (1 - e^{-kL}) \cos(\omega t + \psi_{F1}) \quad (76)$$

$$f_\phi(t) = F_5(t) = 2\rho g a A_{WP} (C + D) e^{-kL} \cos(\omega t + \psi_{F5}) \quad (77)$$

where f_ϕ is the force moment about the y – axis through the center of gravity, L is the draft, and the functions C and D are defined as:

$$C \equiv \left(\frac{L}{2} + \overline{BG} \right) - \frac{1}{k} \quad (78)$$

$$D \equiv \left(\frac{L}{2} - \overline{BG} \right) + \frac{1}{k} \quad (79)$$

Where \overline{BG} is the distance between the buoy’s center of gravity and center of buoyancy (positive value), and L is the draft of the cylindrical section (See Figure 65). For simplicity, equations (76) and (77) can be re-written as:

$$F_1(t) = |F_1| \cos(\omega t + \psi_{F1}) = \text{Re}\{|F_1| e^{i(\omega t + \psi_{F1})}\} \quad (80)$$

and,

$$F_5(t) = |F_5| \cos(\omega t + \psi_{F5}) = \text{Re}\{|F_5|e^{i(\omega t + \psi_{F5})}\} \quad (81)$$

where $|F_1|$ is the magnitude of the surge excitation force and $|F_5|$ is the magnitude of the force moment in pitch. Since the system is linear and time invariant, the resulting displacements will be of the form;

$$x(t) \equiv X_1(t) = |X_1| \sin(\omega t + \psi_{H1}) = \text{Re}\{-|X_1|ie^{i(\omega t + \psi_{H1})}\} \quad (82)$$

and

$$\phi(t) \equiv X_5(t) = |X_5| \sin(\omega t + \psi_{H5}) = \text{Re}\{-|X_5|ie^{i(\omega t + \psi_{H5})}\} \quad (83)$$

where $|X_1|$ and $|X_5|$ are the surge and pitch displacement magnitudes, and ψ_{H1} and ψ_{H5} are the phase shifts between the incident waves and their respective motions. After substituting equations (80) through (83) into equations (74) and (75), and defining the following complex magnitudes (equations (84) through (87)), the equations of motion can be rewritten as equations (88) and (89).

$$\hat{F}_1 \equiv 2\rho g a A_{WP}(1 - e^{-kL})e^{i(\psi_{F1})} \quad (84)$$

$$\hat{F}_5 \equiv 2\rho g a A_{WP}(C + D)e^{-kL}e^{i(\psi_{F5})} \quad (85)$$

$$\hat{X}_1 \equiv |X_1|e^{i(\psi_{H1})} \quad (86)$$

$$\hat{X}_5 \equiv |X_5|e^{i(\psi_{H5})} \quad (87)$$

$$\text{Re}\{[i\omega^2(M_{11} + A_{11})\hat{X}_1 + i\omega^2 A_{15}\hat{X}_5 + \omega B_{11}\hat{X}_1 + \omega B_{15}\hat{X}_5]e^{i(\omega t)}\} = \text{Re}\{\hat{F}_1 e^{i(\omega t)}\} \quad (88)$$

$$\text{Re}\{[i\omega^2(I_{55} + A_{55})\hat{X}_5 + i\omega^2 A_{51}\hat{X}_1 + \omega B_{55}\hat{X}_5 + \omega B_{51}\hat{X}_1 - iC_{55}\hat{X}_5]e^{i(\omega t)}\} = \text{Re}\{\hat{F}_5 e^{i(\omega t)}\} \quad (89)$$

Equations (88) and (89) can be solved simultaneously by making the following substitutions:

$$P \equiv i\omega^2(m + A_{11}) + \omega B_{11} \quad (90)$$

$$Q \equiv i\omega^2 A_{15} + \omega B_{15} \quad (91)$$

$$R \equiv i\omega^2 A_{51} + \omega B_{51} \quad (92)$$

$$S \equiv i\omega^2(I_{55} + A_{55}) + \omega B_{55} - iC_{55} \quad (93)$$

Then,

$$\hat{X}_1 = \frac{\hat{F}_1 S - \hat{F}_5 Q}{PS - QR} \quad (94)$$

$$\hat{X}_5 = \frac{\hat{F}_5 P - \hat{F}_1 R}{PS - QR} \quad (95)$$

Rewriting the above equations in the form below gives the remaining transfer functions for the system response:

$$H_1(\omega) = \frac{\hat{X}_1}{a} = \frac{\hat{F}_1 S - \hat{F}_5 Q}{a(PS - QR)} \quad (96)$$

$$H_5(\omega) = \frac{\hat{X}_5}{ka} = \frac{\hat{F}_5 P - \hat{F}_1 R}{ka(PS - QR)} \quad (97)$$

2.5.3.1.3 HYDRODYNAMIC COEFFICIENTS

For most marine structures, determining the hydrodynamic coefficients to be used in the equations of motion is the most difficult aspect of the seakeeping analysis. For many structures these coefficients can only be obtained through model testing, or numerical approximations. Fortunately, the geometry of the LSRC (i.e. a cylinder) is simple enough that the hydrodynamic impedance coefficients (A_{ij}, B_{ij}) and the hydrostatic restoring coefficients (C_{ij}) can be approximated with good accuracy using analytical methods. The most widely used method for approximating the hydrodynamic properties of long slender objects is *strip theory*. In strip theory, the flow at each cross-section is assumed to be locally two-dimensional. The theory suggests that the hydrodynamic properties of three-dimensional objects (i.e. A_{ij} and B_{ij}) can then be obtained by simply integrating the two-dimensional properties (i.e. a_{ij} and b_{ij}) along the length of the structure. Without further explanation, the formulation of the coefficients obtained from

strip theory can be seen below ($A_{11}, A_{15}, A_{51}, A_{55}, B_{15}$ and B_{51}). Notice that each of these coefficients is associated with flow moving across the cylinder's length. Contributions to the added mass with respect to flow across the lower end-cap (i.e. A_{1j} and A_{5j}) were neglected. However, A_{33} should not be neglected, and was obtained by using half⁶⁸ the added mass of an ellipsoid of revolution with dimensions ($b/a = 0.7$). In three dimensions, ellipsoids are the most general bodies where comparable analytical results are available. For this analysis, the analytical results depicted in Figure 58 were used⁶⁹.

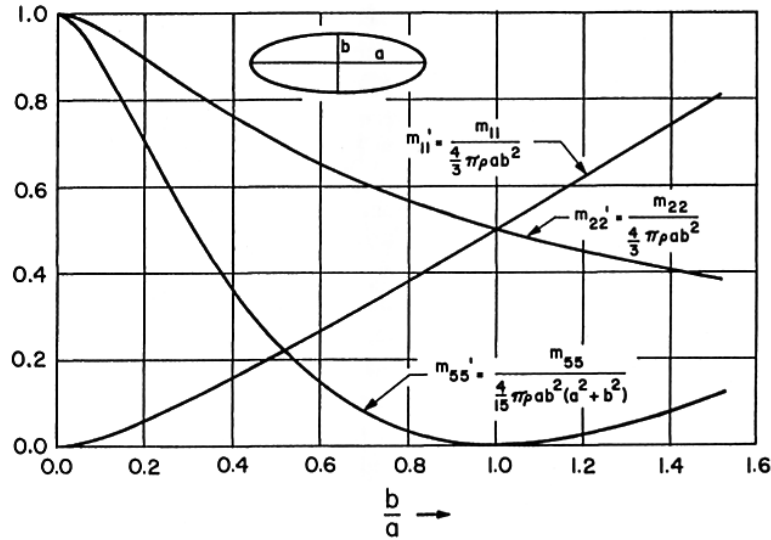


Figure 58. Added mass of an ellipsoid of revolution (Courtesy of J.N. Newman, The MIT Press [25])

Another useful method for determining the hydrodynamic coefficients is given by the *Haskind* relations. These relations can be used to express the damping coefficients in terms of the exciting forces, and require no assumptions regarding the wavelength or body geometry [25]. The relationships state that the damping coefficient will be proportional to the square of the exciting force, and that the resonant response will be inversely proportional to the exciting force. The Haskind relations can be used to approximate the *wave damping* if the resonant frequencies of oscillation are low, and at low frequencies where the heave force can be estimated by its hydrostatic limit. In the case of the LSRC however, the Haskind relations alone are not sufficient. Unlike conventional ship designs, the LSRC's *frictional damping* is significant when compared to the damping which results from “wave making”. Thus, the damping coefficients must also include the effects of drag forces. However, because forces due to drag are nonlinear ($\text{Drag} \propto v^2$), it is necessary to develop a linear approximation for use in equations (57), (74) and (75). The approximation used in this paper assumes that the actual nonlinear drag force and the equivalent linear damping force dissipate the same amount of energy per cycle. Equating these two energies and solving for the damping coefficient gives⁷⁰:

⁶⁸ This is a good assumption when only half of the object is in contact with the water.

⁶⁹ Note: The results in Figure 58 pertain to motions along the x – axis. Thus, dimensions a and b in Figure 58 will be the opposite of those defined in this paper.

⁷⁰ See reference [39], pp.83-84.

$$B = \frac{4}{3\pi} \rho C_D A |X| \omega \quad (98)$$

where, C_D is the coefficient of damping ($C_D = f(\text{Geometry, Reynolds number})$), A is the frontal area, and $|X|$ is the arbitrary constant amplitude necessary to maintain linearity. In this paper, the average amplitude of motion $\overline{|X|}$ is used (i.e. $|X| = \overline{|X|}$). The formulation of the hydrodynamic damping coefficients obtained using both the Haskind relations and the linear approximation of drag can be seen below. The total damping coefficients (i.e. $B_{11}, B_{15}, B_{33}, B_{51}$ and B_{55}) are then obtained by simply adding the two.

ADDED MASS COEFFICIENTS

$$A_{11} = - \int_0^{-L} a_{11} dz = \rho \pi R^2 L$$

$$A_{33} \approx \frac{1}{2} A_{33}^{ellipsoid (b/a=0.7)} = \frac{1}{2} \left[(0.76) \frac{4}{3} \pi \rho b a^2 \right]$$

$$A_{55} = -a_{11} \left[- \int_0^{CG} \ell^2 d\ell - \int_0^{KG} \ell^2 d\ell \right] = \rho \pi R^2 \left(\frac{L^3}{12} + L \overline{BG}^2 \right)$$

$$A_{15} = A_{51} = -a_{11} \left[\int_0^{KG} \ell d\ell - \int_0^{CG} \ell d\ell \right] = \rho \pi R^2 L \overline{BG}$$

$$A_{13} = A_{31} = A_{35} = A_{53} = 0$$

DAMPING COEFFICIENTS

WAVE DAMPING

$$B_{11} = \frac{k}{8\rho g V_g} |F_1|^2 = \frac{\omega k}{4\rho} \left(\frac{|F_1|}{g} \right)^2 \quad (\text{deep water})$$

$$B_{33} = \frac{k}{4\rho g V_g} |F_3|^2 = \frac{\omega k}{2\rho} \left(\frac{|F_3|}{g} \right)^2 \quad (\text{deep water})$$

$$B_{55} = \frac{k}{8\rho g V_g} |F_5|^2 = \frac{\omega k}{4\rho} \left(\frac{|F_5|}{g} \right)^2 \quad (\text{deep water})$$

$$B_{15} = B_{51} = -b_{11} \left[\int_0^{KG} \ell \, d\ell - \int_0^{CG} \ell \, d\ell \right] = b_{11} \overline{LBG}$$

where,

$$b_{11} = \frac{\left| \frac{F_1}{L} \right|^2}{2\rho g V_g} = \frac{\omega}{\rho} \left(\frac{|F_1|}{Lg} \right)^2 \quad (\text{deep water})$$

$$B_{13} = B_{31} = B_{35} = B_{53} = 0$$

FRICTIONAL DAMPING

$$B_{11} = \frac{8}{3\pi} \rho C_D R L |\overline{X}_1| \omega$$

$$B_{33} = \frac{4}{3\pi} \rho C_D A_{WP} |\overline{X}_3| \omega$$

$$B_{55} = -\frac{8}{3\pi} \rho C_D R |\overline{X}_5| \omega \left[-\int_0^{CG} \ell^3 d\ell - \int_0^{KG} \ell^3 d\ell \right] =$$

$$B_{55} = \frac{2}{3\pi} \rho C_D R |\overline{X}_5| \omega \left(\frac{L^4}{8} + 3L^2 \overline{BG}^2 + 2\overline{BG}^4 \right)$$

$$B_{15} = -\frac{8}{3\pi} \rho C_D R |\overline{X}_5| \omega \left[\int_0^{KG} \ell^3 d\ell - \int_0^{CG} \ell^3 d\ell \right] =$$

$$B_{15} = \frac{2}{3\pi} \rho C_D R |\overline{X}_5| \omega (L^3 \overline{BG} + 4L \overline{BG}^3)$$

$$B_{51} = -\frac{8}{3\pi} \rho C_D R |\overline{X}_1| \omega \left[\int_0^{KG} \ell d\ell - \int_0^{CG} \ell d\ell \right] =$$

$$B_{51} = \frac{8}{3\pi} \rho C_D R |\overline{X}_1| \omega (L \overline{BG})$$

$$B_{13} = B_{31} = B_{35} = B_{53} = 0$$

HYDROSTATIC RESTORING COEFFICIENTS

$$C_{33} = \rho g A_{WP} = \rho g \pi R^2$$

$$C_{55} = \rho g \nabla [z_{CG} - z_{CB}] + \rho g \iint_{AWP} x^2 ds = \rho g \nabla \overline{GM} = \rho g \nabla \overline{BG} + \frac{1}{4} \rho g \pi R^4$$

$$C_{11} = C_{13} = C_{31} = C_{15} = C_{51} = C_{35} = C_{53} = 0$$

2.5.3.2 SYSTEM RESPONSE

Once the transfer functions have been determined, everything about the system's response is known. As discussed earlier, the total wave system describing the sea is assumed to be the summation of many (theoretically an infinite number) independent components. This can be written mathematically as equation (99).

$$\eta(t) = \sum_{j=1}^N a_j \sin(\omega_j t - k_j x + \psi_j) \quad (99)$$

Where ψ_j is the random phase angle associated with wave component j . For linear time-invariant systems, this property of superposition also holds true for the response. If the input to the system is the seaway described by equation (99), then the response will be of the form:

$$X(t) = \sum_{j=1}^N a_j |H(\omega_j)| \sin(\omega_j t - k_j x + \psi_j + \psi_{H(\omega_j)}) \quad (100)$$

However, this result is only useful if all the wave components are known. In practice, tabulating the individual wave components for a particular sea system is not practical. Instead, it is more convenient to describe the sea state by a *wave spectrum*. The wave spectrum ($S(\omega)$), also known as a *variance spectrum* or “*energy spectrum*”⁷¹, and can be viewed as a distributed amplitude, or “probability density”⁷², of amplitudes, indicating the energy of the system [27], See Figure 55.

⁷¹ Note: The wave spectrum is not actually an energy spectrum. More accurately, it is a power spectrum.

⁷² Note: This description is loosely applied. The modal frequency is *not* the most probable frequency. Point spectrum's, such as the Bretschneider spectrum, are *not* probability density functions.

Said another way, the wave spectrum is a function that provides all the component amplitudes and frequencies desired to evaluate expressions like equation (99). If the wave spectrum is subdivided into equally spaced frequency components ($\Delta\omega$), each with frequency (ω_j) and spectrum amplitude ($S(\omega_j)$) (See Figure 55), then the wave amplitude (a_j) can be expressed by:

$$a_j = \sqrt{2 S(\omega_j) \Delta\omega} \quad (101)$$

and equations (99) and (100) can be readily evaluated⁷³. Through the use of weather ship stations and satellite data, ocean wave spectra have been developed for various regions of the world. One of the most common wave spectrums, which is also the current International Towing Tank Conference (ITTC) standard, is the Bretschneider spectrum. This spectrum is defined by the formula below,

$$S(\omega) = \frac{1.25}{4} \frac{\omega_m^4}{\omega^5} (H_{1/3})^2 e^{-1.25(\omega_m/\omega)^4} \quad (102)$$

where ω_m is the spectrum's modal frequency (i.e. frequency corresponding to the spectrum's peak amplitude), and $H_{1/3}$ is the ocean's (local) *significant wave height*. The significant wave height is the expected value of any wave, given that it is greater than 66.7% of all observed waves. Said another way, it is the average height of the top 33.3% of all observed waves. This definition also applies to wave heights denoted with different numerical subscripts (i.e. $H_{1/N}$). Although the modal frequency may be selected at will, it is not uncommon to use a modal frequency that satisfies the following relationship:

$$\omega_m = 0.4 \sqrt{\frac{g}{H_{1/3}}} \quad (103)$$

If the selected modal frequency satisfies equation (103), the Bretschneider spectrum reduces to the Pierson-Moskowitz spectrum for fully developed seas. Although developing and decaying seas can often prove to be more limiting, the Pierson-Moskowitz spectrum will be used in this analysis.

The concept of spectra is not limited to defining the ocean surface. Mathematically, a spectrum can be defined for any random process that is stationary and ergodic. For linear time-invariant systems, and if the input is a stationary and ergodic random process, then the response is also stationary and ergodic. In addition, it can be shown that the *response spectrum* is related to the *input spectrum* by the transfer functions derived above. Defining the input spectrum as the

⁷³ Strictly speaking, this interpretation of the sea spectrum is only valid for the limiting case $\delta\omega \rightarrow 0$ and when the number of components $\rightarrow \infty$.

Bretschneider sea spectrum, and the output spectrum as one of the LSRCs motions (i.e. surge, heave or pitch); the following relationship is true.

$$X(\omega) = |H(\omega)|^2 S(\omega) \quad (104)$$

Equation (104) is commonly known as the Wiener-Khinchine relation. $X(t)$ can now be obtained by taking the inverse Fourier Transform of $X(\omega)$. An added benefit to solving for the system's response spectrum is the ability to obtain statistical information about the response. Because the system's response is a stationary and ergodic random process, the response will have statistics (expected values) that are equal to the time averages. Thus, useful information, such as, the probability of pitch exceeding a specified value, or the LSRC's average vertical acceleration in a sea state four, to name a few, can be easily obtained from the system's response spectrum.

2.5.3.3 SEA STATISTICS

In ocean engineering, knowing the system's response to a given input is often not enough. Because the ocean environment (input) is never fully known, a description of the system's response (output) must be also accompanied by a level of confidence. It thus becomes necessary to apply statistics to both the ocean environment as well as the system's response. Fortunately, the statistics used to describe the sea can also be used to calculate the response statistics. The method used in this paper is described below.

While spectra can be characterized by their shape and modal frequency, it is often more meaningful to describe a spectrum with frequency parameters known as *moments*. These moments depend on the spectrum's shape, and can be used to calculate the statistics of interest. Without further explanation, three particularly useful moments are defined below.

$$M_0 = \int_0^{\infty} S(\omega) d\omega = \sigma^2 = \text{Variance} \quad (105)$$

$$M_2 = \int_0^{\infty} \omega^2 S(\omega) d\omega \quad (106)$$

$$M_4 = \int_0^{\infty} \omega^4 S(\omega) d\omega \quad (107)$$

Another parameter that is used to describe the shape of a spectrum is the *spectral broadness parameter* (ϵ). The bandwidth of a spectrum will always be a value between zero and one, and describes how “wide” the spectrum is. Typical values for the ocean are between 0.6 and 0.8. The bandwidth is defined as:

$$\varepsilon = \sqrt{1 - \left(\frac{M_2^2}{M_0 M_4} \right)} \quad (108)$$

In the paragraphs to follow, these relationships will be used to calculate the probability distributions which will govern the system's response.

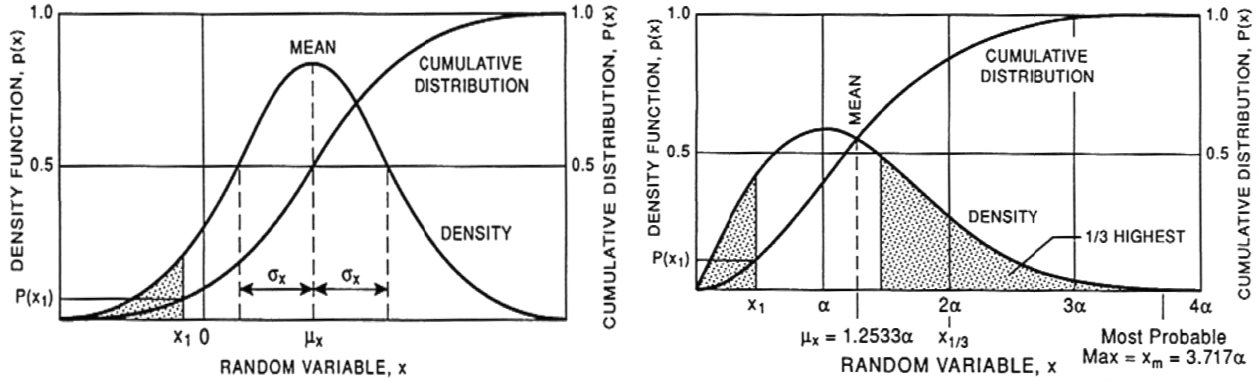


Figure 59. Probability density functions, (a) Gaussian, (b) Rayleigh
(Courtesy of M. Rahman, Oxford University Press [28])

A typical record of waves observed at a fixed point is a continuous irregular function of time (See Figure 55). It is thus reasonable to assume that the sea elevation above (or below) the still water level is a zero-mean process with a Gaussian distribution (See Figure 59(a)). The probability density function for the *sea level* (η) can then be written as:

$$p(\eta) = \frac{1}{\sigma\sqrt{2\pi}} e^{\left(\frac{-\eta^2}{2\sigma^2}\right)} \quad (109)$$

where, σ is the standard deviation ($\sqrt{M_0}$), and σ^2 is the variance (M_0). However, it is not uncommon to observe two consecutive wave minima above the still water level, or two consecutive wave maxima below the still water level. Because the maxima and minima are also random variables, the probability density function of all *maxima* (or *minima*) can be written as:

$$p(\eta^*) = \frac{2/\sigma}{1 + \sqrt{1 - \varepsilon^2}} \left\{ \frac{\varepsilon}{\sqrt{2\pi}} e^{-\frac{1}{2}\left(\frac{\eta^*}{\varepsilon}\right)^2} + \left(\eta^* \sqrt{1 - \varepsilon^2}\right) e^{\left(\frac{-\eta^{*2}}{2}\right)} \left[1 - \frac{1}{\sqrt{2\pi}} \int_{-\infty}^{\eta^* \left(\frac{-\sqrt{1 - \varepsilon^2}}{\varepsilon}\right)} e^{\left(\frac{-\tau^2}{2}\right)} d\tau \right] \right\} \quad (110)$$

where, τ is a dummy variable of integration, and η^* is the non-dimensional elevation of wave maxima (η_m) given by:

$$\eta^* = \frac{\eta_m}{\sqrt{M_0}} > 1 \quad (111)$$

where η_m is the elevation (dimensional) of wave maxima (or minima). In a real ocean, η_m loosely corresponds to an individual wave's amplitude. In an ocean perfectly described by the linear superposition of sinusoidal waveforms, $\eta_m = a$. For broad banded spectrums ($\varepsilon \rightarrow 1$) where the minima consistently fall above the still water level (or the maxima consistently fall below the still water level), the probability density function of wave elevation will approach that of a Gaussian distribution. Plugging $\varepsilon = 1$ into equation (110) gives the non-dimensional form of equation (109). In general, however, sea spectrums are narrow banded⁷⁴. Thus, it is more appropriate to characterize the wave maxima with probability distributions that correspond to low values of ε . Plugging $\varepsilon = 0$ into equation (110) gives:

$$p(\eta^*) = \frac{\eta^*}{\sigma} e^{\left(\frac{-\eta^{*2}}{2}\right)} \quad (112)$$

The result defined by equation (112) is commonly known as the Rayleigh density function (See Figure 59(b)). Although equation (112) was obtained by assuming a bandwidth of zero (i.e. “perfectly” narrow, $\varepsilon = 0$), research has shown that the Rayleigh density function accurately describes the narrow banded seaways most frequently encountered by ships [29]. Thus, the Rayleigh density function will be used to approximate the statistics of the Bretschneider sea spectrum described above. Substituting equation (111) into equation (112), gives the probability density function of the wave amplitude for narrow banded spectrums.

$$p(a) = \frac{a}{M_0} e^{\left(\frac{-a^2}{2M_0}\right)} \quad 0 < a < \infty \quad (113)$$

From this relationship, it can be shown that the expected value of particular wave heights ($H_{1/N}$) and maxima (H^{max}) are proportional to the root mean square wave height ($H_{1/N} \propto H_{RMS} = \sqrt{M_0}$). The most common of these statistics are defined below [29].

⁷⁴ Although the ocean typically exhibits bandwidths (ε) ≈ 0.6 , it is still considered “narrow” overall. As a comparison, a white noise spectrum of infinite broadness has a bandwidth (ε) of only 2/3.

Wave heights:

$$H_{mf} = 0.707\sqrt{M_0} \quad (\text{most frequent wave height}) \quad (114)$$

$$H_{1/1} = 2.5\sqrt{M_0} \quad (\text{average wave height}^{75}) \quad (115)$$

$$H_{1/3} = 4.0\sqrt{M_0} \quad (\text{significant wave height}) \quad (116)$$

$$H_{1/10} = 5.1\sqrt{M_0} \quad (117)$$

Highest expected wave heights in N successive waves:

$$H_{N=100}^{max} = 6.5\sqrt{M_0} \quad (118)$$

$$H_{N=1,000}^{max} = 7.7\sqrt{M_0} \quad (119)$$

$$H_{N=10,000}^{max} = 8.9\sqrt{M_0} \quad (120)$$

Conveniently, the proportionality constants listed above can also be applied to the LSRC's response. This assumption is valid so long as the wave process is Gaussian and the response is linear. Moreover, because the response spectra are generally narrower than the wave spectra, the narrow-banded assumption used to derive these relationships is, in general, *more* appropriate when applied to the response. For spectra with bandwidths less than 0.6, the error committed is typically less than 10% [29]. When applying the above relations to a system's response, it is often more useful to evaluate the system's response amplitudes vice the double amplitudes or "heights". This transformation can be made by simply multiplying the proportionality constants in equations (114) through (120) by a factor of 1/2.

In addition to the wave statistics, it is also useful to know the probabilities associated with the expected response amplitudes. Using an approximation based on the Rayleigh distribution presented above, the probability that the wave amplitude (a) will exceed a particular value (a_0) is given by:

$$p(a \geq a_0) \cong \left(\frac{2\sqrt{1-\varepsilon^2}}{1+\sqrt{1-\varepsilon^2}} \right) e^{\left(\frac{-a_0^2}{2M_0} \right)} \quad (121)$$

⁷⁵ This relationship, after being modified for the response amplitude, is used calculate the constant average amplitudes $|X|$ present in the frictional damping coefficients.

Likewise, equation (121) can be used to calculate the probability that the *response* will exceed a specified limit by simply replacing the amplitude (a) with the response of interest (i.e. $|X|$, $|V|$ or $|A|$), and using the appropriate moment.

2.5.3.4 ASSESSING THE LSRC's SEAKEEPING PERFORMANCE

With the exception of pitch, the displacement response ($X(\omega)$) of the LSRC is not nearly as important as the system's response in acceleration⁷⁶. Conveniently, the Wiener-Khinchine relation can also be used to determine the system's response in both velocity and acceleration. It can be shown that the velocity ($V(\omega)$) and acceleration ($A(\omega)$) spectrums are given by:

$$V(\omega) = \omega^2 |H(\omega)|^2 S(\omega) \quad (122)$$

and

$$A(\omega) = \omega^4 |H(\omega)|^2 S(\omega) \quad (123)$$

Equations (105) through (121) can then be used to determine all the same statistics as previously discussed for the wave heights.

For the LSRC, the seakeeping characteristics of interest will be those that most directly affect the wellbeing of the crew. Because the crew is not expected to perform any significant tasks while waiting to be rescued, it will be sufficient to ensure the crew is comfortable and safe. For this reason the responses of interest will include the LSRCs rotation in pitch, and the accelerations in each of the three motions; surge, heave and pitch. For this analysis, these results will be compared to the U.S. Navy operability criteria (NATO STANAG 4154). These limits are based on numerous studies [30], and are intended to give guidance during ship design. Meeting these criteria will minimize the likelihood of motion sickness, and ensure that will the crew can carry out basic tasks without interference. The NATO limits can be seen in Table 13.

CRITERIA	LIMIT
Motion Sickness Incidence (MSI)	20% of Crew in 4 hours
Motion Incidence Interruption (MII)	1 tip per minute
Roll Amplitude	4.0° RMS
Pitch Amplitude	1.5° RMS
Vertical Acceleration	0.2 g RMS
Lateral Acceleration	0.1 g RMS

Table 13. NATO STANAG 4154 (U.S. Navy) operability criteria

⁷⁶ To a large extent the position and velocity of the LSRC will be transparent to the crew. However, accelerations will produce forces that will be felt only too well.

Compliance with Table 13 does not guarantee good seakeeping characteristics; however, ships that meet these requirements have been found to perform well. Because the guidelines were developed for ships, it is unclear how effective they will be for sailors occupying a “buoy”. In general, the acceleration limits listed above are older criteria that attribute sea sickness, to a large extent, on vertical motions. The more modern MSI and MII criteria replaces the limit for vertical acceleration and takes into account the human sensitivity to different frequencies of motion; however, it does not take into account the habituation associated with spending time at sea [30]. Although the LSRC should be made as seaworthy as possible, the limits listed in Table 13 should not be viewed as criteria for failure. Given the circumstances, it may be necessary to sacrifice crew comfort to permit survival.

2.5.3.5 SEAKEEPING RESULTS

The seakeeping analysis was performed using the program in Appendix VIII. The LSRC demonstrates good seakeeping characteristics in sea states one and two. The results for sea states three and four can be found in Appendix IX, and are summarized in Table 14 below.

CHARACTERISTIC	SEA STATE 3	SEA STATE 4
Pitch (degrees)	4.6 RMS	23.7 RMS
Vertical Acceleration	0.02g RMS	0.12g RMS
Lateral Acceleration due to Surge	0.01g RMS	0.02g RMS
Lateral Acceleration due to Pitch	0.09g RMS	0.21g RMS
Significant Acceleration in Heave (feet/sec ²)	1.6	8.2
Significant Acceleration in Pitch (degrees/sec ²)	15	39

Table 14. Seakeeping results

Despite the low value of \overline{BG} , the LSRC performs well in sea state three; however, the results suggest that the buoy will most likely exceed the STANAG limits for pitch and lateral acceleration⁷⁷. The response in sea state four has similar results with larger violations. This is attributed to the larger RAO amplitudes in acceleration and pitch. For sea states one through three, the resonant frequencies for heave and pitch fall to the left of the sea spectrum modal frequency and are not a concern. The natural frequencies can be observed graphically in Figures 60 and 61, and are given by the equations below:

$$\omega_{n_3} = \sqrt{\frac{C_{33}}{M + A_{33}}} = 0.88 \quad \text{radians/second} \quad (124)$$

$$\omega_{n_5} = \sqrt{\frac{C_{55}}{(I_{55} + A_{55}) - \frac{1}{2}M\overline{BG}^2}} = 0.54 \quad \text{radians/second} \quad (125)$$

When using the Pierson-Moskowitz spectrum the modal frequency is expected to decrease with higher sea states, and will eventually converge with the resonant frequency in heave; thus is the case for sea state four. However, despite the overlap in modal frequencies, the probability of exceeding the vertical acceleration limit due to heave alone is only 29%. Finally, developing seas are not expected to exacerbate the response. Because the capsule's resonant frequencies fall to the left of the sea spectrum's modal frequency (i.e. along the frequency axis), developing seas will only drive the spectrum peaks farther apart.

⁷⁷ It is common practice to combine the lateral acceleration contributions from both surge and pitch, thereby obtaining a single value for comparison with seakeeping criteria. In the case of the LSRC, the contribution from surge is negligible and the contribution from pitch alone is sufficient.

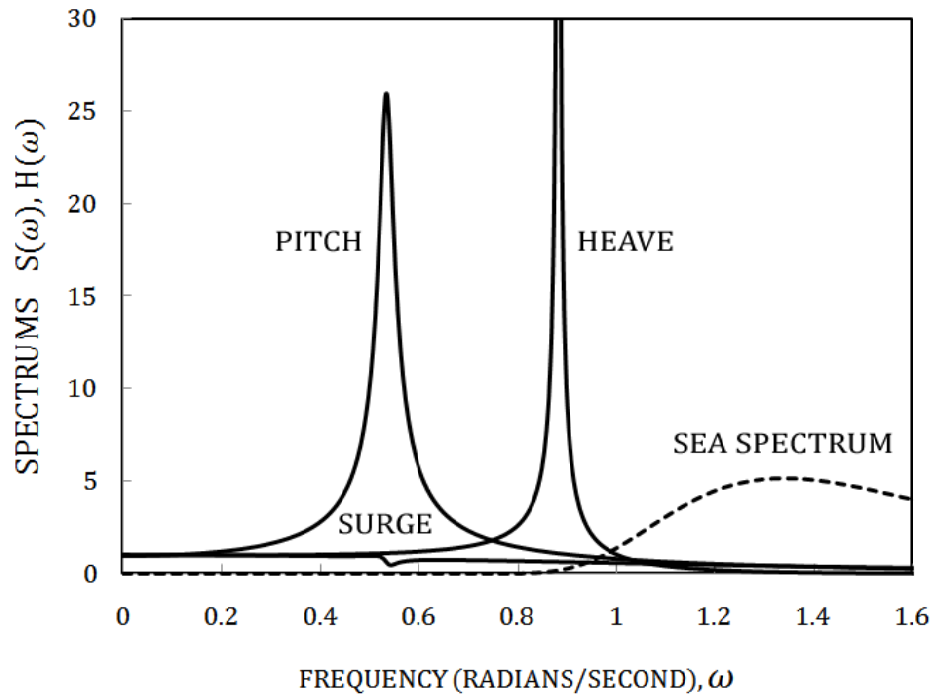


Figure 60. Sea state 3. RAOs and sea spectrum (X100)

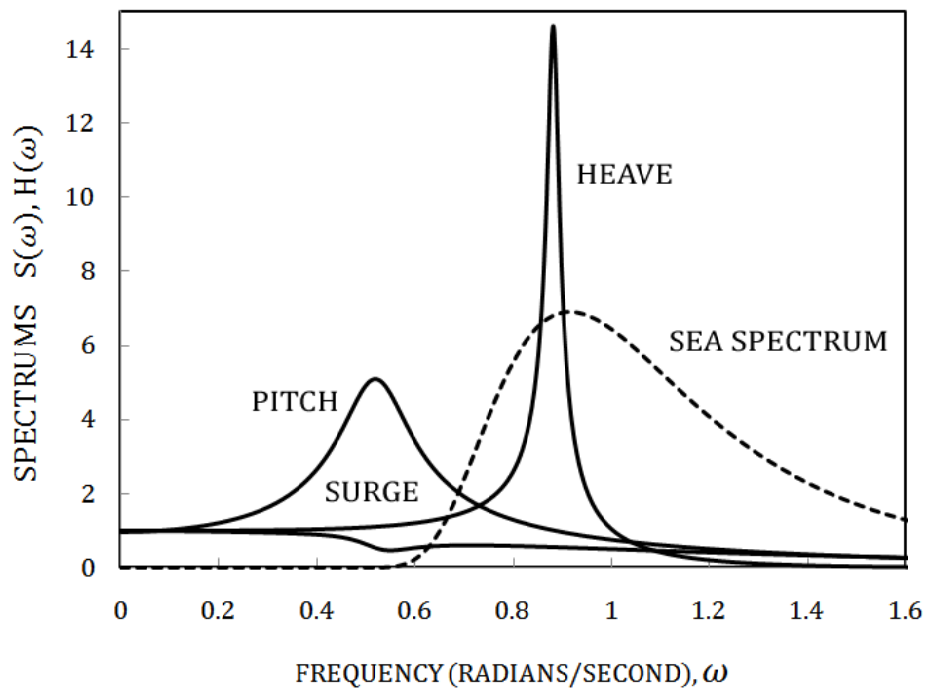


Figure 61. Sea state 4. RAOs and sea spectrum (X20)

Statistics show that the probability of exceeding the STANAG limits in sea state three is 66% for pitch and 56% for lateral acceleration. Likewise, the probabilities for sea state four are 94% and 83%, respectively. The capsule's performance can be visualized by running a time simulation of the response. The pitch response in sea states three and four can be seen in Figures 62 and 63 below.

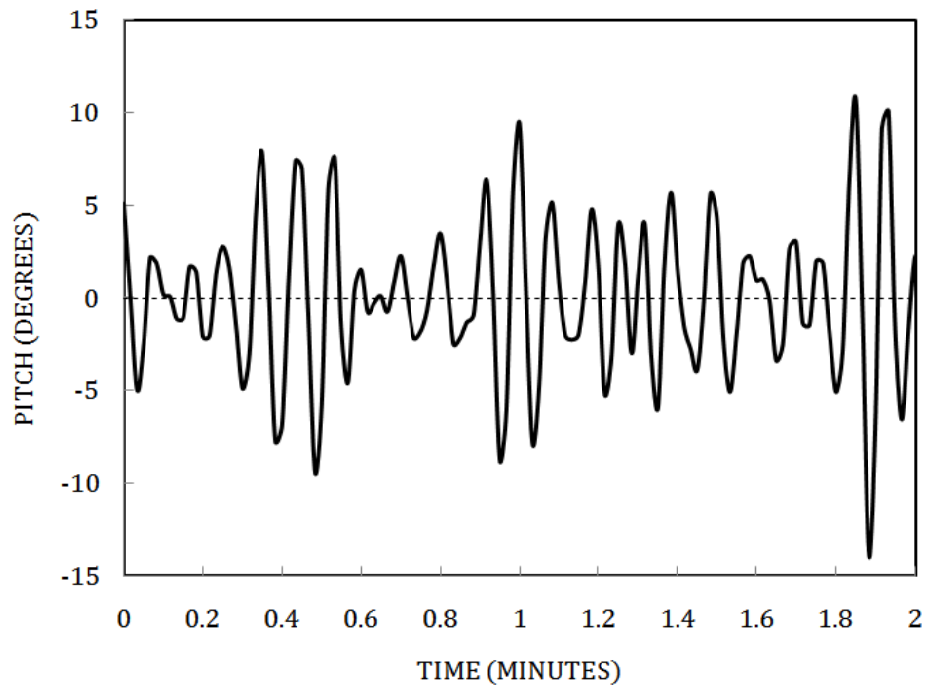


Figure 62. Sea state 3. Time space simulation in pitch

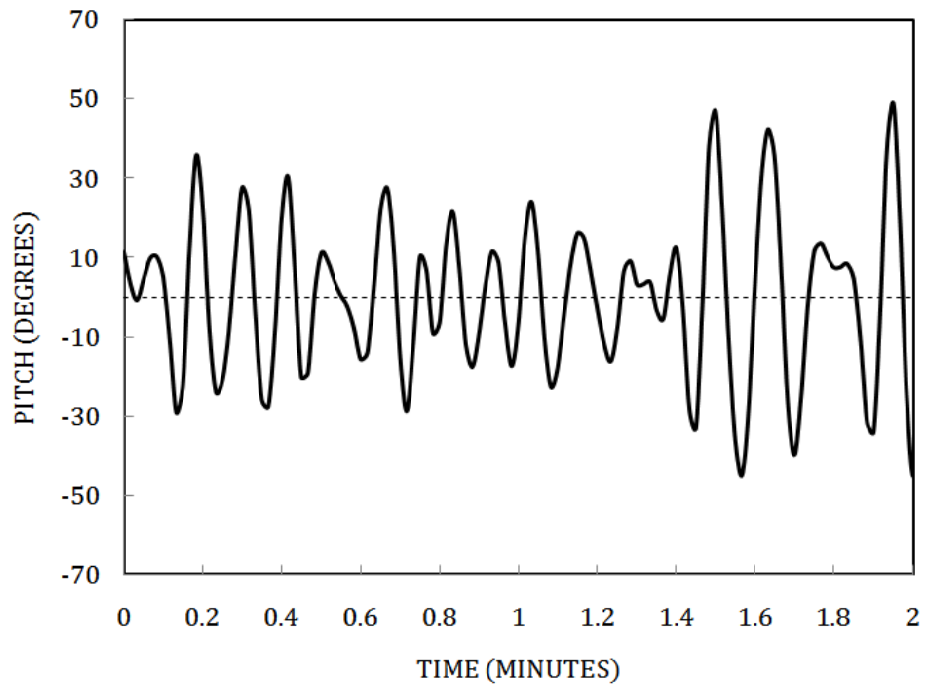


Figure 63. Sea state 4. Time space simulation in pitch

2.6 COST

A detailed cost analysis was not performed for the LSRC. However, some general statements can be made. Restructuring the submarine SAR strategy in such a way that SRCs are relied upon as the primary means of rescue would require approximately 145 capsules similar in size to that of the LSRC. This assumes a U.S. Submarine fleet of 71, each being outfitted with two LSRCs and three ready spares. Assuming a budget similar to that of the SRDRS program (i.e. R&D: \$180M and OMN: ~\$5M per year [31]), each capsule would have to be produced for no more than \$1.2M. If the concept were introduced during new construction (e.g. SSBN(X)), MMT design and fabrication could capitalize on synergies with similar systems using SCN dollars. Because the LSRC will be little more than an oversized, over structured SNDL, this cost target may be feasible. In addition, the large quantity of capsules required will most likely result in substantial learning-curve savings. Finally, the small size and scope of this project will allow for relatively accurate cost estimates. Thus, the program should be able to keep cost over-runs within the established margins.

(INTENTIONALLY LEFT BLANK)

3 CONCLUSIONS AND OBSERVATIONS

Group-assisted rescue methods, such as the SRDRS, are too slow to be used as a primary means of rescue. Further, although the SEIE suit can be used for “prompt” escape, the depth limitations and risk of injury preclude its use as a primary means of rescue. The operational regime of the SRC fills the capability gap that currently exists in the U.S. Navy submarine SAR program (See Figure 8). Therefore, a sound rescue strategy will rely upon group-independent escape methods (i.e. SRCs, RRGs, SRGs and SCs) as the primary means of rescue, and will maintain group-assisted rescue methods (i.e. SRVs and submarine rescue chambers) and individual-escape methods (i.e. buoyant/hooded ascent and ascent with SEIE) as a contingency.

Seventy personnel can fit inside a single SRC the size of a Trident II D-5 missile. In the full load condition, the capsule will displace 43.1 long-tons and have a submerged buoyancy of 3,516 lbm. Mass distribution calculations indicate that the LSRC will exhibit poor stability characteristics due to small values of \overline{BG} (31.6 inches) (See Tables 11 and 12). Holding the freeboard at 1.8 feet, the LSRC is weight limited and any additional ballast must be compensated for. For this reason, reductions in load will be necessary to improve \overline{BG} . Conservatively, a weight margin of 10% was evenly applied to all weight groups (with the exception of fixed ballast). Given the small size of the LSRC, it may be possible to reduce the weight margin for improved \overline{BG} . These results stress the importance of optimizing the LSRC structure based on weight rather than other parameters.

The LSRC will exhibit good seakeeping characteristics in sea states one and two, but will exceed the STANAG pitch and lateral acceleration limits in sea states three and four. With the exception of heave in sea state four, the RAO modal frequencies are much lower than that of the sea spectrum. However, it is expected that improvements in \overline{BG} will have the net effect of bringing the pitch RAO closer to sea spectrum; albeit, the RAO magnitude will decrease. For this reason, improvements in \overline{BG} will help reduce pitch amplitude and resonance will only be a concern in high sea states.

Structural analysis suggests that pressure hull designs utilizing king frames will produce the lightest structures. The scantling optimization routine used in this analysis identified numerous scantling arrangements that could be used in designing the pressure hull; however, the lightest designs maintained shell thickness at 0.75 inches and utilized frames with cross-sectional areas of about 5.2 square inches. Using these members, the optimal frame spacing was determined to be 14 inches for hulls without king frames and 23 inches for hulls with king frames. FEA performed on each structure revealed that the optimal designs for both small frame only pressure hulls and pressure hulls utilizing king frames would fail by shell yield at the “near-frame” location with a safety factor of 1.40 and 1.24, respectively. Modifying the FE model to incorporate imperfections in shape of axisymmetric shell yield revealed that the optimal designs could tolerate imperfections up to 0.5 inches. A similar analysis in which perturbations were introduced in the shape of the most susceptible buckling mode revealed that imperfections of only 0.125 inches could be tolerated before the structure failed prematurely. Results obtained by NAVSEA 05P22 revealed that both designs would fail by multi-wave failure, and only the small frame design used in this paper would meet the objective collapse depth of 2,500 feet. Because this paper did not consider multi-wave failure modes, these finding were not expected.

Consequently, the small frame design was used for the remainder of this analysis. In general, the analytical and numerical results showed good agreement; however, the numerical results proved less conservative. This result was somewhat unexpected since the FFSOR assumed an OOR of 0.5 inches, and the ring stiffeners in the FE model were designed with perfect circularity. The frame stresses calculated by each method are congruent with this inconsistency.

4 FUTURE WORK

4.1 EJECTION PHASE AND ACCENT PHASE

Although the Germans may have been the first to conceive the SRC concept, it was the Russians that perfected its use; or at the very least, fully embraced the concept. Over the last four decades Russia has conducted more tests, and built more models (SRCs) than any other nation. And although difficult to obtain, several documents detailing designs and test results have been published. One such document [32] identifies the major problems encountered in developing SRCs. They are:

- Jamming in the extraction chamber during separation from the submarine
- Excessive rolling of the SRC during ascent

The first problem may arise during separation from the submarine due to, (1) structural deformation resulting from explosive shock or collision, (2) excessive submarine trim and heel, and (3) bottom currents. The second problem results from SRC geometry/mass properties and hydrodynamic phenomena. Models tested by Russian engineers were found to exhibit large angular oscillations, and in many cases, overturning. To overcome these challenges, researchers at the Krylov Central Scientific Research Institute have relied almost entirely on model testing. This is clearly an area for future work. As it pertains to the ejection phase, the survivors must not be placed in a situation in which they are trapped in the capsule due to system failure. A number of ejection systems should be tested for reliability, and each should undergo shock trials to ensure survivability. As for the ascent phase, simulations should be performed to identify instabilities. To test the many loading conditions that may arise during use, recent advances in computational hydrodynamics should be exploited, and scaled model tests should be performed on the most limiting cases.

In addition to the problems identified above, work should be done to assess the dynamics during surface-breaking. Depending on the submerged buoyancy and hydrodynamic drag, the capsule may develop excessive velocities. For the LSRC, the submerged buoyancy is directly related to the freeboard. With a free board of only 1.8 feet, the modified LSRC design presented above has a positive buoyancy of 3,516 lbm (fully submerged). This is significantly greater than that of the Gabler sphere which has a positive buoyancy of only ~661 lbm. In addition, because the LSRC is more streamline in shape designers may need to consider adding breaking appendages such as water streamers and dampening plates.

In 1970, the Office of Naval Research contracted CADCOM Inc. to study the ascent characteristics of a modular escape capsule released from a submerged submarine [33]. This work resulted in a computer program (MODSEC) that could be used to study the real-time motion characteristics of a capsule during ascent. MODSEC was specifically designed to investigate the hydrodynamic behavior of a truncated ellipsoid of revolution (i.e. separable compartment (SC), See Figure 1). However, the software was developed in such a way that the equations of motion or the capsule geometry could be easily changed. Reference [33] is available through the U.S. Department of Commerce, National Technical Information Service (NTIS).

Although MODSEC was developed on legacy machines⁷⁸, the report gives several logic-flowcharts that could be used to reconstruct the work in a modern computer language. Because analytical derivations are also presented, this paper may be a good starting point for someone interested in studying the ascent characteristics of the LSRC.

4.2 MISSILE TUBE SYSTEMS AND INTERFACE

This paper assumes that missile tube systems and interfaces can be designed with relatively little impact on ship performance. By design, the MMT(s) and standard SLBM tubes will have many common features; however, from an engineering perspective the tubes will be significantly different. Because the MMT(s) and associated systems must be designed for collapse depth, and be shock grade A certified, they will be considerably heavier, and may have a significant impact on the submarine's equilibrium polygon. In addition, the submarine-LSRC access hatch will present a considerable design challenge, and may dictate that the tube is unsuitable for other payloads. Finally, additional work should be done to assess the feasibility of using an actual missile tube to house the LSRC. Given the political sensitivity of nuclear weapon systems, the marriage of the two may not be possible. In this case, the LSRC support systems would have to be designed separately; however, existing synergies could still be exploited.

4.3 PSYCHOLOGICAL EFFECTS (CLAUSTROPHOBIA)

Finally, no consideration was given to the human psyche when designing the LSRC. When fully manned, the submariners will experience confinement in the extreme. If these conditions must be tolerated for an extended period, the men may become claustrophobic and behave irrationally. Research performed by NASA may prove useful in this area. Moreover, psychologists should be consulted when manning levels are chosen.

4.4 TEMPERATURE

As discussed in chapter 2, the decision to remove hull insulation was based purely on improving stability. However, data collected during SURVIVEX 2003 and SURVIVEX 2004 suggests that heat exhaustion may be a real concern for survivors occupying the LSRC [34]⁷⁹. In light of this data, NSMRL's final report on SURVIVEX (not yet released) should be reviewed for information relevant to the LSRC design.

⁷⁸ MODSEC was developed for a time-shared PDP-10 computer.

⁷⁹ The final NSMRL report on SURVIVEX 2003 and 2004 has not yet been released (as of May 8, 2009).

BIBLIOGRAPHY

- [1] *Surfacing Rescue Facilities for Submarines*. **Pichugin, G N and Kondratenko, Ye K.** s.l. : Sudostroyeniye, 1998, Vol. 1, pp. 58-61.
- [2] **Polmar, Norman and Moore, Kenneth J.** *Cold War Submarines: The Design and Construction of U.S. and Soviet Submarines*. First Edition. Dulles : Brassey's, Inc., 2004. 1-57488-594-4.
- [3] **Unnithan, Sandeep.** Underwater Ejection. [Online] August 19, 2000. [Cited: May 7, 2009.] <http://www.indianexpress.com/ie/daily/20000819/ina19047.html>.
- [4] *The Rescue Sphere - A Rescue System for Submarines*. **Helischer, C.** s.l. : Naval Forces, 1986, Vol. 7, pp. 33-35.
- [5] *New Blast-Proof System of Rescuing Submarine Crews*. **Abramov, Yu V and Polovinkin, N G.** s.l. : Sudostroyeniye, 2004, Vol. 1, pp. 26-28.
- [6] **Commander, Submarine Force.** Submarine Search and Rescue. *OPLAN 2137*. 2003. N31/012.
- [7] **Miller, David.** *Submarine Disasters*. Guilford : The Lyons Press, 2006. 1-59228-815-4.
- [8] **Monroe-Jones, Edward.** *Submarine Escape and Rescue*. Bangor : Submarine Research Center, 2007. 978-0-9741343-7-6.
- [9] **SRDRS Operations and Training.** Description of Operations for the Submarine Rescue Diving and Recompression System, Revision 6. 2004.
- [10] War Damage Report No. 58. [Online] U.S. Hydrographic Office, January 1, 1949. [Cited: May 7, 2009.] <http://www.ibiblio.org/hyperwar/USN/rep/WDR/WDR58/WDR58-22.html>.
- [11] *Removal of Toxic Gases in Submarines*. **Mazurek, Waldemar.** 3, s.l. : Naval Forces, 2007, Vol. 28, pp. 46-51. 07228880.
- [12] **The Society of Naval Architects and Marine Engineers.** Submarine Pressure-Hull Design. *Principles of Naval Architecture*. New York : s.n., 1967, pp. 206-219.
- [13] **Von Sanden, K and Gunther, K.** *The Strength of Cylindrical Shells, Stiffened by Feames and Bulkheads, Under Uniform External Pressure on All Sides*. 1952. Taylor Model Basin Report T-38.
- [14] **Pulos, J G and Salerno, V L.** *Axisymmetric Elastic Deformations and Stresses in a Ring-Stiffened, Perfectly Circular Cylindrical Shell Under External Hydrostatic Pressure*. West Bethesda, MD : David Taylor Model Basin Report 1497, 1961.
- [15] **Jackson, Harry A.** *Fundamentals of Submarine Concept Design*. s.l. : British Maritime Technology, 1992.
- [16] **Brush, D O and Almroth, B O.** *Buckling of Bars, Plates, and Shells*. New York : McGraw-Hill Book Company, 1975.
- [17] **Kendrick, S.** *The Buckling Under External Pressure of Circular Shells with Evenly Spaced Frames*. s.l. : NCRE Report R-244, 1953.
- [18] **Wenk, E., Jr and Kennard, E H.** *The Weakening Effect of Initial Tilt and Lateral Buckling of Ring Stiffeners on Cylindrical Pressure Vessels*. s.l. : DTMB Report 1073, 1956.
- [19] **European Convention for Constructional Steelwork.** *European Recommendations for Steel Construction: Buckling of Shells (Third Edition)*. 1984.
- [20] **Graphics Research Corporation Ltd.** *Submarine Structures Paramarine (PRSHUL/MNSTR) Systems Specification Document*. Gosport, Hants : s.n., 2000.
- [21] **Timoshenko, S P and Woinowsky-Krieger, S.** *Theory of Plates and Shells (2nd ed.)*. Pennsylvania : McGraw-Hill Book Company, Inc., 1959.
- [22] **McGrattan, R J and Peteros, G A.** *Structural Principles. Submersible Vehicle Systems Design*. Jersey City, NJ : The Society of Naval Architects and Marine Engineers, 1990, pp. 271-304.
- [23] **Timoshenko, S P and Gere, J M.** *Theory of Elastic Stability (2nd ed.)*. Pennsylvania : The Maple Press Company, 1961.
- [24] **ABAQUS, Inc.** *ABAQUS Version 6.5 Documentation*. USA : s.n., 2004.
- [25] **Newman, John Nicholas.** *Marine Hydrodynamics*. Cambridge : The MIT Press, 1977. 0-262-14026-8.

- [26] **Faltinsen, O M.** *Sea Loads on Ships and Offshore Structures*. Cambridge : Cambridge University Press, 1990. 0-521-45870-6.
- [27] **Techet, A H and Triantafyllou, M S.** Spectrum of a Random Process. *Course 13.42 Lecture Notes*. 2004.
- [28] **Rahman, Matiur.** *Water Waves: Relating Modern Theory to Advancing Engineering Applications*. New York : Oxford University Press, 1995. 0-19-853478-7.
- [29] **The Society of Naval Architects and Marine Engineers.** *Motions in Waves and Controllability. Principles of Naval Architecture: Volume III (2nd ed.)*. Jersey City, NJ : Author, 1989, pp. 41-56.
- [30] **Effects of Motion at Sea on Crew Performance: A Survey. Stevens, Samson C and Parsons, Michael G.** 1, January 2002, *Marine Technology*, Vol. 39, pp. 29-47.
- [31] **Fein, Geoff.** SRDRS Gives Navy Improved Sub Rescue Capability. *BNET*. [Online] June 17, 2008. [Cited: May 4, 2009.] http://findarticles.com/p/articles/mi_6712/is_55_238/ai_n29449254/.
- [32] **Negashev, Sergey V, Stambrovskaya, Alla A and Uspenskiy, Andrey L.** *Investigation of Dynamics of Escape Capsule During their Detachment from Submarine and when Breaking the Surface of Water*. St. Petersburg, Russia : The Krylov Central Scientific-Research Institute.
- [33] **CADCOM Inc.** *Simulation Study of a Modular Escape Capsule Released from a Submerged Submarine*. Springfield : U.S. Department of Commerce, National Technical Information Service, 1970.
- [34] *SURVIVEX 2003, Exercise Tests Disabled Submarine Survival. Horn, Wayne G.* 1, s.l. : Undersea Warfare, 2003, Vol. 6, pp. 25-27.
- [35] *Фииуки*. [Online] [Cited: May 7, 2009.] <http://fishki.net/comment.php?id=50536>.
- [36] **Frey, W.** *Russian Submarines: Guardians of the Motherland*. Pennsylvania : Infinity Publishing.com, 2006.
- [37] **Moore, R.** *A Time to Die*. New York : Crown Publishers, 2002.
- [38] **Nash, W A.** *Hydrostatically Loaded Structures: The Structural Mechanics, Analysis and Design of Powered Submersibles*. Tarrytown, NY : Pergamon Press, 1995.
- [39] **Berteaux, H O.** *Buoy Engineering*. New York : John Wiley & Sons, 1976.
- [40] *Naval Architectural Aspects of Submarine Design. Arentzen, E S and Mandel, P.* 1960, Society of Naval Architects and Marine Engineers, pp. 622-692.
- [41] *Effects of Boundary Conditions on the Stability of Cylinders Subject to Lateral and Axial Pressures. Sobel, L H.* 8, s.l. : American Institute of Aeronautics and Astronautics, 1964, Vol. 2.
- [42] **Berteaux, H O, Goldsmith, R A and Schott, W E.** *Heave and Roll Response of Free Floating Bodies of Cylindrical Shape*. Boston, Massachusetts : Woods Hole Oceanographic Institute (Technical Report WHOI-77-12), 1977.
- [43] *Navy Awards Lockheed Martin \$248 Million Contract for Trident II D-5 Missile Production and D-5 Service Life Extension*. [Online] Lockheed Martin, January 29, 2002. [Cited: May 7, 2009.] http://www.lockheedmartin.com/news/press_releases/2002/NavyAwardsLockheedMartin248MillionC.html.
- [44] *UK Nuclear Weapons Plan Unveiled*. [Online] BBC News, December 4, 2006. [Cited: May 7, 2009.] http://news.bbc.co.uk/2/hi/uk_news/politics/6205174.stm.

ACRONYMS

ASDS	Advanced SEAL Delivery System
ASME	American Society of Mechanical Engineers
ASNE	American Society of Naval Engineers
ASW	Anti Submarine Warfare
AUWS	Assessment/Underwater Work System
BASEC	British Admiralty Submarine Escape Committee
CASPA	Carbon Dioxide Self-Powered Absorber
DCS	Decompression Sickness (i.e. the “Bends”)
DISSUB	Distressed (Disabled) Submarine
DSRV	Deep Submergence Rescue Vehicle
DTMB	David Taylor Model Basin
ECCS	European Convention for Constructional Steelwork
FEA	Finite Element Analysis
FFSOR	Full Factorial Scantling Optimization Routine
GMDSS	Global Maritime Distress and Safety System
HDW	Howaldtswerke-Deutsche Werft
IC	Internal Communications
IGI	Inelastic General Instability
IKL	Ingenieur-Kontor Lübeck
IMO	International Maritime Organization
ITTC	International Towing Tank Conference
JMSDF	Japanese Maritime Self Defense Force
LET	Logistics Escape Trunk
LRIT	Long Range Identification and Tracking
MAC	Multiple All-up-round Canister
MMT	Multi-mission Tube
MRE	Meals Ready-to-Eat
NATO	North Atlantic Treaty Organization
NAVSEA	Naval Sea Systems Command
NEDU	Naval Experimental Diving Unit
NSMRL	Naval Submarine Medical Research Laboratory
NTIS	National Technical Information Service
OMN	Operation and Maintenance, Navy
OOF	Out of Fairness

OOD	Out of Roundness
PACU	Portable Atmosphere Control Unit
PDA	Personal Digital Assistant
PNA	Principles of Naval Architecture
PRMS	Pressurized Rescue Module System
R&D	Research and Development
RAO	Response Amplitude Operator
RGS	Rescue/Recovery Gear Ship
ROK	Republic of Korea
ROW	Rest of World
RRG	Reusable Rescue Gear (single man retractable SRC)
SAR	Search and Rescue
SATCOM	Satellite Communications
SC	Separable Compartments (typically the bow)
SCN	Ship Construction New
SCOG	Self Contained Oxygen Generator
SDS	Submarine Decompression System
SEAREX	Automated Senior Survivor Guidance Program
SECT	Submarine Emergency Communications Transmitter Buoy
SEIE	Submarine Escape and Immersion Equipment
SEPIRB	Submarine Emergency Position Indicating Radio Beacon
SHT	Special Hull Treatment
SLBM	Submarine Launched Ballistic Missile
SLCDAU	Soda Lime Carbon Dioxide Absorption Unit
SMERAT	Submarine Escape and Rescue Assistance Team
SNDL	Standard Double Lock Recompression Chamber
SOF	Special Operations Forces
SOLAS	Safety of Life at Sea
SRC	Surfacing Rescue Container (NOTE: SRC should not be confused with the Submarine Rescue Chamber, which will always be spelled out when referenced in this paper)
SRDRS	Submarine Rescue Diving and Recompression System
SRG	Surfacing Rescue Gear (group retractable SRC)
SRV	Submarine Rescue Vehicle
SSBN	Nuclear Ballistic Missile Submarine
SSGN	Guided Missile Submarines
SSK	Hunter-Killer/ASW Submarine

SSN	Nuclear Attack Submarine
STANAG	NATO Standardization Agreement
SUBOPAUTH	Submarine Operating Authority
SWBS	Ship Work Breakdown Structure
TPI	Tons Per inch Immersion
TTFR	Time to First Rescue
TUP	Transfer Under Pressure
UAV	Unmanned Aerial Vehicles
UMO	Undersea Medical Officer
UMO	Undersea Medical Officers
UTS	Ultimate Tensile Strength
UUV	Unmanned Underwater Vehicles
VOC	Volatile Organic Compounds
VOO	Vessel of Opportunity

(INTENTIONALLY LEFT BLANK)

TERMS AND DEFINITIONS (STRUCTURAL ANALYSIS)

A	Constant [non-dimensional]
A_{eff}	Effective frame area [length ²]
A_f	Frame area [length ²]
a	Frame deflection parameter [non-dimensional]
a	Semimajor axis [length]
B	Constant [non-dimensional]
b	Semiminor axis [length]
C	Axial (extensional) stiffness parameter [mass/time ²]
D	Bending stiffness parameter [mass·length ² /time ²]
D_o	Outer diameter of cylindrical shell (i.e. hull) [length]
D_w	Design collapse depth [length]
E	Young's Modulus (HY80: $E \approx 29,500,000$ psi) [mass/length·time ²]
$E1$	First frame parameter, ECCS (measure of frame stability) [non-dimensional]
$E2$	Second frame parameter, ECCS (measure of frame stability) [non-dimensional]
$E3$	Third frame parameter, ECCS (measure of frame stability) [non-dimensional]
e	Frame eccentricity (OOR) [length]
e_w	Frame web eccentricity [length]
F	Constant [length]
F_1	First transcendental function [non-dimensional]
F_2	Second transcendental function [non-dimensional]
F_3	Third transcendental function [non-dimensional]
F_4	Fourth transcendental function [non-dimensional]
$F1$	First frame parameter, SSP74 (measure of frame stability) [non-dimensional]
$F2$	Second frame parameter, SSP74 (measure of frame stability) [non-dimensional]
$F3$	Third frame parameter, SSP74 (measure of frame stability) [non-dimensional]
G	Constant [non-dimensional]
g	Gravitational acceleration [length/time ²]
h_{fl}	Flange breadth [length]
h_w	Web height [length]
I	Moment of inertia of a single frame including a length (L_f) of shell plating [length ⁴]
I_{eff}	Moment of inertia of a single frame including a length (L_{eff}) of shell plating [length ⁴]
I_{req}	Required moment of inertia for king frames [length ⁴]
L	Clear length enclosed by stiffeners ($L_f - t_w$) [length]
L_b	Length between bulkheads [length]

L_D	Largest spacing between an adjacent bulkhead and a deep frame or between adjacent deep frames [length]
L_{beff}	Effective bulkhead spacing [length]
L_{eff}	Effective frame spacing [length]
L_f	Frame spacing [length]
m	Number of half sine waves in the axial direction [non-dimensional]
\bar{m}	Dimensionless wave number along the axis of the cylinder [non-dimensional]
N_θ	Dome circumferential force [mass·length/time ²]
N_ϕ	Dome meridional force [mass·length/time ²]
n	Number of complete sine waves in the circumferential direction [non-dimensional]
n_c^{GI}	Critical buckling mode for shell general instability [non-dimensional]
p	External hydrostatic pressure [mass/length·time ²]
p_c^Y	Critical pressure for shell yielding [mass/length·time ²]
p_c^{Ye}	Critical pressure for end-cap yielding [mass/length·time ²]
p_c^{Be}	Critical pressure for end-cap buckling [mass/length·time ²]
\tilde{p}_c^{Be}	Critical pressure for end-cap buckling (empirical) [mass/length·time ²]
p_c^{LB}	Critical pressure for shell lobar buckling (interframe collapse) [mass/length·time ²]
p_c^{GI}	Critical pressure for shell general instability (overall collapse) [mass/length·time ²]
p_c^{GI*}	Critical pressure for shell general instability ($L = L_{beff}$) [mass/length·time ²]
q	Total radial load acting on a ring frame per inch of circumference [mass/time ²]
R	Outer radius of shell [length]
R_c	Outer crown radius of the torispherical shell [length]
R_f	Radius to the centroid of the frame cross-section [length]
R_k	Outer knuckle radius of the torispherical shell [length]
R_{NA}	Radius to neutral axis of shell-frame composite [length]
R_o	Outer radius of sphere [length]
R_s	Radius to midplane of shell [length]
R_1	Radius to the frame toe [length]
r_o	Radius from the axis of revolution to the parallel circle [length]
r_1	Principle radii of curvature at point one on the dome surface [length]
r_2	Principle radii of curvature at point two on the dome surface [length]
SF_{FY}	Frame yield safety factor [non-dimensional]
SF_{FI}	Frame instability safety factor [non-dimensional]
SF_{GI}	Shell general instability yield safety factor [non-dimensional]
SF_{LB}	Shell lobar buckling safety factor [non-dimensional]
SF_{SY}	Shell yield safety factor [non-dimensional]
t_{fl}	Flange thickness [length]
t_s	Shell thickness [length]

t_w	Web thickness [length]
U	Degree of flexibility provided by frame [non-dimensional]
V	Ratio of shell area under the frame faying flange, to the total frame area plus shell area under frame faying flange [non-dimensional]
α	Ratio of effective frame area to shell area [non-dimensional]
β	Ratio of faying width to frame spacing [non-dimensional]
γ	Beam column effect [non-dimensional]
η_1	First non-dimensional parameter [non-dimensional]
η_2	Second non-dimensional parameter [non-dimensional]
θ	Slenderness parameter [non-dimensional]
θ	Circumferential angle [degrees]
λ	Slenderness ratio [non-dimensional]
ν	Poisson's ratio (HY80: $\nu \approx 0.3$) [non-dimensional]
ρ	Saltwater density ($\rho \approx 1.999$ slugs/feet ³) [mass/length ³]
$\bar{\sigma}$	Von Mises stress [mass/length·time ²]
$\sigma_{bending}$	Frame bending stress [mass/length·time ²]
σ_{hoop}	Frame hoop (direct) stress [mass/length·time ²]
σ_Y	Yield stress (HY80: $\sigma_Y \approx 80,000$ psi) [mass/length·time ²]
$\sigma_{\theta\theta MB}$	Circumferential hoop stress, mid-bay [mass/length·time ²]
$\sigma_{xx MB}$	Longitudinal (axial) stress, mid-bay [mass/length·time ²]
$\sigma_{\theta\theta NF}$	Circumferential hoop stress, near-frame [mass/length·time ²]
$\sigma_{xx NF}$	Longitudinal (axial) stress, near-frame [mass/length·time ²]
φ	Meridional angle [degrees]
ϕ	Modified pressure factor [non-dimensional]
Ψ	Pressure factor [non-dimensional]

Superscripts/Subscripts

e End-cap
 KF King frame (deep frame)

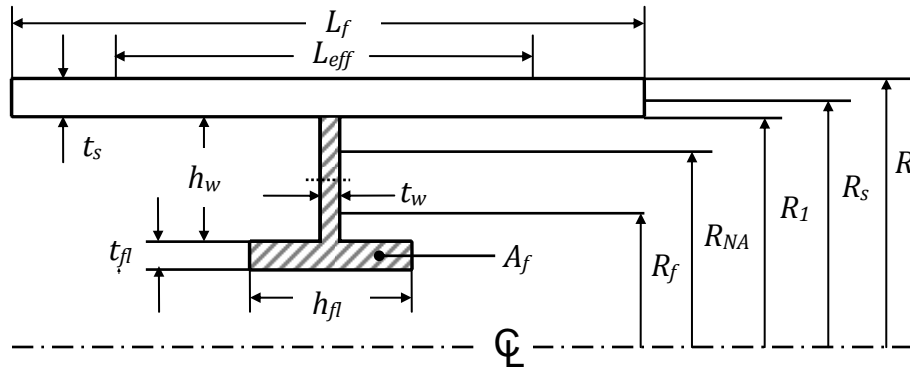


Figure 64. Small frame scantling dimensions and definitions

TERMS AND DEFINITIONS (SEAKEEPING ANALYSIS)

A_{ij}	Added mass in i when accelerated in j [mass]
a	Wave amplitude [length]
a	Semimajor axis [length]
a_0	Particular wave amplitude [length]
\overline{BG}	Distance between center of buoyancy and center of gravity [length]
B_{ij}	Damping coefficient in i with speed in j [mass/time]
b	Semiminor axis [length]
C_D	Coefficient of damping [non-dimensional]
C_{ij}	Hydrostatic restoring coefficient in i when displaced in j [mass/time ²]
D_o	Cylinder diameter [length]
d	Dished end-cap radius center offset from origin [length] (See Figure 65)
F, f	Force [mass·length/time ²]
\overline{GM}	Vertical distance between center of gravity and metacenter [length]
g	Gravitational acceleration [length/time ²]
$H(\omega)$	Transfer function (aka. Response Amplitude Operator (RAO)) [non-dimensional]
H_{mf}	Most frequent wave height [length]
$H_{1/N}$	Average height of top 1/ N percent of all observed waves [length]
I	Moment of Inertia [mass·length ²]
i	$\sqrt{-1}$ [non-dimensional]
$ i $	Magnitude of i [units of i]
\hat{i}	Complex magnitude of i [units of i]
\overline{KG}	Distance from keel to center of gravity [length]
k	Wave number [1/length]
L	Draft of cylindrical section [length] (See Figure 65)
ℓ	Variable of integration [non-dimensional] (See Figure 65)
M	Mass [mass]
M_0	Zeroth moment of a spectrum [length ²]
M_2	Second moment of a spectrum [length ² /time ²]
M_4	Fourth moment of a spectrum [length ² /time ⁴]
p	Probability or probability density
R	Outer radius of shell [length] (See Figure 65)

R_o	Outer radius of sphere [length] (See Figure 65)
\bar{S}	Surface of integration
$S(\omega)$	Wave spectrum (i.e. sea spectrum) [time·length ²]
x	x – axis coordinate [length]
X_1	Surge [length]
X_2	Sway [length]
X_3	Heave [length]
X_4	Roll [radians]
X_5	Pitch [radians]
X_6	Yaw [radians]
y	y – axis coordinate [length]
z	z – axis coordinate [length]
β	Dished end-cap arc angle [radians] (See Figure 65)
Δ	Displacement [mass]
ε	Spectrum bandwidth [non-dimensional]
η	Wave elevation [length]
θ	Circumferential angle [radians]
λ	Wave length [length]
ρ	Density [mass/length ³]
σ	Standard deviation [length]
τ	Dummy variable of integration
Φ_I	Velocity potential function [length ² /time]
ϕ	Pitch angle [radians]
ψ_i	Phase angle of i [1/time]
ω	Wave frequency [1/time]
ω_m	Modal frequency [radians/time]
∇	Volume of displacement [length ³]

Superscripts/Subscripts

<i>dish</i>	Dish type end-cap (See Figure 65)
<i>disk</i>	Disk type end-cap (See Figure 65)
<i>m</i>	Maxima
<i>max</i>	Maximum
<i>FK</i>	Froude-Krylov
<i>I</i>	Incident
<i>RMS</i>	Root mean square
<i>S</i>	Surface
*	Non-dimensional
<i>x, y, z</i>	Cartesian coordinate direction
1,3,5	Surge, Heave and Pitch, respectively

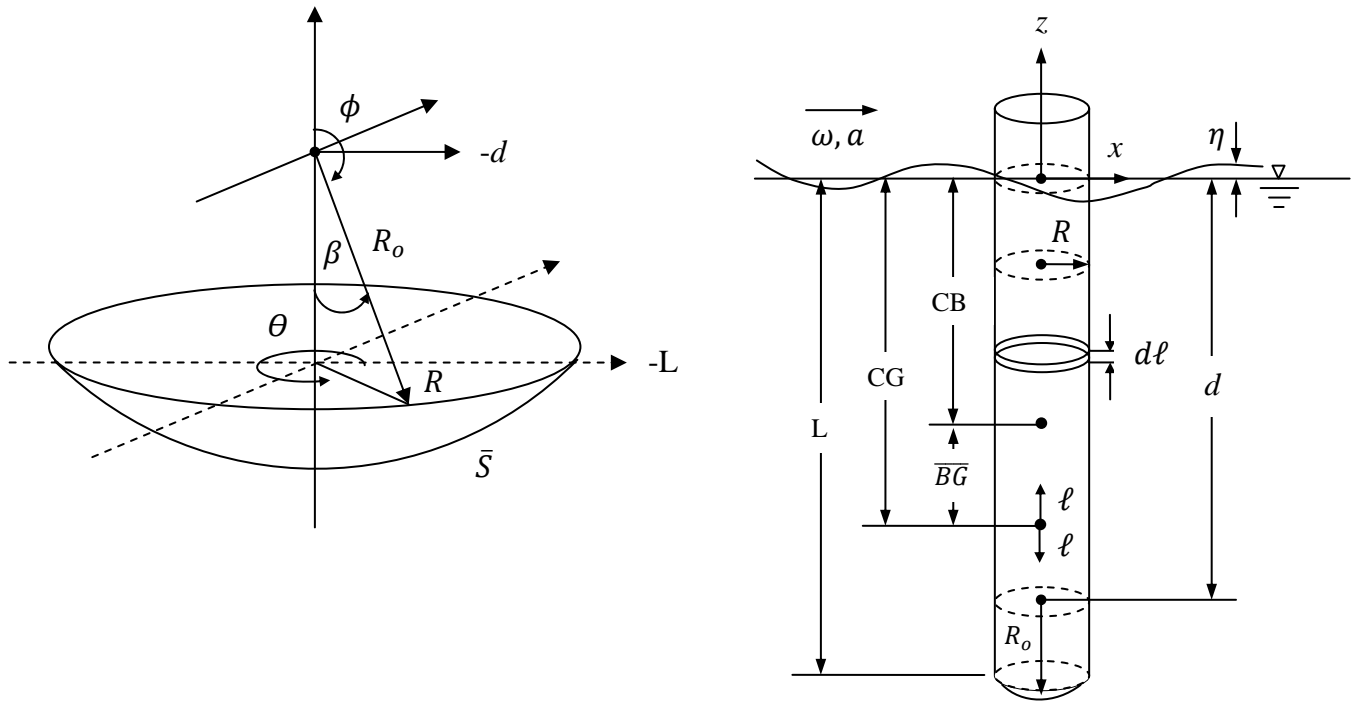


Figure 65. Seakeeping analysis dimensions

(INTENTIONALLY LEFT BLANK)

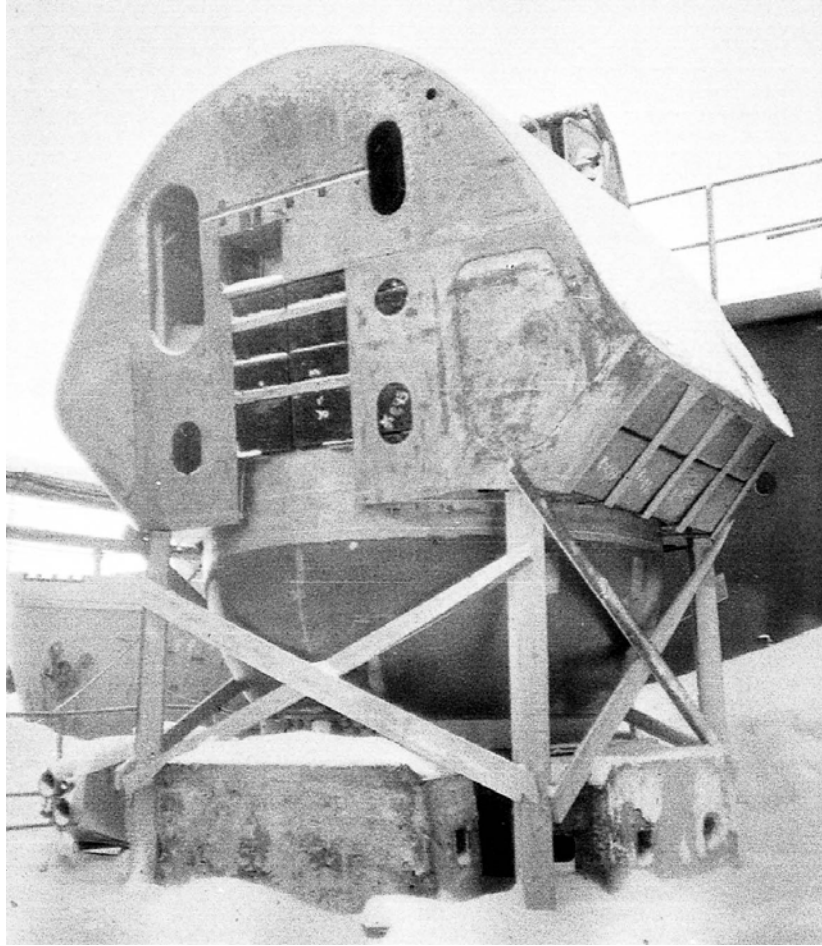
APPENDIX I. SRC Designs



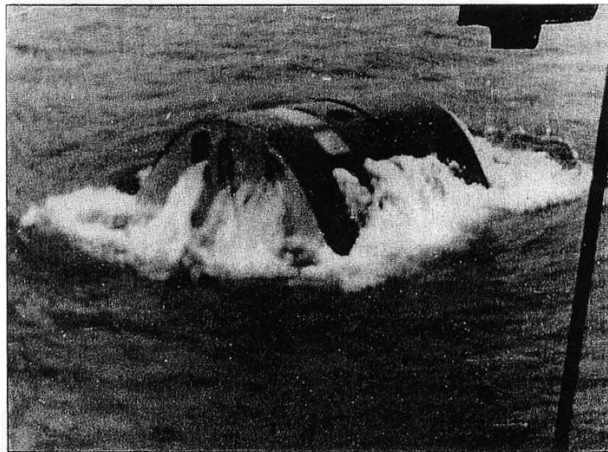
Typhoon class SRC. (removed for maintenance) [35]



Sierra class SRC (courtesy of W. Frey, [36])



Alfa class SRC (courtesy of W. Frey, [36])

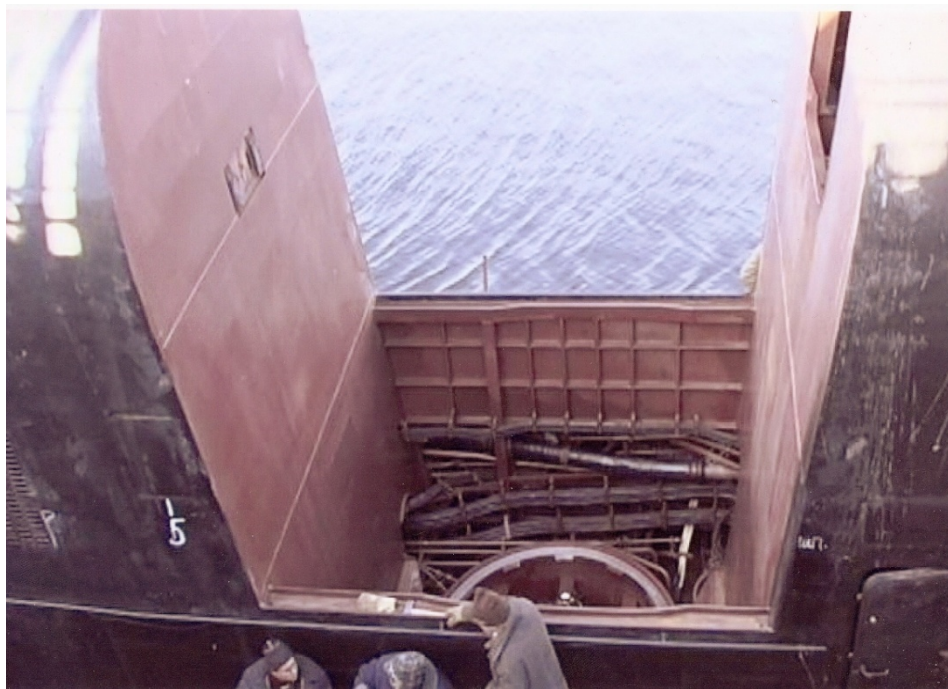


Испытание ВСК ПЛА пр.705

Alfa class SRC surfacing (courtesy of W. Frey, [36])



Akula class SRC (courtesy of W. Frey, [36])



Akula class SRC (courtesy of W. Frey, [36])

(INTENTIONALLY LEFT BLANK)

APPENDIX II. Historical Submarine Escape and Rescue Data

<u>INSTANCE</u>	<u>YEAR</u>	<u>FLAG</u>	<u>DISSUB</u>	<u>DEPTH (FEET)</u>	<u>TTFR (HRS)</u>
1	1851	Germany	Brandtaucher	53	6.5
2	1901	French	Farfadet	<100	NA
3	1903	Germany	U-3	50	1.5
4	1910	Japan	IJNS No. 6	60	NA
5	1915	Germany	UB-57	129	Promptly
6	1916	Britain	HMS E-41	45	2
7	1916	Germany	U-51	90	6
8	1916	Britain	E-41	45	Promptly
9	1916	Danish	Dykkeren	28	Promptly
10	1917	Britain	HMS K-13	200	10
11	1917	Germany	UB-84	<100	NA
12	1919	Chile	Rucumilla (H-3)	56	7
13	1920	USA	USS S-5 (SS-110)	197	51
14	1921	USA	USS S-48 (SS-159)	60	Uncertain
15	1923	USA	USS O-5 (SS-66)	50	31
16	1927	USA	USS S-4 (SS-109)	110	NA
17	1931	Britain	HMS Poseidon (P-99)	130	2.5
18	1939	Britain	HMS Thetis (N-25)	140	16.5
19	1939	USA	USS Squalus (SS-192)	242	28
20	1939	Germany	U-40	115	1.5
21	1940	Germany	U-64	131	Promptly
22	1940	Britain	HMS H-49	70	Promptly
23	1941	Britain	HMS Umpire (N-82)	60	Promptly
24	1941	Britain	HMS P-32	210	Promptly
25	1941	Britain	HMS Perseus (N-36)	170	1
26	1942	Germany	U-512	164	Promptly
27	1942	Germany	U-701	100	Promptly
28	1942	Italy	Iride	<50	2.5
29	1943	Germany	U-533	367	Promptly
30	1943	Germany	U-526	30	NA
31	1943	Britain	HMS Untamed (P-58)	160	NA
32	1943	Britain	HMS X-3	114	Promptly
33	1944	Germany	U-413	89	<1
34	1944	Germany	U-550	318	Uncertain
35	1944	USA	USS Tang (SS-306)	180	7.5
36	1944	Britain	Wellman X	186	0.5
37	1944	Germany	U-741	190	Promptly
38	1944	Germany	U-767	<250	0
39	1944	Britain	HMS Stratagem (P-234)	<200	Promptly
40	1944	Germany	U-859	160	Promptly
41	1945	Germany	U-1195	98	Promptly
42	1945	Germany	U-1199	240	Promptly
43	1945	Britain	XE11	215	0
44	1945	Germany	U-399	190	<0.5
45	1950	Britain	HMS Truculent (P-315)	80	Promptly
46	1981	Soviet Union	C-178 (S-178)	131	31.2
47	1983	Soviet Union	Ckam (K-429)	128	7
48	1988	Peru	BAP Pacocha (SS-48)	140	15.5
49	1989	Soviet Union	Komsomolets (K-278)	5500	0
50	2000	Russia	Kursk (K-141)	350	NA

<u>INSTANCE</u>	<u>METHOD OF ESCAPE/RESCUE</u>
1	Free ascent without individual escape gear
2	Condemned
3	Dry exit through torpedo tube
4	Condemned
5	Free ascent, some with individual escape gear
6	Free ascent without individual escape gear
7	Free ascent with individual escape gear
8	Free ascent without individual escape gear
9	3 Ascent without individual escape gear, 5 Dry exit through hatch
10	2 Free ascent without individual escape gear, 47 Dry exit through torpedo tube
11	Condemned
12	Dry exit through hatch
13	Dry exit through hole cut in pressure hull
14	Dry exit through torpedo tube
15	Dry exit through hatch
16	Condemned
17	Free ascent with individual escape gear
18	Free ascent without individual escape gear
19	Submarine Rescue Chamber
20	Free ascent with individual escape gear
21	Free ascent with individual escape gear
22	Free ascent without individual escape gear
23	Free ascent, most with individual escape gear
24	Free ascent with individual escape gear
25	Free ascent with individual escape gear
26	Free ascent from torpedo tube using individual escape gear
27	Free ascent without individual escape gear
28	Free ascent without individual escape gear
29	Free ascent from torpedo tube using individual escape gear
30	Condemned
31	Condemned
32	Free ascent with individual escape gear
33	Free ascent without individual escape gear
34	Free ascent from torpedo tube using individual escape gear
35	2 Free ascent without individual escape gear, 7 with individual escape gear
36	Free ascent with individual escape gear
37	Free ascent with individual escape gear
38	Free ascent without individual escape gear
39	Free ascent, some with individual escape gear
40	Free ascent without individual escape gear
41	Free ascent from torpedo tube and tower, some with individual escape gear
42	Free ascent from torpedo tube using individual escape gear
43	Free ascent without individual escape gear
44	Free ascent without individual escape gear
45	Free ascent from torpedo tube using individual escape gear
46	Free ascent from torpedo tube, some with individual escape gear
47	Free ascent from torpedo tube using individual escape gear
48	Free ascent from torpedo tube using individual escape gear
49	Surfacing Rescue Container
50	Condemned

INSTANCE OUTCOME

1	3 escaped and survived
2	All 14 died awaiting rescue. Hull tapping stopped after 32 hours
3	28 were rescued, 3 died waiting to be saved
4	All 16 died awaiting rescue
5	6 survived, several men died during ascent
6	All 7 survived
7	5 escaped, 2 died during ascent
8	1 escaped and survived
9	3 escaped, 5 were rescued, 1 died in conning tower
10	2 escaped after 10 hours, 1 died attempting escape, 47 were rescued after 57 hours
11	All 7 died awaiting rescue. Hull tapping stopped after 30 hours
12	All 25 survived
13	Entire crew survived
14	All 41 survived
15	All 2 survived
16	All 34 died awaiting rescue. Hull tapping stopped after 2 hours
17	7 escaped (2 after 2.5 hours and 5 after 6 hours), 1 died during ascent, some had DCS
18	4 escaped, 99 died waiting to be rescued
19	33 men rescued
20	9 escaped, 7 died of hypothermia
21	All 8 survived
22	1 escaped and survived
23	21 escaped, 5 were never found
24	3 escaped, 1 died during ascent, 21 died contemplating escape
25	4 escaped, 3 were never found
26	3 escaped, 2 died during ascent
27	18 escaped, 7 survived
28	7 escaped, 2 died during ascent, 2 died waiting to be rescued
29	3 escaped, 1 died during ascent, and 1 died at surface an hour later
30	12 abandoned ship prior to sinking
31	All 33 died attempting escape. Survivors were alive for at least 4 hours
32	3 escaped and survived
33	1 escaped and survived
34	At least 3 men escaped, all died adrift
35	13 attempted escape, 4 did not succeed
36	1 escaped and survived
37	2 escaped, 1 died after ascent
38	1 escaped and survived
39	10 escaped, 2 died during ascent, some had DCS
40	20 escaped and survived
41	18 survived
42	1 escaped and survived
43	2 escaped and survived
44	1 escaped and survived
45	60 escaped, 50 were never found
46	4 died trapped in submarine, 26 escaped, 3 died on surface, 3 were never found
47	120 escaped, 16 died during ascent
48	21 escaped, 1 died during ascent, 1 suffered brain damage and some DCS
49	4 escaped, 3 died during/after ascent
50	23 died awaiting rescue. Survivors were alive for at least 6.3 hours

(INTENTIONALLY LEFT BLANK)

APPENDIX III. NAVSEA HY80 Stress-Strain Curve Data

SMALL FRAME FLANGE (ROLLED)		KING FRAME FLANGE (ROLLED)		SHELL (ROLLED)	
STRESS (PSI)	STRAIN (IN/IN)	STRESS (PSI)	STRAIN (IN/IN)	STRESS (PSI)	STRAIN (IN/IN)
0	0	0	0	0	0
22303.41	0.000743447	21600.55	0.000720018	21123.43	0.000704114
26845.04	0.000900000	26816.24	0.000900000	26717.24	0.000900000
35359.50	0.001200000	35326.30	0.001200000	34849.52	0.001200000
43340.62	0.001500000	43283.74	0.001500000	42387.45	0.001500000
50408.30	0.001800000	50239.76	0.001800000	49264.99	0.001800000
56723.14	0.002100000	56546.60	0.002100000	55547.32	0.002100000
62347.33	0.002400000	62168.45	0.002400000	61167.25	0.002400000
67226.63	0.002700000	67045.50	0.002700000	66033.36	0.002700000
71171.16	0.003000000	70987.94	0.003000000	69964.80	0.003000000
74459.45	0.003300000	74278.71	0.003300000	73268.09	0.003300000
77051.44	0.003600000	76892.68	0.003600000	75903.58	0.003600000
78664.53	0.003900000	78615.84	0.003900000	77898.73	0.003900000
79565.81	0.004200000	79526.48	0.004200000	79214.06	0.004200000
80052.30	0.004500000	80042.05	0.004500000	79982.89	0.004500000
80201.19	0.004800000	80196.91	0.004800000	80167.45	0.004800000
80297.84	0.005100000	80295.18	0.005100000	80276.75	0.005100000
80369.94	0.005400000	80368.13	0.005400000	80355.44	0.005400000
80426.91	0.005700000	80425.57	0.005700000	80416.35	0.005700000
80473.49	0.006000000	80472.48	0.006000000	80465.49	0.006000000
80512.51	0.006300000	80511.71	0.006300000	80506.27	0.006300000
80545.77	0.006599999	80545.14	0.006599999	80540.79	0.006599999
80574.54	0.006899999	80574.02	0.006899999	80570.48	0.006899999
80599.71	0.007199999	80599.29	0.007199999	80596.38	0.007199999
80621.94	0.007499999	80621.59	0.007499999	80619.15	0.007499999
80641.74	0.007799999	80641.45	0.007799999	80639.39	0.007799999
80659.52	0.008099999	80659.25	0.008099999	80657.49	0.008099999
80675.54	0.008400000	80675.33	0.008400000	80673.81	0.008400000
80690.11	0.008700000	80689.89	0.008700000	80688.59	0.008700000
80703.37	0.009000001	80703.20	0.009000001	80702.05	0.009000001
80715.52	0.009300001	80715.37	0.009300001	80714.37	0.009300001
80726.70	0.009600001	80726.56	0.009600001	80725.66	0.009600001
80737.02	0.009900002	80736.89	0.009900002	80736.10	0.009900002
80746.55	0.010200002	80746.45	0.010200002	80745.73	0.010200002
80755.43	0.010500003	80755.34	0.010500003	80754.70	0.010500003

80763.69	0.010800003	80763.61	0.010800003	80763.03	0.010800003
80771.40	0.011100003	80771.33	0.011100003	80770.81	0.011100003
80778.62	0.011400004	80778.56	0.011400004	80778.09	0.011400004
80785.39	0.011700004	80785.31	0.011700004	80784.90	0.011700004
80791.76	0.012000005	80791.69	0.012000005	80791.31	0.012000005
80797.73	0.012300005	80797.69	0.012300005	80797.34	0.012300005
80803.41	0.012600006	80803.36	0.012600006	80803.02	0.012600006
80808.73	0.012900006	80808.70	0.012900006	80808.40	0.012900006
80813.80	0.013200006	80813.74	0.013200006	80813.48	0.013200006
80818.59	0.013500007	80818.55	0.013500007	80818.30	0.013500007
80823.15	0.013800007	80823.11	0.013800007	80822.88	0.013800007
80827.46	0.014100008	80827.45	0.014100008	80827.23	0.014100008
80831.60	0.014400008	80831.57	0.014400008	80831.36	0.014400008
80835.52	0.014700009	80835.48	0.014700009	80835.30	0.014700009
80839.25	0.015000009	80839.23	0.015000009	80839.06	0.015000009
80842.84	0.015300009	80842.82	0.015300009	80842.66	0.015300009
80846.26	0.015600010	80846.23	0.015600010	80846.09	0.015600010
80849.54	0.015900010	80849.52	0.015900010	80849.38	0.015900010
80852.66	0.016200010	80852.64	0.016200010	80852.52	0.016200010
80855.69	0.016500009	80855.66	0.016500009	80855.54	0.016500009
80858.56	0.016800009	80858.55	0.016800009	80858.43	0.016800009
80861.34	0.017100008	80861.32	0.017100008	80861.21	0.017100008
80864.02	0.017400008	80863.98	0.017400008	80863.89	0.017400008
80866.56	0.017700007	80866.55	0.017700007	80866.46	0.017700007
80869.04	0.018000007	80869.02	0.018000007	80868.94	0.018000007
80876.91	0.018300006	80876.90	0.018300006	80882.31	0.018300006
80884.64	0.018600006	80884.61	0.018600006	80889.96	0.018600006
80892.16	0.018900005	80892.13	0.018900005	80897.39	0.018900005
80910.48	0.019200005	80910.41	0.019200005	80910.16	0.019200005
80917.52	0.019500004	80917.46	0.019500004	80922.73	0.019500004
80929.88	0.019800004	80929.83	0.019800004	80929.57	0.019800004
80947.59	0.020100003	80947.53	0.020100003	80941.75	0.020100003
80953.98	0.020400003	80953.93	0.020400003	80953.69	0.020400003
80965.75	0.020700002	80965.70	0.020700002	80965.47	0.020700002
80971.81	0.021000002	80971.77	0.021000002	80971.55	0.021000002
80988.72	0.021300001	80988.71	0.021300001	80977.48	0.021300001
80994.40	0.021600001	80994.39	0.021600001	80988.80	0.021600001
81000	0.021823216	81000	0.021846645	81000	0.021862550

FRAME WEB
(UNROLLED)

STRESS (PSI)	STRAIN (IN/IN)
0	0
77000	0.002566670
78000	0.002700000
79000	0.002900000
79500	0.003100000
80000	0.004600000
80500	0.010000000
81000	0.020000000

Note: HY80 reaches UTS above 90,000 PSI. If necessary, the stress strain data in this Appendix can be extrapolated linearly along a slope tangent to the last several points.

(INTENTIONALLY LEFT BLANK)

APPENDIX IV. Full Factorial Scantling Optimization Routine (FFSOR)

```

% Program: Full Factorial Scantling Optimization Routine (FFSOR) - Small Frame
% Language: MATLAB Script (M-file)
% Author: LCDR Joshua LaPenna
% Date: June, 2009
% Units: English

% Function: This program calculates the failure pressure of a cylindrical
%           pressure vessel by 5 different failure modes (Yield, General
%           instability, Lobar Buckling, Frame Yield, & Frame Instability)
%           for numerous combinations of structural dimensions. The program
%           gives the user control of 7 parameters (Frame Spacing, Shell
%           Thickness, Web Height, Web Thickness, Flange Height, Flange
%           Thickness, & Length between bulkheads). The program then tests
%           every combination of the given dimensions to arrive at the most
%           efficient design (lowest weight).
clear
clc
close all

%User Input Parameters
g = 32.174; %Gravity (ft/sec^2)
R = 83/2; %Outer Radius of Cylinder (inches)
OD = 2*R; %Outer Diameter of Cylinder (inches)
b = 29; %Minor Semiaxes of Oblate Spheroid – End-cap Height (inches)
v = 0.3; %Poisson's Ratio (Steel)
E = 29500000; %Young's Modulus (steel)(lb/in^2)
sigmaY = 80000; %Yield Strength (steel)(lb/in^2)
rhoW = 1.999; %Density of salt water (slugs/ft^3)
rhoS = 15.134; %Density of steel (slugs/ft^3)
Dw = 2500; %Designed collapse pressure (feet)
SFy = 1.5; %Safety Factor for Yield
SFib = 2.25; %Safety Factor for Lobar Buckling
SFgi = 3.75; %Safety Factor for General Instability
SFfy = 1.5; %Safety Factor for Frame Yield
SFfi = 1.8; %Safety Factor for Frame Instability
e = 0.5; %Eccentricity (inches)
SGTEST=1; %Enter 1 to check solutions against scantling guidelines

% Design A [Minimum Value : Increment : Maximum Value]
% Note: LB = (Compartment length) 407" + (Dome Height) 29"(0.4)

LB = [34.885*12]; %Bulkhead Spacing (inches)
LF = [8:1:36]; %Frame Spacing (inches)
TS = [24/32:1/32:1.25]; %Shell Thickness (inches)
HW = [3:0.25:6]; %Web Height (inches)
TW = [1/4:1/32:3/4]; %Web Thickness (inches)
HFL = [2:1/4:7]; %Flange Width (inches)
TFL = [1/2:1/32:1.25]; %Flange Thickness (inches)

% Selected Scantlings for Design A
% "Hide" line 245 & 255 when running these scantlings (i.e. SG6 does not apply)
% LB = [34.885*12]; %Bulkhead Spacing (inches)

```



```

% LF = [14]; %Frame Spacing (inches)
% TS = [0.75]; %Shell Thickness (inches)
% HW = [6]; %Web Height (inches)
% TW = [0.34375]; %Web Thickness (inches)
% HFL = [4.75]; %Flange Width (inches)
% TFL = [0.65625]; %Flange Thickness (inches)

% Design B [Minimum Value : Increment : Maximum Value]
% Note: SSP74 recommends increasing LB by 5%-10% when using king frames.
% For this analysis, 7.5% is used.

% LB = [12*1.075*12]; %Bulkhead Spacing (inches)
% LF = [12:1:32]; %Frame Spacing (inches)
% TS = [24/32:1/32:1.25]; %Shell Thickness (inches)
% HW = [3:0.25:6.25]; %Web Height (inches)
% TW = [1/4:1/32:3/4]; %Web Thickness (inches)
% HFL = [2:1/4:7]; %Flange Width (inches)
% TFL = [1/2:1/32:1]; %Flange Thickness (inches)

% Selected Scantlings for Design B
% LB = [12*1.075*12]; %Bulkhead Spacing (inches)
% LF = [23]; %Frame Spacing (inches)
% TS = [0.75]; %Shell Thickness (inches)
% HW = [6]; %Web Height (inches)
% TW = [0.34375]; %Web Thickness (inches)
% HFL = [4.75]; %Flange Width (inches)
% TFL = [0.6875]; %Flange Thickness (inches)

%Calculates the total number of scantling combinations
TC=length(LB)*length(LF)*length(TS)*length(HW)*length(TW)*length(HFL)*length(TFL);
combinations=0;
status=0;
ET=0;
solcount=0;

%Sizes matrices for output plots
Best=[0 0 0 0 0 0 0 0 0 0 0 0 0 0 0 0 0 0 0 0];
Poor=[0 0 0 0 0 0 0 0 0 0 0 0 0 0 0 0 0 0 0 0];
Random=[0 0];

%Optimization Loop Begins
for j1=1:length(LF)
    for j2=1:length(TS)
        for j3=1:length(HW)
            for j4=1:length(TW)
                for j5=1:length(HFL)
                    for j6=1:length(TFL)
                        for j7=1:length(LB)
                            combinations=combinations+1;
                            status=status+1;
                            tic;
                            Lf=LF(1,j1);
                            ts=TS(1,j2);
                            hw=HW(1,j3);
                            tw=TW(1,j4);

```

```

hfl=HFL(1,j5);
tfl=TFL(1,j6);
Lb=LB(1,j7);

```

%Derived Parameters

```

Input=[Lf ts hw tw hfl tfl];
Rs=-(ts/2)+R;
theta=Lf*((3*(1-(v^2)))/((Rs*ts)^2))^0.25;
Leff = 1.56*((Rs*ts)^0.5)*((cosh(theta)-cos(theta))/(sinh(theta)+sin(theta)));
ls=Leff*(ts^3)/12;
lw=tw*(hw^3)/12;
lfl=hfl*(tfl^3)/12;
Afl=tfl*hfl;
Aw=tw*hw;
Aseff=ts*Leff;
Af=Afl+Aw;
Weight=((2*rhost*g/1728)*(((R-(ts/2))*Lf*ts)+((R-ts-(hw/2))*tw*hw)+((R-ts-hw-(tfl/2))*hfl*tfl)));
BR=(rhow*g/1728*(R^2)*Lf)/Weight;
ynaf=Afl*((hw+tfl)/2)/(Af); %Distance from web center to frame NA (toward flange is positive)
Rf=R-ts-(hw/2)-ynaf; %Radius to the centroid of the frame cross-section
L=Lf-tw; %Length enclosed by stiffeners
C=(E*ts)/(1-v^2);
D=(E*(ts^3))/(12*(1-v^2));
lwcorf=lw+Aw*(ynaf^2);
lflcorf=lfl+Afl*(((tfl+hw)/2)-(ynaf))^2;
lframe=lwcorf+lflcorf;

ynaLeff=(((hw+tfl)/2)*Afl)-(((hw+ts)/2)*Aseff)/(Aseff+Aw+Afl);
lscor=ls+Aseff*(((ts+hw)/2)+ynaLeff)^2;
lwcor=lw+Aw*(ynaLeff^2);
lflcor=lfl+Afl*(((tfl+hw)/2)-ynaLeff)^2;
leff=lscor+lwcor+lflcor;
Reff=R-ts-(hw/2)-ynaLeff; %Radius to the centroid of the frame-plate (Leff) composite cross-section

Asf=ts*Lf;
lsf=Lf*(ts^3)/12;
ynaLf=(((hw+tfl)/2)*Afl)-(((hw+ts)/2)*Asf)/(Asf+Aw+Afl);
lscorf=lsf+Asf*(((ts+hw)/2)+ynaLf)^2;
lwcorf=lw+Aw*(ynaLf^2);
lflcorf=lfl+Afl*(((tfl+hw)/2)-ynaLf)^2;
l=lscorf+lwcorf+lflcorf;
RNA=R-ts-(hw/2)-ynaLf; %Radius to the centroid of the frame-plate (Lf) composite cross-section

```

%Shell Yield Calculation

```

p=rhow*g*Dw*SFy/144;
Aeff=(R/Rf)*Af;
alpha=Aeff/(Lf*ts);
beta=tw/Lf;
PCY=0; %Initial guess, gamma = 0 implies no beam-column effect
iter=0;
FLAG01=0;
while (1)
    PCYold=PCY;
    iter=iter+1;
    gamma=(PCY/(2*E))*((abs(Rs/ts))^2)*sqrt(3*(1-v^2));

```

```

n1=0.5*sqrt(1-gamma);
n2=0.5*sqrt(1+gamma);
F1=(4/theta)*abs((((cosh(n1*theta))^2)-
((cos(n2*theta))^2))/(((cosh(n1*theta)*sinh(n1*theta))/n1)+((cos(n2*theta)*sin(n2*theta))/n2)));
F2=abs((((cosh(n1*theta)*sin(n2*theta))/n2)+((sinh(n1*theta)*cos(n2*theta))/n1))/(((cosh(n1*theta)*sinh(n
1*theta))/n1)+((cos(n2*theta)*sin(n2*theta))/n2)));
F3=sqrt(3/(1-v^2))*abs((((cos(n2*theta)*sin(n2*theta))/n2)-
((cosh(n1*theta)*sinh(n1*theta))/n1))/(((cosh(n1*theta)*sinh(n1*theta))/n1)+((cos(n2*theta)*sin(n2*theta))/
n2)));
F4=sqrt(3/(1-v^2))*abs((((cosh(n1*theta)*sin(n2*theta))/n2)-
((sinh(n1*theta)*cos(n2*theta))/n1))/(((cosh(n1*theta)*sinh(n1*theta))/n1)+((cos(n2*theta)*sin(n2*theta))/n
2)));
A=(alpha*((1-v)/2))/(alpha+beta+(1-beta)*F1);
B=(F2^2)+(F2*F4*(1-2*v)*sqrt(0.91/(1-v^2)))+(F4^2)*(1-v+v^2)*(0.91/(1-v^2));
G=1.5*(F2-(v*F4*sqrt(0.91/(1-v^2))));
a=(1-(v/2))/(1+(tw*ts/Aeff)+(Lf*ts*F1/Aeff));
sigmattMB=(p*R/ts)*(1-a*(F2+v*F4));
sigmaxxMB=(p*R/ts)*(0.5+a*F4);
sigmattNF=(p*R/ts)*(1-a*(1-v*F3));
sigmaxxNF=(p*R/ts)*(0.5-a*F3);
sigmaMB=sqrt((sigmattMB^2)-(sigmattMB*sigmaxxMB)+(sigmaxxMB^2));
sigmaNF=sqrt((sigmattNF^2)-(sigmattNF*sigmaxxNF)+(sigmaxxNF^2));
sigmaY=[sigmaMB sigmaNF];
sigmaTY=max(sigmaY);
PCY=(sigmaY*ts/Rs)/(sqrt(0.75+((A^2)*B)-(A*G)));
Error=abs((PCY-PCYold)/PCY)*100;
if Error<=0.001,break,end
if iter==1000
    fprintf('\nERROR 01: Shell Yield pressure not found. Try increasing iterations (Line: 183)\n')
    FLAG01=1; break; end
end
if FLAG01==1
    break, break, break, break, break, break, break, break, end
GammaY=PCY/p; %<1 indicates failure
pCY=p;

%Shell Lobar Buckling Calculation (Windenburg Approximation)
p=rhow*g*Dw*SFib/144;
PCLBW=(2.42*E*((ts/(2*Rs))^2.5))/(((1-v^2)^.75)*(((Lf-tw)/(2*Rs))-(0.45*((ts/(2*Rs))^0.5))));
GammaLBW=PCLBW/p; %<1 indicates failure

%General Instability Calculation
p=rhow*g*Dw*SFgi/144; % (lbf/in^2)
mbar=pi*Rs/Lb;
for n=1:20
    PCGIp(1,n)=n;
    PCGIp(2,n)=(E*ts/Rs)*(mbar^4/(((n^2)-1+((mbar^2)/2))*(((n^2)+(mbar^2))^2)))+(E*leff*((n^2)-
1))/(Lf*(Rs^3));
end
[PCGI,NgI]=min(PCGIp(2,:));
nCGI=PCGIp(1,NgI);
GammaGI=PCGI/p; %<1 indicates failure

%Frame Yielding Calculations
p=rhow*g*Dw*SFfy/144;

```



```

solcount=solcount+1;
sizeBest=size(Best);
if sizeBest(1,1)==101
    [br,sr]=min(Best(:,7));
    if qq(1,7)>br
        Best(sr,:)=qq sgm Lb];
    end
else
    Best(sizeBest(1,1)+1,:)=qq sgm Lb];
end
end
end %SG Loop ends

%Stores Worst 100 Results (i.e. lowest BRs) in Matrix Poor
if (q>1)&(sgm==1)
    sizePoor=size(Poor);
    if sizePoor(1,1)==101
        [br,sr]=max(Poor(:,7));
        if qq(1,7)<br
            Poor(sr,:)=qq sgm Lb];
        end
    else
        Poor(sizePoor(1,1)+1,:)=qq sgm Lb];
    end
end

%Stores Random solutions in matrix Random to generate solution space
fracsol=solcount/2000; %(Note: Change denominator to control plot density)
roundfracsol=round(fracsol);
if (q>1)&(sgm==1)&(fracsol==roundfracsol)
    sizeRandom=size(Random);
    Random(sizeRandom(1,1)+1,:)=qq(1,1) qq(1,7)];
end

%Times operations for status output
looptime=toc;
ET=ET+looptime;

%Prints analysis status in command window
if status==50000
    DTG=clock;
    fprintf('\n***PLEASE DO NOT DISTURB COMPUTER. PROGRAM RUNNING***');
    fprintf('\nDate: %g/%g/%g Time: %g:%g\n',DTG(1,2),DTG(1,3),DTG(1,1),DTG(1,4),DTG(1,5));
    fprintf('%g combinations complete (%g percent)\n',combinations,(combinations/TC)*100);
    fprintf('Elapsed time: %g hours\n',ET/3600);
    fprintf('Approximately %g hours remaining\n\n',(TC-combinations)*(ET/combinations)/3600);
    status=0;
end
    end
    end
    end
    end
    end
end %Optimization Loop Ends

```

```

%Informs user if matrix Best is empty
if FLAG01~=1 % FLAG01 Loop Begins
if nnz(Best)==0 %Output Loop Begins
    fprintf('\nAll scantling combinations:\n');
    fprintf('(1) Fail prior to %g feet (and/or)\n',Dw);
    fprintf('(2) Fail first by modes other than shell yield (and/or)\n');
    if SGTEST==1
        fprintf('(3) Do not meet scantling guidelines\n');
    end
else

%Deletes zero vector in Best
Bestsort = sortrows(Best,7);
Bestflip=flipud(Bestsort);
Bestflip(end,:)=[];
%Matrix Bestflip now has 100 rows which are all valid solutions
%Deletes zero vector in Poor
Poorsort = sortrows(Poor,7);
Poorflip=flipud(Poorsort);
Poorflip(end,:)=[];
%Matrix Poorflip now has 100 rows which are all valid solutions
%Deletes zero vector in Random
if nnz(Random)~=0
    Randomsort = sortrows(Random,2);
    Randomflip=flipud(Randomsort);
    Randomflip(end,:)=[];
end

%Calculates Structure Efficiency for elements in Bestflip
No=((Bestflip(:,1).*pCY).*(Bestflip(:,7)))./10000;
Bestout=[Bestflip No];
Bestflip(101:end,:)=[];

%Stores Best 1000 Results in txt file "Best1000Results.txt"
dlmwrite('Best1000Results.txt', Bestout, 'delimiter', '\t', 'precision', 6);

%Combines Best and Poor
Results=[Bestflip;Poorflip];

%Stores solution with best BR in Output
[br,sr]=max(Bestflip(:,7));
Output=[Bestflip(sr,:)];
%Output=[GammaY GammaLBW GammaGI GammaFY GammaFI GammaAve BR nCGI PCY PCLBW
PCGI sigmaTf PCFI Lf ts hw tw hfl tfl Weight sigmaTY sgm Lb]

%Calculates Shell Lobar Buckling Calculation (Brush & Almroth) for comparison
p=rhow*g*Dw*SFlb/144;
mbar=(1*pi*R)/(Output(1,14)-Output(1,17));
C=(E*Output(1,15))/(1-v^2);
D=(E*(Output(1,15)^3))/(12*(1-v^2));
for n=1:20 %Assumes convergence in 20 iterations
    PCLBp(1,n)=n;
end

```

```

PCLBp(2,n)=((((mbar^2)+(n^2))^4)*(D/R^2))+((mbar^4)*(1-
v^2*C))/(R*(((mbar^2)+(n^2))^2)*((n^2)+(0.5*(mbar^2))));
end
[PCLB,Nlb]=min(PCLBp(2,:));
nCLB=PCLBp(1,Nlb);
GammaLB=PCLB/p; %<1 indicates failure

%Calculates frame stress for the scantlings in Output using SF=1
Afl=Output(1,18)*Output(1,19);
Aw=Output(1,16)*Output(1,17);
Af=Afl+Aw;
ynaf=Afl*((Output(1,16)+Output(1,19))/2)/(Af); %Distance from web center to frame NA (toward flange is
positive)
Rf=R-Output(1,15)-(Output(1,16)/2)-ynaf; %Radius to the centroid of the frame cross-section
Rs=-(Output(1,15)/2)+R;
Aeff=(R/Rf)*Af;
alpha=Aeff/(Output(1,14)*Output(1,15));
beta=Output(1,17)/Output(1,14);
theta=Output(1,14)*((3*(1-(v^2)))/((Rs*Output(1,15))^2))^0.25;
gamma=(Output(1,9)/(2*E))*((abs(Rs/Output(1,15)))^2)*sqrt(3*(1-v^2));
n1=0.5*sqrt(1-gamma);
n2=0.5*sqrt(1+gamma);
F1=(4/theta)*abs((((cosh(n1*theta))^2)-
((cos(n2*theta))^2))/(((cosh(n1*theta))*sinh(n1*theta))/n1)+((cos(n2*theta))*sin(n2*theta))/n2));
p=rhow*g*Dw/144;
sigmahoopf=((p*Rf*Output(1,17)*(1-(v/2)))/(Af+(Output(1,17)*Output(1,15))))*(1+(((alpha/beta)*(1-
beta)*F1)/(alpha+beta+(1-beta)*F1)));
sigmabendf=((p)/(Output(1,11)-p))*((E*e*((Output(1,8)^2)-
1)*((Output(1,15)/2)+Output(1,16)+Output(1,19)))/(Rs^2));
sigmaTf=sigmahoopf+sigmabendf;
GammaFY=sigmaY/sigmaTf;
pDDD=p;

%Calculates the pressure at which frame yielding will occur for the scantlings in Output
iter=0;
while (1)
    iter=iter+1;
    p=p+0.1;
    sigmahoopf=((p*Rf*Output(1,17)*(1-(v/2)))/(Af+(Output(1,17)*Output(1,15))))*(1+(((alpha/beta)*(1-
beta)*F1)/(alpha+beta+(1-beta)*F1)));
    sigmabendf=((p)/(Output(1,11)-p))*((E*e*((Output(1,8)^2)-
1)*((Output(1,15)/2)+Output(1,16)+Output(1,19)))/(Rs^2));
    sigmaTfy=sigmahoopf+sigmabendf;
    Error=abs((sigmaY-sigmaTfy)/sigmaY)*100;
    if Error<=0.005,break,end
    if iter==10000
        fprintf('\nERROR 02: Frame Yield pressure not found. Try increasing iterations (Line:
412)\n'),break,end
end
pFY=p; %External hydrostatic pressure at which an individual frame yields

%Displays Results
fprintf('\n*****User Input*****\n\n');
fprintf('Outer Radius of Cylinder (inches): %g\n',R);
fprintf('Length Between Bulkheads (feet): %g\n',Output(1,23)/12);

```

```

fprintf('Design Collapse Depth (feet):                %g\n',Dw);
fprintf('Total Number of Combinations:                %g\n',TC);

fprintf('\n*****Optimum Scantlings*****\n\n');
fprintf('Frame Spacing (inches):                %g\n',Output(1,14));
fprintf('Shell Thickness (inches):                %g\n',Output(1,15));
fprintf('Web Height (inches):                %g\n',Output(1,16));
fprintf('Web Thickness (inches):                %g\n',Output(1,17));
fprintf('Flange Width (inches):                %g\n',Output(1,18));
fprintf('Flange Thickness (inches):                %g\n',Output(1,19));

fprintf('\n*****Optimum Scantling Results*****\n\n');
fprintf('Shell Yield Pressure:                %g psi (%g\n',ceil(Output(1,9)),ceil((Output(1,9)*144)/(rho*Y)));
fprintf('Shell Lobar Buckling Pressure (mode = %g):                %g psi (%g\n',nCLB,ceil(PCLB),ceil((PCLB*144)/(rho*Y)));
fprintf('Shell Lobar Buckling Pressure (Windenburg):                %g psi (%g\n',ceil(Output(1,10)),ceil((Output(1,10)*144)/(rho*Y)));
fprintf('General Instability (Bryant) Buckling Pressure (mode = %g):                %g psi (%g\n',Output(1,8),ceil(Output(1,11)),ceil((Output(1,11)*144)/(rho*Y)));
if iter==10000
    fprintf('Frame Yield Pressure:                No result. See ERROR message above.\n');
else
    fprintf('Frame Yield Pressure:                %g psi (%g\n',ceil(pFY),ceil((pFY*144)/(rho*Y)));
end
fprintf('Frame Von Mises Stress at %g feet (Yield Strength):                %g psi (%g\n',Dw,ceil(sigmaTf),sigmaY);
fprintf('Frame Instability Buckling Pressure:                %g psi (%g\n',ceil(Output(1,13)),ceil((Output(1,13)*144)/(rho*Y)));
fprintf('Safety Factors - Actual (Desired)\n');
fprintf('Shell Yield:                %g (%g)\n',Output(1,9)/pDDD,SFY);
fprintf('Shell Lobar Buckling:                %g (%g)\n',PCLB/pDDD,SFib);
fprintf('General Instability (Bryant):                %g (%g)\n',Output(1,11)/pDDD,SFgi);
if iter==10000
    fprintf('General Instability:                No result. See ERROR message above.\n');
else
    fprintf('Frame Yield:                %g (%g)\n',pFY/pDDD,SFfy);
end
fprintf('Frame Instability:                %g (%g)\n',Output(1,13)/pDDD,SFfi);

fprintf('\n*****Scantling Guidelines*****\n\n');
fprintf('ts*sigmaY/pR:                %g (0.7 - 0.9)\n',Output(1,15)*sigmaY/(pCY*(R-
(Output(1,15)/2))));
fprintf('hw/tw:                %g (15 - 20)\n',Output(1,16)/Output(1,17));
fprintf('hfl/hw:                %g (0.7 - 0.8)\n',Output(1,18)/Output(1,16));
fprintf('Lf/2R:                %g (0.07 - 0.10)\n',Output(1,14)/(2*R));
fprintf('tfl/ts:                %g (0.75 - 1.0)\n',Output(1,19)/Output(1,15));
fprintf('Af/Lf*ts:                %g (0.3 -\n',((Output(1,16)*Output(1,17))+(Output(1,18)*Output(1,19)))/(Output(1,14)*Output(1,15));
fprintf('Lb/2R:                %g (1.5 - 2.0)\n',Output(1,23)/(2*R));
fprintf('Lf:                %g (R/6 = %g)\n',Output(1,14),R/6);
fprintf('((hw+tfl)/R:                %g (0.05 - 0.1)\n',(Output(1,16)+Output(1,19))/R);

```

%Plots Optimization Results (1/GammaY vs 1/BR)


```

figure(1)
plot(1./Results(:,7),1./Results(:,1),'.','markersize',12,'Color','k')
hold on
axis([0 1 0 1]);
xlabel('WEIGHT / BUOYANCY');
ylabel('( P / P_C )');
title(['SCANTLING OPTIMIZATION AT ',num2str(Dw),' FEET']);
if nnz(Random)~=0
plot(1./Randomflip(:,2),1./Randomflip(:,1),'.','markersize',12,'Color','k')
end
hold off

%Calculate Slenderness Ratio & Sai
%Taylor Model Basin Data (Arentzen & Mandel,1960) - Ships with Pc from Experimental Data
ModelsY=[1.25 0.7 0.91 0.8 0.49 0.59 0.69 0.81 0.58 0.59 0.71 1.305 0.89 0.605 0.67 0.655 0.49 0.51
0.508 0.415 0.41 0.48 0.38 0.3 0.23 0.35];
ModelsX=[0.58 0.86 0.885 0.89 0.99 0.977 0.982 0.985 1.08 1.18 1.225 0.96 1.21 1.39 1.4 1.44 1.46 1.59
1.615 1.7 1.8 1.81 1.9 1.925 1.96 2.0];
%Taylor U.S. Submarine Data (Arentzen & Mandel,1960) - Ships with Pc from Equation 92a (Von
Sanden and Gunther)
ShipsY=[1.12 1.09 1.045 1.045 1.09 1.01 1.03 1.21 0.98 1.045];
ShipsX=[0.622 0.62 0.635 0.68 0.685 0.725 0.77 0.78 0.89 1.06];
lamda=(((Output(1,14)/(2*R-Output(1,15)))/((Output(1,15)/(2*R-Output(1,15)))^1.5))*(sigmaY/E))^0.5;
Sai=(Output(1,9))/((2*Output(1,15)*sigmaY)/(2*R-Output(1,15))); %P from Equation (16)
lamdaV1=[1.1:0.01:4.0];
lamdaV2=[0:0.01:1.2];
ordinate1=1.3./(lamdaV1.^2);
ordinate2=ones(1,length(lamdaV2));

%Plots Shell Segment Performance for lightest solution
figure2 = figure;
axes1 = axes('Parent',figure2);
axis(axes1,[0.4 2 0 2]);
box(axes1,'on');
hold(axes1,'all');
plot1 = plot(lamda,Sai,'LineStyle','none','Marker','.','color','k','MarkerSize',17,'Parent',axes1);
plot2 = plot(ModelsX,ModelsY,'LineStyle','none','Marker','+','MarkerSize',5,'color','k','Parent',axes1);
plot3 = plot(ShipsX,ShipsY,'LineStyle','none','Marker','o','color','k','MarkerSize',5,'MarkerFaceColor',[1 1
1],'Parent',axes1);
legend1 = legend(axes1,{'FFSOR RESULT WITH P_C FROM EQUATION (16)','MODELS WITH P_C
FROM EXPERIMENT','SUBS WITH P_C FROM VON SANDEN & GUNTHER
(92a)'},'Location','NorthWest');
annotation1 = annotation(figure2,'textbox','Position',[0.6036 0.3476 0.2161
0.169],'LineStyle','none','FontSize',12,'String',{'\psi = 1.30 / \lambda^2'},'FitHeightToText','on');
box(legend1,'off');
xlabel('SLENDERNESS RATIO, \lambda');
ylabel('PRESSURE FACTOR, \psi');
title('SHELL SEGMENT PERFORMANCE');
hold on
plot(lamdaV1,ordinate1,'color','black','linewidth',1.5);
plot(lamdaV2,ordinate2,'color','black','linewidth',1.5);
hold off
end %Output Loop Ends
end %FLAG01 Loop End

```

APPENDIX V. FFSOR Results – Design A

*****User Input*****

Outer Radius of Cylinder (inches):	41.5
Length Between Bulkheads (feet):	34.885
Design Collapse Depth (feet):	2500
Total Number of Combinations:	57200325

*****Optimum Scantlings*****

Frame Spacing (inches):	14
Shell Thickness (inches):	0.75
Web Height (inches):	6
Web Thickness (inches):	0.34375
Flange Width (inches):	4.75
Flange Thickness (inches):	0.65625

*****Optimum Scantling Results*****

Shell Yield Pressure:	1682 psi (3765 feet)
Shell Lobar Buckling Pressure (mode = 10):	4835 psi (10825 feet)
Shell Lobar Buckling Pressure (Windenburg):	4944 psi (11069 feet)
General Instability (Bryant) Buckling Pressure (mode = 2):	9811 psi (21966 feet)
Frame Yield Pressure:	1682 psi (3766 feet)
Frame Von Mises Stress at 2500 feet (Yield Strength):	51463 psi (80000 psi)
Frame Instability Buckling Pressure:	13063 psi (29248 feet)

Safety Factors - Actual (Desired)	
Shell Yield:	1.50592 (1.5)
Shell Lobar Buckling:	4.32995 (2.25)
General Instability (Bryant):	8.786 (3.75)
Frame Yield:	1.50636 (1.5)
Frame Instability:	11.6988 (1.8)

*****Scantling Guidelines*****

ts*sigmaY/pR:	0.871081 (0.7 - 0.9)
hw/tw:	17.4545 (15 - 20)
hfl/hw:	0.791667 (0.7 - 0.8)
Lf/2R:	0.168675 (0.07 - 0.10)
tfl/ts:	0.875 (0.75 - 1.0)
Af/Lf*ts:	0.493304 (0.3 - 0.6)
Lb/2R:	5.04361 (1.5 - 2.0)
Lf:	14 (R/6 = 6.91667)
(hw+tfl)/R:	0.160392 (0.05 - 0.1)

(INTENTIONALLY LEFT BLANK)

APPENDIX VI. FFSOR Results – Design B (Small Frame)

*****User Input*****

Outer Radius of Cylinder (inches):	41.5
Length Between Bulkheads (feet):	12.9
Design Collapse Depth (feet):	2500
Total Number of Combinations:	30332862

*****Optimum Scantlings*****

Frame Spacing (inches):	23
Shell Thickness (inches):	0.75
Web Height (inches):	6
Web Thickness (inches):	0.34375
Flange Width (inches):	4.75
Flange Thickness (inches):	0.6875

*****Optimum Scantling Results*****

Shell Yield Pressure:	1682 psi (3765 feet)
Shell Lobar Buckling Pressure (mode = 9):	2589 psi (5796 feet)
Shell Lobar Buckling Pressure (Windenburg):	2617 psi (5859 feet)
General Instability (Bryant) Buckling Pressure (mode = 2):	9454 psi (21166 feet)
Frame Yield Pressure:	1699 psi (3803 feet)
Frame Von Mises Stress at 2500 feet (Yield Strength):	50733 psi (80000 psi)
Frame Instability Buckling Pressure:	8937 psi (20008 feet)

Safety Factors - Actual (Desired)

Shell Yield:	1.50599 (1.5)
Shell Lobar Buckling:	2.31832 (2.25)
General Instability (Bryant):	8.46637 (3.75)
Frame Yield:	1.52114 (1.5)
Frame Instability:	8.00317 (1.8)

*****Scantling Guidelines*****

ts*sigmaY/pR:	0.871081 (0.7 - 0.9)
hw/tw:	17.4545 (15 - 20)
hfl/hw:	0.791667 (0.7 - 0.8)
Lf/2R:	0.277108 (0.07 - 0.10)
tfl/ts:	0.916667 (0.75 - 1.0)
Af/Lf*ts:	0.308877 (0.3 - 0.6)
Lb/2R:	1.86506 (1.5 - 2.0)
Lf:	23 (R/6 = 6.91667)
(hw+tfl)/R:	0.161145 (0.05 - 0.1)

(INTENTIONALLY LEFT BLANK)

APPENDIX VII. FFSOR Results – Design B (King Frame)

*****User Input*****

Outer Radius of Cylinder (inches):	41.5
Length Between Bulkheads (feet):	36
Design Collapse Depth (feet):	2500
Total Number of Combinations:	993225

*****Optimum Scantlings*****

King Frame Web Height (inches):	10
King Frame Web Thickness (inches):	0.59375
King Frame Flange Width (inches):	8
King Frame Flange Thickness (inches):	0.96875
King Frame Insert Width (inches):	9.2
King Frame Insert Thickness (inches):	0.225

*****Optimum Scantling Results*****

General Instability (3T-Bryant) Buckling Pressure (mode = 2):	13107	psi	(29345 feet)
King Frame Yield Pressure:	1677	psi	(3755 feet)
King Frame Von Mises Stress at 2500 feet (Yield Strength):	51426	psi	(80000 psi)
King Frame Instability Buckling Pressure:	7593	psi	(16999 feet)
Total Weight of One King Frame:	936	lbf	

Safety Factors - Actual (Desired)

General Instability (3T-Bryant):	11.7379	(3.75)
King Frame Yield:	1.50206	(1.5)
King Frame Instability:	6.79970	(2.25)

*****Scantling Guidelines*****

hw/tw:	16.8421	(15 - 20)
hfl/hw:	0.8	(0.7 - 0.8)
tfl/ts:	0.99359	(0.75 - 1.0)
Lb/2R:	1.73494	(1.5 - 2.0)
E1:	16.8421	(<=21.1232)
E2:	8.25806	(<=19.2029)
E3:	0.00923236	(>=0.00271186)

Required moment of inertia for King Frame plus Leff:	452.466	in^4
Calculated moment of inertia for King Frame plus Leff:	540.953	in^4
King Frame moment of inertia / Small Frame moment of inertia:	13.3323	(~10)
King Frame area / Small Frame area:	2.95743	(~3)

(INTENTIONALLY LEFT BLANK)

APPENDIX VIII. Seakeeping Solver for Cylindrical Spar Buoys

```
% Program:      Seakeeping Solver for Cylindrical Spar Buoys
% Language:     MATLAB Script (M-file)
% Author:       LCDR Joshua LaPenna
% Date:         June, 2009
% Units:        Metric

% Function:      This program analyzes the motion of a cylindrical spar buoy
%               in regular waves. The user has control of buoy mass, lyy
%               center of gravity and end-cap geometry (i.e. a/b), as well as
%               sea state and performance criteria. For each motion, surge, heave
%               and pitch, the program outputs the displacement, velocity and
%               acceleration spectrums, natural frequencies, and typical
%               seakeeping statistics. The program can be easily modified to
%               output forces and moments if desired.
clear
clc
close all

%Physical Properties
rho=1025;           %Seawater density (kilograms/meter^3)
g=9.81456;         %Gravity (meters/sec^2)

%Input Parameters
%Obtained from Final LSRC Design (Solid Works Output)
Le=461*0.0254;      %Length between end-caps (meters) (i.e. cylinder length)
R=41.5*0.0254;      %Cylinder outer radius (meters)
b=0.7*R;            %End-cap semiminor axis (b) (meters)
Mass=96595*0.45359237; %LSRC full load (occupied) Mass (kilograms)
lyy=833680.1;       %LSRC mass moment of inertia about y-axis through CG
KG=5.5;            %Distance between the keel and CG (meters)
Endcap=1;          %To calculate F3hat for disk only, set to 1. For disk and dish, set to 0
VAL=0.2*g;          %Vertical acceleration limit (meters/second^2)
LAL=0.1*g;          %Lateral acceleration limit (meters/second^2)
Pitchmax=4;         %Maximum recommended pitch/roll amplitude (degrees) RMS value
Sea=4;              %Sea state of interest (1-9)
Cd1=1.2;            %Damping coefficient of cylinder in surge (for Le/2R=5, Cd=0.75)
Cd3=0.4;            %Damping coefficient of end-cap in heave
Cd5=1.2;            %Damping coefficient of cylinder in pitch

%Derived Parameters
Disp=Mass/rho;       %Volume displaced by LSRC (meters^3)
Dispe=0.5*(4/3)*pi*b*(R^2); %Volume displaced by lower end-cap (meters^3)
L=(Disp-Dispe)/(pi*(R^2)); %Draft of cylindrical section (meters)
FB=Le-L+(23*0.0254); %Freeboard to hatch opening (meters)
Awp=pi*(R^2);        %Waterplane area (Stillwater) (meters^2)

%LSRC center of buoyancy (distance from surface) (meters)
CB=((Dispe*(L+((4/3)*(b/pi))))+(L*Awp*(L/2)))/(Disp);

CG=L+b-KG;           %LSRC center of gravity (distance from surface) (meters)
BG=CG-CB;            %Distance between CG and CB (meters)
GM=BG+((0.25*pi*(R^4))/Disp); %Metacentric height (meters)
```


%Dished End-cap Parameters

```
Ro=((R^2)+(b^2))/(2*b);           %Sphere radius (meters)
d=L-sqrt((Ro^2)-(R^2));           %Distance from surface to sphere center (meters)
beta=asin(R/Ro);                 %Dished end-cap arc angle (radians)
```

%Define Ocean Environment

%World Meteorological Organization Sea State Codes 1-9

%Mean Significant Wave Height (meters)

```
H13=[0.05 0.3 0.875 1.875 3.25 5.0 7.5 11.5 14];
```

```
wmin=0.001;                       %Minimum frequency (radians)
wmax=2;                           %Maximum frequency (radians)
dw=0.001;                         %Frequency increment (radians)
Omega=[wmin:dw:wmax];             %Frequency range (radians/second)
K=(Omega.^2)./g;                  %Wave number range (radians^2/meter^2)
```

%Calculates Bretschneider Sea Spectrum (S)

```
wm=0.4*sqrt(g/H13(Sea));
Sw=(1.25/4).*(wm^4./Omega.^5).*(H13(Sea)^2).*exp(-1.25.*((wm./Omega).^4));
Sw=Sw+(1E-315);                  %Ensures Sw has all non-zero elements
Awi=(2.*Sw.*dw).^0.5;            %Calculates Vector of Wave Amplitudes A(wi)
```

%Calculates Added Mass (A)

```
A11=rho*Awp*L;
A13=0;
A15=rho*Awp*L*BG;
A31=A13;
A33=0.5*(0.76*(4/3)*pi*rho*b*(R^2));
A35=0;
A51=A15;
A53=A35;
A55=rho*Awp*(((L^3)/12)+(L*(BG^2)));
```

%Calculates Damping Force Coefficients (B)

%B11, B33, B55, B15 & B51 are defined below

```
B13=0;
B31=B13;
B35=0;
B53=B35;
```

%Calculates Restoring Force Coefficients (C)

```
C11=0;
C13=0;
C15=0;
C31=C13;
C33=rho*g*Awp;
C35=0;
C51=C15;
C53=C35;
C55=(rho*g*Disp*(BG))+((1/4)*rho*g*pi*(R^4));
```

%When taking moments about CG:

```
I55=Iyy;
```

```

M15=0;
M51=M15;

%Calculate Forcing Functions (i.e. Forces - F1hat, F3hat & F5hat)
%Calculate Heave Force Complex Amplitude (F3hat)
F3hat_disk=(Awi.*(rho*g*Awp)).*exp(-K.*L); %Equation (66) Note: F3hat = |F3|
if Endcap==0
    step=0;
    for omega=wmin:dw:wmax
        step=step+1;
        k=(omega^2)/g;
        Function=['exp(' num2str(k) '*' num2str(Ro) '*cos(phi)-' num2str(d) ')'*cos(' num2str(k) '*'
num2str(Ro) '*sin(phi)*cos(theta))*cos(phi)*(sin(phi))'];
        Integrand=inline(Function,'theta','phi');
        A=dblquad(Integrand,0,2*pi,pi-beta,pi); %Equation (69)
        A_matrix(1,step)=A;
    end
    step=0;
    for omega=wmin:dw:wmax
        step=step+1;
        k=(omega^2)/g;
        Function=['exp(' num2str(k) '*' num2str(Ro) '*cos(phi)-' num2str(d) ')'*sin(' num2str(k) '*'
num2str(Ro) '*sin(phi)*cos(theta))*cos(phi)*(sin(phi))'];
        Integrand=inline(Function,'theta','phi');
        B=dblquad(Integrand,0,2*pi,pi-beta,pi); %Equation (70)
        B_matrix(1,step)=B;
    end
    Psid=atan(B_matrix./A_matrix);
    F3hat_dish=(sqrt((A_matrix.^2)+(B_matrix.^2))).*(Awi.*((Ro^2)*rho*g)).*exp(i.*(-Psid)); %Equation (73)
    % Plots F3hat_disk and F3hat_dish for comparison
    figure(102)
    plotyy(Omega,abs(F3hat_disk),Omega,abs(F3hat_dish))
end

%Calculate Surge and Pitch Complex Amplitudes (F1hat & F5hat)
%O. M. Faltinsen, page 95
CC=((L/2)+BG)-1./K;
DD=(L/2)-BG+(1./K);
F1hat=((2*rho*g*Awp).*Awi).*(1-exp(-K.*L));
F5hat=((2*rho*g*Awp).*Awi).*(CC+(DD.*exp(-L.*K)));

%Heave Analysis
X3ave=2; %Initial Guess: average heave amplitude
iter=0;
B33H=((Omega.*K)./(2*rho)).*(((abs(F3hat_disk))./g).^2); %Haskind relation
while (1)
    X3ave_old=X3ave;
    iter=iter+1;

    %Calculates Damping Force Coefficient (B)
    B33=B33H+(((4/(3*pi))*rho*Cd3*Awp*X3ave).^2).*(Omega);

    %Calculate Heave Transfer Function (H3)
    X3hat=(F3hat_disk)./(-(Omega.^2).*(Mass+A33)+(i.*Omega.*B33)+C33);
    H3=X3hat./Awi; %Non-dimensional

```

```

%Calculate Heave Response Spectrum (displacement)
SX3=(abs(H3).^2).*Sw;

%Calculates Moments of the Response Spectrum
MoSX3=trapz(Omega,SX3);

%Calculates the Average Heave Amplitude
X3_11=1.25*sqrt(MoSX3);
X3ave=X3_11;
Error3=abs((X3ave-X3ave_old)/X3ave)*100;
if Error3<=0.01,break,end
if iter==100
fprintf('\nB33 did not converge. Try increasing iterations\n'),break,end
end
[max3,row3]=max(abs(H3));
wn3=Omega(row3); %Natural frequency in heave (graphically)
wn3E=(C33/(Mass+A33))^0.5; %Natural frequency in heave (analytical)

%Surge and Pitch Analysis
X1ave=0.3; %Initial Guess: average surge amplitude
X5ave=0.5; %Initial Guess: average pitch amplitude
iter=0;
B11H=((Omega.*K)./(4*rho)).*(((abs(F1hat))./g).^2); %Haskind relation
B15H=(Omega./rho).*(((abs(F1hat))./(L*g)).^2).*(L*BG); %Haskind relation
B51H=B15H;
B55H=((Omega.*K)./(4*rho)).*(((abs(F5hat))./g).^2); %Haskind relation
while (1)
X1ave_old=X1ave;
X5ave_old=X5ave;
iter=iter+1;

%Calculates Damping Force Coefficients (B)
B11=B11H+(((8/(3*pi))*rho*Cd1*R*L*X1ave).*Omega);
B55=B55H+(((2/(3*pi))*rho*Cd5*R*X5ave*((CG^4)+(KG^4))).*Omega);
B15=B15H-(((2/(3*pi))*rho*Cd5*R*X5ave*((KG^4)-(CG^4))).*Omega);
B51=B51H-(((4/(3*pi))*rho*Cd1*R*X1ave*((KG^2)-(CG^2))).*Omega);

%Calculates functions P, Q, R & S (Coupled Pitch and Surge)
PP=(((i).*Omega.^2).*(Mass+A11))+(Omega.*B11)-(i*C11);
QQ=(((i).*Omega.^2).*(M15+A15))+(Omega.*B15)-(i*C15);
RR=(((i).*Omega.^2).*(M51+A51))+(Omega.*B51)-(i*C51);
SS=(((i).*Omega.^2).*(I55+A55))+(Omega.*B55)-(i*C55);

%Seakeeping Analysis
%Calculate Surge Transfer Function (H1)
X1hat=((F1hat.*SS)-(F5hat.*QQ))./((PP.*SS)-(QQ.*RR));
H1=X1hat./Awi; %Non-dimensional

%Calculate Pitch Transfer Function (H5)
X5hat=((F5hat.*PP)-(F1hat.*RR))./((PP.*SS)-(QQ.*RR));
H5=X5hat./((Awi.*K); %Non-dimensional

%Calculates Surge and Pitch Response Spectrums (displacement)

```

```

SX1=(abs(H1).^2).*Sw;
SX5=(abs(H5).^2).*Sw;

%Calculates Moments of the Response Spectrums
MoSX1=trapz(Omega,SX1);
MoSX5=trapz(Omega,SX5);
M2SX5=trapz(Omega,(SX5.*(Omega.^2)));
M4SX5=trapz(Omega,(SX5.*(Omega.^4)));

%Calculates Bandwidths of the Response Spectrums
EpsilonSX5=sqrt(1-((M2SX5^2)/(MoSX5*M4SX5)));

%Calculates the Average Surge and Pitch Amplitudes
X1_11=1.25*sqrt(MoSX1);
X5_11=1.25*sqrt(MoSX5);
X1ave=X1_11;
X5ave=X5_11;
Error1=abs((X1ave-X1ave_old)/X1ave)*100;
Error5=abs((X5ave-X5ave_old)/X5ave)*100;
if (Error1<=0.01)&(Error5<=0.01),break,end
if iter==100
fprintf('\nB11 or B55 did not converge. Try increasing iterations\n'),break,end
end
[max5,row5]=max(abs(H5));
wn5=Omega(row5); %Natural frequency in pitch (graphically)
wn5E=((C55)/((I55+A55)-(0.5*Mass*(BG^2))))^0.5; %Natural frequency in pitch (analytical)

%Calculates Velocity and Acceleration Spectrums
SV1=(Omega.^2).*SX1;
SA1=(Omega.^4).*SX1;
SV3=(Omega.^2).*SX3;
SA3=(Omega.^4).*SX3;
SV5=(Omega.^2).*SX5;
SA5=(Omega.^4).*SX5;

%Calculates Moments of the Acceleration Spectrums
MoSA1=trapz(Omega,SA1);
MoSA3=trapz(Omega,SA3);
MoSA5=trapz(Omega,SA5);

M2SA1=trapz(Omega,(SA1.*(Omega.^2)));
M2SA3=trapz(Omega,(SA3.*(Omega.^2)));
M2SA5=trapz(Omega,(SA5.*(Omega.^2)));

M4SA1=trapz(Omega,(SA1.*(Omega.^4)));
M4SA3=trapz(Omega,(SA3.*(Omega.^4)));
M4SA5=trapz(Omega,(SA5.*(Omega.^4)));

%Calculates Bandwidths of the Acceleration Spectrums
EpsilonSA1=sqrt(1-((M2SA1^2)/(MoSA1*M4SA1)));
EpsilonSA3=sqrt(1-((M2SA3^2)/(MoSA3*M4SA3)));
EpsilonSA5=sqrt(1-((M2SA5^2)/(MoSA5*M4SA5)));

%Calculates the Significant Response Amplitudes

```

%These are the average amplitude of all maxima above a13. Said another
 %way, it is the expected value of the response, given that the response
 %is above a13.

```
A1_13=2*sqrt(MoSA1);
A3_13=2*sqrt(MoSA3);
A5_13=2*sqrt(MoSA5);
```

%Calculates the Average Response Amplitudes

```
X5_11=1.25*sqrt(MoSX5);
A1_11=1.25*sqrt(MoSA1);
A3_11=1.25*sqrt(MoSA3);
A5_11=1.25*sqrt(MoSA5);
```

%Calculates the probability that the response will exceed the motion/acceleration limits

```
ProbX5_Pitchmax=(2*((sqrt(1-(EpsilonSX5^2)))/(1+(sqrt(1-(EpsilonSX5^2))))))*(exp(-
(((Pitchmax*(pi/180))^2)/(2*MoSX5))));
ProbA1_LAL=(2*((sqrt(1-(EpsilonSA1^2)))/(1+(sqrt(1-(EpsilonSA1^2))))))*(exp(-((LAL^2)/(2*MoSA1))));
ProbA3_VAL=(2*((sqrt(1-(EpsilonSA3^2)))/(1+(sqrt(1-(EpsilonSA3^2))))))*(exp(-((VAL^2)/(2*MoSA3))));
ProbA5_LAL=(2*((sqrt(1-(EpsilonSA5^2)))/(1+(sqrt(1-(EpsilonSA5^2))))))*(exp(-
(((LAL/(CG*cos(X5_11)))^2)/(2*MoSA5))));
```

%Output

```
fprintf('\n***** RESULTS *****\n');
fprintf('\nSea State = %g\n',Sea);
fprintf('Significant Wave Height (H13) = %g meters\n',H13(Sea));
fprintf('Sea Spectrum Modal Frequency = %-.23f 1/seconds\n\n',wm);
fprintf('Heave Spectrum Modal Frequency = %-.23f 1/seconds\n',wn3);
fprintf('Pitch Spectrum Modal Frequency = %-.23f 1/seconds\n',wn5);
fprintf('\nAverage Accelerations in Sea State %g :\n',Sea);
fprintf('Surge = %-.21f m/s2\n',A1_11);
fprintf('Heave = %-.21f m/s2\n',A3_11);
fprintf('Pitch = %-.21f deg/s2\n',A5_11*(180/pi));
fprintf('\nSignificant Accelerations in Sea State %g :\n',Sea);
fprintf('Surge = %-.21f m/s2\n',A1_13);
fprintf('Heave = %-.21f m/s2\n',A3_13);
fprintf('Pitch = %-.21f deg/s2\n\n',A5_13*(180/pi));
fprintf('
          NATO STANAG 4154    LSRC PERFORMANCE    PROBABILITY
OF\n');
fprintf('
          LIMIT          IN SEA STATE %g          EXCEEDING LIMIT\n\n',Sea);
fprintf('Pitch:          %-.21f deg (RMS)          %-.21f deg (RMS)          %-.21f
percent\n\n',Pitchmax,sqrt(MoSX5)*(180/pi),ProbX5_Pitchmax*100);
fprintf('Vertical Acceleration (Heave):          %-.22f m/s2 (RMS)          %-.21f m/s2 (RMS)          %-.21f
percent\n\n',VAL,sqrt(MoSA3),ProbA3_VAL*100);
fprintf('Lateral Acceleration (Surge):          %-.22f m/s2 (RMS)          %-.21f m/s2 (RMS)          %-.21f
percent\n\n',LAL,sqrt(MoSA1),ProbA1_LAL*100);
fprintf('Lateral Acceleration (Pitch):          %-.22f m/s2 (RMS)          %-.21f m/s2 (RMS)          %-.21f
percent\n\n',LAL,sqrt(MoSA5)*(CG)*cos(X5_11),ProbA5_LAL*100);
```

%Time Space Simulations

```
Seconds=240; %Duration of time simulation
Psi=rand(1,length(Omega)).*2*pi; %Vector of random phases
time=[0:1:Seconds];
```

%Calculates Surge Response in Time Space

```
PsiH1=angle(H1); %Vector of transfer function phase angles
```

```

for t=0:Seconds
    X1ti=Awi.*abs(H1).*sin(Omega.*t+PsiH1+Psi);
    X1t(t+1)=sum(X1ti);
end

%Calculates Heave Response in Time Space
PsiH3=angle(H3); %Vector of transfer function phase angles
for t=0:Seconds
    X3ti=Awi.*abs(H3).*sin(Omega.*t+PsiH3+Psi);
    X3t(t+1)=sum(X3ti);
end

%Calculates Pitch Response in Time Space
PsiH5=angle(H5); %Vector of transfer function phase angles
for t=0:Seconds
    X5ti=Awi.*abs(H5).*sin(Omega.*t+PsiH5+Psi);
    X5t(t+1)=sum(X5ti);
end

%Plots Bretschneider Spectrum
figure(1)
plot(Omega,Sw,'black','linewidth',1.5);
xlabel('FREQUENCY (RADIAN/SECOND), \omega');
ylabel('Sw');
title(['BRETSCHNEIDER SPECTRUM, SEA STATE = ',num2str(Sea)]);

%Plots Surge Transfer Function H1 (RAO)
figure(2)
plot(Omega,abs(H1),'black','linewidth',1.5);
xlabel('FREQUENCY (RADIAN/SECOND), \omega');
ylabel('|H1|');
title('SURGE TRANSFER FUNCTION');

%Plots Heave Transfer Function H3 (RAO)
figure(3)
plot(Omega,abs(H3),'black','linewidth',1.5);
xlabel('FREQUENCY (RADIAN/SECOND), \omega');
ylabel('|H3|');
title('HEAVE TRANSFER FUNCTION');

%Plots Pitch Transfer Function H5 (RAO)
figure(4)
plot(Omega,abs(H5),'black','linewidth',1.5);
xlabel('FREQUENCY (RADIAN/SECOND), \omega');
ylabel('|H5|');
title('PITCH TRANSFER FUNCTION');

%Plots RAOs and Sea Spectrum
figure(5)
plot(Omega,Sw.*20,'--black','linewidth',1.5);grid;
hold on
plot(Omega,abs(H1),'red','linewidth',1.5)
plot(Omega,abs(H3),'blue','linewidth',1.5)
plot(Omega,abs(H5),'green','linewidth',1.5)

```

```

title(['WAVE ENERGY SPECTRUM AND NATURAL FREQUENCIES, Sea State = ',num2str(Sea)]);
xlabel('FREQUENCY (RADIAN/SECOND), \omega')
ylabel('SPECTRUM')
legend('BRETSCHNEIDER X 20','SURGE','HEAVE','PITCH')
xlim([0 2])
ylim([0 15])
hold off

%Plots Displacement Spectrums
figure(6)
[AX,Hand1,Hand2] = plotyy(Omega,SX1,Omega,SX5.*(180/(pi)),'plot');
set(get(AX(1),'Ylabel'),'String','SURGE, S_1(\omega) AND HEAVE, S_3(\omega)','color','black')
set(get(AX(2),'Ylabel'),'String','PITCH, S_5(\omega)','color','black')
set(Hand1,'LineStyle','--','linewidth',1.5)
set(Hand2,'linewidth',1.5)
title(['DISPLACEMENT SPECTRUMS, SEA STATE = ',num2str(Sea),' H_1/_3 = ',num2str(H13(Sea)),'',
'meters']);
xlabel('FREQUENCY (RADIAN/SECOND), \omega')
hold on
plot(Omega,SX3,'blue','linewidth',1.5)
legend(AX(1),'SURGE','HEAVE')
hold off

%Plots Velocities Spectrums
figure(7)
[AX,Hand1,Hand2] = plotyy(Omega,SV1,Omega,SV5.*(180/(pi)),'plot');
set(get(AX(1),'Ylabel'),'String','SURGE, S_1(\omega) AND HEAVE, S_3(\omega)','color','black')
set(get(AX(2),'Ylabel'),'String','PITCH, S_5(\omega)','color','black')
set(Hand1,'LineStyle','--','linewidth',1.5)
set(Hand2,'linewidth',1.5)
title(['VELOCITY SPECTRUMS, SEA STATE = ',num2str(Sea),' H_1/_3 = ',num2str(H13(Sea)),'',
'meters']);
xlabel('FREQUENCY (RADIAN/SECOND), \omega')
hold on
plot(Omega,SV3,'blue','linewidth',1.5)
legend(AX(1),'SURGE','HEAVE')
hold off

%Plots Accelerations Spectrums
figure(8)
[AX,Hand1,Hand2] = plotyy(Omega,SA1,Omega,SA5.*(180/(pi)),'plot');
set(get(AX(1),'Ylabel'),'String','SURGE, S_1(\omega) AND HEAVE, S_3(\omega)','color','black')
set(get(AX(2),'Ylabel'),'String','PITCH, S_5(\omega)','color','black')
set(Hand1,'LineStyle','--','linewidth',1.5)
set(Hand2,'linewidth',1.5)
title(['ACCELERATION SPECTRUMS, SEA STATE = ',num2str(Sea),' H_1/_3 = ',num2str(H13(Sea)),'',
'meters']);
xlabel('FREQUENCY (RADIAN/SECOND), \omega')
hold on
plot(Omega,SA3,'blue','linewidth',1.5)
legend(AX(1),'SURGE','HEAVE')
hold off

%Plots Surge Response in Time Space
figure(9)

```

```

plot(time./60,X1t,'black','linewidth',1.25);
xlabel('Time (Minutes)');
ylabel('Surge (Meters)');
title(['Surge Response, SEA STATE = ',num2str(Sea),' H_1/_3 = ',num2str(H13(Sea)),' , meters']);

```

%Plots Heave Response in Time Space

```

figure(10)
plot(time./60,X3t,'black','linewidth',1.25);
xlabel('Time (Minutes)');
ylabel('Heave (Meters)');
title(['Heave Response, SEA STATE = ',num2str(Sea),' H_1/_3 = ',num2str(H13(Sea)),' , meters']);

```

%Plots Pitch Response in Time Space

```

figure(11)
plot(time./60,X5t*(180/pi),'black','linewidth',1.25);
xlabel('Time (Minutes)');
ylabel('Pitch (Degrees)');
title(['Pitch Response, SEA STATE = ',num2str(Sea),' H_1/_3 = ',num2str(H13(Sea)),' , meters']);

```


(INTENTIONALLY LEFT BLANK)

APPENDIX IX. Seakeeping Results

***** RESULTS *****

Sea State = 3

Significant Wave Height (H13) = 0.875 meters

Sea Spectrum Modal Frequency = 1.340 1/seconds

Heave Spectrum Modal Frequency = 0.882 1/seconds

Pitch Spectrum Modal Frequency = 0.535 1/seconds

Average Accelerations in Sea State 3 :

Surge = 0.2 m/s²

Heave = 0.3 m/s²

Pitch = 9.6 deg/s²

Significant Accelerations in Sea State 3 :

Surge = 0.3 m/s²

Heave = 0.5 m/s²

Pitch = 15.4 deg/s²

	NATO STANAG 4154 LIMIT	LSRC PERFORMANCE IN SEA STATE 3	PROBABILITY OF EXCEEDING LIMIT
Pitch:	4.0 deg (RMS)	4.6 deg (RMS)	65.9 percent
Vertical Acceleration (Heave):	1.96 m/s ² (RMS)	0.2 m/s ² (RMS)	0.0 percent
Lateral Acceleration (Surge):	0.98 m/s ² (RMS)	0.1 m/s ² (RMS)	0.0 percent
Lateral Acceleration (Pitch):	0.98 m/s ² (RMS)	0.9 m/s ² (RMS)	55.9 percent

***** RESULTS *****

Sea State = 4

Significant Wave Height (H13) = 1.875 meters

Sea Spectrum Modal Frequency = 0.915 1/seconds

Heave Spectrum Modal Frequency = 0.881 1/seconds

Pitch Spectrum Modal Frequency = 0.520 1/seconds

Average Accelerations in Sea State 4 :

Surge = 0.3 m/s²

Heave = 1.6 m/s²

Pitch = 24.4 deg/s²

Significant Accelerations in Sea State 4 :

Surge = 0.5 m/s²

Heave = 2.5 m/s²

Pitch = 39.0 deg/s²

	NATO STANAG 4154 LIMIT	LSRC PERFORMANCE IN SEA STATE 3	PROBABILITY OF EXCEEDING LIMIT
Pitch:	4.0 deg (RMS)	23.7 deg (RMS)	93.7 percent
Vertical Acceleration (Heave):	1.96 m/s ² (RMS)	1.2 m/s ² (RMS)	28.6 percent
Lateral Acceleration (Surge):	0.98 m/s ² (RMS)	0.2 m/s ² (RMS)	0.0 percent
Lateral Acceleration (Pitch):	0.98 m/s ² (RMS)	2.1 m/s ² (RMS)	83.4 percent